IMPERIAL COLLEGE LONDON

Understanding the impact of bioprocess conditions on monoclonal antibody glycosylation in mammalian cell cultures through experimental and computational analyses

Si Nga Sou

January 2016

Department of Chemical Engineering

Imperial College London

South Kensington Campus

London SW7 2AZ

A thesis submitted to Imperial College London in partial fulfilment of the requirements of the degree of Doctor of Philosophy

[…] “Sometimes I wished I could swim in the sea of cell culture, talk to the cells in person and find out exactly what they need to process the ideal rProduct.” Si Nga Sou

Abstract

With positive outcomes from medical treatments, monoclonal antibodies (mAbs) are to date the best-selling biologics in the pharmaceutical market. The fact that a lot of blockbuster drugs are facing the period of patent cliffs and patents of many of them are due to expire in the next 5 years, places an urgency for better, cheaper and more efficient bioproduction processes, as well as the development of novel drugs and biosimilars. To address to this issue, application of the Quality by Design paradigm that was introduced by the Food and Drug Administration (FDA) is of paramount importance. Medical values and safety of monoclonal antibodies have been reported to rely on the carbohydrate structures that are attached to the mAb N-linked glycosylation site on each constant region. Fc-N-linked glycosylation is considered as a critical quality attribute (CQA) of these therapeutic proteins under the scope of Quality by Design. It was also reported that different bioprocess conditions during recombinant mAb production directly impact glycan compositions and their distribution on the molecules, although the mechanism behind this change is not fully understood. This lack of understanding limits process design and optimisation. To address this issue we examined the effect of mild hypothermia (32°C) and the different recombinant expression systems on mAb N-linked glycosylation, using experiments, flux balance analysis (FBA) and mechanistic modelling to identify resulting differences in cell metabolism. A defined mathematical model that mechanistically and quantitatively describes CHO cell behaviour and metabolism, mAb synthesis and its N-linked glycosylation profiles before and after the induction of mild hypothermia in SGE and TGE expression systems was also constructed, which we believe is the first quantitative model that relates mild hypothermia and TGE system to the four elements mentioned above. Not only does the model aid understanding of the way bioprocess conditions affect product quality, it also provides a platform for bioprocess design, control and optimisation in industry and helps the implementation of the Quality by Design principles. Results obtained from our computational studies suggested glycosyltransferases to be the key players for changes observed among different bioprocess conditions, based on results obtained from this thesis we then manipulated the expression of galactosyltransferase in particular, through a proof-of-concept experiment using miRNAs.

Acknowledgements

I firstly would like to express my gratitude to my academic supervisors Dr. Cleo Kontoravdi and Dr. Karen M Polizzi, for their exceptional support, guidance, knowledge, inspiration and encouragement throughout the past four years of my PhD study. I would like to thank my industrial supervisors Dr. Christopher Sellick and Dr. Ken Lee for their supervision, arrangement of experiments and assistance. I also sincerely thank Kalpana Nayyar, Andrew Smith and Neil Birkett from MedImmune plc for their assistance in glycan, mAb titre analyses and mAb purification, respectively. I thankfully acknowledge the Biotechnology and Biological Sciences Research Council (BBSRC) and Bioprocessing Research Industry Club (BRIC) for my PhD studentship, as well as the financial contribution and technical supports of MedImmune plc. A special thank you to Dr. Ioscani Jimenez Del Val and Dr. Philip Jedrzejewski for their valuable advice and support on the model development and application, as well as Dr Sarantos Kyriakopoulos for his full patience in passing me his knowledge on flux balance analysis. And of course a special thanks to my dearest Dr. Philip Jedrzejewski and Dr. Ioanna Stefani for their moral support and accompany throughout the four year period. Lastly I would like to give a big thank you to my family and Philip Jedrzejewski for the patience and love, which helped me to get through stressful periods during my study.

Declaration

I hereby certify that all material in this thesis which is not my own work has been properly acknowledged.

Si Nga Sou

London, U.K.

January, 2016

Notation

- ECM : Extracellular matrix
- $F_{in,feed}$: inlet flow rate of Feed C (CD EfficientFeed^{TM}C AGT^{TM})
- $F_{in,\ Glc}$: inlet flow rate of glucose only feed
- F_{out} : Outlet flow rate of the bioreactor
- $F_{out,NSD}$: NSD transport rate
- $F_{out,nucloetide}$: Nucleotide transport rate
- $F_{out,UDPGalNAc}$: UDPGalNAc transport rate
- $F_{out,CMPNeu5Ac}$: CMPNeu5Ac transport rate
- $F_{out,ATP}$: ATP transport rate
- $F_{out,CTP}$: CTP transport rate
- $F_{out,GTP}$: GTP transport rate
- $F_{out,UTP}$: UTP transport rate
- K_A : mAb assembly rate constant
- K_{asn} : Monod constant for growth with respect to asparagine
- K_{asp} : Monod constant for growth with respect to aspartate
- K_{arg} : Monod constant for growth with respect to arginine
- K_{glc} : Monod constant for growth with respect to glucose
- K_{glu} : Monod constant for growth with respect to glutamate
- K_{Lac} : Monod constant for growth with respect to lactate
- K_{lysis} : Specific lysis rate of CHO cells within the bioreactor
- K_{lys} : Monod constant for growth with respect to lysine
- K_{pro} : Monod constant for growth with respect to proline
- K_{PEI} : Monod constant for growth with respect to PEI
- $K_{d,amm}$: Constant for cell death by ammonia
- KI_{amm} : Inhibition constant for growth with respect to ammonia
- KI_{lac} : Inhibition constant for growth with respect to lactate

- $K_{amm,gln}$: Monod constant for ammonia production from glutamine
- Kd_{HC} : mRNA decay rate of mAb heavy chain
- Kd_{LC} : mRNA decay rate of mAb light chain
- K_{ER} : Rate constant for ER-to-Golgi antibody transport
- K_G : Rate constant for Golgi-to-ECM antibody transport
- $K_{glc,ATP}$: Saturation constant of glucose with respect to ATP
- $K_{gln,ATP}$: Saturation constant of glutamine with respect to ATP
- $K_{UTP,glc}$: Saturation constant of UTP with respect to glucose
- $K_{UTP,gln}$: Saturation constant of UTP with respect to glutamine
- $K_{UTP,ATP}$: Saturation constant of UTP with respect to ATP
- $K_{GTP,glc}$: Saturation constant of GTP with respect to glucose
- $K_{GTP,gln}$: Saturation constant of GTP with respect to glutamine
- $K_{GTP,ATP}$: Saturation constant of GTP with respect to ATP
- $K_{CTP,glc}$: Saturation constant of CTP with respect to glucose
- $K_{CTP,gln}$: Saturation constant of CTP with respect to glutamine
- $K_{CTP,ATP}$: Saturation constant of CTP with respect to ATP
- $K_{UDPGlcNAc,glc}$: Saturation constant of UDPGlcNAc with respect to glucose
- $K_{UDPGlcNAc,gln}$: Saturation constant of UDPGlcNAc with respect to glutamine
- $K_{UDPGlcNAc,UTP}$: Saturation constant of UDPGlcNAc with respect to UTP
- $K_{UDPGlc,glc}$: Saturation constant of UDPGlc with respect to glucose
- $K_{UDPGlc,UTP}$: Saturation constant of UDPGlc with respect to UTP
- $K_{GDPMan,glc}$: Saturation constant of GDPMan with respect to glucose
- $K_{GDPMan,GTP}$: Saturation constant of GDPMan with respect to GTP
- $K_{UDPGalNAc,UDPGlcNAc}$: Saturation constant of UDPGalNAc with respect to UDPGlcNAc
- $K_{CMPNeu5Ac,UDPGlcNAc}$: Saturation constant of CMPNeu5Ac with respect to UDPGlcNAc
- $K_{gln,CMPNeu5Ac}$: Saturation constant of glutamine with respect to CMPNeu5Ac
- $K_{UDPGal,UDPGlc}$: Saturation constant of UDPGal with respect to UDPGlc
- $K_{GDPFuc,GDPMan}$: Saturation constant of GDPFuc with respect to GDPMan
- $K_{i,CMPNeu5Ac}$: Competitive product inhibition constant
- $K_{i,GDPFuc}$: Non-competitive product inhibition constant
- $K_{i,CMPNeu5Ac,UDPGlcNAc}$: Transport inhibition of CMPNeu5Ac by UDPGlcNAc
- $K_{out,nucleotide}$: Consumption rate of nucleotide
- $K_{TP,nucleotide}$: Saturation coefficient of nucleotide transport

- $K_{TP,NSD}$: Saturation coefficient of NSD transport
- $K_{TP,UDPGalNAc}$: Saturation coefficient of UDPGalNAc transport
- $K_{TP,CMPNeu5Ac}$: Saturation coefficient of CMPNeu5Ac transport
- $K_{TP,UDPGlcNAc}$: Saturation coefficient of UDPGlcNAc transport
- $K_{TP,UDPGlc}$: Saturation coefficient of UDPGlc transport
- $K_{TP,UDPGal}$: Saturation coefficient of UDPGal transport
- $K_{TP,GDPMan}$: Saturation coefficient of GDPMan transport
- $K_{TP,GDPFuc}$: Saturation coefficient of GDPFuc transport
- $K_{d,ManI\ D}$: Enzyme dissociation constant of ManI on substrate Man_6
- $K_{d,ManII\ A}$: Enzyme dissociation constant of ManII on substrate Man_5
- $K_{d,GnTII}$: Enzyme dissociation constant of GnTII on substrate $CoreGlcNAc_1$
- $K_{d,GalT\ a1A}$: Enzyme dissociation constant of GalT on substrate $CoreGlcNAc_2$ (α-1,3 arm)
- $K_{d,GalT\ a1B}$: Enzyme dissociation constant of GalT on substrate $CoreGlcNAc_2$ (α-1,6 arm)
- $K_{d,GalT\ a2A}$: Enzyme dissociation constant of GalT on substrate $CoreGlcNAc_2Gal_1$ (α-1,6 arm)
- $K_{d,Fuc\ A}$: Enzyme dissociation constant of FucT on substrate $CoreGlcNAc_2$
- $k_{T,[Asn]}$: Menten constant of asparagine transport into the cell from culture medium
- $k_{T,[Glc]}$: Menten constant of glucose transport into the cell from culture medium
- $k_{T,[Lac]}$: Menten constant of lactate transport into the cell from culture medium
- LC : mAb light chain
- m_{glc} : maintenance coefficient of glucose
- p_{gln} : synthesis coefficient of glutamine
- N_{HC} : mAb heavy chain DNA copy number
- N_{LC} : mAb light chain DNA copy number
- $N_{glc,ATP}$: Number of glucose required for ATP synthesis
- $N_{glc,GTP}$: Number of glucose required for GTP synthesis
- $N_{glc,UTP}$: Number of glucose required for UTP synthesis
- $N_{glc,UDPGlc}$: Number of glucose required for UDPGlc synthesis
- $N_{glc,UDPGlcNAc}$: Number of glucose required for UDPGlcNAc synthesis
- $N_{glc,GDPMan}$: Number of glucose required for GDPMan synthesis
- $N_{gln,ATP}$: Number of glutamine required for ATP synthesis
- $N_{gln,GTP}$: Number of glutamine required for GTP synthesis
- $N_{gln,UTP}$: Number of glutamine required for UTP synthesis
- $N_{gln,CTP}$: Number of glutamine required for CTP synthesis

- $N_{gln,UDPGlcNAc}$: Number of glutamine required for UDPGlcNAc synthesis
- $N_{gln,CMPNeu5Ac}$: Number of glutamine required for CMPNeu5Ac synthesis
- $N_{ATP,CTP}$: Number of ATP required for CTP synthesis
- $N_{ATP,GTP}$: Number of ATP required for GTP synthesis
- $N_{ATP,UTP}$: Number of ATP required for UTP synthesis
- $N_{glyc,cell}$: Total number of glycan per cell
- $N_{NSD,glyc}$: Number of NSD consumed per host cell N-linked glycan
- $N_{UDPGalNAc,glyc}$: Number of UDPGalNAc consumed per host cell N-linked glycan
- $N_{CMPNeu5Ac,glyc}$: Number of CMPNeu5Ac consumed per host cell N-linked glycan
- $N_{NSD,mAb}$: Number of NSD consumed per mAb Fc-glycan
- $N_{glyc,mAb}$: Number of glycan per a molecule of mAb
- *PEI* : 25kDa linear polyethylenimine transfection reagent
- q_{asn} : Specific rate of asparagine consumption
- q_{asp} : Specific rate of aspartate consumption
- q_{arg} : Specific rate of arginine consumption
- q_{amm} : Specific rate of ammonia production
- q_{glc} : Specific rate of glucose consumption
- q_{glu} : Specific rate of glutamate consumption
- q_{gln} : Specific rate of glutamine consumption
- q_{lac} : Specific rate of lactate consumption
- q_{ys} : Specific rate of lysine consumption
- q_{pro} : Specific rate of proline consumption
- q_{mAb} : Specific rate of mAb production
- r_{NSD}: NSD synthesis rate from glucose or/and glutamine
- $r_{nucleotide}$: rate of nucleotide synthesis
- r_{ATP}: rate of ATP synthesis
- r_{GTP}: rate of GTP synthesis
- r_{CTP}: rate of CTP synthesis
- r_{UTP}: rate of UTP synthesis
- $r_{UDPGlcNAc}$: UDP-GlcNAc synthesis rate from glucose and glutamine
- r_{UDPGlc}: UDP-Glc synthesis rate from glucose
- r_{GDPMan}: GDP-Man synthesis rate from glucose
- $r_{UDPGalNAc}$: UDP-GalNAc synthesis rate from UDP-GlcNAc
- $r_{CMPNeu5Ac}$: CMP-Neu5Ac synthesis from UDP-GlcNAc

- r_{UDPGal}: UDP-Gal synthesis rate from UDP-Glc
- r_{GDPFuc}: GDP-Fuc synthesis rate from GDP-Man
- $r_{met,glc}$: rate of other biochemical reactions based on glucose
- $r_{met,gln}$: rate of other biochemical reactions based on glutamine
- R_{HC} : rate of mAb heavy chain consumption in mAb assembly
- R_{LC} : rate of mAb light chain consumption in mAb assembly
- S_{HC} : transcription rate of mAb heavy chain
- S_{LC} : transcription rate of mAb light chain
- T_{HC} : translation rate of mAb heavy chain
- T_{LC} : translation rate of mAb light chain
- V : Volume of cell culture
- $V_{max,nucleotide}$: Maximum turnover rate of nucleotide
- $V_{max,ATP}$: Maximum turnover rate of ATP
- $V_{max,CTP}$: Maximum turnover rate of CTP
- $V_{max,GTP}$: Maximum turnover rate of GTP
- $V_{max,UTP}$: Maximum turnover rate of UTP
- $V_{max,NSD}$: Maximum turnover rate of NSD
- $V_{max,UDPGlcNAc}$: Maximum turnover rate of UDPGlcNAc
- $V_{max,UDPGlc}$: Maximum turnover rate of UDPGlc
- $V_{max,GDPMan}$: Maximum turnover rate of GDPMan
- $V_{max,UDPGalNAc}$: Maximum turnover rate of UDPGalNAc
- $V_{max,UDPGal}$: Maximum turnover rate of UDPGal
- $V_{max,CMPNeu5Ac}$: Maximum turnover rate of CMPNeu5Ac
- $V_{max,GDPFuc}$: Maximum turnover rate of GDPFuc
- V_{cell} : volume of a CHO cell
- X_v : Viable cell density in the bioreactor
- X_t : Total cell density in the bioreactor
- $Y_{arg,glu}$: Yield of arginine on glutamate
- $Y_{glu,gln}$: Yield of glutamate on glutamine
- $Y_{gln,glu}$: Yield of glutamine on glutamate
- $Y_{lac,glc}$: Yield of lactate on glucose
- $Y_{lys,glu}$: Yield of lysine on glutamate
- $Y_{pro,glu}$: Yield of proline on glutamate
- $Y_{x_v,asn}$: Yield of biomass on asparagine

- $Y_{x_v,asp}$: Yield of biomass on aspartate
- $Y_{x_v,arg}$: Yield of biomass on arginine
- $Y_{x_v,amm}$: Yield of biomass on ammonia
- $Y_{x_v,glc}$: Yield of biomass on glucose
- $Y_{x_v,glu}$: Yield of biomass on glutamate
- $Y_{x_v,gln}$: Yield of biomass on glutamine
- $Y_{x_v,lac}$: Yield of biomass on lactate
- $Y_{x_v,lys}$: Yield of biomass on lysine
- $Y_{x_v,pro}$: Yield of biomass on proline
- ε_1 : ER glycosylation efficiency factor
- ε_2 : Golgi glycosylation efficiency factor
- $f_{lim,}$: Nutrient limitation
- $f_{inh,}$: Product inhibition
- μ : Specific CHO cell growth rate
- μ_d : Specific CHO cell death rate
- μ_{max} : Maximum specific growth rate
- $\mu_{d,max}$: Maximum specific death rate
- λ /MW: Molecular weight of mAb
- *UDP-GlcNAc*: Intracellular uridine diphosphate N-acetylglucosamine concentration
- *UDP-Glc*: Intracellular concentration of uridine diphosphate glucose concentration
- *GDP-Man*: Intracellular concentration of guanosine diphosphate mannose
- *UDP-GalNAc*: Intracellular uridine diphosphate N-acetylgalactosamine concentration
- *CMP-Neu5Ac*: Intracellular cytosine monophosphate N-acetylneuraminic acid concentration
- *UDP-Gal*: Intracellular uridine diphosphate galactose concentration
- *GDP-Fuc*: Intracellular guanosine diphosphate fucose concentration
- *[ATP]* : Intracellular concentration of adenosine triphosphate
- *[GTP]* : Intracellular concentration of guanosine triphosphate
- *[CTP]* : Intracellular concentration of cytidine triphosphate
- *[UTP]* : Intracellular concentration of uridine triphosphate
- *[Asn]* : Extracellular concentration of asparagine
- *[Asp]* : Extracellular concentration of aspartate
- *[Arg]* : Extracellular concentration of arginine
- *[Glc]* : Extracellular concentration of glucose
- *[Glu]* : Extracellular concentration of glutamate

- *[Gln]* : Extracellular concentration of glutamate
- *[Lac]* : Extracellular concentration of lactate
- *[Lys]* : Extracellular concentration of lysince
- *[Pro]* : Extracellular concentration of proline
- *[PEI]* : Concentration of PEI
- *[HC*]: mAb heavy chain concentration
- *[LC]* : mAb light chain concentration
- $[HC_2LC_2]_{ER}$: Fully assembled mAb molecule in the ER
- $[HC_2LC_2]_G$: Fully assembled mAb molecule in the Golgi apparatus
- *[mHC]* : mRNA production of mAb heavy chain
- *[mLC]* : mRNA production of mAb light chain
- *[mAb]* : secreted mAb concentration
- $[Asn_{in,feed}]$: inlet asparagine concentration in CD EfficientFeed^{TM}C AGT^{TM}
- $[Asp_{in,feed}]$: inlet aspartate concentration in CD EfficientFeed^{TM}C AGT^{TM}
- $[Arg_{in,feed}]$: inlet arginine concentration in CD EfficientFeed^{TM}C AGT^{TM}
- $[Glc_{in,feed}]$: inlet glucose concentration in CD EfficientFeed^{TM}C AGT^{TM}
- $[Glu_{in,feed}]$: inlet glutamate concentration in CD EfficientFeed^{TM}C AGT^{TM}
- $[Lys_{in,feed}]$: inlet lysine concentration in CD EfficientFeed^{TM}C AGT^{TM}
- $[Pro_{in,feed}]$: inlet proline concentration in CD EfficientFeed^{TM}C AGT^{TM}
- $[Glc_{in,Glc}]$: inlet glucose concentration in in glucose-only feed
- $[Glc_{int}]$ *:* intracellular concentration of glucose
- $[Gln_{int}]$ *:* intracellular concentration of glutamine
- *[mHC]* : mRNA production of mAb heavy chain
- *ManI*: α-1,2 Mannosidase I
- *GnTI*: α-1,3 N-acetylglucosaminyl transferase I
- *ManII*: α-1,3/α-1,6 Mannosidase II
- *GnTII*: α-1,6 N-acetylglucosaminyl transferase II
- *FucT*: α-1,6 Fucosyltransferase (also known as FUT8)
- *GalT*: β-1,4 Galactosyltransferase

Contents

List of figures

List of tables

Chapter 1
Introduction

Since the approval of the first chimeric monoclonal antibody by the U.S. Food and Drug Administration (FDA) in 1986, a total of 44 monoclonal antibody (mAb) products were approved and marketed. This class of biopharmaceutical product is emerging at a significant rate, with an approval rate of approximately 4 to 5 products per year by the FDA (Ecker et al. 2015). According to the global sales forecast report on biologics by EvaluatePharma in 2014, mAb products will be five of the top 10 best-selling products in the world by 2020. Humira®, an anti-tumour necrosis factor α mAb that is used to treat Crohn's disease, remains as the top selling worldwhile product (Figure 1) (EvaluatePharma 2014). However, 2015-2020 are indeed challenging years for the biopharmaceutical industry, product patents of at least 13 blockbuster mAbs including Humira®, Remicade®, Rituxan®, Lucentis® and many others are at risk of patent expiry (Mullard 2012). This imposes urgency to improve the turnover rate of current mAb development, as well as developing novel biologics and biosimilars for post-patent recovery. To date more than 300 mAb product candidates are in the industrial R&D pipeline, with Nivolumab® being the top most valuable R&D project and the most exciting anti-cancer product that targets programmed cell death-1 pathway (EvaluatePharma 2014). In all ways, to keep up with the fast growing demand for prescription drugs and to ease the risk of the upcoming patent cliff, it is essential for the pharmaceutical industry to investigate efficient production methods with an aim of increasing product yield and efficacy, and to shorten production period.

	Product	Generic Name	Company	Pharmacological Class	WW Product Sales ($m) 2013	2020	CAGR	Market Status
1	Humira	adalimumab	Abbvie + Eisai	Anti-tumour necrosis factor alpha MAb	11,014	12,707	+2%	Marketed
2	Lantus	insulin glargine recombinant	Sanofi	Insulin	7,592	10,252	+4%	Marketed
3	Enbrel	etanercept	Amgen + Takeda + Pfizer	Tumour necrosis factor alpha inhibitor	8,778	8,572	-0%	Marketed
4	Remicade	infliximab	JNJ + Merck & Co + Mitsubishi	Anti-tumour necrosis factor alpha MAb	8,367	8,217	-0%	Marketed
5	Sovaldi	sofosbuvir	Gilead Sciences	Hepatitis C nucleoside NS5B polymerase inhibitor	139	8,027	+78%	Marketed
6	Januvia/Janumet	sitagliptin phosphate	Merck & Co + Daewoong	Dipeptidyl peptidase IV inhibitor	5,842	6,895	+2%	Marketed
7	Avastin	bevacizumab	Roche	Anti-VEGF MAb	6,751	6,613	-0%	Marketed
8	Xarelto	rivaroxaban	Bayer + JNJ	Factor Xa inhibitor	1,948	6,414	+19%	Marketed
9	Nivolumab	nivolumab	Bristol-Myers Squibb + Ono	Anti-programmed death-1 MAb	-	6,361		R&D
10	Tecfidera	dimethyl fumarate	Biogen Idec	Nuclear factor erythroid 2-related factor (Nrf2) pathway activator	876	6,310	+33%	Marketed

Figure 1. Top 10 selling pharmaceutical products in the world. This is modified from the sales forecast report of (EvaluatePharma 2014).

To fulfil this aim, the biopharmaceutical sector can no longer rely on the traditional "Quality by Testing (QbT)" methodology, where quality of products from experiments is only assessed at the end of the process and products are discarded if they fail to meet specification set by the FDA, without looking into the reason for the failure (Hubert et al. 2014). Not only does QbT increase drug production cost, it also lengthens the time required to pass all stages of clinical trials and for the product to be released into the market. As a result, in 2006 the U.S. FDA encouraged the implementation of the "Quality by Design (QbD)" paradigm. QbD relates critical quality attributes (CQAs) of the target protein to bioprocess parameters. Through prior knowledge of the product in different bioprocess conditions, relevant parameters can be altered accordingly in defined product design spaces along the production process and quality can be incorporated into the final products (Rathore and Winkle 2009). To satisfy the principle of QbD during pharmaceutical production requires a thorough understanding of the relationship between process parameters and the CQA of the target product.

In mammalian cells, nascent polypeptides are subject to post-translational modifications to give functionality; such modifications also generate variations within the same species. Protein glycosylation is a commonly observed protein modification. In the case of Immunoglobulin G (IgG), N-linked glycosylation of mAb has been extensively studied and oligosaccharides are found on the Asn_{297} on the C_H2 domain of each heavy chain within its Fc-region. Although it is less studied, Fab regions of mAb molecules are also glycosylated. Fab regions recognise and bind to target antigens to initiate immunomodulation and their antigen binding affinity and avidity are dependent upon the N-glycan structure of Fab fragments (Man Sung et al. 1993). The Fc-domain of the mAb is functionally important owing to the activation of downstream immune effector mechanisms upon binding to

different types of Fcγ receptors. Oligosaccharide chains on the C_H2 domains of both heavy chains affect the protein structure of the binding site and sometimes glycans themselves are involved in the receptor-binding to initiate effects. However, cell metabolism and the process of mAb production including mAb productivity and glycosylation are cell-line, bioprocess condition and product dependent. As a result, product quality can be built into the Fc region during mAb manufacturing to modulate its immune effector function. During recombinant IgG production, mAb glycoforms are regarded as a CQA. Improved understanding of how a certain process condition influences the mAb Fc glycosylation therefore allows specific design of experiment (DoE) and consistant generation of mAb molecules with the desired function. In return, it improves product yield and efficacy, alongside with reduced manufacturing time and cost (Kozlowski and Swann 2006).

The main focus of this study was to thoroughly investigate the impact of mild hypothermic cell culture temperatures and transient gene expression on mAb productivity and mAb Fc N-linked glycosylation. These bioprocess conditions were specifically chosen, as they had the potential to increase the specific productivity of recombinant products, as well as shorten the time-frame for mAb production. In brief, mild hypothermia during cell culture (e.g. temperature shift from 37°C to 30 - 33°C) is a common industrial practice that is used to increase mAb production yield during the fermentation process (Yoon et al. 2006). By lowering the cell culture temperature, it provides a prolonged period of time at high cell density and viability, which typically results in a higher integral viable cell density as well as higher mAb titre. On the other hand, transient gene expression (TGE) is a fast emerging methodology employed during bioproduction. Traditionally, plasmids of recombinant DNA are transfected and expressed within mammalian hosts in a stable manner through stable gene expression (SGE), where target genes are integrated into the host cell genome. This method generates high volumetric yield of recombinant materials, but the process of rProtein synthesis is time-consuming and labour-intensive. As opposed to SGE, TGE is an alternative DNA transfection methodology where target genes of interest are temporarily expressed within host cells without genome integration. This method reduces the time required for clonal selection and cell line expansion, which in turn, speeds up the overall production process. Despite the usefulness of both conditions discussed, each bears its own limitations which could have negative effects on the CQAs of products under the examined bioprocesses.

Within this context, the main goal of this work was to establish linkages between process conditions and CQAs through experimental and computational analyses. We aimed to create a thorough understanding of the impact of each condition on intracellular mechanisms with respect to five main indicators: CHO cell growth profile, nutrient and amino acid metabolism, mAb synthesis, nucleotide and NSD metabolism and mAb Fc N-linked glycosylation. Only through complete understanding of how one or a combination of different conditions affect the cellular behaviour, cell

metabolism and product synthesis, one can identify the underlying causes of differences arising from each bioprocess condition, and design experiments accordingly to generate optimal products.

In addition to experimental analyses, computational approaches are becoming increasingly useful for systems analysis, interpretation of experimental data and to generate estimates for product quality post-fermentation. The use of modelling tools allows us to examine specific parameters that would otherwise be difficult to investigate experimentally, such as the kinetic properties of enzymes involved in N-linked glycosylation. In this study we analysed the metabolic distribution of carbon within cells that were under the influence of each bioprocess condition, through flux balance analysis. In conjunction with the FBA study, mechanistic models that are capable of describing the five aspects of intracellular mechanisms mentioned above were developed for conditions that were examined in this study. The proposed mechanistic models were to be developed based on existing models from Kontoravdi et al. (2010b) and Jimenez del Val et al. (2011). With an aim to compare the respective model outputs from each expression system under different culture temperatures, the developed models provided insights into how differences in product quality arise from the two expression systems. By developing mechanistic models that are capable of representing the biological systems under SGE and TGE, we aimed to close the loop between model outputs and experimental system and provide a platform for bioprocess design, control and optimisation in industry and will assist the implementation of the Quality by Design principles.

The thesis commences with a thorough review of important literature in Chapter 2 that focuses on mAb N-linked glycosylation, this includes its biosynthetic process, structure and function of these attached sugar molecules, their impacts of product glycosylation on drug efficacy, and describing the relationship between bioprocess conditions and mAb glycosylation, with the main focus on mild hypothermic culture temperature and transient gene expression system. The chapter continues with a description of potential approaches that can be applied to identify the underlying mechanisms of cellular processes upon culturing mammalian cells under different bioprocess conditions, which will include the use of various experimental approaches, understanding the cellular metabolic distribution of nutrients and energy through flux balance analysis studies, as well as a description on mechanistic mathematical models from past relevant literatures, the thesis will outline the construction and the assumption of models that were developed to describe host cell dynamics, mAb synthesis, NSD metabolism and the process of N-linked Fc-glycosylation within the Golgi apparatus. The thesis continues by outlining a list of experimental methods that are practised throughout the entire research project in Chapter 3. Our research commences with an investigation of the impact of mild hypothermia on mAb glycosylation in stable CHO transfectants, through the combination of experimental and mathematically analyses presented in Chapter 4 and 5. With similar analytic approaches, the work in the thesis is further extended in Chapter 6 and 7 to examine the effect of transient gene expression on product quality, and a full comparison between stable and transient

gene expression systems, with respect to cellular metabolism, product production and glycosylation, is carried out. Based on the knowledge and understanding that is obtained from the research, a proof-of-concept experiment described in Chapter 8 is developed with an aim to improve mAb glycosylation through manipulating the expression of key glycosyltransferases. Finally the thesis closes with an overall conclusion, which includes the presentation of the main findings of the work and comments on future studies that can potentially be carried out to further improve our understanding of similar matters within the field of biopharmaceutical production in Chapter 9.

Chapter 2
Literature Review

2.1. Monoclonal antibodies – structure and endogenous function

Monoclonal antibodies (mAbs), also known as Immunoglobulins (Igs), are glycoprotein molecules that play an important role in the human immune system. They are formed of four polypeptide chains, two identical heavy and two identical light chains, which form a Y-shape (Figure 2). Igs are heterogeneous in their structures and functions, in which variations arise from differences in the amino-acid sequence of the heavy chains. Each heavy chain consists of one variable domain that is responsible for antigen recognition, and various constant regions that trigger immune response. Isotypes of mAb molecules differ by the number of constant domains, e.g. IgG, IgD, IgE and IgA have three constant domains whereas IgM has four. On the other hand, each light chain has one variable and one constant domain only. The C-termini of the heavy chains are joined together by disulphide bonds at the hinge region and form the crystallizable fragment (Fc) of the mAb, while variable regions of light chains are brought into line with those of the heavy chains to form the antigen-binding fragment (Fab) region. To date, IgGs are the most widely studied antibodies and are further grouped into IgG_1, IgG_2, IgG_3 and IgG4 according to their respective abundances in human serum. Owing to its large quantity in serum (~75% of all immunoglobulins) (Kukrer et al. 2010), recombinant mAbs produced are mostly subgroups of IgGs.

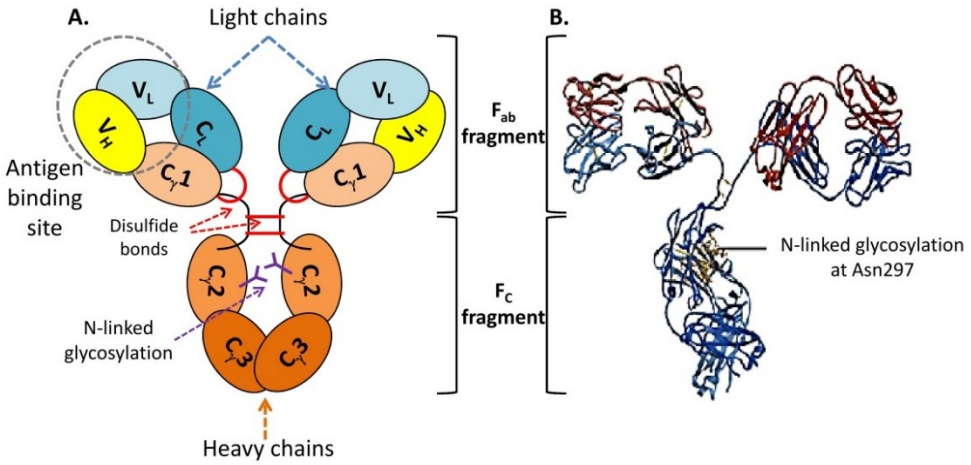

Figure 2. Monoclonal antibody IgG structure. A. IgG mAb possesses a "Y-shape" structure, which comprises two identical heavy and two identical light chains that are joined together by disulfide bonds. Each IgG molecule has two Fab fragments for antigen binding, and one Fc region for functional effector activation. B. X-ray crystallography derived IgG ribbon structure. One N-linked oligosaccharide chain is attached to the Asn 297 amino acid residue of each of the heavy chain CH_2 IgG backbone (Lehninger et al. 2008).

Upon an invasion of pathogens into the human body, our cells trigger a series of immune responses which stimulate the plasma B-cells to produce antibodies with Fab regions that are specific for the targeted antigens. While the Fab region of the mAb recognizes and binds to the antigen, clearance of the pathogen depends on mechanism of the Fc region. Focusing on the IgG isotypes, binding to the Fc region of IgGs can activate various immune effector functions. An example is antibody-dependent cellular cytotoxicity (ADCC), which lyses and kills antigens with granules secreted by granulocytes such as NK cells or neutrophils, when the Fc of the mAb-antigen immune complex is bound by the FcγIII receptor on NK cells or FcγII-A receptor on neutrophils respectively (Janeway 2005). Alternatively complement-dependent cytotoxicity (CDC) is activated, in which the Fc of the antigen-bound mAb binds to the C1 complement complex to activate the complement system. The pathogen is eventually engulfed and eliminated by the membrane attack complex formed during the complement process (Janeway 2005). Moreover, Kaneko et al. showed that the glycosylation pattern on the Fc region of an IgG changes between a pro- and an anti-inflammatory response; this regulates the immune system (Kaneko et al. 2006).

2.2. Monoclonal antibodies as a class of therapeutics (biologics)

Owing to the specificity and functionality towards target pathogens in triggering immune responses, mAbs are excellent candidates as therapeutics for various numbers of diseases. Drug

production is slowly and increasingly shifting from the generation of chemically defined-small molecules to pharmaceutical products that are produced in mammalian hosts (biologics). In the case of monoclonal antibodies, technology involved in mAb generation has advanced dramatically since the development of the first mAb in mice in 1975 (Kohler and Milstein 1975). The hybridoma technique developed by Kohler and Milstein in 1975 involved the fusion of immortal myeloma cells with B-lymphocytes from murine spleen cells that were immunised with specific antigen. To increase target specificity, Boulianne et al. (1984) generated chimeric humanised mAb production in mice and in 1994 mAb were successfully synthesized from the transgenic humanised murine model (Green et al. 1994). To bypass the necessity for animal immunisation, recombinant expression of fully humanised mAb products was then developed using phase display (Clementi et al. 2012). Throughout the history of mAb production, a lot of efforts has gone into cell line development, host cell identification, establishment of clonal libraries, as well as investigations into different expression systems, in order to improve the efficiency of product production. At least 30 approved mAbs were synthesized in the past 35 years and they are clinically active; these include the blockbuster products Humira® and Renucade® which are anti-inflammatory drugs that inhibit the TNF-α receptor; anti-cancer mAbs such as Rituxan® and Herceptin® which target specific types of cancer, or Avastin® that limits cancer cell metastasis; or many others that function against autoimmunity, viral infection or diabetes, or treatments towards neurodegenration such as Alzheimer's disorder (Kyriakopoulos and Kontoravdi 2014b).

2.3. Fc N-linked glycosylation of therapeutic mAbs

In addition to product yield, mAb efficacy and safety are important factors in biopharmaceutical production, which is highly influenced by the oligosaccharide-chains that are attached to the Fc-region of a mAb molecule. In mammalian cells, nascent polypeptides are subject to post-translational modifications to give functionality; such modifications also generate variations within the same species. Protein glycosylation is a commonly observed protein modification. Two types of protein glycosylation exist: asparagine-linked (N-linked) and serine/threonine-linked (O-linked). While O-linked glycosylation is not common in secreted proteins and in the case of mAbs reports are mostly related to human IgA_1 (Allen et al. 1995). On the other hand, N-linked glycosylation of IgG has been extensively studied and oligosaccharides are found on the Asn_{297} on the C_H2 domain of each heavy chain within its Fc-region. Protein glycosylation is also observed on the variable (V) regions of the IgG light and heavy chains. For instance mass spectrometric analysis showed that the IgG-Fab region of an anti-melanoma mouse IgG_3 monoclonal antibody exhibited hypergalalactosylation and sialylation (Muthing et al. 2003). However, owing to the relatively low

abundance of Fab-glycosylation in IgG (an average of around 15-20%), N-linked Fc-oligosaccharides remains the main focus in this study.

2.3.1. Synthetic process of N-linked glycosylation

N-linked glycosylation involves a N-acetylglucosamine (GlcNAc) molecule covalently attached (β-linkage) to the asparagine residue of the protein with an amino-acid sequence Asn-Xaa-Ser/Thr, where X represents any amino acid except proline. N-linked glycosylation commences in the ER where the dolichol-linked precursor oligosaccharide ($GlcNAc_2Man_9Glc_3$) is synthesized in the ER lumen; and then transferred *en bloc* onto the nascent polypeptide chain by an oligosaccharyltransferase. Next, glycan-bound protein polypeptide undergoes the folding process with the terminal glucose (Glc) residues acting as a quality control to ensure correct protein folding. In brief, two glucose molecules are removed from the core $GlcNAc_2Man_9Glc_3$ attached on the nascent polypeptide by glucosidases I & II, leaving the glycan core monoglucosylated. The monoglucocylated glycoprotein interacts with lectins on calnexin and calreticulin to initiate the Calnexin-Calreticulim cycle for correct protein folding. When bound to calnexin and calreticulin chaperone proteins, the glycoprotein is catalysed by the thiol-disculphide oxidoreductase ERp57 and encourages the formation of disulphide bonds on the bound-glycoprotein. The glycoprotein is protected from any pre-mature degradation during the folding process when bound to calnexin and calreticulin. The cleavage of the remaining single glucose by glucosidase II releases the glycoprotein from the complex. If the protein is correctly folded, it exits the ER and is transported into the Golgi apparatus for downstream processing. However, a single glucose molecule can be re-added by UDP-Glc:glucosyltransferase (UGGT) to protein that is not properly folded and re-enter into the Calnexin-Calreticulin cycle (Ellgaard and Helenius 2003). In addition to UGGT and chaperone proetins which aid protein folding, ER-manosidase I (ERManI) recognises terminally misfolded-proteins within the ER, trimming one α1,2-linked mannose residue to yield Man_8 structure. ERManI involves highly in the process of Endoplasmic-reticulum-associated protein degradation (ERAD), in which the removal of a single mannose initiates subsequent degradation of misfolded proteins (Avezov et al. 2008). While within the Golgi apparatus, mannose (Man) residues are trimmed from the oligosaccharide to give a $GlcNAc_2Man_5$ structure in the cis-Golgi; addition of GlcNAc and further Man sugar trimming take place in the medial Golgi; downstream sugar-transfer reactions such as the additions of galactose (Gal), fucose (Fuc) and N-acetylneuraminic acid/sialic acid (Neu5Ac) in the trans-Golgi generate IgG with complex glycan patterns. The glycoprotein is now ready to be secreted into the extracellular matrix for harvesting (Taylor and Drickamer 2003) (Figure 3).

Many precise enzymatic reactions are required in order to accurately process the attached oligosaccharides, these include glycosidases that remove and transferases which add sugar residues onto the growing oligosaccharide chain. Both glycosidases and transferases are substrate specific and only act on specific glycan linkages. For instance, mannosidase I removes terminal mannose residues that are in α1,2 linkages in oligo-mannose oligosaccharide $Man_9(GlcNAc)_2$, while mannosidase II hydrolyses both α1,3 linkages and α1,6 linked terminal mannoses in mannosyl-oligosaccharides. There are also five different N-acetylglucosaminyltransferases that catalyse the addition of N-acetylglucosamine (GlcNAc) residues during N-linked glycosylation, in which each enzyme works upon specific mannosyl-glycoproteins and attaches GlcNAc residues with precise beta-linkages (Krambeck and Betenbaugh 2005). Since the availability of enzymes and co-substrates relies on intracellular conditions, variations in glycan pattern arise. There are two main types of glycan variation in general: 1. glycan macro-heterogeneity, which refers to the glycosylation site occupancy along the amino-acid sequence of the polypeptide chain; and 2. Glycan micro-heterogeneity that denotes the differences in glycan pattern of an oligosaccharide chain during processing inside the Golgi apparatus. In addition to enzyme availability, the availability of nucleotide sugar donors (NSDs) also contributes to glycan variations. NSDs are glycosyl-donors and protein glycosylation reactions rely on the presence of these 'activated sugars'; as a result, the availability of NSD species have a direct impact on the mAb glycosylation.

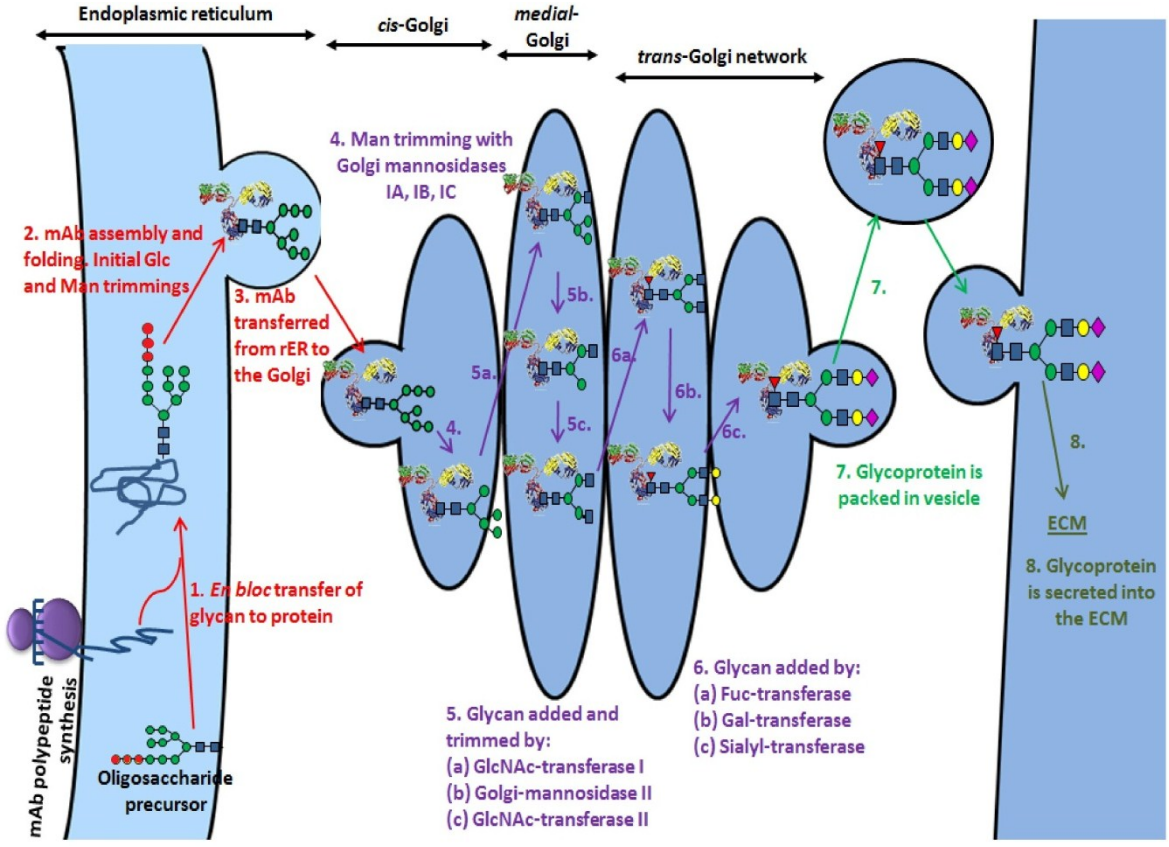

Figure 3. mAb glycoprotein processing. Upon mAb polypeptides and oligosaccharide precursor synthesis, glycans are *en bloc* transfer onto Asn_{297} of the HC polypeptides. mAb is assembled and folded and initial glycan trimming happens with 3 terminal Glc and 1 Man removed. mAb-$GlcNAc_2Man_8$ is transported into the Golgi apparatus for downstream glycan processing. Mannose trimming generates mAb-GlcNAc2Man5 structure in the *cis*-Golgi; 1 GlcNAc is added, followed by 2 Man trimming and second GlcNAc addition in the *medial*- Golgi. In the *trans*-Golgi, 1 Fuc, 2 Gal and 2 NeuAc are added to yield bi-antennary structure for IgG. Glycoprotein is then packed inside a vesicle and is secreted into the ECM for functions. mAb: monoclonal antibody; rER: rough endoplasmic reticulum; Glc: Glucose (●); GlcNAc: N-acetyl-glucosamine (■); Man: mannose (●); Gal: Galactose (●); Fuc: fucose (▼); NeuAc: sialic acid (◆); ECM: extracellular matrix.

2.3.2. Nucleotide sugar donors (NSDs) – building blocks for protein glycosylation

Nucleotide sugar donors are substrates of sugar transferases during glycan processing. Each NSD molecule comprises one nucleotide and one sugar residue. Table 1 shows common structures of NSD molecules that are involved in mAb glycosylation, which are normally UDP-glucose (UDP-Glc), UDP-galactose (UDP-Gal), UDP-N-Acetylhexosamine (UDP-HexNAc) including UDP-GlcNAc and UDP-GalNAc; GDP-mannose (GDP-Man) and GDP-fucose (GDP-Fuc), together with CMP-N-acetylneuraminic acid (CMP-Neu5Ac), or in other word, CMP-sialic acid. In the case of IgG, UDP-GlcNAc molecules are mostly responsible for glycan branching, while glycan elongation is usually carried out by the addition of species such as UDP-Gal and CMP-Neu5Ac. In theory, mammalian cells can generate all types of sugar from carbon and nitrogen sources e.g. glucose or fructose, and various amino acids; and extracellular feeding of different carbon sources affects the overall NSD production and consequently alters protein glycosylation. However the actual NSD synthetic pathway is more complex than that (Murrell et al. 2004), where competitive enzymatic inhibition and product inhibition is common within the network. Figure 4 illustrates a simplified diagram of the NSD synthetic pathway, which indicates the consumption of glucose, galactose, fructose and glutamine within the NSD biosynthetic network. It also shows the synthetic pathway of each NSD species (labelled in different colour schemes).

Table 1. Common nucleotide sugar donor (NSD) observed during IgG N-linked glycosylation. GDP-Man and UDP-GlcNAc are transported into the ER, while UDP-Gal, UDP-GlcNAc, GDP-Fuc and CMP-sialic acid are found transported into the Golgi apparatus for glycan processing. UDP: Uridine-diphosphate; GDP: Guanidine-diphosphate; CMP: Cytidine-monophosphate; GlcNAc: N-acetyl-glucosamine (■); Man: mannose (●); Gal: Galactose (○); Fuc: fucose (▼); NeuAc: sialic acid (◆); ECM: extracellular matrix.

NSD	Structure	NSD	Structure
UDP-GlcNAc	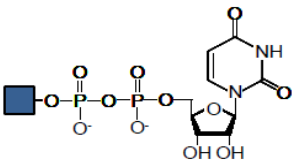	GDP-Fuc	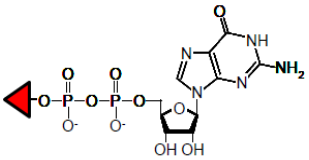
UDP-Gal	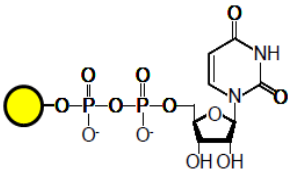	CMP-sialic acid	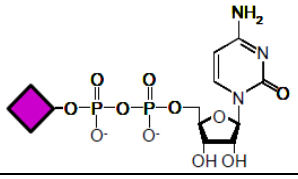
GDP-Man	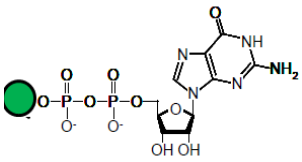		

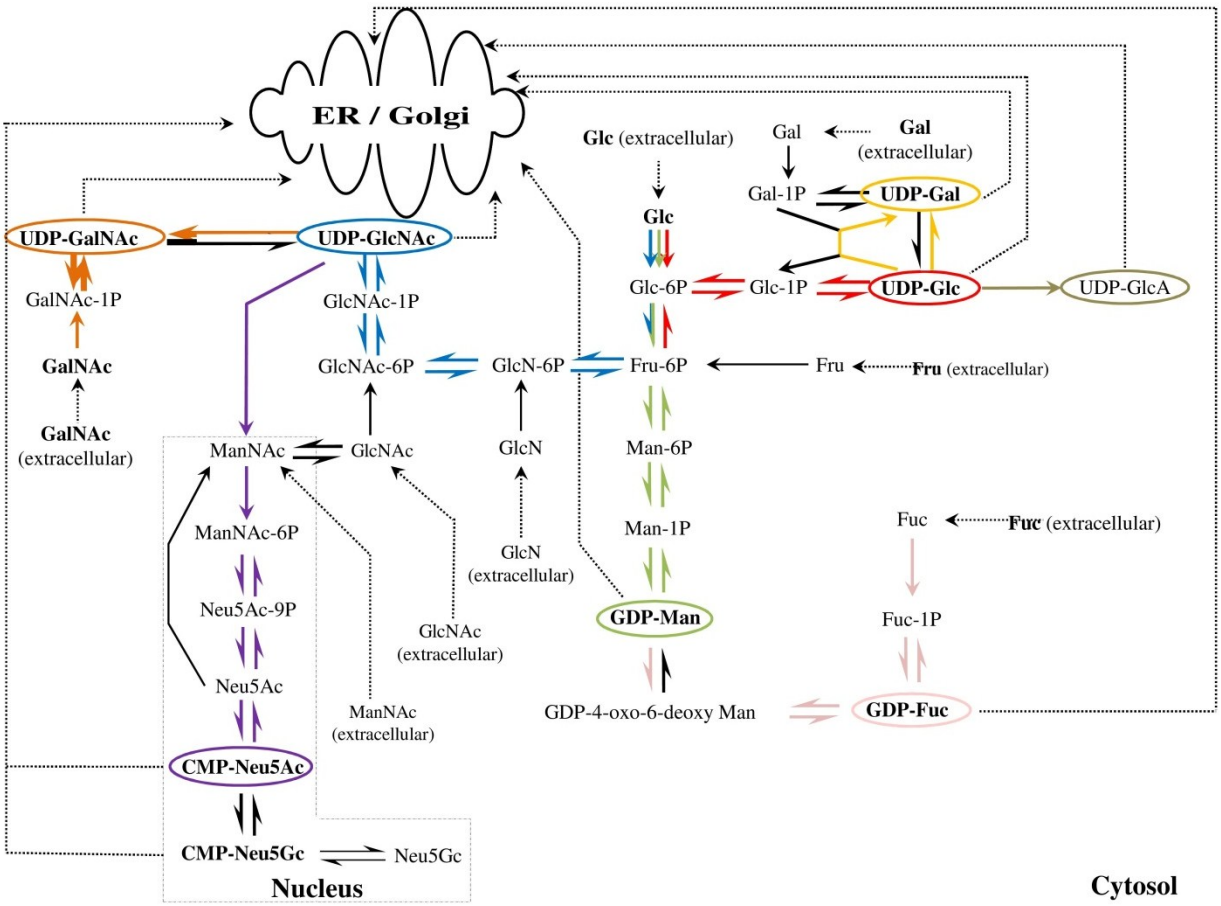

Figure 4. NSD biosynthetic pathway in mammalian cells. Raw materials that are required for NSD metabolism are sugar residues: glucose (Glc), galactose (Gal), glucosamine (GlcN), fucose (Fuc) and mannose (Man), as well as nucleotide-precursors. NSD products are transported in the ER or the Golgi for protein glycosylation. Apart from CMP-Neu5Ac which is synthesized within the nucleus, the rest of the NSD species are produced in the cytosol. Synthetic pathways for various NSDs are labelled in the following colour scheme to indicate their sources: Red: UPD-Glc; Yellow: UDP-Gal; Light green: GDP-Man; Olive green: UDP-GlcA; Pink: GDP-Fuc; Blue: UDP-GlcNAc; Brown: UDP-GalNAc; Purple: CMP-Neu5Ac. This is modified from Murrell et al. (2004).

2.3.3. N-linked glycosylation – structure and function

All N-linked glycans possess a common core structure which comprises two GlcNAc and three mannose residues (Asn-GlcNac$_2$Man$_3$), with two GlcNAc bound to the asparagine of the protein backbone in the β-1,4 conformation, followed by a β-1,4 linkage by the first mannose and two extra mannoses additions each via α-1,3 and α-1,6 linkages which form two arms to initial glycan bi-antennary structure (Figure 5 A). Depending on the availability of glycosyltransferases and NSDs, other residues are added onto the oligosaccharide during glycan processing in the Golgi apparatus. High-mannose structures are produced when solely mannose residues are added to both arms (Figure 5 B). Complex glycan pattern may have two or more antennae with various other sugar types

extending from the core-structure, or fucose residues directly attached to the protein backbone-bound GlcNAc (Figure 5 C). Hybrid structure, on the other hand, represents a partially under-processed glycan structure, with predominantly mannose residues on one single branch (Figure 5 D). In general, Chinese hamster ovary (CHO) cells are the most industrially used host cells. The commercially CHO-derived IgGs are nearly 90 % core-fucosylated; they are sometimes sialylated (~ 10%) and are usually bi-antennary. However, CHO cells do not naturally possess bisecting-GlcNAc (Kobata 2000; Liu et al. 2011). Figure 6 illustrates some common types of Fc-glycosylation patterns that are observed in IgG generated from CHO cells.

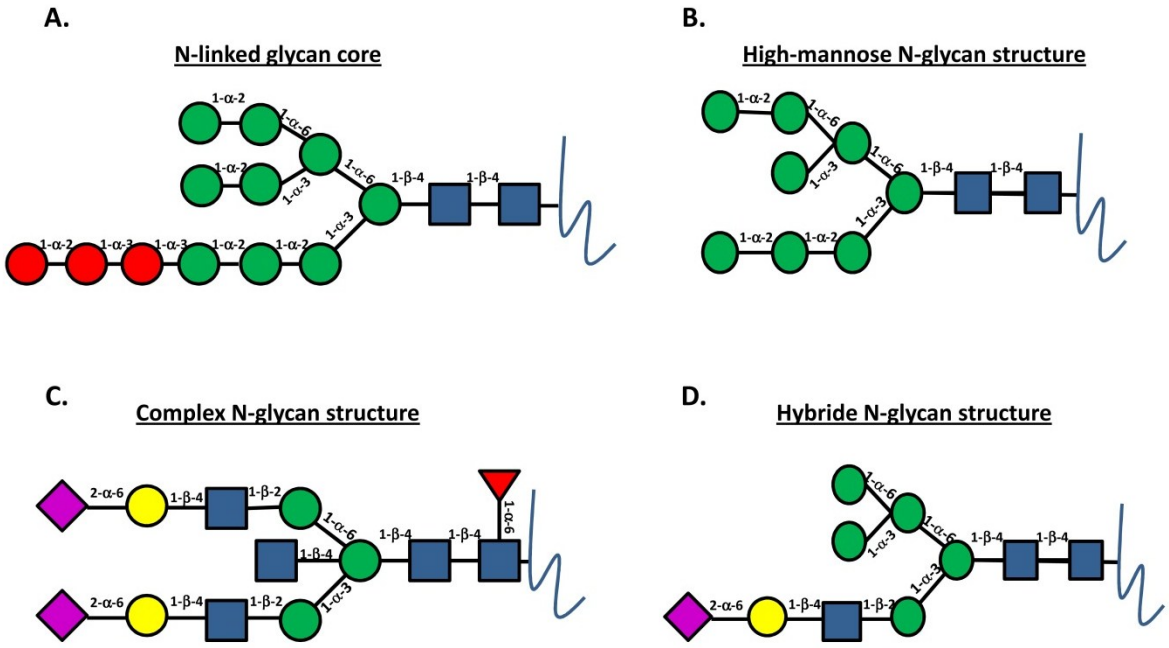

Figure 5. Three main types of N-linked glycan structure. A. The conserved core structure of N-linked glycans. B. High-mannose N-glycan structure, with mannose residues (Man5 – Man9 in mammalian cells) added to the core structure. C. Complex structure of N-glycosylation. Different types of sugar residues are added to the non-reducing end of the core mannoses. Bi- or multi- antennary structures can be observed, together with core fucosylation. D. Hybrid N-glycan is the combination between high-mannose and complex-glycan structure. Glc: Glucose (); GlcNAc: N-acetyl-glucosamine (); Man: mannose (); Gal: Galactose (); Fuc: fucose ( ); NeuAc: sialic acid ( ).

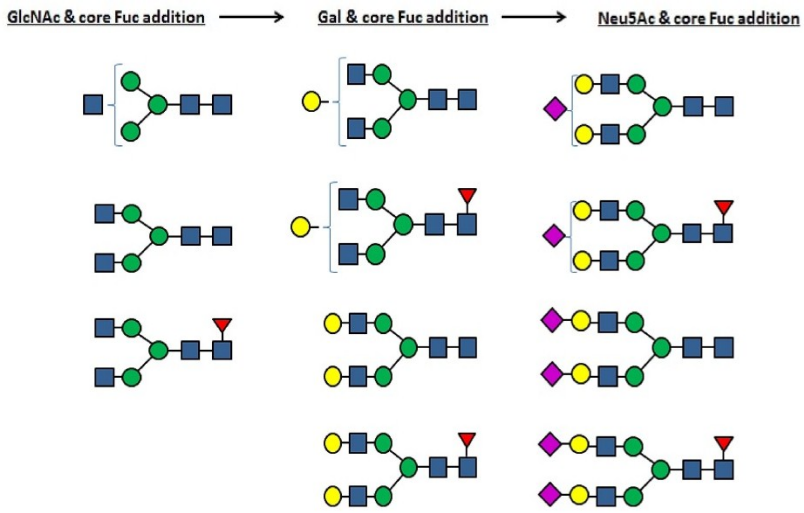

Figure 6. Common glycan structures found on Fc-region of IgG expressed in CHO cells. Fc-glycan of IgG produced by CHO cells are usually b-antennary, ranges from single non-reducing GlcNAc addition to the N-glycan core, to galactose and sialic acid residues on either/both arms. Core fucosylation can be observed in any stage of Fc-glycan processing. GlcNAc: N-acetyl-glucosamine (▬); Man: mannose (●); Gal: Galactose (○); Fuc: fucose (▼); NeuAc: sialic acid (◆).

Regardless of the type of glycoprotein, sugars that are attached contribute to protein folding, stability, trafficking, biological activities and serum clearance. Firstly, glycan addition aids protein folding, where terminal glucose molecules assist glycoprotein folding via the calnexin-calreticulum cycle in the ER (Taylor and Drickamer 2003). In addition, other study demonstrated that a single attachment of high-mannose sugar chain onto the asparagine24 of Ribonuclease B (RNaseB) increased ribonuclease stability, through reduced chemical exchanges between its protein amide hydrogen protons which encouraged a more thermodynamically stable structure (Joao et al. 1992). Moreover, protein clearance rate is directly related to the stability of the molecules. Furthermore, intracellular signaling through adenylate cyclase activation, is only possible when pituitary hormones are glycosylated (Taylor and Drickamer 2003).

In terms of mAb functionality, binding of the Fc-domains to different types of Fcγ receptors activate downstream immune effectors through cascade reactions. Oligosaccharides attached on the C_H2 domains of both heavy chains can alter the protein structure of the binding site, and the sugars themselves may sometimes be involved in receptor-binding. Depending on the type of sugar pattern on a mAb molecule, its immune activity varies. For example, Shinkawa et al. (2003) discovered that the absence of core fucosylation could lead to an increase in ADCC activity of approximately 50-fold. With the help of the IgG-FcγRIIIa crystal structure, studies in 2011 revealed that the high affinity

achieved in non-fucosylated mAb species, was mediated by the proximal carbohydrate-carbohydrate interaction between the mAb molecule and the FcγRIIIa receptor (Figure 7 A), where the presence of a core-fucose was demonstrated to extend the substrate-receptor distance (Figure 7 B) (Ferrara et al. 2011). In addition, Zou et al. (2011) argued that bisecting GlcNAc also contribute to enhanced ADCC activity since an increase in IgG-Fc-FcγRIIIa binding was observed independently of core fucosylation.

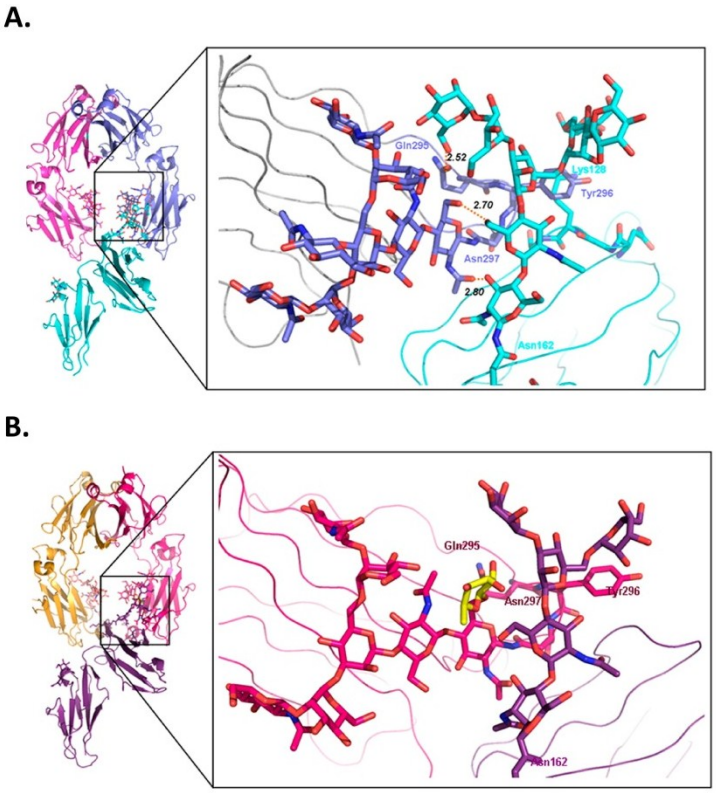

Figure 7. Interaction interphases between A. non-fucosylated Fc-fragment (blue), or B. fucosylated Fc-domain (magenta), and the glycosylated Fc-receptor (cyan in (A) and dark violet in (B). The core fucose in the fucosylated species is highlighted in yellow. Distances of hydrogen bonds between the receptor and the Fc-fragments are shown. This is taken from Ferrara et al. (2011).

On the other hand, Hodoniczky et al. (2005) demonstrated that terminal galactosylation in the Fc-region of a mAb molecule increased CDC activity. This was explained by the higher affinity of the mAb Fc-fragment to the C1q complement molecule, which was observed upon the stable interaction between terminal galactose and Fc-amino acids, initiated through a Fc-conformational change (Figure 8). Moreover, galactosylated IgG_1 molecules increase CDC receptor binding by enhancing structural rigidity via the interaction between terminal galactose molecules and lysine246 of the IgG (Houde et al. 2010; Raju 2008).

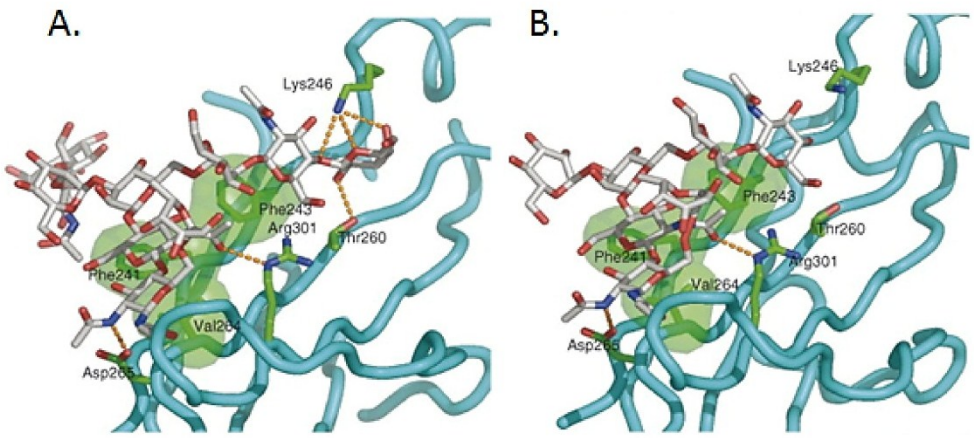

Figure 8. Hydropholic and hydrophilic interactions between Fc-glycan and Fc-amino-acid residues in the crystal structures of G2 and G0 mAb species. A. Crystal structure of mAb Fc-G2. A total of six hydrogen-bonds were observed between G2-sugar residues and Fc-backbone. B. Only 2 H-bonds were found between Fc-G0 sugars and its amino acids. G2-terminating oligosaccharides give mAb a stable Fc structure for CDC activation. These are taken from Raju (2008). "Permission is granted by the right holder Elsevier to reproduced this image for this thesis"

While mAb galactosylation improves CDC activity, terminal sialic acid residues on the oligosaccharide chain increase mAb serum half-life (Hossler et al. 2009). Moreover, sialic acids also serve as immune modulators by exerting an anti-inflammatory response upon the interaction between the α-2,6 attached Neu5Ac molecules on the intravenous immunoglobulin (IVIG) and the FcγRIIB inhibitory receptor (Kaneko et al. 2006). In contrast, high mannose structure on the Fc domain of an IgG molecule increases serum clearance in human (Goetze et al. 2011), which can potentially reduce the effective period of the drug within a human body.

Changes in mAb Fc-sialylation, galactosylation and fucosylation are often key biomarkers in many autoimmune and inflammatory diseases. For example, IgG molecules found in patients with rheumatoid arthritis are N-linked sialyted and fucosylated, but they lack terminal galactosylation, where approximately 50% are observed to be non-galactosylated (Parekh et al. 1985). As a result it alters the conformational structure of these mAb molecules and consequently affects IgG-leukocyte interaction to initiate proper immune responses (Krapp et al. 2003). Similarly, a drop in mAb Fc-galactosylation is also observed in patients with osteoarthritis, Lambert-Eaton myasthenic syndrome and myasthenia gravis (Selman et al. 2011). These studies show the importance of IgG Fc-galactosylation in immunology.

2.4. The impact of bioprocess condition on mAb synthesis and glycosylation

The previous section illustrates the importance of mAb glycosylation in activating immune responses in medical treatments. However, it is difficult to control and produce mAb molecules with one specific glycoform. Protein glycosylation within the ER and the Golgi apparatus relies on several factors including the abundance of different NSD species and the availability and catalytic efficiency of glycosyltransferases. These factors are very prone to vary with changes in the culture conditions during recombinant mAb production. As a result thorough understanding of the impact of each bioprocess condition on mAb production, including protein glycosylation, will be a good first-step to employing the Quality by Design strategy. In this part of the chapter, common bioprocess conditions or practices, such as the use of different host cell lines, the levels of culture pH, osmolarity, temperature, gaseous exchange and feeding and media supplementation will be discussed. These will be followed by a single section that will describe in detail how transient gene expression (TGE) affects product production, with respect to the method of transfection, and a combination of different cell culture process parameters that are practiced under the TGE system.

2.4.1. Host cell lines

Owing to the ability to obtain human-like post-translational modifications, mammalian cells are by far the most commonly employed cell type during recombinant mAb production. The most frequently used commercial cell lines for mAb synthesis include Chinese hamster ovary (CHO) and mouse NS0 myeloma cells. Since mammalian cells of different types originate from different species, they possess diverse levels of cellular machinery (e.g. enzyme expression) and metabolic activity, and the heterogeneity of mAb Fc-glycoforms of IgG molecules generated from different types of mammalian cell lines is therefore high. For example, despite the fact that both CHO and NS0 cells are capable of producing mAb with galactosylated bi-antennary sugar structures, CHO cells process the addition of terminal galactose residues through β-1,4-linkages, whereas NS0 cells possess the α-1,3 glycosyltransferase that CHO cells do not and form bi-galactosylation Galα-1,3Galβ-1,4GlcNAc on one antenna (Umana et al. 1999b). It was later revealed by Hills et al. (2001a) that a possible steric hindrance of β-1,4 galactosyltransferases, or lower binding affinity of this enzyme to UDP-Gal than α-1,3 galactosyltransferases, could have contributed to the different linkages. Most importantly, α-1,3 galactose linkages are immunogenic in humans (Jenkins et al. 1996). Furthermore, both α-1,3

fucosyltransferase and N-acetylglucosaminyltransferase III (GnTIII) enzymes are not present in CHO cells and peripheral fucose and bisecting GlcNAc additions are therefore not possible (Butler 2006).

In addition, humans only generate terminal N-acetylneuraminic acids (NANAs) while other species, such as rhesus monkey, goat and rat are capable of producing N-glycosylneuraminic acids (NGNAs) (Raju et al. 2000). Since NGNA-bearing glycoproteins produced in mouse NS0 cells are immunogenic in humans, CHO cells are better hosts for recombinant mAb production. However CHO cells are incapable of generating Neu5Ac addition via α-2,6 linkages which are essential for activation of anti-inflammatory response in humans (Butler 2006).

On the other hand, other organisms such as yeast *Pichia pastoris,* produce mAb molecules with multi-antennary high mannose structures on their Fc-regions, which can trigger immunogenic responses in humans (Liu et al. 2011). Insect cells are not able to process sialic acid addition owing to the absence of enzymes for CMP-Neu5Ac NSD production. They also lack GnTII glucosyltransferase and some other transport proteins that are necessary for NSD transport within the lumen of the Golgi apparatus (del Val et al. 2010); making insect cells a less favourable host for recombinant mAb production. Plants, on the other hand, have special glycosyltransferases that can generate sugar patterns such as xylose, which are immunogenic and glycoengineering is therefore necessary in order to produce human-like Fc-glycosylation (Castilho et al. 2011; Tekoah et al. 2004). Furthermore, bacterial systems lack the post-translational machinery for N-linked glycosylation; but humanized yeasts and bacteria with engineered machineries can produce proteins with human-like qualities. For instance, an enteropathogenic bacterium *Campylobacter jejuni* was discovered to possess the ability for N-linked glycosylation (Linton et al. 2002) Wacker and colleagues made use of this unique property of *C. jejuni* and reconstituted a functional N-linked glycosylation pathway into *Escherichia coli* by transferring the *pgl* gene cluster that encodes N-linked-equivalent glycosyltransferases (Wacker et al. 2002). Schwarz et al. (2010) modified this system based on the knowledge of the lipid-linked oligosaccharide (LLO) and replaced the bacterial Bacillosamine-Asn linkages with an eukaryotic GlcNAc-Asn linkages. This glycoengineering approach was later transferred to *Salmonella enterica serovar Typhimurium* (Wacker et al. 2006).

2.4.2. Feeding of nutrients, amino acids and other media supplements

Glucose (Glc) and glutamine (Gln) are the main carbon and nitrogen sources during most cell culture. Glucose is the main carbon source for most mammalian cells and it has been shown to have a

great impact on the glycan-macroheterogeneity on recombinant glycoproteins (Nyberg et al. 1999). All NSD species, including UDP-Glc, UDP-Gal and UDP-GlcNAc which play important roles in mAb glycosylation in CHO cultures, are all biosynthesized indirectly from glucose and other glycolytic intermediates. Glucose depletion therefore directly reduces the NSD pool for glycan-synthesis. Glycan microheterogeneity is also affected upon glucose and glutamine limitation. Truncated glycan structures with reduced terminal sialic acid addition and increased mannosylation were observed in medium containing less than 0.7 mM glucose and 0.1 mM glutamine in IFN-γ producing CHO cell lines (Chee Furng Wong et al. 2005). On the other hand, glucose and glutamine are required for CMP-Neu5Ac synthesis. Synthesized UDP-GlcNAc molecules are converted into ManNAc which is a substrate for CMP-Neu5Ac production. As a result, the reduced level of UDP-GlcNAc lowers the CMP-Neu5Ac availability. D-Glucosamine supplementation can directly increase the UDP-GlcNAc pool, but its negative impacts on CMP-Neu5Ac synthesis suggests the presence of product inhibition where high UDP-GlcNAc concentration limits CMP-Neu5Ac transport into the Golgi-network for glycan processing (Pels Rijcken et al. 1995) and only extracellular supplement of ManNAc can bypass the transport inhibition and increase the yield of sialic acid. The impact of glucose starvation on intracellular UDP-HexNAc concentrations was also found in the study conducted by Fan et al. (2015). Alongside, they also observed increased concentrations of UDP-Glc and UDP-Gal, accompanied by a higher occupancy of galactose in the attached glycans during glucose starvation. Moreoever, changes in cellular activities such as energy metabolism, cytoskeleton, protein expression and cell signalling were observed when cells entered a limited glucose uptake phase in perfusion cultures (Wingens et al. 2015).

Tailored feedings to improve NSD contents for protein galactosylation were attempted in 2001 by Hills et al. (2001b) by galactose supplementation in the culture medium. Despite 5-fold increase in UDP-Gal level, minimal change in β-1,4 galactosylation was observed. Ever since then, different feeding strategies were examined. In 2011, a mixture of manganese chloride, galactose and uridine has also been shown to improve mAb terminal galactosylation. Gramer et al. (2011) demonstrated through experimental studies, that 8 times the amount of 1 mM uridine, 0.002 mM manganese chloride ($MnCl_2$) and 5 mM galactose mixture improved the overall product galactosylation by 18% and 24% in two distinctive cell lines. CHO cell performance was suggested to remain unchanged at this level of uridine-$MnCl_2$-Gal supplementation, although slight cell growth impedance was observed when the mixture was 20 times higher or beyond. Despite enhancing protein galactosylation by increasing the intracellular UDP-Gal concentration, it activates intracellular sialidase activity which can lead to Fc-desialylation (Butler 2006). In addition, Grainger and James (2013) adjusted concentrations of manganese, galactose and uridine in culture media by the use of the

design of experiment sreponse surface modelling (DoE-RSM) developed by the group, and positive result in galactosylation was achieved.

Amino acids are essential for cell growth and a lot of intracellular mechanisms, such as nucleic acid production, energy generation through the TCA cycle, intracellular signalling. Amino acids are also crucial building blocks for protein translation, and the production of all host cell proteins including key enzymes, and in the case of biopharmaceutical industry, the recombinant products. In comparison to batch CHO cell culture, cells that were fed with designed feeds achieved a 50% higher product yield when 40% of nutrients were added on top of the designed feeds (Kyriakopoulos and Kontoravdi 2014b). Histidine (His), tryptophan (Trp) and asparagine (Asn) were shown in this study to be always depleted in CHO cell cultures; this suggests high demands of these amino acids for cell growth and protein synthesis.

Other chemical supplements, such as sodium butyrate, valproic acid (VPA) or dimethyl sulfoxide (DMSO) were shown to increase mAb productivity, by introducing cell cycle arrest and stabilizing the heavy and light chain mRNAs. Some studies looked into the effect of sodium butyrate addition on mAb glycosylation, they showed that 1 mM sodium-butyrate induced a two-fold increase in α-2,6 sialylation of α-2,6 sialyltransferase-engineered CHO-expressing interferon-γ (Lamotte et al. 1999). At the same time, 1 mM valproic acid was demonstrated to halt cultured cells at the G1 growth phase and attenuated sialyltransferase activity, this provided a transient suppression of α-2,3 Neu5Ac addition onto glycan chains of C6-glioma (Bacon et al. 1997). In addition, valproic acid was demonstrated to increase the expression of chaperones in the ER and the cytosol to regulate protein folding, such as chaperones binding immunoglobulin protein (BiP), protein disulfide-isomerase (PDI), calreticulin and heat-shock protein 70 (HSP-70) (Kim et al. 2005). DMSO is sometimes added during cell culture to improve cell viability and product yield. In the case of L1/Ig5-6 (cell adhesion molecule with Ig domain 5 & 6) that were expressed in the insect *Spodoptera frugiperda* cells, Gouveia et al. (2010) achieved a slight increase in high-mannose glycoforms upon DMSO addition.

2.4.3. Metabolic wastes and cell culture pH

Mammalian cells secret ammonia and lactate as metabolic by-products. Not only do the accumulation of ammonia and lactate in culture medium affect cell growth and protein yields, it is also suggested to influence product glycosylation. Firstly, ammonia and lactate directly affect cell culture pH and the pH within the Golgi apparatus. This affects activities of many relevant host cell

enzymes, including glycosyltransferases that are responsible for protein glycosylation. Rothman et al. (1989) showed that N-linked glycosylation of IgGs that were expressed in hybridoma cell line altered upon a pH shift within the Golgi apparatus. Another study also demonstrated that at pH 6.9, a very mild acidic environment contributed by lactate accumulation which is very common during fermentation, the lowest sialic acid content was found in IgG_3 that were expressed in murine cell lines (Muthing et al. 2003). One of the most noticeable changes upon increased levels of ammonia in cell culture is the reduced level of terminal sialytion. Studies showed that 15 mM of ammonia increased UDP-GlcNAc and UDP-GalNAc production, which in turn inhibited sialic acid transport through competitive inhibitions. In addition, a rise in the UDP-GalNAc level was shown to limit the availability of UDP-Gal molecules that are necessary for protein galactosylation (Butler 2006).

2.4.4. Levels of DOT, pCO_2 and medium osmolarity

Dissolved oxygen tension (DOT) is another culture parameter that affects mAb Fc-glycosylation. A non-constant DOT was shown to impede hybridoma cell growth, without significantly affecting the overall mAb production yield (Serrato et al. 2004). Results in this study showed that at low dissolved oxygen tension at 10% DOT (where normal *in vivo* DOT is 12.5 - 25.0% (Richter et al. 1972)) reduced Fc-galactosylation in hybridoma cells (Kunkel et al. 1998) and decreased sialyltransferase activity in CHO cells were observed (Chotigeat et al. 1994). The observed effects can be explained by the reduced consumption of glucose which eventually lowered the UDP-Gal concentration pool, alongside with increased production of lactate which shifted culture pH and consequently affect intracellular enzymatic activities. Serrato et al. (2004) however observed an increase in mAb Fc-sialylation from oscillating DOT, which was shown to reduce the steric hindrance of sialyltransferase and increased protein sialylation.

On the other hand, not only does high medium osmolarity impede cell viability, changes in both medium osmolarity and in CO_2 partial pressure (pCO_2) altered the Fc-glycosylation pattern on mAb molecules. Schmelzer and Miller (2002) demonstrated a 20% decrease in IgG_{2a}-mannose contents, with either increase in pCO_2 (from 40 to 195 mmHg) or a rise in osmolarity (from 320 to 435 mOsm/kg). In addition to decreases in mannosylation, high medium osmolarity induced by sodium chloride (NaCl) addition was shown to reduce the Fc-galactose profile in IgG_{2a}, while surprisingly high level of pCO_2 yielded the opposite effect. Hyperosmostic stress, on the other hand, affect cell growth and mAb productivity. Shen et al. (2010) demonstrated substantial increases in the specific productivity of Fc-fusion-protein upon the induction of hyperosmostic conditions in batch

CHO cell culture, but the overall titre remained unchanged due to the reduction in viable cell concentration (Reddy and Miller 1994; Shen et al. 2010). In 2012, with the combination of experimental and computational approaches, Ho et al. (2012b) showed a positive correlation between hyperosmotic conditions and mAb production in GS-NS0 cells, where she showed 100% increase in the specific IgG mRNA transcription rates were accompanied by the improvement observed in the specific product productivity (q_P). Interestingly, reduction in medium osmolarity from 300 mOsm kg^{-1} to 150 mOsm kg^{-1} was also shown to enhance q_{mAb} by 128% in CHO cultures, by increasing the total cytoplasmic pool of IgG mRNAs by 1.4-fold (Lee and Lee 2001).

2.4.5. Mild hypothermic cell culture temperature

Mild hypothermia during cell culture (e.g. temperature shift from 36.5°C to 32°C) is commonly employed to increase the specific recombinant product productivity (Kantardjieff et al. 2010; Yee et al. 2009). Cells are normally cultured at physiological temperature during the start of the fermentation until desired viable cell density is obtained; the temperature is then lowered to mild hypothermic levels (ranges from 28°C to 34°C), where the rates of cell growth are compensated by the increases in q_P. The magnitude of the increase in q_P varies among experiments, where the fold-change of productivity fluctuates from 0- to 14-fold (Becerra et al. 2012) and such impact is likely to be highly cell line and product dependent. A study from Becerra et al. (2011) attempted to investigate the reason for non-improved q_P during mild hypothermic conditions, and concluded that increase in q_P was not promoted when high growth rate of host cells was achieved.

Despite the usefulness of mild hypothermic temperatures in recombinant protein production, there is no single theory that solely explains how this effect arises. The first theory behind this impact is related to cell growth, where cells experience a partial cell cycle arrest at the G_1/G_0 phase upon the introduction of mild hypothermia (Sunley et al. 2008), alongside with increase in product productivity. By maintaining high cell viability, lowering culture temperature provides a prolonged cell growth period and a higher integral viable cell density is achieved. At the same time, some studies also showed that cell apoptosis was delayed in mild hypothermic cultures (Moore et al. 1995; Moore et al. 1997). A substantial number of studies were carried out and results showed that the defence mechanism of cells against programmed cell death was stronger, where the expression of bcl-2, an anti-apoptotic protein increased at 30°C (Slikker et al. 2001). In addition to prolonged cell viability, other cell mechanisms, such as cytoskeleton reorganization, were suggested to change at reduced culture temperatures. Transcriptomic studies showed that at 32°C, cytoskeleton-related filament genes

including *Ckap4*, *Arpc5*, *Mid1ip1* and *Vim* were overexpressed to assist vesicle transport, the process of endocytosis and subsequently protein secretion (Yee et al. 2009). In addition, mild hypothermic conditions were shown to have affected protein synthesis from transcription level, where the mRNA decay rates of recombinant species were lower at reduced temperatures (Fox et al. 2005). Other studies also observed an increase in the recombinant EPO protein yield in response to the higher EPO mRNA level (Yoon et al. 2003). This observation was not limited to just gene transcription, proteomic studies revealed that expression of proteins responsible for cell growth regulation, anti-apoptosis, cytoskeleton organisation, protein chaperones, as well as CAP-independent translational machinery, were up-regulated to improve protein translation (Baik et al. 2006; Kumar et al. 2008). As a result, effects of mild hypothermic conditions are rather extensive, and it is not just limited to improving q_P.

Although the effect of mild hypothermia on mAb Fc-glycosylation is still under investigation, studies suggested that its impact on product quality is indeed cell line and product dependent. While some studies observed no significant difference in product glycosylation between physiological and mild hypothermic conditions (Bollati-Fogolin et al. 2005; Yoon et al. 2003), other studies showed that EPO glycoproteins expressed at mild hypothermic temperature (32^{o}C) in CHO cells were less branched and had lower sialic acid contents (Ahn et al. 2008). Moreover, Nam et al. (2008) observed an increase in sialic acid and decrease in fucosylation in CHO cell expressing secreted human placental alkaline phosphatase (SEAP). It is highly possible that gene expression of glycosyltransferases or NSD biosynthetic enzymes are affected at lower temperature, possibly by retaining cells within the G_0/G_1 phase of cell cycle (Marchant et al. 2008).

2.4.6. Cell line engineering

In addition to monitoring and adjusting process parameters, engineered recombinant protein glycosylation through overexpression or silencing of target genes, for instance genes for different glycosyltransferases, is a very popular approach to achieve desired glycoforms on noval mAb and biosimilars. Such attempts aimed to produce mAbs with specific biological functions or to avoid the expression of mAbs with glycan structures that are potentially immunogenic to humans. In addition to the availability of NSD species, expression level and activity of glycosyltransferases control the processing of oligosaccharides attached on recombinant products. Table 2 shows a list of glycosidases and glycosyltransferases that are active in mAb Fc-glycosylation. The most targeted enzymes in Table 2 that are involved in glyco-engineering are N-acetylglucosaminyltransferase (GnT), galactosyltransferase (GalT), fucosyltransferase (FucT) and sialyltransferase (SiaT), since additions of

branched GlcNAc, terminal Gal, core Fuc and terminal Neu5Ac residues are the most influential components in determining the efficacy of a drug. In 1999, the first attempt to overexpress N-acetylglucosylaminlytransferases III and V (GnT III & V) in a tetracycline-regulated manner was carried out, with an aim to introduce bisecting GlcNAc and multi-antennary structures to products produced in CHO-DUKX cells. Despite the huge success in generating the desired glycoforms, the overexpression of GnT III & V enzymes greatly impeded cell growth (Umana et al. 1999a). In the same year, Weikert et al. (1999) suggested the possibility of genetically-engineering CHO cells to obtain glycoforms with terminal galactose or sialic acid residues, which encouraged CDC activity and modulated inflammation. The group showed that by overexpressing human β-1,4 galactosyltransferase (GalT) or α-2,3 sialyltransferase (SiaT) gene in CHO cells, the level of terminal galactosylation was increased and more than 90% of IgG Fc-regions were sialylated (Weikert et al. 1999). In addition, siRNA expression against α-1,6 fucosyltransferase (FUT8) gene reduced the expression of the target FucT and produced mAb molecules with approximately 60% reduction in Fc-fucosylation. This increased ADCC activity by 100-fold (Mori et al. 2004). Genetic engineering is therefore proven to have high potential in adapting the QbD principle, but process optimisation is indeed necessary to minimise possible side-effects that could be generated from engineered cell lines.

In 2011, the assembled genomic data of CHO-K1 cells was for the first time available to the public and this marked a big break-through in the field of recombinant protein production in mammalian cells. Within the 2.45 Gb of the genomic sequence analysed, 24,383 genes, including genes that are involved in glycosylation, viral susceptibility etc. are predicted (Xu et al. 2011). Ever since then a lot of studies were conducted to improve the data set of the CHO transciptome (Rupp et al. 2014). Moreover, many new experimental ideas and concepts emerged from this discovery; one of these emerging fields is microRNA. MicroRNAs (miRNAs) are short non-coding RNAs that play a role in regulating mammalian gene expression (Bartel 2004) and their potential in regulating cellular networks and processes is high. Advances in miRNA technology and the CHO genome analysis enable us to investigate the functionality of miRNAs in CHO cells. The application of miRNAs in mAb bioprocessing aims to improve mAb production in terms of its quality and quantity becomes possible.

Studies from both Lin et al. (2011) and Maccani et al. (2014) profiled miRNA expression between non-producing and rProtein-producing cell lines, and among expressing cell lines. Results from their studies showed that significant differences in miRNA expression were predominately between producers and non-producers. miRNA genes such as miR-21-5p and miR-10b-5p, which are responsible for controlling cell proliferation, cell death and migration are expressed differently in

recombinant protein producing cells (Krichevsky and Gabriely 2009; Lin et al. 2012). In 2014, Jadhav et al. (2014a) generated stable CHO cell lines with over-expressions of miR-17 or miR-17-inclusive clusters, and they managed to achieve an improvement in cell growth rates and rProtein productivity from these engineered cell lines. These studies highlighted the huge potential of miRNA in the field of bioprocessing, as well as the possibility of manipulating key process enzymes through miRNA control.

Table 2. List of enzymes that are commonly employed during N-linked Fc-glycosylation in *homo sapiens*.

Enzyme	EC number	Substrate	Location
oligosaccharyl-transferase	EC 2.1.1.119	dolichol phosphate-$GlcNAc_2Man_9Glc_3$	Endoplasmic reticulum
mannosyl-oligosaccharide glucosidase	EC:3.2.1.106	Asn-$GlcNAc_2Man_9Glc_3$	Endoplasmic reticulum
α-1,3-glucosidase I	EC:3.2.1.84	Asn-$GlcNAc_2Man_9Glc_2$	Endoplasmic reticulum
α-1,3-glucosidase II	EC:3.2.1.84	Asn-$GlcNAc_2Man_9Glc$	Endoplasmic reticulum
Endoplasmic reticulum mannosyl-oligosaccharide 1,2-α-mannosidase I	EC:3.2.1.113	Asn-$GlcNAc_2Man_9$ Asn-$GlcNAc_2Man_{(8\text{-}6)}$ (at high enzyme concentration)	Endoplasmic reticulum
mannosyl-oligosaccharide α-1,2-mannosidase	EC:3.2.1.113	Asn-$GlcNAc_2Man_{(9\text{-}6)}$	*cis*-Golgi apparatus
α-mannosidase II	EC:3.2.1.114	Asn-$GlcNAc_2Man_5GlcNAc$	medial Golgi apparatus
α-1,3-mannosyl-glycoprotein β-1,2-N-acetylglucosaminyltransferase I	EC:2.4.1.101	Asn-$GlcNAc_2Man_5$	medial Golgi apparatus
α-1,6-mannosyl-glycoprotein β-1,2-N-acetylglucosaminyltransferase II	EC:2.4.1.143	Asn-$GlcNAc_2Man_3GlcNAc$	medial Golgi apparatus
core α-1,6-fucosyltransferase	EC:2.4.1.68	Asn-$GlcNAc_2Man_3GlcNAc_2$	medial Golgi apparatus
β-1,4-galactosyltransferase	EC:2.4.1.22/90/38	Asn-$GlcNAc_2Man_3GlcNAc_2$	*trans*-Golgi apparatus
		Asn-$GlcNAc_2FucMan_3GlcNAc_2$	
		Asn-$GlcNAc_2Man_3GlcNAc_2Gal$	
		Asn-$GlcNAc_2FucMan_3GlcNAc_2Gal$	
β-galactoside α-2,6-sialyltransferase	EC:2.4.99.1	Asn-$GlcNAc_2Man_3GlcNAc_2Gal_2$	*trans*-Golgi apparatus
		Asn-$GlcNAc_2FucMan_3GlcNAc_2Gal_2$	
		Asn-$GlcNAc_2Man_3GlcNAc_2Gal_2NeuAc$	
		Asn-$GlcNAc_2FucMan_3GlcNAc_2Gal_2NeuAc$	

2.5. Transient gene expression in recombinant protein production

Transient gene expression (TGE) is becoming industrially relevant and a more popular method for recombinant protein expression mostly due to its capability of fast rProduct production, in comparison to the traditional stable transfection methods. CHO and human kidney HEK-293 cell lines are typical mammalian hosts for the transient system. However the main obstacle of this approach, for CHO cells in particular, is the relatively low protein yield that one can achieve. As a result, a lot of studies focus on ways to improve mAb productivity through TGE optimization, which includes improving transfection efficiency, determining the best transfection method/reagent for each cell type, as well as exploring impacts of culture parameters (temperature, pH, nutrient supply etc.) on mAb production and Fc-glycosylation in the TGE system.

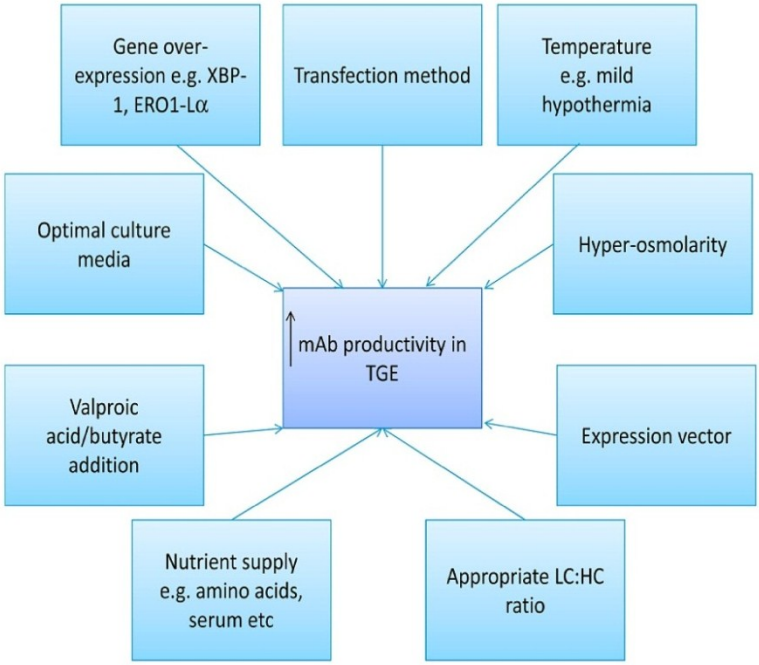

Figure 9. Factors that are known to affect mAb production yield in transient gene expression.

Owing to the huge drawback of TGE in production yield, the main goal of most studies focused on methods to increase rProtein productivity. Figure 9 shows key parameters that are considered during TGE process optimization. Results showed that the amount of mAb protein production in TGE was highly dependent on the actual transient transfection method, the expression vector in which mAb heavy and light chains were expressed, together with other culture parameters such as culture temperature, osmolarity and supplement addition.

2.5.1. Transient gene transfection methodology

Target genetic material can be taken up by host cells in two main ways: delivery through chemical or physical approaches. There are several chemical transfection reagents, e.g. polyethylenimine (PEI), lipofectamine™ 2000, *Trans*IT-PRO™ and calcium phosphate. Of these, Sou et al. (2013) evaluated the first three chemical transfection reagents mentioned above and demonstrated *Trans*IT-PRO™ to be the more efficient reagent, but it was not the most-cost-effective option. As a result, polyethylenimine still remains the preferred option; it provides efficient transfection (40 - 90%) in most cell lines and it is cost-effective (Ehrhardt et al. 2006; Morrow 2008).

PEI works by forming polyplexes with target DNA which give it an overall positive charge, interact with the negatively charged host cell membrane and foreign DNA is eventually taken up into the cell (Figure 10 D). With the use of 1:4 DNA to linear 25 kDa PEI ratio during transfection of CHO-DG44 cells, Rajendra et al. (2011a) achieved a mAb yield of 250 mg/L in 0.5 L batch cultures over 14 days. Other studies demonstrated a 3-fold increase in mAb titre in cultured CHO-T cells with a DNA:PEI ratio of 1:4, when compared to cation-lipid transfection reagent Freestyle™ MAX (Codamo et al. 2011a). The high transfectability of PEI-mediated transient transfection in HEK293 cells was so shown to achieve IgG protein titres of up to 1 g/L (Backliwal et al. 2008b). Owing to the relatively lower cost of PEI and its possibility for large-scale protein expression, PEI has become a standard chemical transfection reagent used in TGE in industry.

Lipofectamine™ 2000, on the other hand, is a cation-lipid formulation transfection reagent that forms liposomes in aqueous media. These liposomes trap DNA within them, form complexes that fuse with the host cell plasma membrane for DNA entry into the cytoplasm (Figure 10 C). With the use of Lipofectamine™ 2000, *Epi*-CHO expression plasmid and the introduction of mild hypothermic condition, Codamo et al. (2011b) obtained a mAb titre of 140 mg/L. Despite the high mAb productivity achieved in this study, transfection efficiency from using Lipofectamine™ 2000 was not sustained in prolonged high cell density cultures, and the high reagent cost makes Lipofectamine™ not economically viable for large-scale operation.

*Trans*IT-PRO™ employs both mechanisms of action and works by forming lipopolyplexes with DNA, which then form electrostatic interactions with the negatively charged cell membrane. These lipopolyplexes are thought to be taken into the cell via endocytosis. The use of this reagent

involves an optional proprietary transfection booster PROBoost which was shown to enhance gene expression in a medium-dependent manner.

Electroporation, on the other hand, is a non-chemical/physical transfection method which utilizes external electrical field pulses to permeabilize host cell membrane and allow DNA plasmid of interest to enter into the cell (Figure 10 B). Electroporation is suggested to be an efficient method for TGE in both human embryonic kidney HEK293 and CHO cells. The advantage of electroporation over chemical transfection reagents is the high transfection efficiency and the low cytotoxicity. Maurisse et al. (2010) achieved a transient gene transfection efficiency of 93% with GFP-plasmid in HEK293 cells, while 100% transfection efficiency and a 1.5-fold increase in mAb productivity were achieved in IgG heavy and light chain DNA plasmids transfected CHO-S cells through repeated cycle of transient transfections (Pichler et al. 2011). Moreover, with a combination of an optimized electroporation transfection method and commercial feedings, Cain et al. (2013) generated a mAb volumetric yield of 200-600 mg/L in an engineered CHOS-XE cell line.

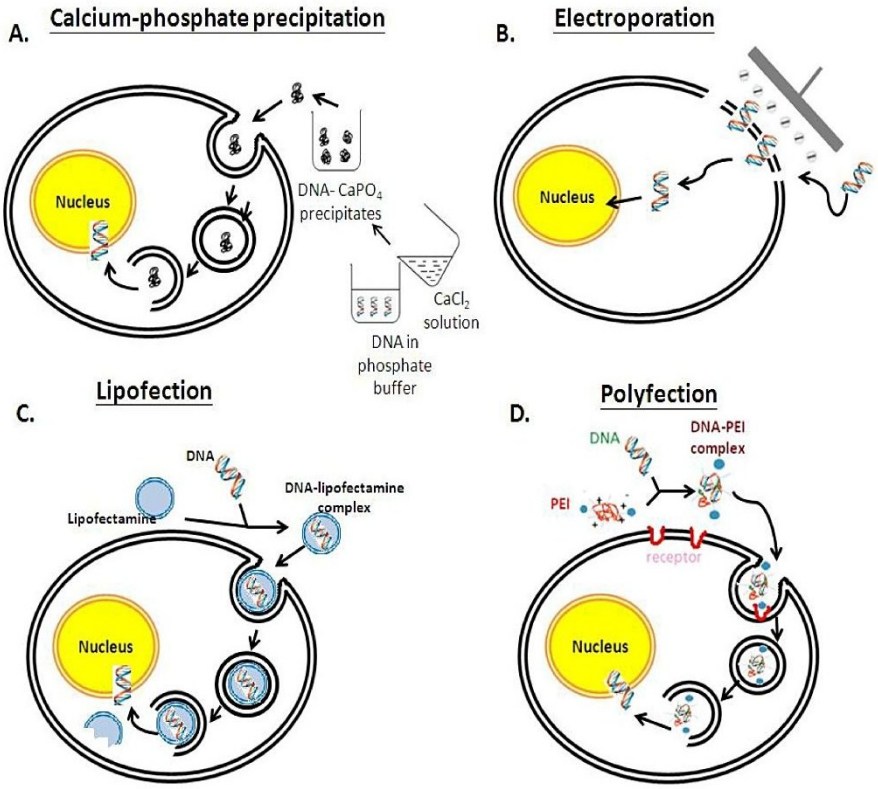

Figure 10. Different methods of DNA delivery in TGE. A. Calcium-phosphate precipitation. DNA is co-precipitated with $CaPO_4$, complex is phagocytosed by and released into the host cell. B. Electroporation. Application of external pulses induces potential difference on the cell membrane, this creates tiny pores on membrane for the entry of target DNA into the cell. C. Lipofection. Lipofectamine™ forms complex with target DNA, the complex is endocytosed in to the cell, endosome lyses and DNA material is released. D. Polyfection. PEI is mixed with target DNA and PEI-DNA complex enters into the cell via ligand-mediated endocytosis. Endosomal-release of DNA happens inside the cell.

2.5.2. HC:LC ratio and expression vector

Co-transfection of heavy (HC) and light (LC) chains in two separate expression vectors into mammalian hosts, or the incorporation of both HC and LC into a single vector under the control of multiple promoters, are common plasmids used in TGE (Bebbington et al. 1992; Brezinsky et al. 2003). However, the lack of control over the expression levels of each gene in these circumstances results in non-expressing clonal production and a huge variation in HC:LC ratio among clones. mAb HC:LC ratio maintenance is clearly a factor that affects the final product concentration and therefore optimum ratio is necessary. Studies from Ho et al. (2012a) suggested the optimal HC:LC ratio in mAb expression and protein aggregation prevention in CHO-K1 cells to be 1:4, while 1:3 was recommended in CHO-S cells (Cain et al. 2013). To improve the transfection efficiency of multiple genes, a method with internal ribosomal entry site (IRES) element was introduced. IRES is a nucleotide sequence that enables a 5' cap-independent translation initiation to initiate mRNA translation without the need of passing through the start codon. By positioning the IRES element 5' of the target gene, it initiates the process of translation by attracting the eukaryotic ribosome to the mRNA molecule. Figure 11 A illustrates ways in such two IRES elements are incorporated, with one being placed before the HC/LC first gene and the other before the selection marker gene. Such gene/IRES arrangement forms a tricistronic expression vector which enhanced mAb expression by 10-fold (Ho et al. 2012a). Results from this study also showed that by placing the LC gene as the first gene of interest, it generated a further 2-fold increase in protein yield than that with HC being placed first. In this case, the use of multiple IRES elements exerted a tight control over the HC:LC ratio among clones, this increased the production of fully assembled mAb, and dramatically reduced the number of non-expressing clones.

The *Epi*-CHO expression system is another approach to maximize mAb production. *Epi*-CHO expression comprises one DNA vector with a Polymavirus origin (PyOri) and an Epstein Barr-Virus nuclear antigen-1 (EBNA-1), which is transfected into CHO cells (Figure 11 B) (Codamo et al. 2011b). Not only does this system maintain consistent HC:LC ratio, the combined use of the *Epi*-CHO system and optimized bioprocesses generated a 4-fold increase in mAb concentration per μg of DNA transfected, in contrast to the non-*Epi*-CHO system (Codamo et al. 2011a), and yielded a mAb titre of around 140 mg/L. PyOri and EBNA-1 encourage episomal replication of DNA in suspension cultures and segregation of DNA into daughter cells, respectively, via better plasmid-nuclear matrix contacts and thus increases the levels of mAb expression and product titre (Kunaparaju et al. 2005).

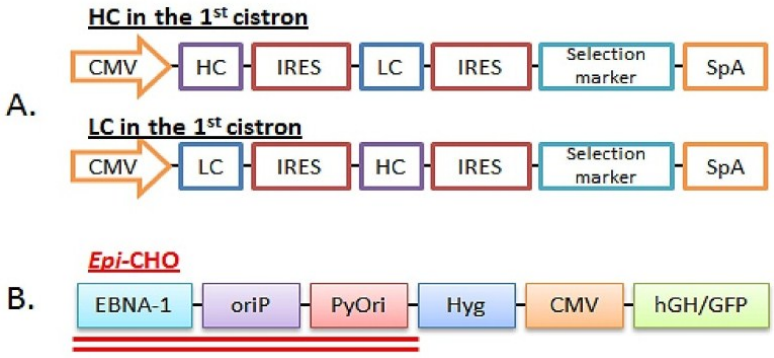

Figure 11. Expression vectors employed in mAb expression in TGE. A. Expression vectors with the use of two internal ribosomal entry site (IRES) elements, which are responsible for the transcription of genes in the 2nd cistron and the selection marker gene. The 1st cistron is controlled by the CMV and it can either be HC or the LC gene. B. The *Epi*-CHO expression vector design comprises of Epstein Barr-Virus nuclear antigen-1 (EBNA-1) and the Polymavirus (Py) origin (PyOri) elements. CMV: Cytomegalovirus; HC: heavy chain; LC: light chain; SpA: simian virus 40 early polyadenylation signal.

By engineering a CHO cell line that co-expresses both the EBNA-1 and an EBV origin of replication (OriP), and a recombinant GS gene expression system that is now widely employed in CHO cells to improve rProtein yields (Courtete et al. 2012). Daramola et al. (2014) managed to achieve a high-yielding TGE system that constantly expresses around 150 mg/L of IgG product, under a non-optimised TGE transfection method. This simple change in expression vector is shown to be a very successfully, rapid and scalable TGE system.With improvements in both DNA transfection and culture process, including optimising the PEI:DNA ratio and reducing culture temperatures to 34°C, the group achieved a 300-fold increases in product expression and generated nearly 2 g/L of secreted IgG in a 6 L Wave-bioreactor.

2.5.3. Post-translational regulatory element

In addition to the impact of expression vectors on TGE-rProtein production, vector optimization with the use of post-translational regulatory elements (PTREs) is another approach that can employed to enhance recombinant expression. In brief, the expression of rProtein per copy of target is often determined by rates of mRNA synthesis and degradation, translation and post-translational modification (Kaufman 2000). PTREs such as native introns and the incorporation of woodchunk hepatitis virus regulatory elements (WPRE) were reported to enhance product expression in TGE. For example, by improving mRNA stability and secretion, a full length mammalian cyotomaegalovirus (CMV) with intron A provided a very high level of both transient mRNA and protein expression in CHO-K1 (Xia et al. 2006). Moreover, WPRE within the expression vector alone

increased the efficiency of mRNA transport, RNA processing and translation (Wulhfard et al. 2008). This system obtained a 10-fold increase in transient IgG protein titres under mild hypothermic conditions (Zhu 2012).

2.5.4. Transfection cell density

CHO cell density upon transient gene transfection is another culture parameter that can be considered when optimizing the TGE system for mAb production. Studies conducted by Backliwal et al. (2008b) showed that a high cell density of HEK 293 cells of around 2 x 10^7 cells/ml, increased transient gene expression regardless of medium type. Rajendra et al. (2011b) specifically examined the effect of transfection cell density on TGE and the group demonstrated the highest volumetric mAb production with an IgG titre of almost 190 mg/L, was achieved at a CHO cell density of 4 x 10^6 cells/ml. However, the effect of host cell density on mAb production is rather heterogeneous, it is highly cell-line, product and bioprocess dependent, and hence process optimization is necessary.

2.5.5. Hyperosmolarity in TGE

Similar to its impact of rProtein expression on stable transfectants, hyperosmolarity is suggested to be a cost-effective way to improve production yields in TGE. Studies in hybridoma cell culture showed a positive correlation between mAb titres and culture osmolarity in TGE (Lin et al. 1999). These effects were translated into CHO-DG44 rProtein expression where a 4-fold increase in mAb titre was achieved upon a single rise in hyperosmotic pressure from 320 mOsm/kg to 490 mOsm/kg with an addition of 90 mM NaCl in BioWhittaker™ proCHO5 medium (Zhang et al. 2010b). Increasing medium osmolarity delayed cell growth, increased cell viability, induced partial cell cycle arrest and increased HC and LC mRNA stabilities (Zhang et al. 2010b). However as suggested earlier in this chapter, the counter-effects of hyperosmolarity on host cell growth were shown to limit further mAb production and process optimization was required. Ryu et al. (2000) demonstrated a positive impact of glycine betaine, an osmo-protective agent, on mAb production, in which the addition of glycine betaine in hyperosmolar medium improved cell growth by an extra 50% - 75% and protein productivity by 40%. Previous studies examined the mechanism of glycine betaine in hyperosmotic conditions and it was suggested that this chemical agent might function through thermodynamic stabilization of macromolecules that are essential in cell growth and cell proliferation (Oyaas et al. 1995).

2.5.6. Mild hypothermia in TGE

The effect of mild hypothermic culture temperature in TGE systems appears to be more potent than that in the stable gene expression (SGE) system. A TGE study by Galbraith et al. (2006) generated a 3-fold increase in the accumulated mAb titres when CHO-K1SV cells were maintained at 32°C post transfection. Two years after this study, Wulhfard and colleagues brought Galbraith's experiments further and showed that a temperature shift 4 h after transfection provided the best mAb yield, with approximately 10-fold increase in titre at 31°C; although the effect of mild hypothermia was shown to be expression vector dependent (Wulhfard et al. 2008). In addition, this group also observed an increase in the integral cell viability, but reduction in both nutrient consumption and metabolic waste production upon mild hypothermia, which was coupled with increased mAb heavy and light chain mRNA transcription. Marchant et al. (2008) looked into the mechanism of increased cell viability at mild hypothermic temperature in TGE and revealed that cells entered prolonged G_0/G_1 at 32°C (Table 3). The induced partial cell cycle arrest enables higher viable cell density with a prolonged survival period. The mild cold-stress helped stabilize and increase the HC and LC mRNA contents and improved mRNA translation and mAb folding with an up-regulation in chaperone expression (Cain et al. 2013). Furthermore, genetic changes have been monitored during temperature shift where a non-coding RNA molecule micro-RNA mir-7 expression was massively down-regulated at 32°C and SEAP productivity was raised compared to CHO-K1 cells cultured at 37°C. This was the first attempt to link culture condition, genetic variation and recombinant protein productivity (Barron et al. 2011).

Table 3. Cell cycle distribution of GS-CHO cells expressing IgG_4 at 37°C and 32°C (Table adapted from (Marchant et al. 2008)). Five different time-points were analysed. Black shade: Go/G1-phase; black and white squares: G2-phase; white shade: S-phase of cell cycle. "Permission is granted by the right holder Springer to reproduced this image for this thesis"

GS-CHO	Time (hours)				
Temperature (°C)	72	96	120	144	216
37					
32					

2.5.7. Chemical supplementation in TGE

Studies demonstrated that the supplementation of 1.25% DMSO during cell culture in TGE has significantly improved mAb expression by almost 100%, in which DMSO was suggested to help maintaining DNA stability post-transfection. A similar effect was observed when 3 mM of lithium acetate (LiAc) was introduced during cell culture (Ye et al. 2009). The addition of both chemicals mentioned was performed 72 h post-transfection and feedings occurred every 2 to 4 days, in combination with glucose, amino acids and vitamin supplements. Alternatively, addition of 2.5 mM valproic acid (VPA) or 2 mM sodium butyrate boosted mAb production in CHO-DG44 cells by 3.5- to 4-fold during transient expression (Backliwal et al. 2008c; Wulhfard et al. 2010). VPA and sodium-butyrate are histone-deacetylation inhibitors and the process of histone acetylation directly influences gene transcription rate. In these studies, VPA or sodium-butyrate addition increased the RNA polymerase accessibility to histone, thus enhanced gene transcription and possibly assisted mRNA stabilization (Wulhfard et al. 2010). Similar to valproate, lithium and butyrate also induce the expression of chaperones which assist protein folding during mAb production.

2.5.8. Overexpression of accessory genes

The overexpression of other genes or accessary proteins such as X-box protein-1 unspliced or XBP-1 spliced isoform (XBP-1 or XBP-1S), endoplasmic reticulum oxidoreductase (ERO1-Lα) and Torsin A are also suggested to promote mAb protein expression in TGE. XBP-1 is a transcription factor that control cell differentiation and protein folding, and its spliced form XBP-1S is activated during unfolded protein response (UPR) to alleviate stress within the endoplasmic reticulum and induces biosynthesis within the ER (Lee et al. 2003). ERO1-Lα, on the other hand, catalyses the formation of disulfide bonds on protein disulfide isomerase (PDI), which plays an important role in protein folding and redox signaling (Sevier and Kaiser 2006). While Torsin A is an adenosine triphosphatase (ATPase)/heat-shock protein hsp104 that encourages protein de-aggregation. Studies showed that XBP-1 overexpression in mAb-expressing CHO-T cells under hypothermic condition increased total mAb concentration by 36% (Codamo et al. 2011a). Cain et al. (2013) later overexpressed both XBP-1S and ERO1-Lα in CHO-S cells and achieved 5.3- to 6.2-fold increases in recombinant mAb production. Despite the usefulness of overexpressed ERO1-Lα in the TGE system, no/negative effects in rProtein expression were observed in stable gene expression (SGE) systems (Mohan and Lee 2010). The different impact of ERO1-Lα overexpression observed in TGE and SGE could be due to disulfide bond formation being hindered by the high plasmid dosage in TGE (which is lower in SGE), thus it effectively increased recombinant protein productivity. Torsin A, in addition,

improved IgG_4 production to a similar extent as XBP-1 (Josse et al. 2010). Co-expression of an anti-apoptotic protein Bcl-xL in CHO-S undergoing TGE also showed reduced levels of cell apoptosis and increased the overall rProtein titre by 100% (Zustiak et al. 2014).

2.5.9. Impact of TGE on mAb Fc-glycosylation

Fc-glycosylation of mAb expressed in cells undergoing TGE is rarely examined and to date only a few studies have directly compared protein glycosylation patterns of stably- and transiently expressed mAbs. It is highly likely that oligosaccharide contents of mAb vary between stable and transient gene expressions. Cellular stress can affect mAb folding in TGE, the retention time of the mAb within the ER might lengthen, and this could potentially affect glycan macroheterogeneity. Under mild hypothermic conditions in TGE, significant changes in galactose abundance were observed, where mAb proteins generated under TGE contained reduced levels of G1F and G2F glycoforms, than those that were stably expressed (Galbraith et al. 2006). Moreover, addition of DMSO or LiAc in BioWhittaker™ UltraCHO media in mAbs synthesized under TGE possessed higher abundance of G1F and G2F structures but a reduced level of G0F glycan contents, when compared to those from the non-chemical supplement transient pool. High fractions of high mannose structures were also observed (Ye et al. 2009).

2.6. Flux balance analysis – towards the understanding of cellular metabolic distribution

Nearly all cellular processes are directly or indirectly linked to the cellular metabolic pathway of a living organism, which contains enormous numbers of biological and chemical reactions involving the synthesis and activities of thousands of enzymes, metabolites, proteins and signalling molecules. Metabolic networks are the basis of life and they control cell growth and cell division, generate responses towards extracellular changes, and manage the process of reproduction. In the case of rProtein production, the rates of each reaction in metabolic networks of the host cells control how key metabolites are being processed within a cell and the amount of materials that flow from one reaction to another in a defined time period. Through cell metabolism one can determine the amount of nutrients and amino acids that are converted into useful metabolites such as nucleic acids, nucleotides and NSD species that are essential for protein glycosylation. Thorough understanding of the flow of each metabolite based on reactions within intracellular metabolic networks enables researchers to determine where and how each metabolite is being utilised under a set of bioprocess

conditions, in order to generate feeding plans that aim to optimise a certain process and improve both quality and quantity of the synthesized products.

There are two approaches to analyse metabolic flux distribution, these include flux balance analysis which is a constraint-based method, or metabolic flux analysis method. Flux balance analysis (FBA) is based on constraints that are normally the cellular inputs and outputs that are observed experimentally during cell culture. In FBA, metabolic networks are represented by a number of mass balances. By using the specified model structure and its model constraints, the FBA suggests the metabolic flux distribution of a cell at a specified steady state by optimising an indicated parameter, such as cell growth or rProtein production (Chen et al. 2011). In addition, FBA can also guide genetic engineering efforts to direct carbon and nitrogen fluxes towards product generation. On the other hand, metabolic flux analysis (MFA) is based on measurements of internal carbon and energy fluxes, which are usually determined through isotopic labelling (Srour et al. 2011). Isotopic labelling works through feeding cell cultures with a known amount of labelled substrates, and determining concentrations of labelled metabolic intermediates and end products are analysed. MFA can also be based on stoichiometric fluxes. This approach is data driven with external rate measurements in small-scale network models (Antoniewicz 2015). By using complex computational tools, resulting flux maps of metabolic networks are estimated, based on optimised balances between internal fluxes and labelled and external flux measurements (Chen et al. 2011).

Both approaches can successfully describe intracellular metabolic fluxes, but only to a limited degree based on the way each method is set up. FBA manages to describe metabolic flux within the optimised solution space, any others outside this indicated space are not estimated, and as a result it is essential to have the right network in FBA in order to ensure the validity of the model. Moreover, FBA is limited to just estimating internal fluxes and does not provide concentration values. In contrast, isotopic labelling-based MFA is usually quantitative. Results from the MFA show the exact measurements of intracellular metabolites from ^{13}C-labelling which bear the labelled element and it enables the direct trace of consumed materials through the metabolic network. However, the main drawback of the MFA method is that only the exchange of fluxes that contained the certain type of isotopic element, such as ^{13}C-isotope for carbon measurements, can be revealed; flows of other non-targeted metabolism therefore are excluded in the study and they cannot be traced. Furthermore, the experimental set-up of isotopic labelling is not as straightforward as those in the FBA studies, where only simple concentration measurements are required to constrain the FBA model. Isotopic labelling experiments are extremely useful and precise, but equipment and labour-training required might not

be readily available in every research environment and complex computational tools are required to analyse and deduce the map of fluxomes.

2.7. Mechanistic mathematical models

To establish mechanistic models that represent biological activities, such as the synthesis of mAb molecules within the host cells, detailed understanding of dynamic cellular processes like cell growth, and metabolism, the process of transcription, translation and secretion of recombinant proteins, as well as the process of protein assembly and post-translational modification within the ER and the Golgi apparatus are essential. Structured models for mammalian cell system account for the intracellular processes, while unstructured models treat the biological system as a black box. These models can also be segregated or unsegregated, according to whether the cell population is considered to be heterogeneous or homogeneous, respectively (Sidoli et al. 2006).

2.7.1. Modelling host cell dynamics and rProtein synthesis

A host cell dynamics model describes cellular activities along the period of cell culture in bioproduction. It usually describes changes of cellular activities such as cell growth, cell metabolism including nutrients, wastes, amino acid metabolism, as well as protein synthesis through gene expression, product translation, assembly and secretion. The first mathematical model for mAb production was developed by Bibila and Flickinger (1991). They developed a structured unsegregated steady-state kinetic model that described the process of mAb synthesis, assembly and secretion in murine hybridoma cells. The model includes heavy and light chain gene copy numbers, their respective rates of gene transcription and mRNA decay. The model developed by Bibila and Flickinger (1991) also includes HC and LC polypeptide balances, the kinetics of the mAb assembly reactions in both cell growth exponential and stationary phases in a batch culture mode, and the rate of antibody secretion from the ER to the Golgi apparatus. The model assumes mAb assembly occurs according to these reactions: $H+H \rightarrow H_2$, $H_2+L \rightarrow H_2L$, $H_2L+L \rightarrow H_2L_2$, where $[H_2]$ and $[H_2L]$ were the assembly intermediate concontrations. This reaction network is known to hold true for IgG_1 products. This inital model comprised 16 equations with 31 model parameters, where parameters are either measured experimentally or derived from existing literature. This model provides the basis for predicting effects of gene dosage, rates of specific cell growth, IgG assembly and mAb secretion.

In 2000, Jang and Barford developed an unstructured model that described cell growth and production of mAb in hybridoma cell lines. In brief, the model includes material balances for hybridoma cell growth and mAb synthesis, glucose and glutamine consumption, and lactate and ammonia production under batch or fed-batch modes (Jang and Barford 2000). This model assumes that viable cells were divided into non-cycling (G_0 or arrested in G_1 phase) and cycling (DNA replicable cells) cell cycle phases, where the model assumes G1 arrested viable cells to contribute to an increase in mAb productivity in fed-batch culture. This model has successfully predicted cellular behaviour in the late exponential growth phase capturing reduced cell growth, nutrient uptake and waste production. However, the main drawback is the inability to simulate amino acid metabolism, which cell growth and other cellular reactions are highly dependent upon. This imposes a problem in representing the metabolism of macromolecules.

Kontoravdi et al. (2005) combined models of Bibila and Flickinger (1991) and Jang and Barford (2000), and generated a single model that monitors both mAb synthesis and cellular metabolisms in hybridoma cells. In addition to the inlet and outlet concentrations of glucose and glutamine, their maintenance coefficients are also included in this model to better capture cell metabolism. This was inspired by Abbott and Clamen (1973) which demonstrated a direct positive relationship between cellular maintenance and protein yield coefficient. Instead of considering the model as one single cell, Kontoravdi et al. (2005) adapted the total cell model from Tatiraju et al. (1999), as well as substituting the concept of cell cycle dependent mAb synthesis with the differentiation between proliferating and non-proliferating cells in the model. This is a hybrid unstructured/structured model, which considers the reactions of cellular metabolism to occur in one open cellular environment, but mAb production in a structured environment, commencing from gene transcription in the cell nucleus, protein translation in the cytosol and cell membrane of the ER, followed by polypeptide assembly and protein processing in the ER and Golgi apparatus, and IgG secretion in the ECM. Furthermore, global parameter sensitivity analysis (GSA) was conducted based on the Sobol' method and experimentally determined parameters were reduced from 30 to 8 in this model. This significantly reduced the number of model validation experiments.

Shifting from hybridoma cell lines, O'Callaghan et al. (2010) constructed a mathematical model that described mAb IgG_4 synthesis and secretion in different GS-CHO cell lines. This model did not focus on cell dynamics or metabolism, but concentrated on mRNA and polypeptide production of heavy and light chains as well as their respective mRNA stabilities. It examines the effects of HC and LC mRNA translation and mAb assembly, on the specific rate of productivity of heavy (q_{HC2}) and light chain (q_{LC2}) mRNA, as well as IgG_4 (q_{IgG4}). Based on the theoretical models of Percy et al.

(1975) in which the covalent assembly of different IgG molecules was dependent on the probability of disulphide bond-formation between heavy-heavy chains or between heavy-light chains, two potential assembly models of IgG_4 were developed. The first model describes mAb assembly in the fashion of $H+H \rightarrow H_2$, $H_2+L \rightarrow H_2L$, $H_2L+L \rightarrow H_2L_2$, while the second model assumes mAb assembly to follow the 2 x ($H+L \rightarrow HL$), $HL+HL \rightarrow H_2L_2$ pathway (Figure 12). Model simulations in this study showed that an excess in LC transcription and translation was observed, and it was HC mRNA and protein production that was direcly proportional to mAb synthesis rate. Moreover, the empirical model developed by McLeod et al. (2011) attempted to distinguish the limitation of cellular processes on GS-CHO-producing mAb synthesis and model estimation from this group suggested that processes such as mAb folding, assembly and secretion did not significantly affect mAb production, but it was gene transcription that exerted a significant control on antibody production.

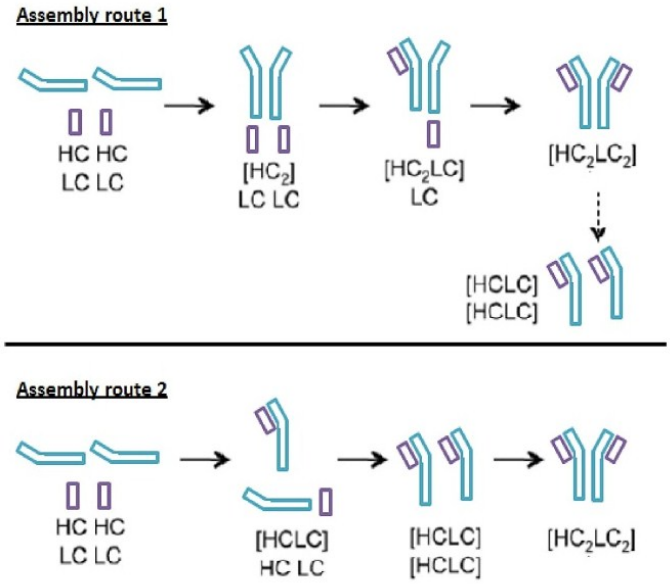

Figure 12. The two mAb assembly routes of mAb examined in O'Callaghan models. The first assembly route proposes that two heavy chains assemble first, followed by the sequential addition of the two remaining light chains. The second mAb assembly route suggests the formation of heavy-light chain hybrids, followed by the combination of the two hybrids to form fully assembled mAb.

In addition to developing cell dynamics models that estimate cell growth and cellular behaviour as well as mAb synthesis as a whole, some model frameworks were developed to predict changes in cellular behaviour under a target condition. For instance, Fox et al. (2004) developed a mathematical model that predicted the optimal time point to introduce mild hypothermia during cell culture in order to generate maximal rProtein production yield. In this proposed model, he assumed that various parameters related to cell growth and product synthesis changed from one culture temperature to another, and two separate parameter sets were employed in his model that

corresponded to physiological and mild hypothermic temperatures, respectively. The separate parameter set approach was later adapted by Munzer et al. (2015) in his unstructured cell dynamics model, in which cell cycle was taken into account when determining the best temperature shift time point for maximal product productivity.

The use of mathematical modelling tools are not only limited to products that are generated from stable cell lines, but also those that are transiently expressed. By removing material balances that represented recombinant gene transcription and mRNA decay in the mAb synthetic model developed specifically for CHO cells by O'Callaghan et al. (2010), and at the same time coupling the model with terms of cell growth and UPR-regulated protein folding, the model was capable of describing the production of seven "difficult to express" mAbs. The modified model also identified the induction of the unfolded protein response (UPR) to be the factor that increased rates of mAb folding and assembly, but reduced cell proliferation (Pybus et al. 2014a). The model managed to monitor and predict the impact of UPR induction on transient mAb expression in UPR-engineered CHO cell lines, which makes it a potential predictive tool for cell line engineering. In the same year, Pybus et al. (2014b) developed a mathematical model that predicts transient mAb production based on the amino acid/mRNA sequences of the constant regions on both heavy and light chains. This modelling methodology served as an *in silico* screening tool for transient protein expression during early mAb development.

2.7.2. mAb N-linked Fc-glycosylation models

Systems biology and computational tools are useful when it comes to process optimisation. Mathematical models are therefore developed based on this principle to aid experimental design. In 1996, the first model that described N-linked glycan attachment in mAb molecules was developed by Shelikoff et al. (1996). This structured kinetic model of glycosylation focuses on Fc-glycan macro-heterogeneity and describes the initial attachment of oligosaccharide precursors onto potential N-linked glycosylation sites on the nascent polypeptide chain in the ER. The model assumes that the process of glycosylation happens co-translationally; Shelikoff et al considered the ER as a plug-flow reactor (PFR) and initial glycosylation occurred proximal to the ER membrane. Predictions generated from this model for glycosylation site occupancy are dependent upon the level of sugar substrate within the system, the catalytic activity of membrane-bound glycosyltransferases under first order kinetics, as well as the competition between protein folding and glycan attachment. Despite the inability of this model to generate quantitative predictions, it qualitatively suggested that fractional glycosylation site occupancy was dependent on the rate of mRNA elongation, in which optimal

elongation rate provided a balance between protein folding and mAb glycosylation. A more recent computational model on macro-heterogeneity was developed in 2005. This model made use of a neural network and deduced the probability of site occupancy based on the amino sequence around the glycosylation site (Senger and Karim 2005). Dependent on the application, the model developed by Senger and Karim (2005) requires fewer parameter inputs, which is a very useful method when the enzyme kinetic mechanism of glycan attachment is not required.

In contrast, micro-heterogeneity of N-linked glycosylation, which describes changes of glycoform within the sugar chain attached to the glycoprotein, was first modelled by Umaña and Bailey in 1997 (Umana and Bailey 1997). Their model considered only the central reaction network of glycan biosynthesis, where core glycan and subsequent additions of GlcNAc and Gal residues were involved (Figure 13). This model contained a total of 33 sugar residues, 33 reactions and eight enzymes, and assumed the Golgi apparatus network as four continuously-stirred tank reactors (CSTRs) (Figure 14), where contents within each Golgi compartments were homogeneous. Enzyme kinetics for glycosyltransferases involved in this model was represented by simple Michaelis-Menten kinetics without consideration on any product or competitive inhibition. This model provided qualitative predictions on the distribution of different glycan structures based on the expression and the localisation of N-linked glycan related enzymes, as well the length of Golgi retention period of these enzymes. Through knock-out experiments on glycosyltransferases, the model was capable of predicting the effect of glycan engineering on glycan structure distribution. However, this model neglected the contribution of nucleotide sugar donors and has limited the ability to consider the impact of extracellular environment on N-linked glycosylation. Despite these limitations, this model provided a basis for the development of future N-linked glycosylation models.

Krambeck & Betenbaugh in 2005 extended the glycosylation model developed by Umaña and Bailey, where the model considered the addition of other sugar residues such as core fucose and sialic acid onto the bi-antennary structure, or other possible extended antennae with galactosamine addition (Krambeck and Betenbaugh 2005). Similar to the Umaña's model, the model of Krambeck considered the Golgi apparatus as four consecutive CSTRs (Figure 14), but the number of overall reactions increased to 22,871 including 7,565 glycan structures. To accommodate the addition of extra sugar species, kinetic parameters for fucose and sialic acid transferases were included in this model. While Umaña's model only considered simple Michaelis-Menten enzyme kinetics, Krambeck's model took into account competitive inhibition, and assumed constant enzyme kinetics among the four Golgi compartments. Model parameters were adjusted in this model to generate matching simulations to experimental data of the target glycoprotein and the model was capable of describing the effect of

glycoengineering on mAb glycosylation. However, Krambeck assumed the same level of nucleotide sugar donors entering into each Golgi compartment. As a result the direct impact of cellular metabolism on mAb glycosylation could not be assessed. Later in 2009, Krambeck and colleagues improved the existing model by introducing additional enzymes. Together with a molecular mass cut-off through MALDI-TOF mass spectrometry, this group managed to predict about 10,000 sugar structures in their model, which enabled complete sets of glycan structures and enzymatic reactions within a mass-range to be revealed (Krambeck et al. 2009). Improvements in this model enabled glycan analysis in diseased cells.

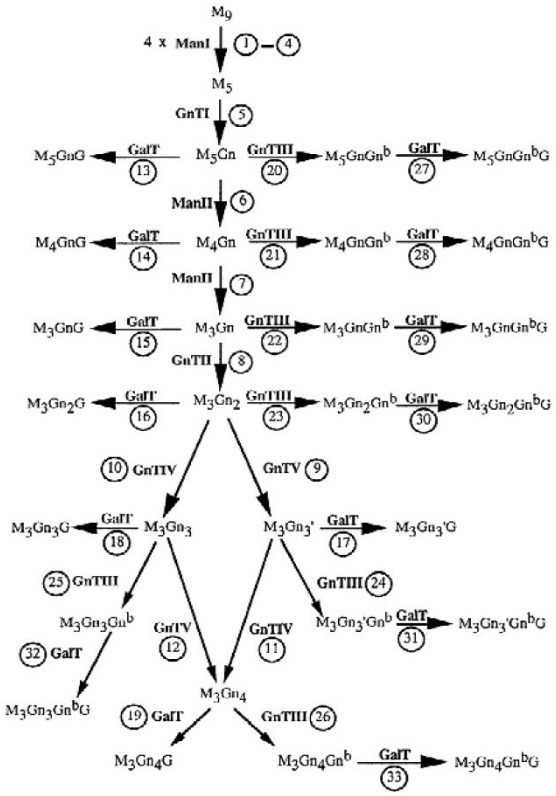

Figure 13. The central reaction network of IgG Fc-N-linked glycosylation. This reaction network only considers enzymes and reactions that are involved in forming GlcNAc terminating-N-glycan structure ($GlcNAc_2Man_3GlcNAc_2$-Asn297). In total 33 reactions and 8 different enzymes are involved. This is adapted from Umana and Bailey (1997). "Permission is granted by the right holder John Wiley & Sons, Inc to reproduced this image for this thesis"

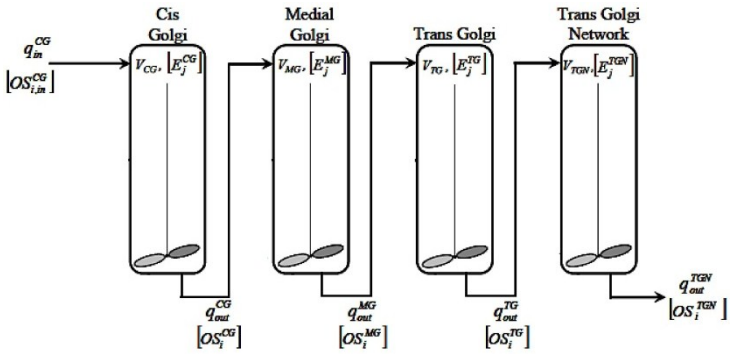

Figure 14. Schematic of the Golgi apparatus as 4 CSTRs. Umana and Bailey (1997), Krambeck and Betenbaugh (2005), Krambeck et al. (2009) and Hossler et al. (2007) considered the Golgi apparatus as 4 CSTRs in their proposed mathematical models for mAb Fc-N-glycosylation. This taken from del Val et al. (2010). "Permission is granted by the right holder American Institute of Chemical Engineers to reproduced this image for this thesis"

By using similar kinetic parameters with the previous two models, Hossler et al. (2007) developed two mathematical models based on certain assumptions on the Golgi structure. The first model employed a similar approach as the previous two and considered the Golgi apparatus as four CSTRs, while the second model considered the Golgi as a series of four PFRs. Hossler and colleagues compared predictions on mAb glycosylation between the two developed models and their observations suggested that model simulations generated from the PFR approach better represented experimental results, especially in predicting the abundance of high-mannose structures. In addition, the model assumed each Golgi compartment to have a different enzyme distribution and NSD concentration. The localisation of glycosyltransferases helped optimise the amount of terminal glycan structure. Lastly, competitive inhibition was included in the kinetic rate expressions. Compared to previous models, this model allowed better understanding of the actual N-linked glycosylation process and enabled better predictions of experimental data. By incorporating the information on enzyme localisation, the model had high potential of describing the genetic manipulation on these enzymes, which made it very useful for the field of glycoengineering.

In 2011, Jimenez del Val and collaborators extended Hossler's model and introduced the Golgi network as one single PFR, which is in line with the concept of Golgi maturation (Figure 15) (Jimenez del Val et al. 2011). In addition to including nucleotide sugar donors as substrates for Fc-glycosylation, the kinetic rate expression of each glycosyltransferase involved, as well as rates of NSD transport protein moving from cell cytosol into the lumen of Golgi apparatus, were taken into account in their model construction. Moreover, the concept of recycling glycosyltransferases and transport proteins was also included within the PFR model. In terms of glycosyltransferase enzyme kinetics, reported competitive and product inhibitions were included along with known kinetic

mechanisms, such as sequential and random Bi-Bi enzyme reactions. Unknown parameters from both enzymatic and protein transport processes were directly estimated for this model. The model aimed to establish a link between intracellular N-glycosylation processes and cellular mechanisms. As a result, computational simulations were capable of generating a more thorough description of commercial recombinant mAb N-glycosylation structures. At the same time the model was able to predict glycan patterns of the recombinant product after the genetic knockout of the fucosyltransferase gene, replicating pre-existing experimental data. This model offers the potential of examining the effect of extracellular bioprocess conditions on the Fc-glycosylation profile.

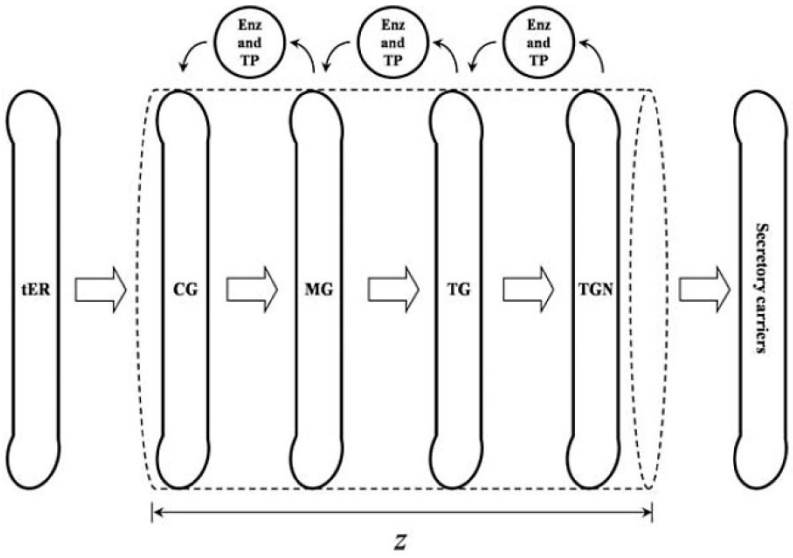

Figure 15. Golgi apparatus maturation in single PFR model. Jimenez del Val et al. (2011) considered the entire Golgi apparatus network as one PFR. Glycoproteins transit from the *cis*-Golgi to the *trans*-Golgi network, in which enzymes, NSD and processed glycoproteins are transported between compartments via vesicles, along the PFR (dotted lined). Figure adapted from Jimenez del Val et al. (2011). "Permission is granted by the right holder American Institute of Chemical Engineers to reproduced this image for this thesis"

2.7.3. Combined mathematical model of cellular processes and mAb N-linked Fc-glycosylation model

The work by Kontoravdi et al. (2007) is believed to be the first report that attempted to relate mAb Fc-glycosylation to cellular metabolic networks, by combining the cell dynamics model that was developed in 2005 with the Umaña and Bailey's glycosylation model to generate a single mathematical model that described cellular processes, metabolism and Fc-N-glycosylation of mAb. Model simulations showed successful predictions for nutrient consumption and protein synthesis, and generated predictions for their effect on mAb Fc-glycosylation. Despite the simplified version of the Umaña and Bailey model, this was the first attempt to extend the effect of bioprocess conditions on the intracellular glycosylation processes.

Based on the model structure of the N-linked glycosylation model developed by Jimenez del Val et al. (2011), Jedrzejewski et al. (2014) further integrated the model with a kinetic cell growth module, where the model described nucleotide sugar donor (NSD) synthesis based on the consumption of glucose and glutamine during the fermentation process. This approach directly relates the process of Fc-glycosylation to cell metabolism, which is subject to vary upon changes in the extracellular environment. Jedrzejewski and colleagues demonstrated that the model was capable of describing time-course concentration profiles of both nucleotide and NSD synthesis, as well as accurately predicted mAb Fc-glycan patterns in a hybridoma cell line. Instead of relating cell metabolism and Fc-glycosylation by using absolute concentrations of nutrients and metabolites, Kaveh et al. (2013) coupled nutrient metabolism to NSD synthesis and N-linked Golgi glycosylation via metabolic flux analysis (MFA). This model approach enabled accurate predictions on the trend of mAb Fc-glycosylation in CHO cultures.

By coupling cellular metabolic networks to NSD synthesis and protein glycosylation, these models are crucial steps towards *in silico* analysis of the impact of bioprocess condition during cell culture on mAb production and glycosylation.

2.8. Discussion and project motivation

In this chapter, literature review was presented covering the topics of protein glycosylation and its effect on protein drug efficacy, as well as experimental investigations on the impact of bioprocess conditions on the antibody glycosylation. This was followed by an overview of computational efforts to describe protein glycosylation in the ER and the Golgi apparatus and the latest efforts to develop predictive tools that link the extracellular environment with the final product glycoforms.

Given the research questions arising from this review, the main aim of our research was to investigate the impact of different bioprocess conditions on mAb Fc-glycosylation. Of particular interest, was the effect of mild hypothermia and the implications of transient gene expression compared to the standard process of fed-batch culture of CHO cells stably expressing monoclonal antibodies. As mentioned within the content of this chapter, many studies have focused on understanding the underlying mechanism behind the advantageous effect of mild hypothermic conditions on recombinant protein production. However, the relationship among mild hypothermic conditions, changes in cell metabolism, mAb synthesis as well as Fc-glycosylation, is not well

established. The same problem applies to transient gene expression, where cell metabolism is already shown to be very different from the traditional stable method but very little is known about the impact of cellular changes on Fc-glycosylation. As a result, the first part of our study focused on the following points:

- Identifying contributing factors to mAb production and mAb Fc-glycosylation changes under mild hypothermic conditions, through detailed examination of changes within host cell metabolic pathways by experimental and FBA study, and
- Comparing mAb synthesis and Fc-glycosylation in TGE systems at different cell culture temperatures with the respective profiles in SGE systems.

Despite advances in model development in terms of representing cellular activities under certain bioprocess conditions, most models describe their impacts under a single aspect and very few of them relate process conditions to cellular performance and product quality through a single model, especially when it comes to modelling the impact of transient gene expression on product glycosylation. As a result, the second part of this thesis attempts to fill this gap and develops a biological mathematical model that mechanistically describes the impact of mild hypothermia or transient gene expression on product glycosylation, as a result of changes in cell metabolism. The proposed model is developed with an aim to capture the variation in Fc-glycosylation in response to changes in the extracellular environment. By satisfying this intention, the model will help revealing limitation in cellular activity that CHO cells are experiencing under a specific culture condition. By identifying the bottlenecks within each bioprocess, improvements can be implemented into the manufacturing process and this will satisfy the quality by design regime. Our proposed mathematical model will serve as a useful analytic tool in host cell characterisation, as well as a predictive tool for Fc-glycosylation under different bioprocess conditions.

Chapter 3
Experimental materials and methods

3.1. Cell culture

3.1.1. Cell line, maintenance and storage

IgG-producing (SGE) or blank (TGE) Chinese hamster ovary CHO-T cell lines (MedImmune, Cambridge, UK) were revived separately and cultured in CD-CHO medium (Life Technologies, Paisley, U.K.) with starting concentrations of 25.81 mM of glucose and 1.36 mM of glutamate in cultures. In the case of the IgG-producing cells for SGE, cells were supplemented with 50 μM methionine sulfoximine (MSX) during the first and second passages only. Depending on the culture volume, cells were grown in Erlenmeyer flasks or in roller bottles (Corning Inc., NY, USA) at 150 rpm in humidified 36.5°C incubator with 5% CO_2 supply and were subcultured in fresh medium every three days at a seeding density of 3 x 10^5 viable cells/mL. Cell concentration and cell viability were measured by ViCell® (Beckman Coulter, CA, U.S.A.). For storage, cell pellet containing 1 x 10^7 viable cells were resuspended in 1 mL of freezing agent which consisted of 92.5% CD-CHO medium and 7.5% dimethyl sulfoxide (DMSO; Sigma-Aldrich, Dorset, UK). Cell vials were stored at -80°C for 20 h in a Nalgene® Mr Frosty prior to being transferred to liquid nitrogen (-160°C) for long term storage.

3.1.2. Cell system and Operation

All experiments mentioned in this thesis, with an exception of the glycosyltransferase manipulation experiment described in Chapter 8 where Erlenmeyer flasks were used, were carried out in triplicate 1.5 L stirred tank DASGIP bioreactors (DASGIP Technology, Juelich, Germany). After three cell passages, CHO cells were transferred into the bioreactor system with an initial culture volume of 0.9 L and a viable cell density of 8 x 10^5 cells/mL in each vessel. Within the 14-day cell culture period, the pH was maintained at 6.9±0.1 and culture temperature was maintained at 36.5°C, or with a temperature shift to 32°C at various points of cell culture depending on the experiment, as indicated in Table 4. The stirring speed was at 150 rpm and CO_2 air concentration was maintained at 5% v/v. On days 2, 4, 6, 8, 10 and 12 of the culture period, the cultures were supplemented with 10% v/v CD EfficientFeedTM C AGT™ Nutrient supplement (Life Technologies, Paisley, U.K.), or with 10% v/v of a proprietary feed x (MedImmune, Cambridge, U.K.) as indicated in Table 5. Excessive foaming was eased by 5 mL additions of 15% antifoam C (Sigma-Aldrich, Dorset, U.K.).

Table 4. Timing of temperature shift in each experiment with different bioprocess conditions.

Chapter number	Bioprocess condition	Time of temperature shift to 32°C
4, 6, 8	SGE, physiological	Does not apply
4, 6, 8	SGE, mild hypothermia	Day 6
6	TGE, physiological	Does not apply
6	TGE, mild hypothermia	Day 2 (24 h post-DNA transfection)
8	miRNA transfection, mild hypothermia	Day 6
8	null vector transfection, mild hypothermia	Day 6

Table 5. Type of nutrient supplement in each experiment with different bioprocess conditions.

Chapter number	Bioprocess condition	10 % v/v CD EfficientFeed™ C AGT™
4, 6, 8	SGE, physiological	√
4, 6, 8	SGE, mild hypothermia	√
6	TGE, physiological	√
6	TGE, mild hypothermia	√
8	miRNA transfection, mild hypothermia	√
8	null vector transfection, mild hypothermia	√

3.2. Transient gene expression (TGE)

3.2.1. Transfection method

Transient transfections were performed in the TGE experiment in Chapter 6 and glycosyltransferase manipulation experiment in Chapter 8. Transient transfection in the former was carried in each bioreactor 24 h after cell inoculation (day 1), at a cell density of 2 x 10^6 cells/mL, while DNA/miRNA vectors were transfected in each shake flask culture on day 5, at a viable cell concentration of 1 x 10^7 cells/mL. Table 6 shows the respective type and amount of DNA vectors transfected in each experiment. To transfect, respective amount of DNA vectors were mixed with 125 mM NaCl-diluted linear PEI 25,000 Da (Polysciences Europe GmbH, Germany) in a ratio of 5:1 PEI:DNA. The mixture was incubated for 2 min at room temperature prior to additions to the cells. Transfection protocol (not vector construction) was adapted from Daramola et al. (2014).

Table 6. Type and amount of vectors used in transient gene expression in each experiment.

Chapter number	Bioprocess condition	DNA/miRNA plasmid	Amount of vector transfected (μg)	Culture volume at transfection (L)
6	TGE, physiological	♦Human IgG heavy chain (HC HuG1) ♦Human IgG light chain (LC HuKappa) (MedImmune, Cambridge, UK)	1 mg of total DNA per 1L of culture volume	0.9
6	TGE, mild hypothermia			
8	miRNA transfection, mild hypothermia	♦cgr-miR-500 in pcDNA4/TO vector ♦cgr-miR-501-5p in pcDNA4/TO vector ♦cgr-miR-181d in pcDNA4/TO vector	0.05, 0.10, 0.25 & 0.50 mg of each miRNA vectors per 1L of culture in 4 separate conditions	0.1
8	null transfection, mild hypothermia	♦pcDNA4/TO vector	0.15 mg per 1L of culture volume	

3.2.2. miRNA vector construction

Table 7 shows miRNA sequences for cgr-miR-500, cgr-miR-501-5p and cgr-miR-181d. Each designed miRNA sequence with compatible sticky ends for *Eco*RI and *Pst*I (Sigma-Aldrich, Dorset, UK) was inserted between the *Eco*RI and *Pst*I sites in three separate pcDNA4/TO expression vectors. After vector verification through DNA sequencing, each miRNA containing vector was progagated in *E.coli* DH5α and purified by the Qiagen Plasmid Maxi Kit (Qiagen, Manchester, UK) according to the manufacturer's instructions.

Table 7. miRNA sequences.

Chapter number	miRNA	Accession number	Sequence
8	cgr-miR-500	MIMAT0023974	5'-AAUGCACCUGGGCAAGGGUUC-3'
	cgr-miR-501-5p	MIMAT0023975	5'-AAUCCUUUGUCCCUGGGUGGAAAUGC-3'
	cgr-mir-181d	MI0020423	5'-GUCACAAUCAACAUUCAUUGUUGUCGGUGGGUUGUGAUGAGGAGGCCAGACCCACCGGGGGAUGAAUGUCACUGUGGCUGG-3'

3.3. Analytical assays

On a daily basis, samples of 10 mL were withdrawn for polypeptide, nucleotide sugar donor (NSD), and heavy and light chain DNA/mRNA and glycosyltransferase mRNA analyses. Samples were centrifuged for 5 min at 200 rpm in an Eppendorf microfuge. Supernatants were stored at -80°C and cell pellets were washed twice with PBS prior to storage at -80°C. Extracellular nutrient and mAb concentrations were quantified in clarified supernatants.

3.3.1. Nutrients, metabolites and secreted mAb concentrations

Extracellular concentrations of glucose, lactate and ammonia in supernatant samples were determined using the YSI Bioprofiler 800 (NOVA Biomedical, MA, U.S.A.). Extracellular amino acid quantification was performed with a Waters Acquity ultra-performance liquid chromatography

(UPLC, Waters, Hertfordshire, U.K.) using the AccQ-tag kit according to the manufacturer's instructions. Secreted mAb titre was determined using a Protein-A affinity chromatography method. Specific consumption and production rates of nutrients and metabolites were calculated by plotting the integral viable cell concentration (IVCC) against the cumulative concentration as in Kyriakopoulos et al. (2013).

3.3.2. DNA and RNA extraction and cDNA preparation

Total DNA and RNA content of each sample was extracted from pellets containing 5 x 10^6 cells according to the manufacturer's protocols for the All prep DNA/RNA mini purification kit (Qiagen, Manchester, U.K.). Using 1 μL of the RT Primer Mix of the QuantiTect Reverse Transcription Kit (Qiagen, Manchester, U.K.), 300 ng of extracted total RNA from each sample was reversed transcribed into cDNA according to the manufacturer's instructions.

3.3.3. mAb heavy and light chain, glycosyltransferase mRNA quantification

To determine the DNA copy number and mRNA expression levels of mAb heavy (HC HuG1) and light chains (LC HuKappa), as well as 8 glycosyltransferases, namely 2 N-acetylglucosaminyltransferases (GnTI and GnTII), 3 galactosyltransferases (β-GalTI, II and III), fucosyltransferase (FucT), UDP-Gal transporter and UDP-GlcNAc transporter, quantitative real-time polymerase chain reaction (qRT-PCR) was performed in each sample. Each cDNA sample transcribed in **(3.3.2)** was analysed in triplicate using PCR. PCR experiments were carried out in a 96 well-plate using 5 μL of 2x SYBR Green Supermix (Sigma-Aldrich, Dorset, U.K.), 0.64 μL of cDNA and 500 nM of each primer pair and ddH_2O to make a total of 10 μL of reaction volume per well. Non-template controls were carried out for each PCR. PCR experiments were initiated with SYBR Green activation at 95 °C for 3 min followed by 40 cycles of 95°C for 30 s, 60°C for 75 s and 72°C for 30 s. DNA melting curve was performed from 65°C to 95°C (read every 0.3°C) to verify product integrity. Results were compared to the C_t-number of house-keeping gene β-actin for relative analysis, while DNA copy number was calculated from a calibration curve of known DNA concentrations. Table 8 shows the primer sequences of glycosyltransferases and those of heavy and light chains are available on request.

Table 8. Forward and reverse primer pairs used in qRT-PCR experiments.

Chapter number	Type	Glycosyltransferase	Accession Number	Primer pair sequence
4,6,8	N-acetylglucosaminyl-transferase	GnT I		5'-CTGGGTGTCATGGATGACCT-3' 5'-CTAATTCCAGCTAGGATC-3'
		GnT II		5'-GATGATTATAACTGGGACTGG-3' 5'-TGACTCAATTTGGGCACTCTG-3'
	Galactosyltransferase	β-Gal T I	AF318896	5'-GACCTGGAGCTTTTGGCAAA-3' 5'-GGGATAATGATGGCCACCTTG-3'
		β-Gal T II	AY117536	5'-CCTTCTCTGCCTGCTGCACT-3' 5'-CTGGGCTTCGGATACTGAAGC-3'
		β-Gal T III	AY117537	5'-AACTGCCATAATTGTGCCCC-3' 5'-TGCCATATGCAAGCTGCTG-3'
	Fucosyltransferase	FucT		5'-TATGGCACCCAGCGAACACTC-3' 5'-TTCACCTGACCAGTGTCCAG-3'
	Nucleotide sugar transporter	UDP-Gal Transporter	AF299335	5'-ACACACTCAAGCTCGCGGT-3' 5'-TGTCACCTGGAAAGTGGCAG-3'
		UDP-GlcNAc Transporter		5'-CAGGAGTTGCTTTTGTACAG-3' 5'-GCTGTGAGAACTGCCATGAG-3'

3.3.4. Determination of heavy and light chain mRNA half-lives

To estimate the stability of heavy and light chain mRNA molecules in SGE, duplicate shake flask experiments were performed at both 36.5°C and 32°C. On day 6, 65 μM of the transcription inhibitor DRB (5,6 dichloro-1 β-D-ribofuranosyl benzinmidazole, Sigma-Aldrich, Dorset, U.K.) dissolved in 100% ethanol (VWR, Lutterworth, U.K.) was added to block cell transcription. The same volume of ethanol was added to control cultures at both temperatures to compensate for the effect of ethanol on the cells. 5 x 10^6 cells/mL were collected from each culture at 0, 3, 6, 9, 12 hours after the inhibitor/ethanol additions. Transcribed cDNA from each sample was quantified by qRT-PCR. Results were normalized to a standard curve generated with known amounts of the HC/LC plasmids and their respective C_t-values. mRNA levels were determined from the standard curve and decay rates were calculated.

3.3.5. Intracellular mAb polypeptides and assembly intermediate analysis

Pellets from 2 x 10^6 viable cells were washed with 0.9% NaCl solution at 4°C before being resuspended in 125 µL of CellLytic™ M solution (Sigma-Aldrich, Dorset, U.K.) supplemented with 1% (v/v) protease inhibitor cocktail (Sigma-Aldrich, Dorset, U.K.). Extraction method is adapted from Ho et al. (2012b). Mixtures were incubated at room temperature for 10 min with shaking prior to centrifugation at 18,000 x g for 15 min to pellet cell debris. Soluble protein-containing supernatant was stored at -80°C prior to Western blot analysis. One part of 4x NuPAGE sample buffer was added to 3 parts of each sample and 100, 10, 1 & 0.1 µg of purified IgG controls (provided by MedImmune, Cambridge, U.K.). Samples and standards were run on a 4 - 20% Precast Protein gel (Thermo Scientific, Horsham, U.K.) in Tris-HEPES running buffer at 115 V for 50 min. The polyacrylamide gel was washed twice with dH_2O before being transferred in a semi-dry transfer system (Bio-Rad, Hertfordshire, U.K.) onto a methanol-activated PVDF transfer membrane (Milipore, Watford, U.K.) at 0.3 A for 40 min. Upon successful transfer, the blot was prepared using the WesternBreeze® Chemiluminescent Anti-Goat-Kit (Life Technologies, Paisley, U.K.) according to the manufacturer's instructions, with 1:1000 horseradish peroxidase (HRP)-conjugated goat anti-human IgG Fc (Jackson Immunoresearch, PA, U.S.A.) and a 10 min exposure time (FujiFilm, Bedford, U.K.). The intensity of each band was quantified using MYImageAnalysis Software Manual (Thermo Scientific, Horsham, U.K.) and concentration in each sample was compared to the IgG protein standards.

3.3.6. Analysis of galactosyltransferase III (GalTIII) protein expression

2 x 10^7 viable cells were pelleted and rinsed with 4°C PBS prior to cell lysis in 200 µL of M-PER Mammalian protein extraction reagent (Thermo Scientific, Horsham, U.K.) supplemented with 1% (v/v) protease inhibitor cocktail (Sigma-Aldrich, Dorset, U.K.). Sampled were gently shaken for 10 min before sonication on ice using 3 times of 5 seconds, with 25 seconds intervals in between each sonication and an amplitude power of 20. Cell debris was removed by centrifugation at 14,000 x g for 15 min. Membrane protein-containing supernatant was stored at -80°C prior to Western blot analysis as described in **(3.3.4)**, with an exception of an additional 10 min incubation at 100°C before gel electrophoresis. β-1,4-Gal-T3 Antibody (N20) (Santa Cruz Biotechnology, Texas, USA) was used as primary antibody for Western blotting and protein concentration in each sample was compared to known concentrations of β-1,4Gal-T3 (N20) blocking peptide (Santa Cruz Biotechnology, Texas, USA).

3.3.7. Extraction of intracellular NSD and analysis

Intracellular nucleotide sugars were extracted by an acetonitrile extraction method (Dietmair et al. 2010; Viant et al. 2005). In brief, 400 µL of ice cold 50% v/v aqueous acetonitrile was added to a cell pellet containing 2 x 10^6 cells. The mixture was incubated on ice for 10 min before centrifugation at 18,000 x g for 5 min at 0°C. Supernatant was dried thoroughly using a SpeedVac (Savant Inc. Laboratory, MI, U.S.A.). Dried samples were resuspended in 150 µL of deionised water and were filtered using 0.2-µm syringe filter units (Fisher Scientific, Loughborough, U.K.) before HPAEC analysis. The NSD analytical method was based on del Val et al. (2013), using a CarboPac PA-1 column with a PA-1 guard column (Dionex, CA, USA). Elution of samples, namely 10 nucleotides - ATP, CTP, GTP, UTP, AMP, ADP, CMP, GMP, UMP and UDP, as well as 9 nucleotide sugar compounds- CMP-Neu5Ac, UDP-GalNAc, UDP-GlcNAc, UDP-Gal, UDP-Glc, GDP-Glc, GDP-Fuc, GDP-Man and UDP-GlcA, was performed using a gradient of E1 (3 mM NaOH) and E2 (1.5 M sodium acetate in 3 mM NaOH) buffers as mobile phases. Detection of all species was carried out at two absorbance wavelengths: 271.6 nm for all cysteine-bearing species and 262.1 nm for all other compounds. The elution profile of each of these species is shown in Appendix I Figure 1 and is also presented in del Val et al. (2013).

3.3.8. mAb glycan analysis

Purified mAb samples with concentration range of 1.25 - 7.5 mg/mL were prepared for glycan analysis using the ProfilerPro Glycan Profiling Kit (PerkinElmer, MA, U.S.A.). 8 µL of each sample was first denatured in the Denaturing Plate containing 3 µL of denaturing solution for 10 min at 70°C. 11 µL of denatured material was transferred to Peptide-N-Glycosidase F (PNGase F) Plate and was incubated at 37°C for 1 h to cleave the glycan from the protein. 8 µL of the digested sample was transferred to the Labelling Plate and was incubated at 55°C for 2 h for glycan labelling, where glycans were derivitised with charged fluorophores. Dried samples were reconstituted in 100 µL of molecular grade water and glycan analysis was performed by the LabChip® GXII instrument (PerkinElmer, MA, U.S.A.). Glycan samples are separated in this method based on a microchip based capillary electrophoresis. The chip contains a set of micro-channels that are linked to both the separation channel and the buffer well, in which one of the micro-channels connects to a capillary below that sip samples through from the sampling plate during experiment. Micro-channels contain either buffers or sieving gel and each glycan sample moves along the sieving gel based on its electrophoretic mobility, and it produces a migration profile which is dependent on the charge, mass

and structure properties such as different glycosidic linkages, α or β bondings and the composition of the saccharide itself. The migration time of each glycan species is normalised to that of the glucose peaks in the glycan ladder by the LabChip GXII software to yield the size of the peaks, while at the same time each sample glycan peak is identified by comparing them to the migration time of known glycan standards that are analysed in the buffer as the samples. This glycan analytic method is capable of resolving glycan structures including high mannoses, hybrid and complexed structures.

3.4. Flux balance analysis

The R workspace (R Development Core Team 2010) and the Sybil package (Gelius-Dietrich et al. 2013) were used to perform the FBA. The metabolic network was constructed based on the one proposed by Carinhas et al. (2013) using the biomass composition proposed by Selvarasu et al. (2012) for CHO cells, but excluding cystine. The final model consisted of 120 metabolites, 97 intracellular reactions and 57 transport equations, as shown in the Appendix I Table 1 and also presented in Kyriakopoulos and Kontoravdi (2014a). The model was optimised by assuming maximum biomass and IgG accumulation during exponential phase, and maximum IgG accumulation at stationary phase. The FBA was constrained by the experimentally measured extracellular fluxes of amino acids, glucose, lactate, ammonia and observed growth rate and specific productivity. Specifically, the upper and lower bounds were set within one standard deviation of experimentally measured fluxes while those fluxes that were not measured were set at ±20% from those reported in (Carinhas et al. 2013). In order to examine the glucose fluxes to nucleotide and NSD production for glycosylation, GlcNAc, GalNAc, Man, Fuc, Gal and Neu5Gc were added in the biomass equation. The amount of each NSD necessary for host cell protein and recombinant product glycosylation, was estimated based on the MS glycan study in North et al. (2010), the occurring frequency of N- and O-linked glycans on host cell proteins based on Apweiler et al. (1999), and the mAb glycan entity in this study. These data were then used to calculate the respective stoichiometric coefficients (mmol per gram of dry cell weight, mmol/gDCW) that were incorporated in the biomass equation and used in the FBA analysis.

Chapter 4
How does mild hypothermia affect recombinant monoclonal antibody glycosylation in stable transfectants?

As illustrated in Chapter 2, the glycan compositions and their distribution on the recombinant monoclonal antibodies (mAbs) are directly impacted by the bioprocess conditions during mammalian cell culture. To understand further the mechanism behind this change, it is necessary to investigate and identify any relevant changes in cell metabolism among different bioprocess conditions. This chapter will examine the effect of mild hypothermia during cell culture on mAb N-linked glycosylation, using the experimental framework that was outlined in Chapter 3. "Permission is granted from Wiley Periodicals, Inc. to use the all materials from the granted publication in this Chapter"

4.1. Background and aims

In order to keep up with the increasing demand of monoclonal antibodies in the pharmaceutical market, one has to increase the specific productivity of recombinant protein (q_{prod}) via optimisation of industrial bioprocesses is necessary. To address this issue, biphasic culture methods based on temperature shift are often used as an approach to increase recombinant protein (rProtein) yield. It was reported by Nam et al. (2008) that a temperature shift from 37°C to 33°C in suspension Chinese Hamster ovary (CHO) cell culture increased the specific productivity of recombinant secreted human placental alkaline phosphate (SEAP) by 8-fold. In response to the cold-shock, CHO cells experienced reduction in the rate of nutrient consumption and production of biological waste (Chuppa

et al. 1997). It was also reported that CHO cell population was partially arrested in G_0/G_1 phase of cell cycle upon the induction of mild hypothermia (Marchant et al. 2008), together with reduced rate of decay in transcriptional species and changes in protein translation, folding and trafficking efficiencies (Cain et al. 2013). As a result with the improvement in rProtein yield, mild hypothermic conditions (30°C - 34°C) are frequently employed in industrial practices (Wulhfard et al. 2008).

Despite the positive outcomes of mild hypothermia in rProtein production, few investigations have been made into its effects on protein glycosylation, and in the case of an IgG, the N-linked glycan pattern on the Fc-domain. As discussed in Chapter 2, the carbohydrate moieties on the mAb Fc-regions determine the binding affinity of mAbs to their respective Fcγ receptors and subsequent ability to activate downstream immune responses. The final composition of these sugars is susceptible to changes, and is dependent on the expression levels and the activities of glycosyltransferases, as well as the availability of nucleotide sugar donors (NSDs) within a cell, which are in turn affected by different nutrient feedings and cell metabolism. Changes along the cell metabolic pathway in response to temperature shift can therefore impact mAb glycosylation.

To ensure the efficacy of a target drug, one must control the consistency in mAb quality and this can be fulfilled through thorough understanding of the relationship between cell metabolism, mAb synthesis and Fc-glycosylation in sub-physiological temperatures. In this chapter, we examined the impact of mild hypothermia on an IgG-expressing cell line and compared the culture performance at different temperatures with respect to cell growth, metabolic profiles including nutrients, biological wastes, amino acids and NSDs, mAb synthesis such as heavy and light chain mRNA and assembly intermediates, mAb glycan profiles and glycosyltransferase expression levels. To better understand and generate a bigger picture of the intracellular metabolic network, we performed flux balance analysis (FBA) based on the data sets from both temperatures and calculated the differences in metabolic flux changes upon the induction of mild hypothermia.

4.2. Results

4.2.1. CHO cell culture behaviour and mAb production profile during mild hypothermia

To investigate the impact of mild hypothermia, two sets of experiments were carried out: 14-day CHO cell fed-batch culture at 36.5°C, or with a temperature shift from 36.5°C to 32°C on day 6

(late exponential phase). Day 6 is chosen as the temperature shift day because it is the time period between cells leaving exponential growth phase and entering into stationary phase; the introduction of mild hypothermia to cells at that period ensures sufficiently high cell density for recombinant protein production, at the same time compromising for the decrease in cell concentration that mild hypothermic condition induces. Figure 16 A and Figure 16 B show the growth profiles of CHO cell cultures and the volumetric and specific mAb productivities at both temperatures. When compared to culture at 36.5°C, cells that are temperature-shifted to 32°C maintain a high viability of 98.2% on harvest day, with only a 10.0% reduction in their IVCC. Reduction in viable cell concentration observed at 32°C is most likely a result of lower rate of cell growth. The prolonged cell viability and slower rate of cell growth observed could be explained by the work of Marchant et al. (2008), in which the group demonstrated cells undergo a partial cell cycle arrest in mild hypothermic conditions and cell division was delayed.

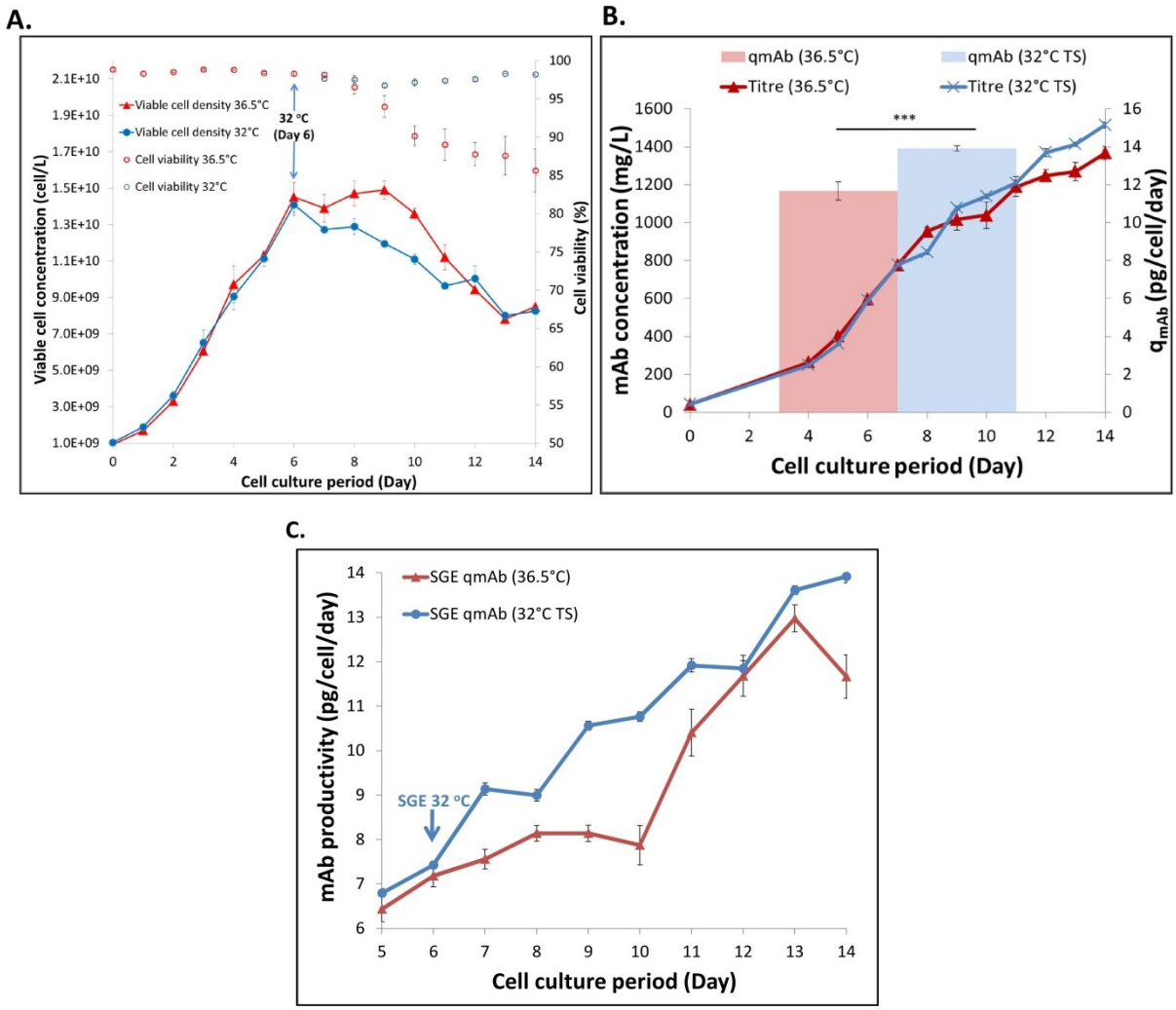

Figure 16. Cell growth, volumetric titre and specific productivity (q_{mAb}) of secreted IgG at 36.5°C and with a temperature shift to 32°C. Viable cell concentration and cell viability profiles were measured along the period of cell culture (A), together with the q_{mAb} which was calculated based on terminal secreted product and accumulated mAb concentration profile of both temperatures (B). (C). Dynamic q_{mAb} profile after the induction of mild hypothermic

condition. Results are average measurements at 36.5°C (n=6) and 32°C (n=3). The error bars represent the standard deviation of the samples. TS: Temperature shift.

Along with increased cell viability, a 25% rise in the specific mAb productivity (q_{mAb}) is observed in 32°C cultures. Figure 16 C shows the dynamic profile of q_{mAb} upon the induction of mild hypothermia. Our analysis here clearly shows that the rate of mAb synthesis per cell is enhanced at 32°C. To better elucidate the reason for the increase in q_{mAb} at lower temperature, intracellular species produced in the mAb synthesis process were experimentally quantified. The results show that the HC mRNA expression level is higher at 32°C (Figure 17 A and Figure 17 B), and the overall net concentrations of H_2 and H_2L mAb assembly intermediates increase by at least 2-fold upon temperature shift (Figure 17 C and Figure 17 D), these together contribute to the 25% rise in secreted mAb production. In both mRNA and polypeptide concentrations, our results also suggest the HC to be the rate-determining species for mAb synthesis, with the increase in HC mRNA transcripts at 32°C being advantageous for overall mAb production. This is in good agreement with the findings of O'Callaghan et al. (2010), which concluded that q_{mAb} was controlled mostly by the rate of HC translation. In addition, a lower culture temperature is shown to stabilise both HC and LC mRNA, with 14% and 22% reductions in HC and LC mRNA decay rates (Table 9), respectively. Our findings correlate with that in Oliveira and McCarthy (1995)., which demonstrated the relationship between mRNA degradation and attenuation in protein translation. Despite increased net difference in H_2L between the two temperatures, the fact that comparable LC mRNA concentrations and rapid decrease of H_2L level on day 12 were observed in this study suggests that the rate of light chain addition is slower at 32°C, thus resulting in the accumulation of intracellular H_2L species and limiting further increase in mAb productivity.

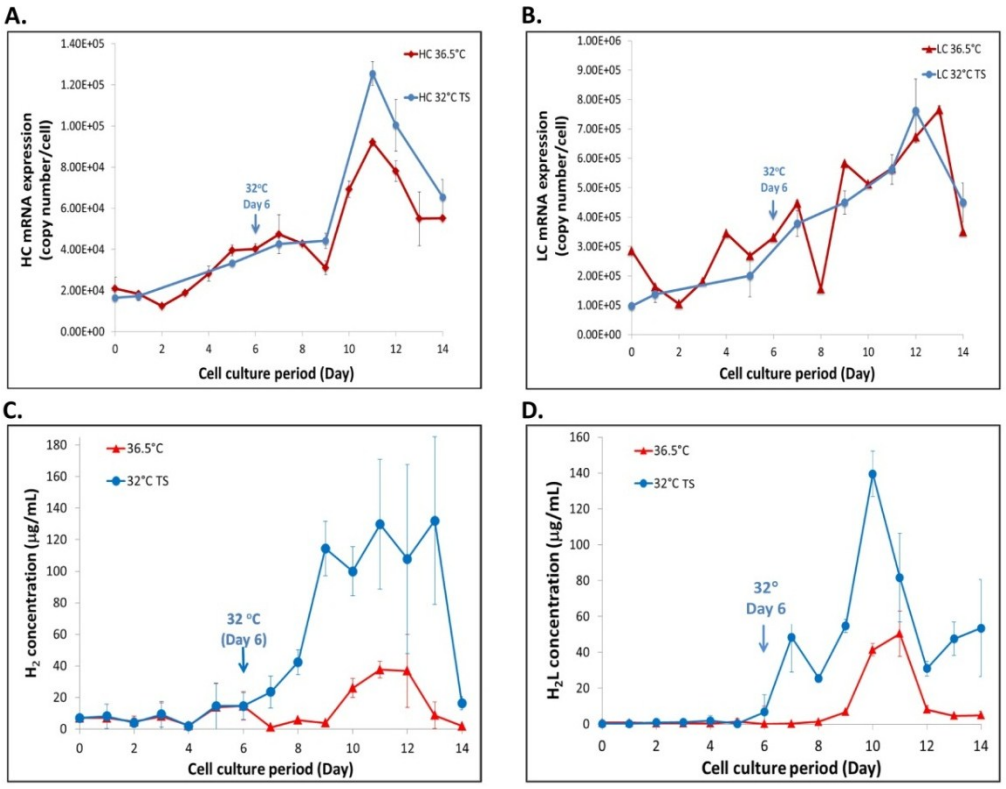

Figure 17. Concentration profiles of heavy (A) and light chain (B) mRNA and H2 (C), H2L (D) intracellular assembly intermediates of IgG molecules at 36.5°C and 32°C TS. Results were average measurements at 36.5°C (n=6) and 32°C TS (n=3). The error bars represent the standard deviation of the samples. TS: Temperature shift.

Table 9. Overview of heavy and light chain mRNA stability at 36.5°C and with temperature shifted to 32°C on day 6.

Species	Rate of decay (h^{-1})	
	36.5 °C	32 °C (Day 6)
HC mRNA	4.7×10^{-2} ($\pm 5.9 \times 10^{-5}$)	4.0×10^{-2} ($\pm 2.3 \times 10^{-4}$)
LC mRNA	5.9×10^{-3} ($\pm 4.7 \times 10^{-5}$)	4.6×10^{-3} ($\pm 3.8 \times 10^{-4}$)

4.2.2. The impact of mild hypothermia on NSD synthesis and mAb glycosylation

To evaluate product quality, the final secreted mAb Fc-glycan profile was analyzed on days 8, 10, 12 and 14 for both temperatures using the LabChip method described in Chaper 3. With respect to

time, the terminal glycan structures observed in harvest products are comparable to those on days 8, 10 and 12. With mild hypothermia, alongside the increase in mAb protein titre, we observe a significant increase in the proportion of IgG molecules with underprocessed glycan structures, with approximately 3% and 17% increase in G0 and G0F, respectively and 15% and 3% reduction in G1F and G2F, respectively on day 12 (Figure 18 A).

At cellular level, the rate of mAb galactosylation is determined. In good agreement with the phenotypic quality of the secreted mAb, Figure 18 B suggests that the rate of mAb galactosylation per cell per day is significantly lower at 32°C, with an average of 35% reduction in the addition rate of galactose residues on each assembled mAb molecule.

A.

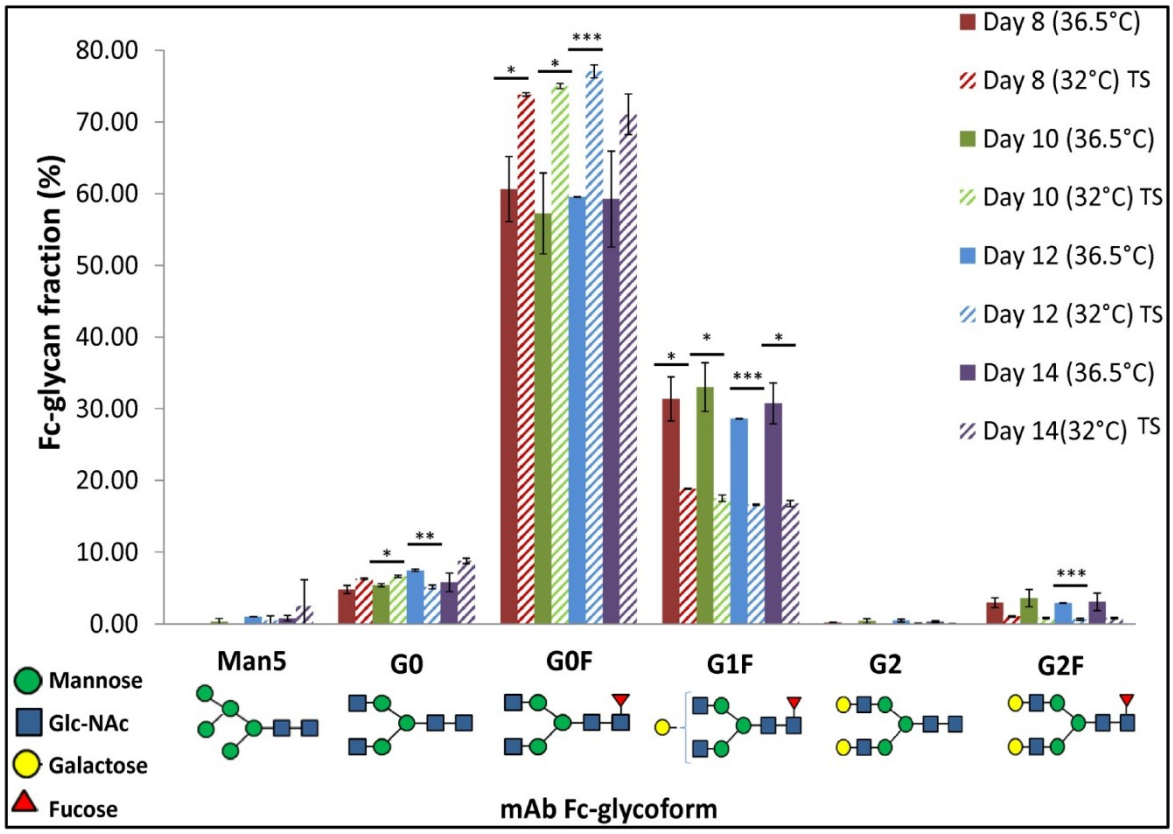

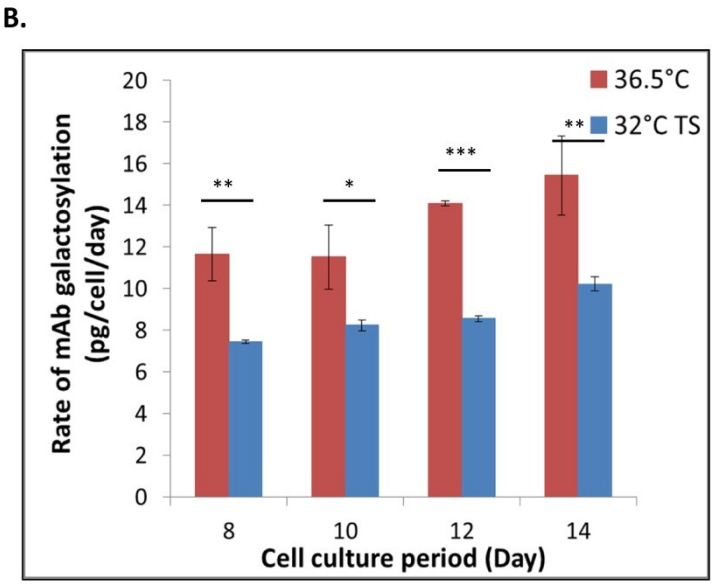

Figure 18. Glycan profile of the secreted IgG. (A). Fractions of 6 glycan structures: Man5, G0, G0F, G1F, G2 and G2F on the secreted IgG products were determined. (B). Rate of mAb galactosylation. Results were average measurements at 36.5°C (n=6) and 32°C (n=3). The error bars represent the standard deviation of the samples. Statistical significance was calculated using a Student's t-test and was represented by: *$p \leq 0.05$(*), $p \leq 0.01$(**) and $p \leq 0.001$(***)*. TS: Temperature shift.

Murrell et al. (2004) demonstrated the complexity of the intracellular NSD synthetic pathway, where the type of sugar source (glucose, galactose, mannose etc.) and the uptake rate affected the production of nucleotide sugars (Figure 4, Chapter 2), building components for protein glycosylation. The availability of glutamine in the system is also critical for nucleotide synthesis. Quantification of the intracellular NSD concentrations is therefore necessary to understand the relationship between CHO cell metabolism and product glycosylation. UDP-Glc is essential in the initiation of N-linked glycosylation due to its role in the generation of the dolichol-linked precursor oligosaccharide ($GlcNAc_2Man_9Glc_3$) in the ER lumen. The intracellular concentration of UDP-Glc remains similar at exponential phase. However, due in part to reduced consumption of glucose during mild hypothermia, the amounts of UDP-Glc, UDP-Gal and UDP-GlcNAc (essential for glycan branching and elongation) within the cells largely decrease upon temperature shift (Figures 19 A-C). The sudden increase in UDP-Gal on day 14 however, could have resulted from the conversion of UDP-Glc, which exhibits a concomitant decrease. Despite the useful analysis described above, fluctuating levels of UDP-Gal and substantial number of non-detected data points in Figure 19 C reduces the confidence of the data. It is therefore not appropriate to rely solely on the data in Figure 19 and an alternative analysis of cell metabolic distribution by flux balance analysis is examined later in this chapter.

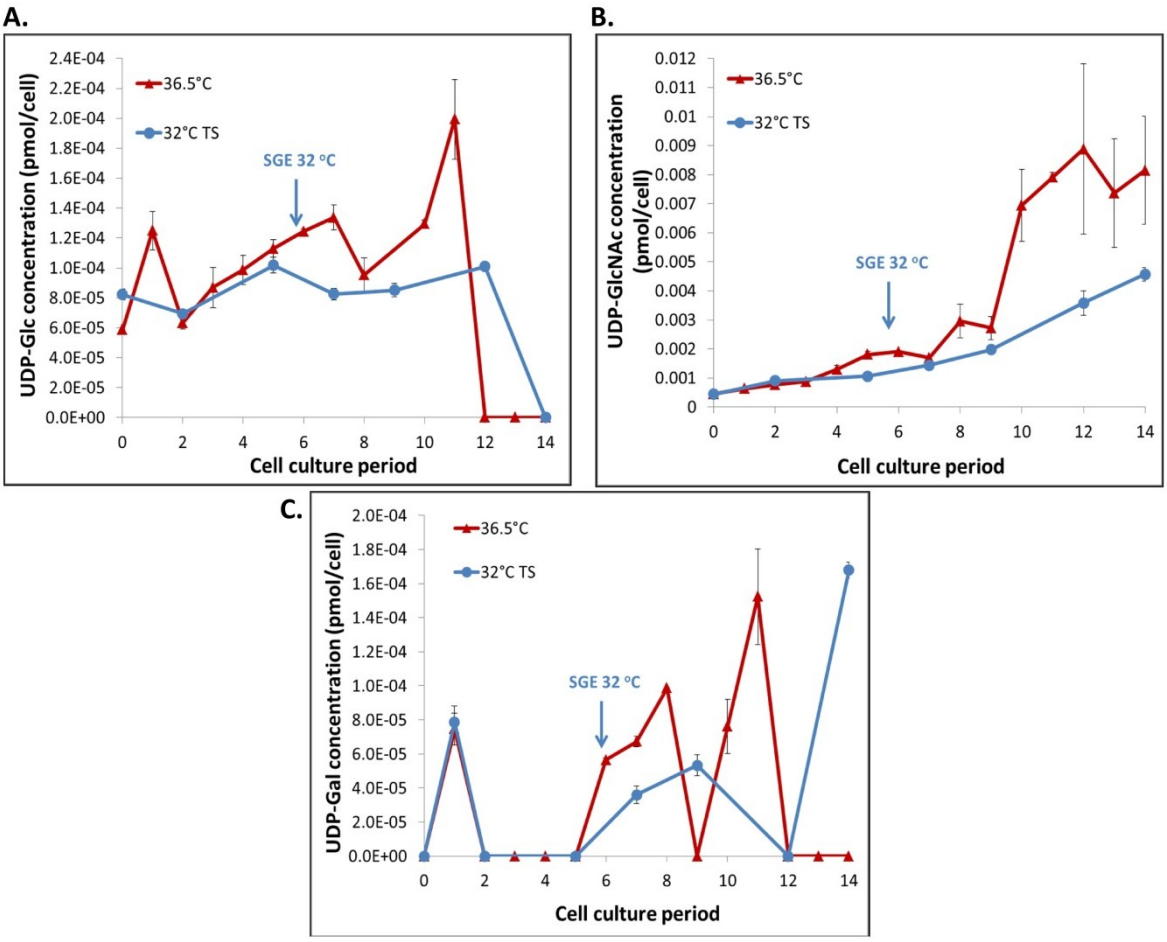

Figure 19. NSD profiles of the secreted IgG. Concentrations of UDP-Glc (A), UDP-GlcNAc (B) and UDP-Gal (C) were measured experimentally. Results were average measurements at 36.5°C (n=6) and 32°C (n=3). The error bars represent the standard deviation of the samples. Any values that are under detection limit of the HPLC method decribed in Chapter 3 are regarded as 0.0. Statistical significance was calculated using a Student's t-test and was represented by: *$p \leq 0.05$(*), $p \leq 0.01$(**) and $p \leq 0.001$(***)*. TS: Temperature shift.

4.2.3. Impact of mild hypothermia on expression of genes related to N-glycosylation

From the glycan analysis we observe a decrease in the galactosylated glycan structures in the secreted mAb produced at 32°C. In addition to cell metabolic adjustments induced by mild hypothermia, which affects the availability of key NSDs for glycoform formation, the expression of the glycosyltransferases that perform the glycan processing can also be a contributing factor to glycan alternation. A number of studies have reported changes in the host cell proteome upon sub-physiological temperature culturing (Underhill and Smales (2007); Baik et al. (2006); Dietmair et al. (2012)), including changes to ER chaperone levels, metabolism, and transport. It is therefore

worthwhile to examine the effect of mild hypothermia on the expression of proteins involved in N-linked glycosylation. In this chapter we investigated the mRNA expression levels of 6 NSD glycosyltransferase enzymes, namely 2 N-acetylglucosaminyltransferases (GnTI and GnTII), which are involved in glycan branching, 3 galactosyltransferases (β-GalTI, II and III) and fucosyltransferase (FucT). In addition, we examined the mRNA expression levels of 2 transporters for UDP-Gal and UDP-GlcNAc, which are responsible for exchange of their respective NSDs between the Golgi apparatus and the cell cytosol. Figure 20 describes the transcript expression profiles at both temperatures. The glycosyltransferases GnTII, β-GalTI, β-GalTIII, and FucT show significantly lower mRNA expression levels at 32°C. Significant decreases in the transcript level of GnTII at 32°C shows that under stable gene expression, formation of bi-antennary glycan structures could be limited by the reduced culture temperature. On the other hand, GnTI, β-GalTII and the two transporters examined do not show major variation in their expression levels, apart from a drop in mRNA level of UDP-GlcNAc transporter at day 14 of the cultures subjected to mild hypothermia.

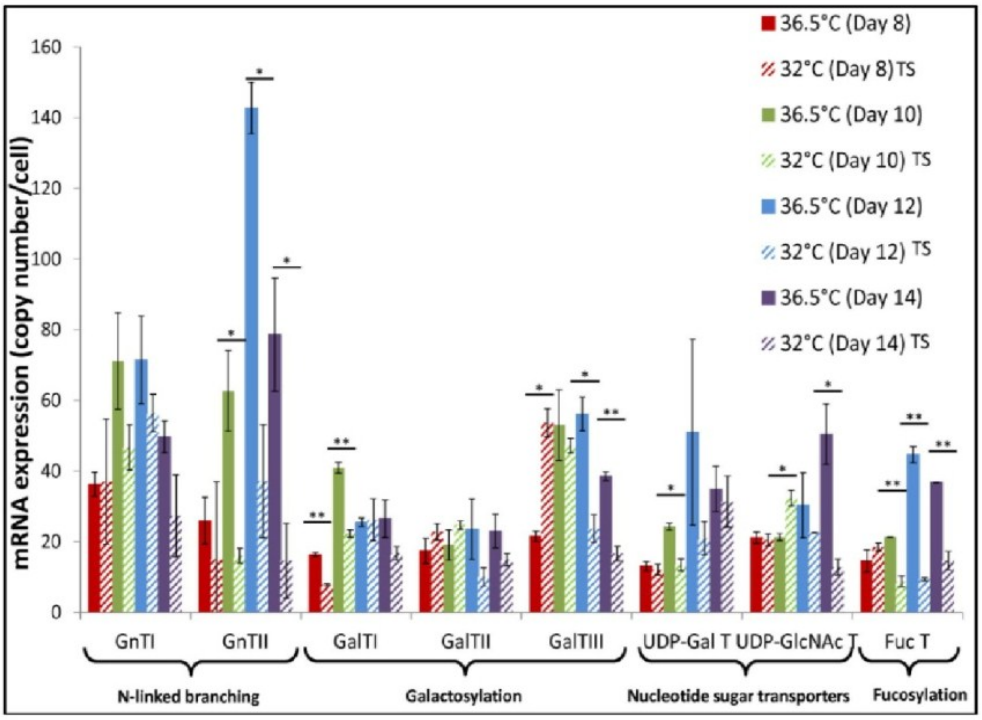

Figure 20. Expression profile of the enzymes involved in N-linked glycosylation. Results were average measurements at 36.5°C (n=6) and 32°C (n=3). The error bars represent the standard deviation of the samples. Statistical significance was calculated using a Student's t-test and was represented by: *p≤0.05(*), p≤0.01(**) and p≤0.001(***)*.TS: Temperature shift.

Within all three GalT enzymes examined in this chapter, GalTIII appears to be most affected by mild hypothermia. As a result, protein expression of GalTIII was further examined. Our results show that the downregulation of the β-GalTIII gene expression observed at 32°C is further supported

by the reduction in β-1,4-GalT-III protein expression in cells cultured in mild hypothermic condition (Figure 21). The increase in β-GalTIII protein on day 14 could be in response to the rise in UDP-Gal within the cells (Figure 19 C). Despite observing decreases in the protein expression of GalTIII, in this case we cannot be absolutely certain that it is entirely GalTIII that catalyses the addition of galactose residues and the expression levels of GalTI and GalTII should also be included in future experiments.

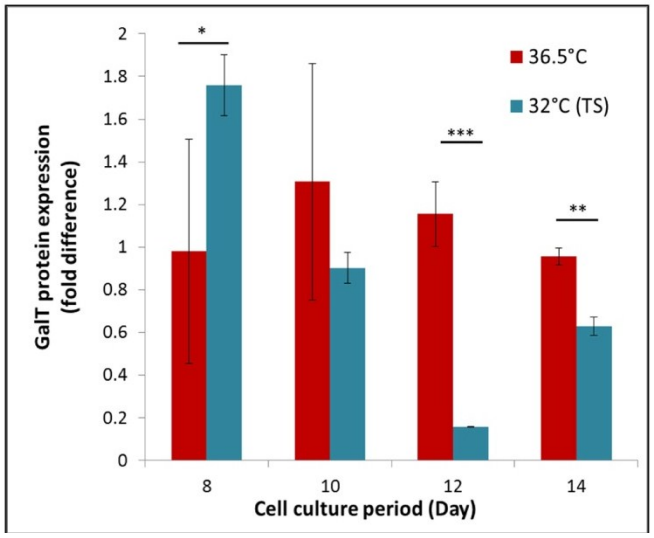

Figure 21. The relative difference in galactosyltransferase III (β-GalTIII) protein expression. Results were average measurements at 36.5°C (n=6) and 32°C (n=3). The error bars represent the standard deviation of the samples. Statistical significance was calculated using a Student's t-test and was represented by: *p≤0.05(*), p≤0.01(**) and p≤0.001(***)*.TS: Temperature shift.

4.2.4. The impact of mild hypothermia on CHO cell metabolism through FBA and experimental studies

Prompted by the reduction in NSD availability observed at 32°C and the low reliability of the experimentally determined UDP-Gal data, FBA was applied to understand how lower culture temperature impacted CHO cell metabolism. Prior to performing the FBA, the consumption and production rates of each exometabolite were calculated with the rate calculation code of Kyriakopoulos (2014). Table 10 shows the calculated production and consumption rates of each exometabolite during the exponential and stationary phase at both temperatures. The overall amino acid and glucose exchanges from the extracellular environment are higher at exponential than at stationary phase. By comparing the two temperatures at stationary phase, we can see reductions in the consumption rates of most metabolites at 32°C, including amino acids isoleucine, leucine and valine

in which approximately 50% reduction in their consumption rates are observed. Also, a shift from lactate production to consumption is suggested, which correlates well with experimental data. The rate of IgG production is also higher at 32°C. In addition, the increase consumption rate of ammonia at 32°C corresponds well to the increase production of glutamine. The FBA was then constrained with the rates of exometabolites, maximum q_{mab} and growth rate (μ) during exponential (days 3-6) growth and maximum q_{mab} and exometabolite uptake/production rates only at late exponential/stationary phase (days 7-10).

Table 10. Average specific metabolic production and consumption rates for 36.5°C and with temperature shifted to 32°C on day 6. Average rates were calculated from n=6 and n=3 at 36.5°C and with temperature shift, respectively.

	Consumption/production rate (femtomol/cell/day)						% difference
	Exponential phase[1]		Stationary phase[2]				
	36.5°C		36.5°C		32°C (TS[3])		
	VALUE	STDEV	VALUE	STDEV	VALUE	STDEV	32°C vs 36.5°C
Ala	**196.2**	12.2	**110.7**	28.8	**15.1**	3.1	**-86.3**
Amm	**-8.5**	9.9	**-1.7**	10.2	**-60.3**	1.4	**3549.8**
Arg	**-38.9**	5.1	**-13.3**	5.5	**-20.9**	2.4	**57.1**
Asn	**-175.9**	10.2	**-50.0**	3.5	**-72.6**	4.1	**45.1**
Asp	**-186.8**	18.1	**-158.3**	12.0	**-122.9**	6.8	**-22.3**
Glc	**-696.0**	245.4	**-545.1**	83.8	**-268.9**	49.0	**-50.7**
Gln	**17.5**	5.6	**43.3**	5.1	**149.0**	1.4	**244.2**
Glu	**-33.5**	3.7	**-21.4**	3.3	**-11.8**	1.8	**-44.8**
Gly	**29.8**	7.5	**27.8**	8.1	**22.5**	0.8	**-19.1**
His	**-14.3**	3.0	**-4.2**	3.9	**-5.4**	2.2	**28.9**
Ile	**-53.9**	8.1	**-33.7**	8.1	**-13.3**	5.4	**-60.6**
Lac	**82.2**	76.5	**-109.8**	61.8	**-321.6**	7.9	**192.9**
Leu	**-117.9**	14.8	**-75.6**	15.1	**-33.0**	6.3	**-56.3**
Lys	**-59.6**	8.7	**-20.9**	9.9	**-36.4**	5.3	**74.0**
Met	**-15.9**	2.3	**-5.8**	2.5	**-4.9**	2.0	**-15.9**
Phe	**-26.1**	3.6	**-10.2**	3.8	**-8.4**	2.2	**-17.4**
Pro	**-43.5**	4.6	**-17.9**	6.1	**-21.3**	4.1	**18.5**
Ser	**-162.2**	14.8	**-58.4**	13.9	**-63.4**	5.7	**8.5**
Thr	**-42.5**	6.1	**-18.0**	7.3	**-11.1**	4.0	**-38.4**
Trp	**-9.2**	2.0	**-3.7**	2.3	**-2.6**	2.0	**-28.8**
Tyr	**-34.0**	3.8	**-12.4**	3.3	**-8.3**	2.1	**-33.5**
Val	**-74.6**	9.1	**-44.1**	10.3	**-26.5**	4.9	**-39.9**
IgG	**15.5**	0.7	**7.7**	1.7	**12.8**	1.0	**67.0**
	Specific growth rate (day^{-1})						
μ	**0.3**	0.0	**0.02**	0.0	**0.0**	0.0	**-100.0**

[1]Exponential phase: day 3-6. [2]Stationary phase: day 7-10. [3]TS: Temperature shift.
Negative value: consumption. Positive value: production.
Red: % increase in species at 32°C. Black: % decrease in species at 32°C.

Results from the FBA (Figure 22) show that during exponential growth, the flux of glucose entering the TCA cycle through glycolysis is less than that during stationary phase, when there is

increased storage of carbon as glycogen. There are also higher fluxes from the TCA cycle into biomass, IgG, amino acid and energy generation to sustain exponential cell growth. At 36.5°C, the flux of glucose from glycolysis to the TCA cycle during stationary phase increases and the TCA cycle is more efficient, with reduced flow of species toward biomass/IgG production. However upon mild hypothermia, lactate becomes the main fuel for the TCA cycle, with no carbon loss to glycogen production. This metabolic shift from glucose to lactate is supported by the dramatic drop in extracellular lactate concentration observed experimentally (Figure 23 B).

While most of the product generated from glycolysis is consumed within the TCA cycle at 36.5°C, at 32°C less energy is spent on the TCA cycle and the consumption of glutamate is higher (Figure 23 D). Glutamate fluxes towards glutamine and aspartate syntheses increases with mild hypothermia, which contributed to the increase in IgG production. Moreover, the conversion rate from glucose-6-phosphate into ribulose-5-phosphate (R5P) and NADPH is 21 times lower at 32°C. This contributes to reduced synthetic rates of nucleotide, NSD and lipids. Table 11 illustrates the lower fluxes of carbon and energy sources entering all the three synthetic pathways at 32°C, accompanied by increased production of glutamine and a high exchange rate of glutamine from the cell cytosol to the extracellular environment. In addition, the synthesis of UDP-N-acetylhexosamine (UDP-GlcNAc, UDP-GalNAc) requires glutamine and a reduced flux of glutamine into nucleotide/NSD synthesis is suggested by the FBA, which can explain the decrease in UDP-GlcNAc concentration measured experimentally.

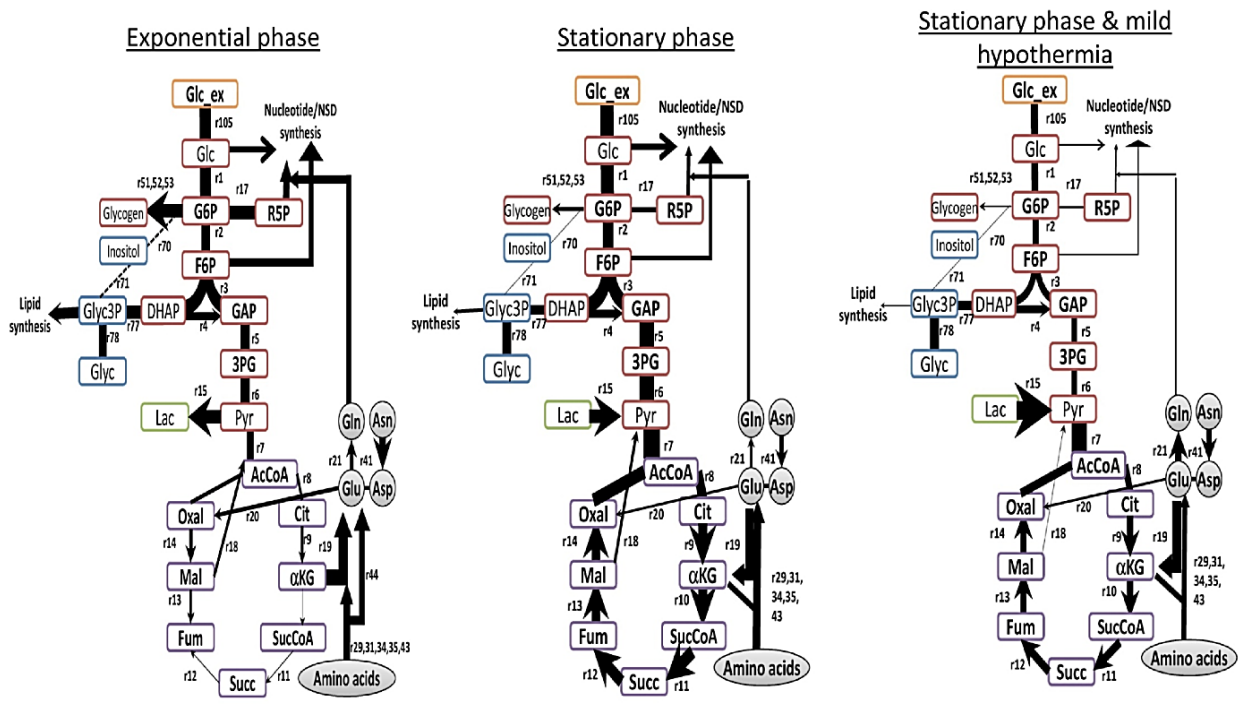

Figure 22. Central carbon metabolism of CHO cells at exponential growth (days 3-6), stationary phase (days 7-10) at 36.5°C and stationary phase coupled with mild hypothermia. Thickness of an arrow indicates the relative flux within the system. This is simplified to include carbon lost to glycerol, glycogen and lactate production, together with nucleotide, NSD, lipid and key amino acid synthesis.

Table 11. FBA estimated flux values in nucleotide synthesis, lipid synthesis and protein glycosylation during stationary phase at 36.5°C and 32°C.

Reaction	Equation		Subsystem	Flux value (femtomol/cell/day)		
				36.5°C (Day 3-6)	36.5°C (Day7-10)	32°C (Day7-10)
54	[c] : R5P + ATP --> PRPP + AMP	Irreversible	Nucleotide	50.34	6.26	0.30
55	[c] : PRPP + (2) Gln + Gly + Asp + (5) ATP + CO2 + (2) N10FTHF --> IMP + (2) Glu + Fum + (5) ADP + (2) THF	Irreversible	Nucleotide	8.00	1.00	0.00
56	[c] : IMP + Asp + GTP --> AMPRN + Fum + GDP	Irreversible	Nucleotide	4.72	0.59	0.00
57	[c] : IMP + Gln + ATP + NAD --> GMPRN + Glu + AMP + NADH	Irreversible	Nucleotide	3.27	0.41	0.00
58	[c] : HCO3 + NH4 + Asp + (2) ATP + NAD --> Orotate + (2) ADP + NADH	Irreversible	Nucleotide	42.34	5.26	0.30
59	[c] : Orotate + PRPP --> UMPRN + CO2	Irreversible	Nucleotide	42.34	5.26	0.30
60	[c] : UMPRN + Gln + ATP --> CMPRN + Glu + ADP	Irreversible	Nucleotide	3.43	0.43	0.00
61	[c] : AMPRN --> dAMP	Irreversible	Nucleotide	1.19	0.15	0.00
62	[c] : GMPRN --> dGMP	Irreversible	Nucleotide	0.89	0.11	0.00
63	[c] : CMPRN --> dCMP	Irreversible	Nucleotide	0.85	0.11	0.00
64	[c] : UMPRN --> dTMP	Irreversible	Nucleotide	1.18	0.15	0.00
65	[c] : Choline + ATP --> Pcholine + ADP	Irreversible	Lipid	6.76	2.77	2.63
66	[c] : Pcholine + (18) AcCoA + Glyc3P + (22) ATP + (33) NADH --> PC + (16) ADP + (6) AMP + (33) NAD + (18) CoASH	Irreversible	Lipid	5.27	0.66	0.00
67	[c] : PC + Ser <==> PS + Choline	Reversible	Lipid	1.55	0.19	0.00
68	[c] : PS --> PE + CO2	Irreversible	Lipid	1.41	0.18	0.00
69	[c] : Choline + Glyc3P <==> Glyc3PC	Reversible	Lipid	3.53	3.53	3.53
70	[c] : G6P --> Inositol	Irreversible	Lipid	0.51	0.06	0.00
71	[c] : Inositol + (18) AcCoA + Glyc3P + (22) ATP + (33) NADH --> PI + (16) ADP + (6) AMP + (33) NAD + (18) CoASH	Irreversible	Lipid	0.51	0.06	0.00
72	[c] : (18) AcCoA + (2) Glyc3P + (22) ATP + (33) NADH --> PG + (16) ADP + (6) AMP + (33) NAD + (18) CoASH	Irreversible	Lipid	0.45	0.06	0.00
73	[c] : (2) PG --> DPG + Glyc	Irreversible	Lipid	0.19	0.02	0.00
74	[c] : (16) AcCoA + Ser + Choline + (16) ATP + (29) NADPH --> SM + (2) CO2 + (14) ADP + (2) AMP + (29) NADP + (16) CoASH	Irreversible	Lipid	0.44	0.06	0.00
75	[c] : (18) AcCoA + (18) ATP + (14) NADPH --> Cholesterol + (9) CO2 + (18) ADP + (14) NADP + (18) CoASH	Irreversible	Lipid	0.98	0.12	0.00
79	[c] : UDPG <==> UDPGal	Reversible	Glycosylation	3.93	0.46	0.30
80	[c] : Glc + ATP + GTP --> GDPMann + ADP	Irreversible	Glycosylation	8.45	1.17	0.61
81	[c] : F6P + Gln + AcCoA + UTP --> UDPNAG + Glu + CoASH	Irreversible	Glycosylation	8.29	1.53	0.76
82	[c] : UDPNAG + ATP + 3PG + CTP --> CMPNeu5Ac + UDP + ADP	Irreversible	Glycosylation	0.98	0.07	0.00
83	[c] : GDPMann + NADPH --> GDPFuc + NADP	Irreversible	Glycosylation	0.79	0.28	0.15
84	[c] : UDPNAG <==> UDP + GlcNAc	Reversible	Glycosylation	5.00	0.78	0.00
85	[c] : UDPNAG <==> UDPGalNAc	Reversible	Glycosylation	1.42	0.18	0.00
86	[c] : UDPGalNAc <==> GalNAc + UDP	Reversible	Glycosylation	1.42	0.18	0.00
87	[c] : GDPMann <==> Mann + GDP	Reversible	Glycosylation	7.13	0.58	0.00
88	[c] : UDPGal <==> Gal + UDP	Reversible	Glycosylation	3.58	0.25	0.00
89	[c] : CMPNeu5Ac <==> CMP + Neu5Ac	Reversible	Glycosylation	0.60	0.07	0.00
90	[c] : GDPFuc <==> GDP + Fuc	Reversible	Glycosylation	0.61	0.18	0.00

On the other hand through experiments, CHO cells were shown to be metabolically less active when the temperature was lowered to 32°C at late exponential phase. Glucose is the main carbon source in the cultures and at 32°C we observe a reduction in glucose consumption, reflected by the higher extracellular glucose concentration in Figure 23 A. This coincides with the estimation from the FBA where less glucose enters into glycolysis. On the other hand, an increase in extracellular ammonia concentration is measured upon temperature shift (days 6 - 10), but this levels out at 36.5°C on day 10, when most ammonia is consumed to generate glutamine (Figure 23 C).

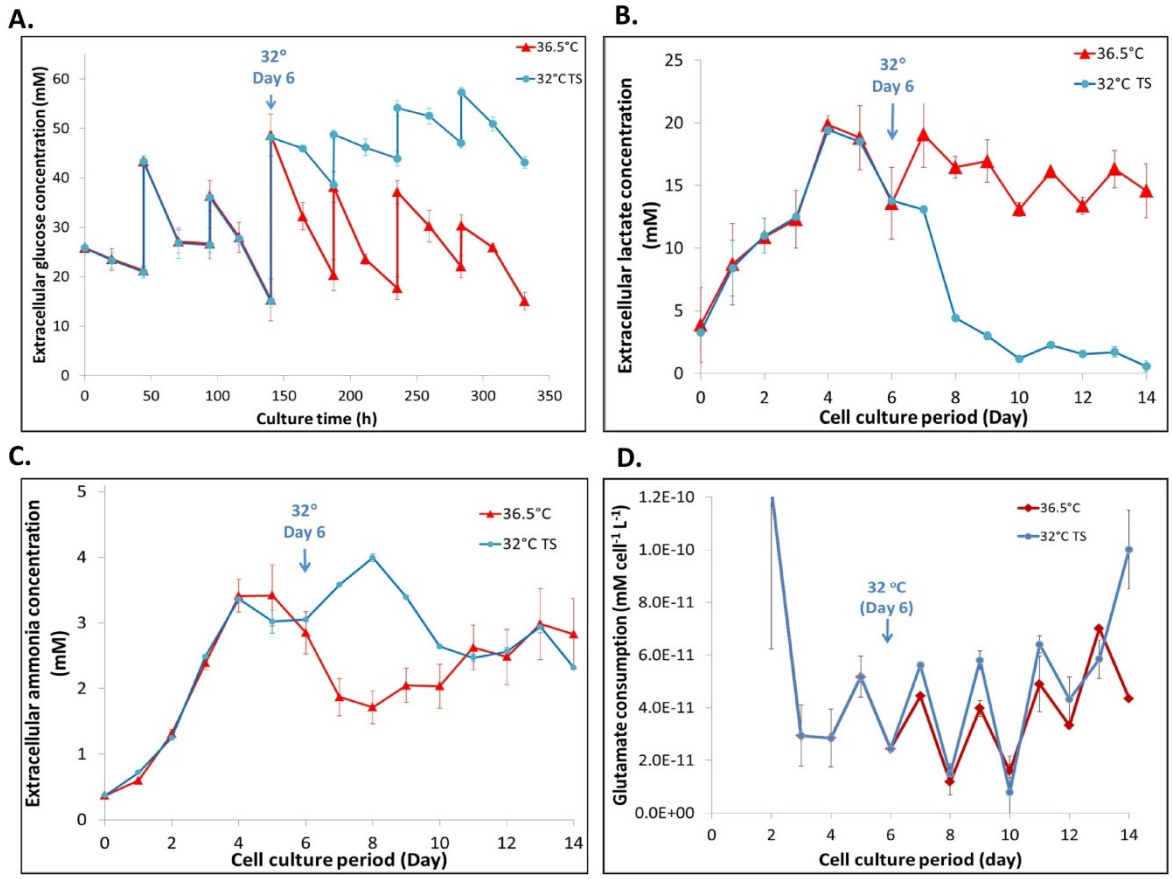

Figure 23. An overview of extracellular metabolite concentrations. Concentration profiles of extracellular glucose (A), lactate (B), ammonia (C) and glutamate consumption profile (D) when CHO cells were culture at 36.5°C or under mild hypothermia at 32°C introduced on day 6. Results were average measurements at 36.5°C (n=6) and 32°C (n=3). The error bars represent the standard deviation of the samples. TS: Temperature shift.

4.3. Discussion

The adaptation that CHO cells undergo in response to mild hypothermia leads to significant changes in the productivity and the glycoform composition of the mAb. The prolonged cell viability observed in this study could be explained by the work of Marchant et al. (2008), which demonstrated that cells experienced a partial cell cycle arrest upon mild hypothermia. As a result, more energy is generated within the TCA cycle to sustain other intracellular activities, such as mAb protein synthesis and trafficking which promoted recombinant mAb production.

As one would expect at exponential growth, higher proportions of energy and amino acids are consumed for biomass formation, while reduced energy utilization for cell growth is observed at stationary phase. During mild hypothermia, there is an increased net flux of amino acids into IgG

protein synthesis, which is illustrated by a 25% rise in the rate of mAb production. As a result of slower cell metabolism, more energy becomes available to be channelled towards protein production, which could have consequently led to reduced availability for protein glycosylation.

In addition, the reduced consumption of glucose that is experimentally observed is mirrored by a lower influx of extracellular glucose into glycolysis as shown by the FBA, where a metabolic shift to lactate consumption is triggered by the reduced production of NADH. This is to maintain the TCA cycle efficiency during stationary phase. However, the synthesis of nucleotides and nucleotide sugars relies on the availability of glucose and glycolysis species namely glucose-6-phosphate and fructose-6-phosphate, together with R5P generated from the pentose-phosphate pathway, which is fuelled from glycolysis. The reduced metabolic rates in these suggested pathways results in lower synthetic rates of the glycosylation substrates. Moreover, the transcript levels of GnTII, β-GalTs and FucT are shown to be lower under mild hypothermia, accompanied by reduced β-GalT protein expression. Therefore, a decrease in NSD synthesis, particularly UDP-Gal, together with lower glycosyltransferase expression levels limits the production of glycan profiles requiring terminal galactosylation. Given that some previous studies observed no significant effect of mild hypothermia on product glycosylation (Ahn et al. (2008); Bollati-Fogolin et al. (2005); Yoon et al. (2003)), we conclude that the effect of mild hypothermia could be product and/or cell line, as well as bioprocess condition specific. Barb and Prestegard (2011) suggested that lower temperature impacts Fc-N-glycan mobility; this in turn could affect the accessibility of the glycan chain to glycosyltransferases. However, further investigation would be necessary to verify this.

In addition, lipid synthesis relies on availability of G6P, AcCoA and various amino acids. The decrease in lipid synthesis calculated by the FBA is in good agreement with findings from Ahn and Antoniewicz (2012), where higher producing cell lines synthesize fewer lipids. The lower availability of lipids could affect the generation of cell membrane and transport vesicles, which are important for the Golgi apparatus structure and the embedment of NSD transporters and glycosyltransferases on the Golgi membrane to initiate functions.

By combining experimental data with the FBA approach, we can begin to understand the link between the increase in mAb synthesis, the deceleration in cell metabolism and reduced maturation of mAb glycan structures during mild hypothermia. Figure 24 provides a summary of how mAb glycosylation can be influenced in biphasic culture temperature. The decrease in cell metabolism reduces NSD synthesis, which along with lower glycosyltransferase expression (β-GalT in particular) directly impacts the process of protein glycosylation. Under mild hypothermia, a higher proportion of

energy and amino acid consumption is used for product formation rather than NSD synthesis. By exploring this relationship, it may be possible to predict changes in glycan structure based on the effects of different bioprocess conditions on cell metabolism, as well as develop improved feeding strategies and cell line engineering to target specific glycan patterns.

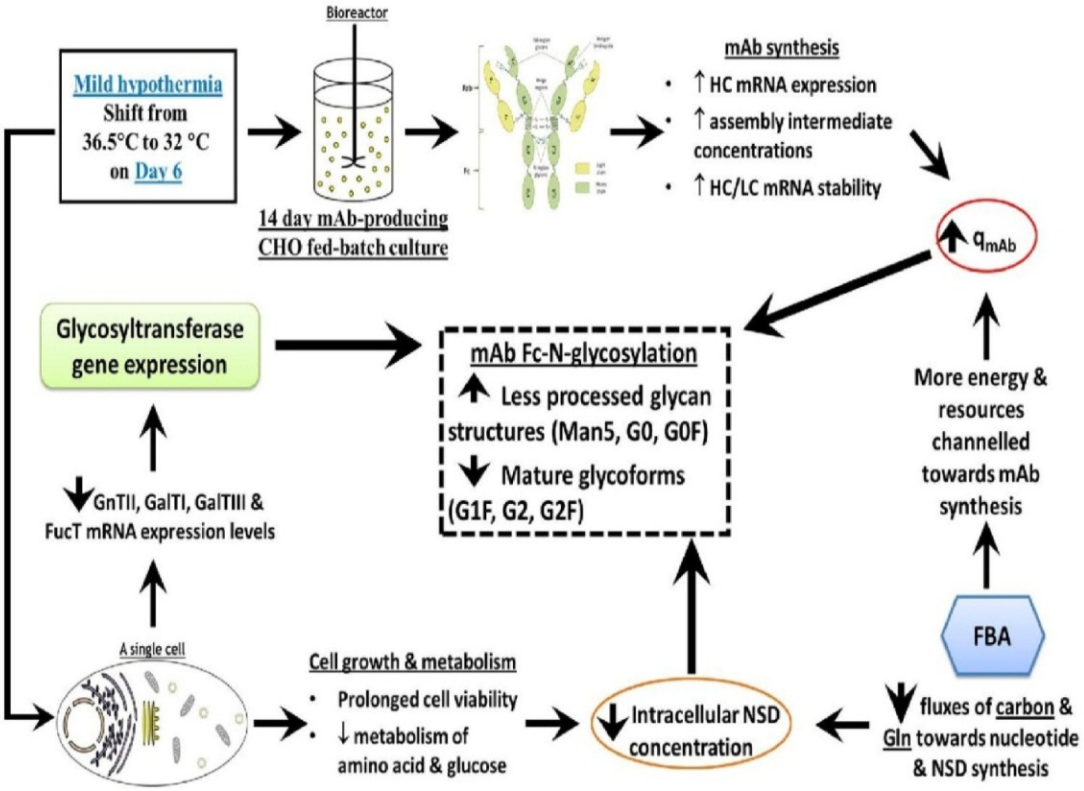

Figure 24. A summary of the impact of mild hypothermia on mAb glycosylation.

4.4. Concluding remarks

By exploring the impact of mild hypothermia on mAb Fc-glycosylation through cell metabolism in this chapter, we observed a counter-balance between mAb production and glycosylation. Mild hypothermic conditions that are introduced at late exponential/early stationary phase resulted in increase in recombinant IgG production, but lower rates of cell metabolism. The product quality, however, is influenced by culture temperature, with a higher fraction of the under-processed glycan structures and a reduced number of terminal galactosylation species found in the secreted IgG produced at 32°C. The relationship between lower cell metabolic rates, an increased IgG

titre and the variation in product glycosylation is better established through the use of the FBA. Calculated fluxomes revealed an overall lower cell metabolism at 32°C during stationary phase, together with decreased fluxes of carbon, energy and glutamine into nucleotide, NSD and lipid syntheses. More energy and metabolites are estimated to contribute to a higher mAb productivity (Yoon et al. 2006), which further limits the amount of resources available for mAb glycosylation. Furthermore, expression levels of key enzymes for N-linked glycan branching and elongation are downregulated, this contributes to the generation of under-processed glycan structures such as G0 and G0F and restricts the addition of terminal galactoses in the secreted product, lowering the efficacy of the IgG molecule. This chapter allows better understanding of the behaviour of CHO cells in mild hypothermic conditions and demonstrated its impact on mAb Fc-glycosylation. The knowledge and findings obtained from this chapter prepare a platform for investigations in later chapters, where a mechanistic approach is used to nail down the fundamental understanding of the effect of mild hypothermia on CHO cells.

Chapter 5
Computational analysis of mAb glycosylation in response to mild hypothermia in stable CHO transfectants

In addition to experimental and flux balance analyses, a defined mathematical model that mechanistically and quantitatively describes CHO cell behaviour and metabolism, mAb synthesis and its N-linked glycosylation profiles before and after the induction of mild hypothermia was constructed. The use of mathematical modelling aims to aid understanding of the way bioprocess conditions affect product quality, estimate biological rates that would be difficult to determine experimentally, and estimate acceptable ranges of process parameters, which will be beneficial for bioprocess design, control and optimisation.

The proposed model consists of four modules that describe CHO cell growth with nutrient metabolism, mAb synthesis, nucleotide sugar donor (NSD) metabolism and mAb Fc glycosylation. Each module is a separate model and they are linked together via common parameters and variables to form a final complex entity that describes mAb Fc N-linked glycoforms. Figure 25 shows each component and its interactions within the complex model, as well as lists of model outputs that link one module to another. In brief, the model commences with the description of CHO cell growth, extracellular nutrient metabolism and mAb synthesis. Parameters estimated for this module are fed into the nucleotide and NSD model (Figure 25), adapted from Jimenez del Val (2013), which describes the NSD synthetic network based on the nutrient (e.g. glucose and glutamine) input from the cell dynamics module. Lastly the outputs from the NSD model listed in Figure 25, are integrated into

the glycan model developed by Jimenez del Val et al. (2011) and to describe N-linked Fc glycan patterns on mAb. This chapter describes the development of the modular model and compared the model outputs between the physiological and mild hypothermia temperatures.

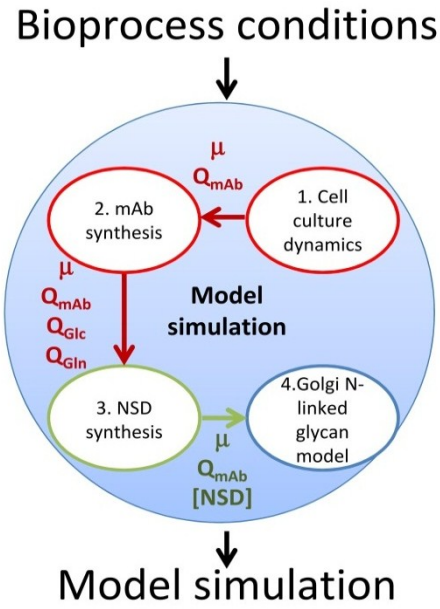

Figure 25. The modularity of the developed mathematical model and the interactions of each individual component within the overall model. Common model parameters that are fed from one module to another are also indicated.

5.1. Cell culture dynamics model

The cell culture dynamics model is modified from previous work on antibody-producing hybridoma cell culture (Kontoravdi et al. 2010a). The first unstructured part describing fed-batch cell culture is constructed based on Monod kinetics; it describes cell growth and death based on the extracellular concentrations of glucose and amino acids, together with metabolic waste such as ammonia and lactate. The process of mAb synthesis, starting from mRNA transcription, polypeptide translation to mAb secretion, is illustrated in the structured part of the model and this synthetic process is described based on the HC_2-LC-LC assembly method.

5.1.1. Cell growth and death

This part of the model comprises of material balances that describe the viable and total cell populations inside a bioreactor. Glucose, lactate and certain amino acids, namely asparagine, aspartate, glutamine, glutamate, arginine, lysine and proline, are assumed to be the key nutrients that determine the specific cell growth rate, while ammonia are the main metabolites that determine the

specific cell death rate. The bioreactor is assumed to be well mixed. The volume of the cell culture is dependent on the inlet and outlet flow rates and can be described as:

$$\frac{dV}{dt} = F_{in,feed} + F_{in,Glc} - F_{out} \quad \text{...Eq. 1}$$

where, V indicates the total culture volume within the reactor and $F_{in,\,feed}$, $F_{in,\,Glc}$, F_{out} are the inlet flow rate of Feed C (CD EfficientFeed™ C AGT™), that of the glucose only feed, and the outlet flow rate of the bioreactor, respectively. The material balance for the viable cell population is:

$$\frac{d(VX_V)}{dt} = \mu V X_v - \mu_d V X_v - F_{out} X_v \quad \text{...Eq. 2}$$

where, X_v is the viable cell density in the bioreactor (*cell/L*) and μ, μ_d are the specific CHO cell growth and death rates (h^{-1}), respectively. The material balance for the total cell population in the bioreactor includes:

$$\frac{d(VX_t)}{dt} = \mu V X_v - K_{lysis}\, V(X_t - X_v) - F_{out} X_t \quad \text{...Eq. 3}$$

where, K_{lysis} describes the specific lysis rate of CHO cells within the bioreactor, while X_t represents the total cell concentration (*cell/L*).

Glucose, lactate and specific amino acids are regarded as the growth limiting factors, while metabolic wastes namely ammonia and lactate serve as the growth inhibiting factors. Owing to the absence of glutamine in the media and feeds, glutamine is not considered to be growth-limiting. Monod type kinetics is used to determine the specific growth rate (μ) using the following equations:

$$\mu = \mu_{max} f_{lim}\, f_{inh} \quad \text{...Eq. 4}$$

where, μ_{max} is the maximum specific growth rate (h^{-1}) and $f_{lim,}\, f_{inh}$ are the nutrient limitation and product inhibition, respectively. $f_{lim,} f_{inh}$ are defined as:

$$f_{lim} = \left(\frac{[Glc]}{K_{glc} + [Glc]}\right)\left(\frac{[Lac]}{K_{lac} + [Lac]}\right)\left(\frac{[Asn]}{K_{asn} + [Asn]}\right)\left(\frac{[Asp]}{K_{asp} + [Asp]}\right)$$
$$\left(\frac{[Glu]}{K_{glu} + [Glu]}\right)\left(\frac{[Arg]}{K_{Arg} + [Arg]}\right)\left(\frac{[Lys]}{K_{Lys} + [Lys]}\right)\left(\frac{[Pro]}{K_{pro} + [Pro]}\right) \quad \text{...Eq. 5}$$

$$f_{inh} = \left(\frac{KI_{amm}}{KI_{amm} + [Amm]}\right)\left(\frac{KI_{lac}}{KI_{lac} + [Lac]}\right) \quad \text{...Eq. 6}$$

where, *[Glc], [Lac], [Asn], [Asp], [Glu], [Arg], [Lys], [Pro]* and *[Amm]* represent the extracellular concentrations of glucose, lactate, asparagine, aspartate, glutamate, arginine, lysine, proline and ammonia (*mM*), respectively. $K_{glc,}$ $K_{lac,}$ $K_{asn,}$ $K_{asp,}$ $K_{glu,}$ $K_{arg,}$ $K_{lys,}$ K_{pro} are the Monod constants for growth with respect to glucose, lactate, asparagine, aspartate, glutamate, arginine, lysine and proline (*mM*), respectively, while KI_{amm} and KI_{lac} are the inhibition constants for ammonia and lactate (*mM*), respectively.

Owing to the nature of CHO cells, which consume both glucose and lactate as carbon sources at different points of the culture period, lactate is included as both a limiting and an inhibition factor for growth in equation 5 and 6. In the case of cell death, ammonia is assumed to be the main contributing factor and the specific death rate (μ_d) is described as the equation below:

$$\mu_d = \frac{\mu_{d,max}}{1 + \left(\frac{K_{d,amm}}{[Amm]}\right)} \quad \text{...Eq. 7}$$

where, $\mu_{d,max}$ is the maximum specific death rate (h^{-1}), and $K_{d,amm}$ is the constant for cell death by ammonia (*mM*).

5.1.2. CHO cell metabolism

By assuming perfect mixing, good control of pH, culture temperature and the levels of dissolved oxygen, gases and carbon dioxide within the bioreactor environment, nutrients, namely glucose, lactate and amino acids are the main carbon and nitrogen sources for cell biomass formation, mAb production and other cellular processes such as NSD, lipid and host protein syntheses. The following material balances describe concentrations of nutrients and waste products:

For glucose:

$$\frac{d(V[Glc])}{dt} = q_{glc}X_vV + F_{in,feed}\left[Glc_{in,feed}\right] + F_{in,glc}\left[Glc_{in,glc}\right] - F_{out}[Glc] \quad \text{...Eq. 8}$$

$$q_{glc} = -\frac{\mu}{Y_{x_v,glc}} - m_{glc} \quad \text{...Eq. 9}$$

where, *[Glc], [Glc$_{in,feed}$]* and *[Glc$_{in,glc}$]* represent glucose concentrations in culture medium, inlet glucose concentration in CD EfficientFeed™ C AGT™ and in glucose-only feed, respectively. q_{glc} indicates the specific rate of glucose consumption (*mmol cell^{-1}h^{-1}*), $Y_{x_v,glc}$ is the yield of biomass on glucose (*cell mmol^{-1}*), while m_{glc} is the maintenance coefficient of glucose (*mmol cell^{-1}h^{-1}*) which conceptually represents the consumption of glucose for other metabolic activities that are not cell growth related.

Despite lactate being a by-product from glucose metabolism, it is consumed by cells when they experience a metabolic shift from lactate production to lactate consumption, and serves as an additional carbon source. The lactate concentration and its specific rate of production are shown in the equations below:

$$\frac{d(V[Lac])}{dt} = q_{lac}X_vV - F_{out}[Lac] \quad \text{...Eq. 10}$$

$$q_{lac} = q_{glc}Y_{lac,glc} - \left(\frac{\mu}{Y_{x_v,lac}} + k_{T,[Lac]}[Lac]\right)\left(\frac{[Lac]}{[Lac] + K_{lac}}\right) \quad \text{...Eq. 11}$$

where, q_{lac} is the specific rate of lactate consumption (*mmol cell^{-1}h^{-1}*), $Y_{x_v,lac}$ indicates the yield of biomass on lactate (*cell mmol^{-1}*), $k_{T,[Lac]}$is the Michaelis-Menten constant of lactate transport into the cells from culture medium (*h^{-1}*) and K_{lac} is the Monod constant with respect to lactate.

In equation 11, the term $\left(\frac{[Lac]}{[Lac]+K_{lac}}\right)$ functions as a modulator for lactate production/consumption upon main carbon metabolic shift to lactate during late exponential growth phase. When *[Lac]* > K_{lac}, $\left(\frac{[Lac]}{[Lac]+K_{lac}}\right)$ is close to 1, it encourages lactate consumption. Inversely when *[Lac]* < K_{lac} , K_{lac} dominates the term and the value of $\left(\frac{[Lac]}{[Lac]+K_{lac}}\right)$ is small and thus limits lactate consumption.

In addition to glucose and lactate, amino acids play a significant role in cell maintenance, metabolism and protein production. Amino acid metabolism also contributes to ammonia

accumulation, which in turn impacts cell death. The material balances described below track the concentrations of various amino acids in the bioreactor throughout the culture period. Firstly, for asparagine:

$$\frac{d(V[Asn])}{dt} = q_{asn}X_vV + F_{in,feed}\left[Asn_{in,feed}\right] - F_{out}[Asn] \quad \text{...Eq. 12}$$

$$q_{asn} = -\frac{\mu}{Y_{x_v,asn}} - k_{T,[Asn]}[Asn] \quad \text{...Eq. 13}$$

where, $[Asn_{in,feed}]$ is the concentration of asparagine in CD EfficientFeed™ C AGT™ (mM) and q_{asn} is the specific rate of asparagine consumption ($mmol\ cell^{-1}\ h^{-1}$). $Y_{x_v,asn}$ denotes to the yield of biomass on asparagine ($cell\ mmol^{-1}$), while $k_{T,[Asn]}$ is the constant for asparagine transport into the cells from culture medium (h^{-1}).

Similarly for aspartate:

$$\frac{d(V[Asp])}{dt} = q_{asp}X_vV + F_{in,feed}\left[Asp_{in,feed}\right] - F_{out}[Asp] \quad \text{...Eq. 14}$$

$$q_{asp} = q_{asn}Y_{asp,asn} - \frac{\mu}{Y_{x_v,asp}} \quad \text{...Eq. 15}$$

where, $[Asp_{in,feed}]$ is the concentration of aspartate in CD EfficientFeed™ C AGT™ (mM) and q_{asp} is the specific rate of aspartate consumption ($mmol\ cell^{-1}\ h^{-1}$). $Y_{x_v,asp}$ and $Y_{asp,asn}$ denote the yield of biomass on asparagine ($cell\ mmol^{-1}$) and the yield of aspartate from asparagine ($mmol/mmol$), respectively.

For glutamate:

$$\frac{d(V[Glu])}{dt} = q_{glu}X_vV + F_{in,feed}\left[Glu_{in,feed}\right] - F_{out}[Glu] \quad \text{...Eq. 16}$$

$$q_{glu} = q_{gln}Y_{glu,gln} - q_{glu}Y_{gln,glu} - q_{glu}Y_{arg,glu} - q_{glu}Y_{lys,glu} - q_{glu}Y_{pro,glu} - \frac{\mu}{Y_{x_v,glu}} \quad \text{...Eq. 17}$$

where, $[Glu_{in,feed}]$ is the concentration of glutamate in CD EfficientFeed™ C AGT™ (mM) and q_{glu} is the specific rate of aspartate consumption ($mmol\ cell^{-1}\ h^{-1}$). Some amino acids are consumed to yield other molecules that are essential for cellular processes. To represent this, $Y_{x_v,glu}$, $Y_{glu,gln,}$ $Y_{gln,glu,}$ $Y_{arg,glu.}$ $Y_{lys,glu}$ and $Y_{pro,glu.}$ are used to denote the yield of biomass on glutamate ($cell\ mmol^{-1}$), and the yields of glutamate on glutamine, glutamine on glutamate, arginine on glutamate, lysine on glutamate and proline on glutamate ($mmol/mmol$), respectively.

The material balance for glutamine is given as:

$$\frac{d(V[Gln])}{dt} = q_{gln}X_vV - F_{out}[Gln] \quad \text{...Eq. 18}$$

$$q_{gln} = q_{glu}Y_{gln,glu} - \frac{\mu}{Y_{x_v,gln}} + p_{gln}\left(\frac{[Amm]}{[Amm] + K_{amm,gln}}\right) \quad \text{...Eq. 19}$$

where, q_{gln} is the specific rate of aspartate consumption ($mmol\ cell^{-1}\ h^{-1}$). $Y_{x_v,gln}$ and $Y_{gln,glu}$ denote the yield of biomass on glutamine ($cell\ mmol^{-1}$) and the yield of glutamine from glutamate ($mmol/mmol$), respectively. p_{gln} is the glutamine producing coefficient of ($mmol\ cell^{-1}\ h^{-1}$) and $K_{amm,gln}$ is the Monod constant for ammonia production from glutamine.

In addition, for arginine, lysine and proline we can write the following material balances:

$$\frac{d(V[Arg])}{dt} = q_{arg}X_vV + F_{in,feed}\left[Arg_{in,feed}\right] - F_{out}[Arg] \quad \text{...Eq. 20}$$

$$q_{arg} = q_{glu}Y_{arg,glu} - \frac{\mu}{Y_{x_v,arg}} \quad \text{...Eq. 21}$$

$$\frac{d(V[Lys])}{dt} = q_{lys}X_vV + F_{in,feed}\left[Lys_{in,feed}\right] - F_{out}[Lys] \quad \text{...Eq. 22}$$

$$q_{lys} = q_{glu}Y_{lys,glu} - \frac{\mu}{Y_{x_v,lys}} \quad \text{...Eq. 23}$$

$$\frac{d(V[Pro])}{dt} = q_{pro}X_vV + F_{in,feed}\left[Pro_{in,feed}\right] - F_{out}[Pro] \quad \text{...Eq. 24}$$

$$q_{pro} = q_{glu}Y_{pro,glu} - \frac{\mu}{Y_{x_v,pro}} \quad \text{...Eq. 25}$$

where, $[Arg_{in,feed}]$, $[Lys_{in,feed}]$ and $[Pro_{in,feed}]$ are concentrations of arginine, lysine and proline in CD EfficientFeed™ C AGT™ (mM), respectively. q_{arg}, q_{lys} and q_{pro} are specific rates of arginine, lysine and proline consumption ($mmol\ cell^{-1}\ h^{-1}$). While $Y_{x_v,arg}$, $Y_{x_v,lys}$ and $Y_{x_v,pro}$ denote to the yield of biomass on arginine, lysine and proline ($cell\ mmol^{-1}$).

These amino acids are chosen to be included in this model as they are most significant contributors to ammonia accumulation. Cells produce and consume ammonia to produce asparagine, aspartate, glutamine and glutamate in particular, within cellular metabolic pathways, as illustrated in Figure 26.

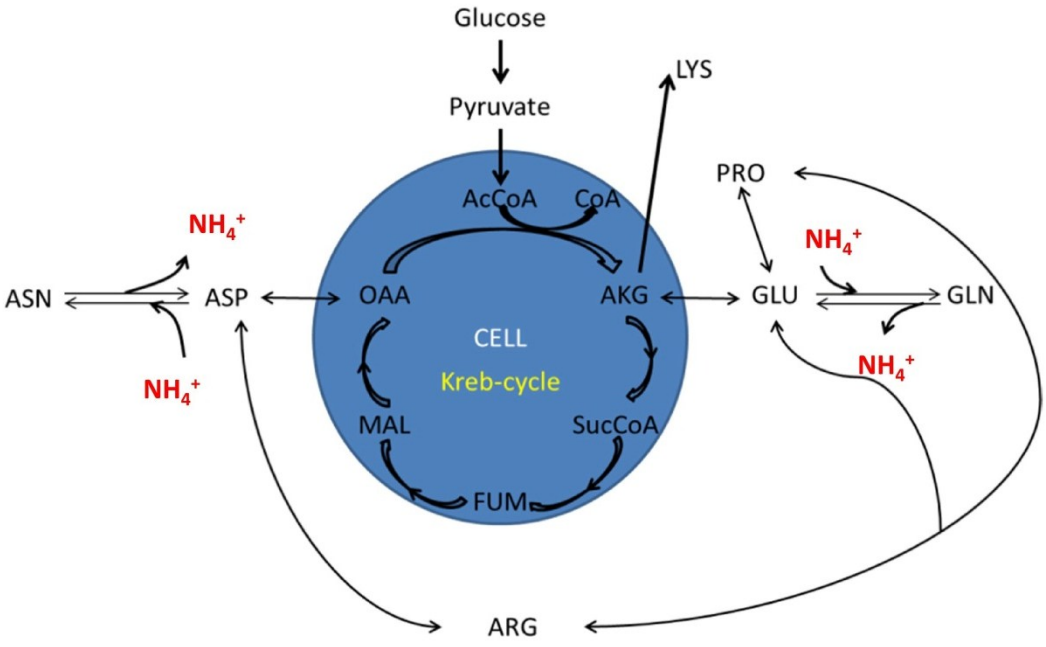

Figure 26. Intracellular metabolic network of various amino acids and their contributions to ammonia metabolism.

According to the network described above, the material balance of extracellular ammonia can be written as:

$$\frac{d(V[Amm])}{dt} = q_{amm}X_vV - F_{out}[Amm] \quad \text{...Eq. 26}$$

$$q_{amm} = -q_{gln} - q_{asn}Y_{asp,asn} - q_{arg} + \frac{\mu}{Y_{x_v,amm}} \quad \text{...Eq. 27}$$

where, q_{amm} and $Y_{x_v,amm}$ represent the specific rate of ammonia production (*mmol cell*$^{-1}$ *h*$^{-1}$) and the yield of viable cells on ammonia, respectively.

5.1.3. mAb synthesis

The third part of this model describes the mAb synthetic process. Given the first two elements of the model are developed in an unstructured manner, a structured model is constructed to describe mAb production based on the transcription and translation of heavy and light chains, as well as the formation of relevant assembly intermediates. It also describes the transport of mAbs from the endoplasmic reticulum (ER), along the Golgi apparatus to the extracellular matrix (ECM) for secretion. Reaction rates in this part of the work are largely based on mass action kinetics. The model assumes the absence of fragmented heavy and light chains, and it follows the HC_2-LC-LC assembly pathway for mAb synthesis (Bibila and Flickinger 1991):

$$HC + HC \leftrightarrow HC_2$$

$$HC_2 + LC \leftrightarrow HC_2LC$$

$$HC_2LC + LC \leftrightarrow HC_2LC_2$$

The material balances for heavy and light chain mRNA production within the ER are defined as:

$$\frac{d[mHC]}{dt} = N_{HC}S_{HC} - Kd_{HC}[mHC] - \mu[mHC] \quad \text{...Eq. 1}$$

$$\frac{d[mLC]}{dt} = N_{LC}S_{LC} - Kd_{LC}[mLC] - \mu[mLC] \quad \text{...Eq. 2}$$

In equation 28 and 29, mRNA production of heavy and light chains (*[mHC]* and *[mLC]*, respectively) are defined based on the heavy and light chain DNA copy numbers N_{HC} and N_{LC} (*gene copy/cell*), the transcription rates of both species S_{HC} and S_{LC} (*mRNA/gene/h*), the rate of cell growth μ and the mRNA decay rates of both chains Kd_{HC} and Kd_{LC} (h^{-1}). In addition, the free intracellular heavy and light chain material balances produced within the ER are defined as:

$$\frac{d[HC]}{dt} = [mHC]T_{HC} + \mu[mHC] - R_{HC} \quad \text{...Eq. 3}$$

$$R_{HC} = \frac{2}{3}K_A[HC]^2 \quad \text{...Eq. 31}$$

$$\frac{d[LC]}{dt} = [mLC]T_{LC} + \mu[mLC] - R_{LC} \quad \text{...Eq. 32}$$

$$R_{LC} = 2K_A[HC_2]\,[LC] + K_A[HC_2L]\,[LC] \quad \text{...Eq. 33}$$

where, *[HC]* and *[LC]* represent the polypeptide concentrations of heavy and light chains (*chain/cell*) These two species are described based on mRNA concentrations of heavy and light chains, translation rates T_{HC} and T_{LC} (*chain/mRNA/h*), rate of cell growth, while R_{HC} and R_{LC} are the rates of heavy and light chain consumption in assembly (*chain/cell/h*). Based on the HC_2-LC-LC mAb assembly sequence, R_{HC} and R_{LC} are defined by the polypeptide concentrations and K_A, which indicates the assembly rate constant (*molecule/cell/h*).

Similarly, the intracellular ER balances are performed on the assembly intermediates as:

$$\frac{d[HC_2]}{dt} = \frac{1}{3}K_A[HC_2] - 2K_A[HC_2][LC] - \mu[HC_2] \quad \text{...Eq. 4}$$

$$\frac{d[HC_2LC]}{dt} = 2K_A[HC_2][LC] - K_A[HC_2LC][LC] - \mu[HC_2LC] \quad \text{...Eq. 35}$$

where, *[HC_2], [HC_2LC]* are the concentrations of the assembly intermediates in the ER (*molecule/cell*).

Fully assembled mAb molecules pass along the ER and the Golgi apparatus as $[HC_2LC_2]_{ER}$ and $[HC_2LC_2]_G$ (*molecule/cell*) respectively, for post-translational modification. Their material balances can be defined as:

$$\frac{d[HC_2LC_2]_{ER}}{dt} = K_A[HC_2L][LC] - K_{ER}[HC_2LC_2]_{ER} - \mu[HC_2LC_2]_{ER} \quad \text{...Eq. 5}$$

$$\frac{d[HC_2LC_2]_G}{dt} = \varepsilon_1 K_{ER}[HC_2LC_2]_{ER} - K_G[HC_2LC_2]_G - \mu[HC_2LC_2]_G \quad \text{...Eq. 37}$$

where, K_{ER} and K_G are rate constants for ER-to-Golgi antibody transport and Golgi-to-ECM antibody transport (h^{-1}), respectively, while ε_1 dictates the ER glycosylation efficiency factor (dimensionless).

Upon successful post-translational modification, fully assembled mAb molecules are secreted into the ECM and expressed as *[mAb]* and the material balance is described as:

$$\frac{d[mAb]\,V}{dt} = q_{mAb}X_v V - F_{out}[mAb] \quad \text{...Eq. 6}$$

$$q_{mAb} = Y_{mAb,\mu}\,\varepsilon_2 \lambda K_G[HC_2LC_2]_G \quad \text{...Eq. 39}$$

where, q_{mAb} is the specific mAb production rate (*mg/cell/h*), λ is the molecular weight of mAb (*g/mol*), and ε_2 is the Golgi glycosylation efficiency factor. $Y_{mAb,\mu}$ refers to the yield of mAb product under a given cell growth rate ($mg\ h^{-1}$).

A feeding time schedule is included in this model to represent the 10% v/v commercial CD EfficientFeed™ C AGT™ feed and glucose only feed (a full time schedule can be found in the Appendix II Table 1). By incorporating X_v and μ in equations 28 to 39, it becomes possible to capture the synthetic network of mAb based on the cellular behaviours, while detailed material balances from mRNA transcription, to polypeptide translation and product transport enable estimations of parameters such as product assembly and secretion rates that would otherwise be difficult to determine experimentally.

5.2. Nucleotide and NSD metabolic model

In order to relate extracellular conditions to intracellular NSD metabolism, the current cell dynamic model is limited and a new extension of the model is required. The computational outputs from the cell dynamic model are implemented in a NSD model, previously developed by Dr Ioscani Jimenez del Val, is based on simple Michaelis-Menten saturation kinetics (Jimenez del Val 2013). In brief, this NSD model is constructed based on the assumption that glucose and glutamine are the only nutrient supporting the NSD synthetic pathway. This model does not account for every reaction within the NSD pathway; synthetic pathways of each NSD species are lumped together in a way that only rate-limiting pathways are being considered, as illustrated in Figure 27. This model accounts for 9 species within the NSD metabolic network, namely Glc_{int}, Gln_{int}, UDP-GlcNAc, UDP-Glc, GDP-Man, UDP-GalNAc, CMP-Neu5Ac, UDP-Gal, GDP-Fuc. The NSD model presented in this Chapter is adapted from that described above (Jimenez del Val 2013) with most of the material balances remaining unchanged. The following features have been added:

1. A glutamine synthesis term incorporated in the intracellular gluctamine material balance to account for the nature of the GS-CHO cell line.

2. Material balances for four nucleotides: ATP, UTP, CTP and GTP.

3. Terms for NSD production from nucleotides in the rate of NSD synthesis (r_{NSD}).

4. Within each of the NSD transport term ($F_{out,NSD}$), and consumption terms for host cell glycan structures, where the previous model only accounted for NSD consumption for antibody product glycosylation.

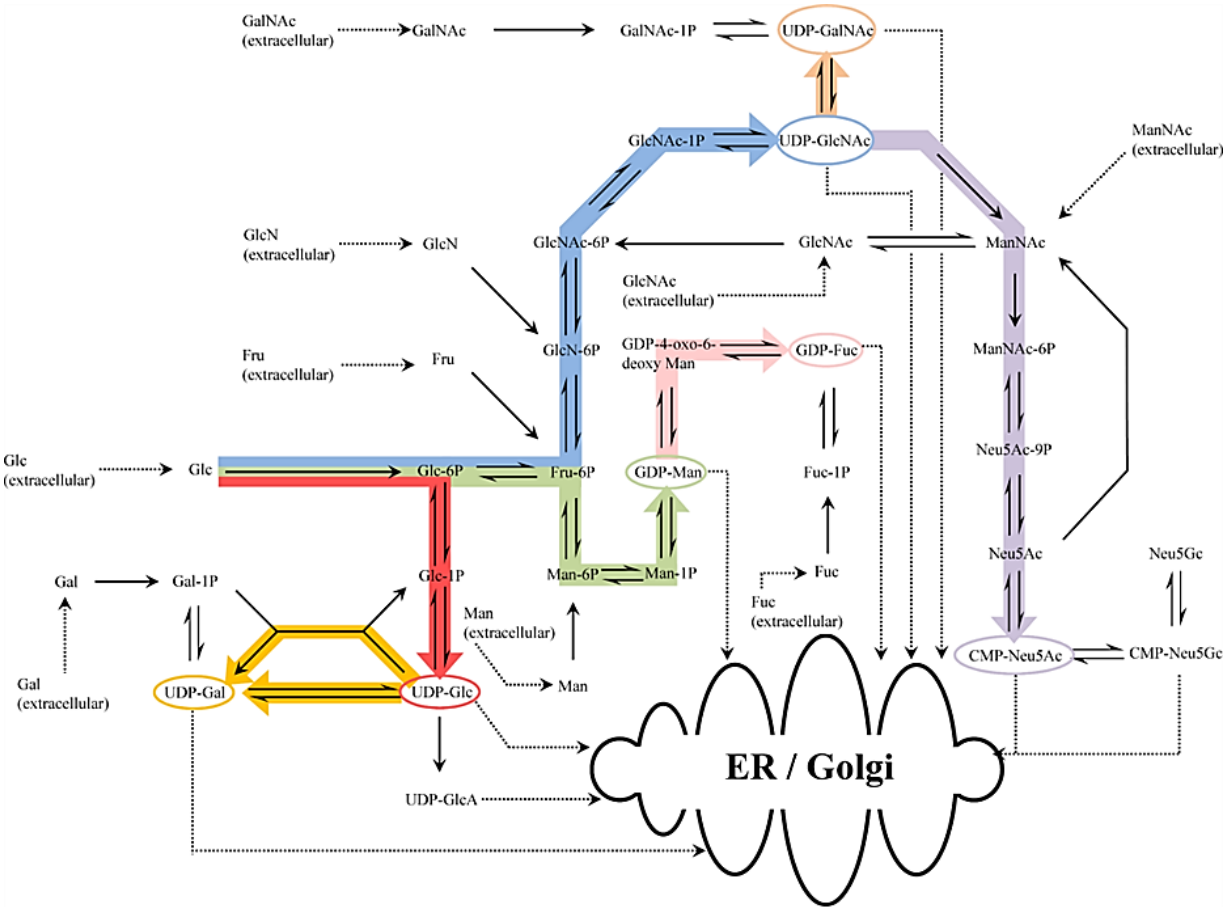

Figure 27. Reduced NSD biosynthetic pathway (Jedrzejewski et al. 2014). Lumped reaction for each NSD biosynthetic reaction from glucose and glutamine is identified by different coloured arrows, where blue represents single UDP-GlcNAc reaction, red for single UDP-Glc reaction, yellow for UDP-Gal, green for GDP-Man, pink for GDP-Fuc orange for UDP-GalNAc and purple for CMP-Neu5Ac.

5.2.1. Nucleotide metabolic model

The biosynthesis of NSDs requires two components: nutrients (e.g. glucose and glutamine) and nucleotides. The intracellular concentrations of glucose and glutamine are defined in Equation 40 to 43 below:

$$\frac{d[Glc_{int}]}{dt} = \frac{q_{glc}}{V_{cell}} - (N_{glc,ATP} r_{ATP} + N_{glc,GTP} r_{GTP} + N_{glc,UTP} r_{UTP} + N_{glc,UDPGlcNAc} r_{UDPGlcNAc} + N_{glc,UDPGlc} r_{UDPGlc} + N_{glc,GDPMan} r_{GDPMan} + r_{met,glc}) \quad \text{...Eq. 40}$$

$$\frac{d[Gln_{int}]}{dt} = \frac{q_{gln}}{V_{cell}}\left(\frac{q_{gln,syn}}{q_{gln}} - 1\right) - \left(N_{gln,ATP}r_{ATP} + N_{gln,CTP}r_{CTP} + N_{gln,GTP}r_{GTP} + N_{gln,UTP}r_{UTP} + N_{gln,UDPGlcNAc}r_{UDPGlcNAc} + N_{glc,CMPNeu5Ac}r_{CMPNeu5Ac} + r_{met,gln}\right) \quad \text{...Eq. 41}$$

$$r_{met,glc} = q_{glc}\frac{f_{glc}}{V_{cell}} \quad \text{...Eq. 42}$$

$$r_{met,gln} = q_{gln}\frac{f_{gln}}{V_{cell}} \quad \text{...Eq. 43}$$

where, $[Glc_{int}]$ and $[Gln_{int}]$ represent the intracellular concentration of glucose and glutamine, respectively. $[Glc_{int}]$ is expressed in *[mM],* while a conversion factor of 1e3 is included in $[Gln_{int}]$ as it is expressed in *[μM]*. V_{cell} is the average volume of the CHO cell *(dm^3)*. $N_{glc,nucleotide}$ and $N_{gln,nucleotide}$ indicate the concentration of intracellular glucose or glutamine required for each named nucleotide synthesis *(mmol/mmol)*. Similarly $N_{glc,NSD}$ and $N_{gln,NSD}$ represent the consumption of intracellular glucose and glutamine in respective NSD production *(mmol/mmol)*. Moreover, $r_{met,glc}$ and $r_{met,gln}$ indicate other biochemical reactions where intracellular glucose and glutamine are consumed as f_{glc} and f_{gln}.

In order to more accurately estimate each NSD concentration within a cell, it is helpful to consider the dynamics of ATP, UTP, GTP and CTP concentrations in the NSD model. Material balances for ATP, UTP, GTP and CTP are defined by the production and consumption of these four species during NSD production only, but not accounting for other species within the nucleotide synthetic pathways, such as nucleoside mono- or di-phosphates, or other amino acids. Equations 44 to 47 described below show the material balances for intracellular nucleotides:

$$\frac{d[ATP]}{dt} = r_{ATP} - \left(N_{ATP,CTP}\,r_{CTP} + N_{ATP,GTP}\,r_{GTP} + N_{ATP,UTP}\,r_{UTP}\right) - F_{out,ATP} \quad \text{...Eq. 44}$$

$$\frac{d[UTP]}{dt} = r_{UTP} - r_{CTP} - r_{UDPGlcNAc} - r_{UDPGlc} - F_{out,UTP} \quad \text{...Eq. 45}$$

$$\frac{d[GTP]}{dt} = r_{GTP} - r_{GDPMan} - F_{out,GTP} \quad \text{...Eq. 46}$$

$$\frac{d[CTP]}{dt} = r_{CTP} - r_{GDPMan} - F_{out,CTP} \quad \text{...Eq. 47}$$

where, $N_{ATP,CTP}$, $N_{ATP,GTP}$ and $N_{ATP,UTP}$ *(mmol/mmol)* represent the number of ATP required during CTP, GTP and UTP synthesis, respectively. $r_{nucleotide}$ *(h^{-1})* represents the overall rate of nucleotide synthesis and they are defined by:

$$r_{ATP} = V_{max,ATP}\left(\frac{[Glc_{int}]}{K_{glc,ATP} + [Glc_{int}]}\right)\left(\frac{[Gln_{int}]}{K_{gln,ATP} + [Gln_{int}]}\right) \quad \text{...Eq. 48}$$

$$r_{UTP} = V_{max,UTP}\left(\frac{[Glc_{int}]}{K_{UTP,glc} + [Glc_{int}]}\right)\left(\frac{[Gln_{int}]}{K_{UTP,gln} + [Gln_{int}]}\right)\left(\frac{[ATP]}{K_{UTP,ATP} + [ATP]}\right) \quad \text{...Eq. 49}$$

$$r_{GTP} = V_{max,GTP}\left(\frac{[Glc_{int}]}{K_{GTP,glc} + [Glc_{int}]}\right)\left(\frac{[Gln_{int}]}{K_{GTP,gln} + [Gln_{int}]}\right)\left(\frac{[ATP]}{K_{GTP,ATP} + [ATP]}\right) \quad \text{...Eq. 50}$$

$$r_{CTP} = V_{max,CTP}\left(\frac{[Gln_{int}]}{K_{CTP,gln} + [Gln_{int}]}\right)\left(\frac{[ATP]}{K_{CTP,ATP} + [ATP]}\right)\left(\frac{[UTP]}{K_{CTP,UTP} + [UTP]}\right) \quad \text{...Eq. 51}$$

where, $V_{max,nucleotide}$ is the maximum turnover rate $\left(\frac{mmol_{nucleotide}}{L_{cell}\,hr}\right)$ and $K_{x,y}$ is the saturation constant of species x with respect to species y *(mM)*. The synthetic rates of nucleotides therefore relate the intracellular concentrations of glucose and glutamine, while in the case of UTP, GTP and CTP their productions are also dependent on ATP as an energy source.

The transport rate of each nucleotide $\left(F_{out,nucleotide}\right)$ is defined as:

$$F_{out,nucleotide} = K_{out,nucleotide}\left(\frac{[Nucleotide]}{K_{TP,nucleotide} + [Nucleotide]}\right) \quad \text{...Eq. 52}$$

where, $K_{out,nucleotide}$ is the consumption rate of nucleotide *(h^{-1})* and $K_{TP,nucleotide}$ denotes to the saturation coefficient of nucleotide transport (*mM*).

5.2.2. NSD synthetic model

With material balances for nucleotide synthesis described above, it is now possible to relate NSD production with both nutrients and nucleotide dynamics within the cell throughout the culture period. By using the same set of material balances for intracellular NSDs as described in Jimenez del Val (2013), we modified the r_{NSD} equations and included nucleotide consumption terms for the production of each NSD species. The updated NSD synthetic rates are now defined in equation 53 to 59.

$$r_{UDPGlcNAc} = V_{max,UDPGlcNAc}\left(\frac{[Glc_{int}]}{K_{UDPGlcNAc,glc}+[Glc_{int}]}\right)\left(\frac{[Gln_{int}]}{K_{UDPGlcNAc,gln}+[Gln_{int}]}\right)\left(\frac{[UTP]}{K_{UDPGlcNAc,UTP}+[UTP]}\right) \quad \text{...Eq. 53}$$

$$r_{UDPGlc} = V_{max,UDPGlc}\left(\frac{[Glc_{int}]}{K_{UDPGlc,glc} + [Glc_{int}]}\right)\left(\frac{[UTP]}{K_{UDPGlc,UTP} + [UTP]}\right) \quad \text{...Eq. 54}$$

$$r_{GDPMan} = V_{max,GDPMan}\left(\frac{[Glc_{int}]}{K_{GDPMan,glc} + [Glc_{int}]}\right)\left(\frac{[GTP]}{K_{GDPMan,GTP} + [GTP]}\right) \quad \text{...Eq. 55}$$

$$r_{UDPGalNAc} = V_{max,UDPGalNAc}\left(\frac{[UDPGlcNAc]}{K_{UDPGalNAc,UDPGlcNAc} + [UDPGlcNAc]}\right) \quad \text{...Eq. 56}$$

$$r_{CMPNeu5Ac} = \left(\frac{V_{max,CMPNeu5Ac}\,[UDPGlcNAc]}{K_{CMPNeu5Ac,UDPGlcNAc}+[UDPGlcNAc]}\right)\left(\frac{[CTP]}{1+\frac{[CMPNeu5Ac]}{Ki,CMPNeu5Ac}}\right)\left(\frac{[Gln_{int}]}{K_{gln,CMPNeu5Ac}+[Gln_{int}]}\right) \quad \text{...Eq. 57}$$

$$r_{UDPGal} = V_{max,UDPGal}\left(\frac{[UDPGlc]}{K_{UDPGal,UDPGlc} + [UDPGlc]}\right) \quad \text{...Eq. 58}$$

$$r_{GDPFuc} = \left(\frac{V_{max,GDPFuc}\,[GDPMan]}{K_{GDPFuc,GDPMan}\left(1+\frac{[GDPMan]}{K_{GDPFuc,GDPMan}}+\left(\frac{[GDPMan]}{K_{GDPFuc,GDPMan}}\frac{[GDPFuc]}{K_{i,GDPFuc}}\right)+\frac{[GDPFuc]}{K_{i,GDPFuc}}\right)}\right) \quad \text{...Eq. 59}$$

where, $V_{max,NSD}$ is the maximum turnover rate $\left(\frac{mmol_{NSD}}{L_{cell}\,hr}\right)$ and $K_{x,y}$ is the saturation constant of species x with respect to species y *(mM)*.While all rates of NSD syntheses relate to concentrations of nutrients and nucleotides, $r_{CMPNeu5Ac}$ and r_{GDPFuc} also account for competitive product inhibition constants $K_{i,CMPNeu5Ac}$ and non-competitive inhibition constant $K_{i,GDPFuc}$, respectively *(mM)*.

In addition to modifying material balances that define the rates of NSD synthesis, the third change in the model involves the incorporation of NSD consumption for host cell protein glycosylation in material balances that define the rate of NSD transport into the Golgi apparatus. The following material balance defines the transport rates for UDP-GlcNAc, UDP-Glc, UDP-Gal, GDP-Fuc and GDP-Man:

$$F_{out,NSD} = \frac{[NSD]}{K_{TP,NSD}+[NSD]}\left[\left(\frac{\mu}{V_{cell}}N_{glyc,cell}N_{NSD,glyc}\right)+\left(\frac{q_{mAb}}{V_{cell}}N_{glyc,mAb}N_{NSD,mAb}\frac{1}{MW}\right)\right] \quad \text{...Eq. 60}$$

Equation 60 consists of two parts: the first part contains a Michealis-Menten saturation kinetics term that includes a transport protein saturation constant $K_{TP,NSD}$ *(mM)*, as illustrated by (Jimenez del Val 2013). The latter shows transport terms for NSD consumption rates for both host cell and antibody product glycosylation, which are functions of cell growth and specific mAb productivity, respectively. Based on the calculations from Harrison et al. (2002) and Selvarasu et al. (2012) on the average host cell weights and biomass composition, together with the q_{mAb} of our secreted IgG molecules that were experimentally determined, the total number of glycan per cell $\left(N_{glyc,cell}\right)$ *(mmol/cell)* and the number of NSD consumed per host cell N-linked glycan $\left(N_{NSD,glyc}\right)$ *($mmol_{NSD}/mmol_{glycan}$)* were calculated (Raman et al. 2006). In addition, the number of NSD consumed per mAb Fc-glycan $N_{NSD,mAb}$ *($mmol_{NSD}/mmol_{glycan}$)* was calculated from Fc-glycan compositions that were experimentally determined, while $N_{glyc,mAb}$, which is the number of glycan per a molecule of product *($mol_{gly}\ mol_{mAbFc}^{-1}$)*, is always 2 in the case of an IgG.

In the case of UDP-GalNAc and CMP-Neu5Ac, material balances for their NSD transport rates are different. Since our CHO cell line does not consume UDP-GalNAc for product glycosylation, the consumption term for UDP-GalNAc on mAb glycan is therefore omitted and its rate of transport is defined as:

$$F_{out,UDPGalNAc} = \left(\frac{[UDPGalNAc]}{K_{TP,UDPGalNAc} + [UDPGalNAc]}\right)\left(\frac{\mu}{V_{cell}} N_{glyc,cell} N_{UDPGalNAc,glyc}\right) \quad \text{...Eq. 61}$$

The same case applies to CMP-Neu5Ac, where our product is not sialylated, therefore only NSD consumption for host cell proteins is being considered. In addition, owing to the competitive product inhibition of the CMP-Neu5Ac Golgi transporter protein by the presence of UDP-GlcNAc (Pels Rijcken et al. 1995), a transport inhibition term of CMP-Neu5Ac by UDP-GlcNAc $\left(K_{i,CMPNeu5Ac,UDPGlcNAc}\right)$ is included in the material balance for the rate of CMP-Neu5Ac transport and it is defined as:

$$F_{out,CMPNeu5Ac} = \frac{[CMPNeu5Ac]\frac{\mu}{V_{cell}} N_{glyc,cell} N_{CMPNeu5Ac,glyc}}{K_{TP,CMPNeu5Ac}\left(1 + \frac{[CMPNeu5Ac]}{K_{TP,CMPNeu5Ac}} + \frac{[UDPGlcNAc]}{K_{i,CMPNeu5Ac,UDPGlcNAc}}\right)} \quad \text{...Eq. 62}$$

By considering as well the consumption rates of NSDs on host cell protein glycans, the updated NSD model better describes the distribution of each NSD species towards product glycosylation, which eventually provides a better estimation towards mAb Fc-glycan prediction in the final glycosylation model.

5.3. Golgi N-linked glycosylation model

Estimated outputs from the NSD model are next fed into a Golgi N-linked mAb Fc-glycosylation model that was adapted from the developed model by Jimenez del Val et al. (2011) to relate CHO cellular metabolism to the process of mAb glycosylation within the Golgi apparatus. While the model developed by Jimenez del Val et al. (2011) considers the concentration of NSD species within the Golgi apparatus by including the rate of transport of each NSD species into the Golgi apparatus, the adapted model that is used in this thesis relates the cytosolic concentration of NSD species directly to the Golgi N-linked model. The adapted model is capable of estimating the

antibody product Fc-glycoforms through describing the process of glycosylation within the Golgi apparatus of a cell. The model is constructed based on a Golgi cisternae maturation regime, where the Golgi apparatus is modelled as a single, continuous plug-flow reactor (PFR). The model assumes successful assembly of mAb with the endoplasmic reticulum and addition of the glycan precursor. The mAb molecule then travels along each compartment of the Golgi in a similar manner as flow of material in a PFR. The localisation of each glycosyltransferase and transport protein is optimised using data from Rabouille et al. (1995), and each appears in a sequential manner within the Golgi apparatus. Material balances for the catalytic reactions of the glycosyltransferases within this model are developed based on three main kinetic mechanisms: ManI & II follow the simple Michaelis-Menten kinetics with competitive and product inhibitions; GnTI & II and GalT also possess the kinetic mechanism above, but they work in a sequential Bi-Bi order; FucT on the other hand follows the random-order Bi-Bi kinetics with competitive and product inhibitions taken into account. The glycan model is a 3-dimentional model that describes Fc-glycoform maturation with respect to cell culture time as well as length of the Golgi apparatus.

To better adapt this glycan model to experimental conditions in our case, some model inputs were modified. Specifically, the overall CHO cell volume and the glycan concentration of mAb entering the Golgi apparatus are re-calculated based on mAb concentration achieved in each condition, while the minimal concentrations of glycosyltransferases required for the assumption of 100% processing by the model, are re-estimated. Since our adapted model includes cytosolic concentration of NSD species, re-estimation of saturation constants of each glycosyltransferase is therefore essential.

5.4. Comparing model simulation results between physiological and mild hypothermic conditions

The model described above was then simulated in gPROMS v.4.0.0 (Process Systems Enterprise Ltd), for two experimental conditions: SGE fed-batch culture at 36.5°C or with a temperature shift to 32°C induced on day 6 (late-exponential phase). By using the same model structure for both conditions, model simulation results from two parameter sets were compared across the two process conditions.

5.4.1. CHO cell culture dynamics and mAb production estimation and discussion

Both parameter sets of the model were simulated and their respective parameters were estimated from the experimental profiles for nutrients, metabolites, total and viable CHO cell concentrations and mAb synthesis including product transcripts and polypeptides. Figure 28 A and Figure 28 B show that simulated results from our cell dynamic model represent our fed-batch experimental data on viable and total cell densities well at both temperatures, correctly capturing the slight reduction in cell density upon temperature shift. In addition, glucose, lactate and ammonia are described effectively by both sets of parameter values of the model (Figures 29 A – C), including all feeding points, nutrient consumption rates and the metabolic shift from lactate production to consumption upon the induction of mild hypothermia. The model simulations for various amino acids are also in good agreements with our experimental concentrations, showing that the consumption of these amino acids is lower at reduced temperature. The model also manages to predict the increase of glutamine in culture medium at 32°C (Figures 30 A – G).

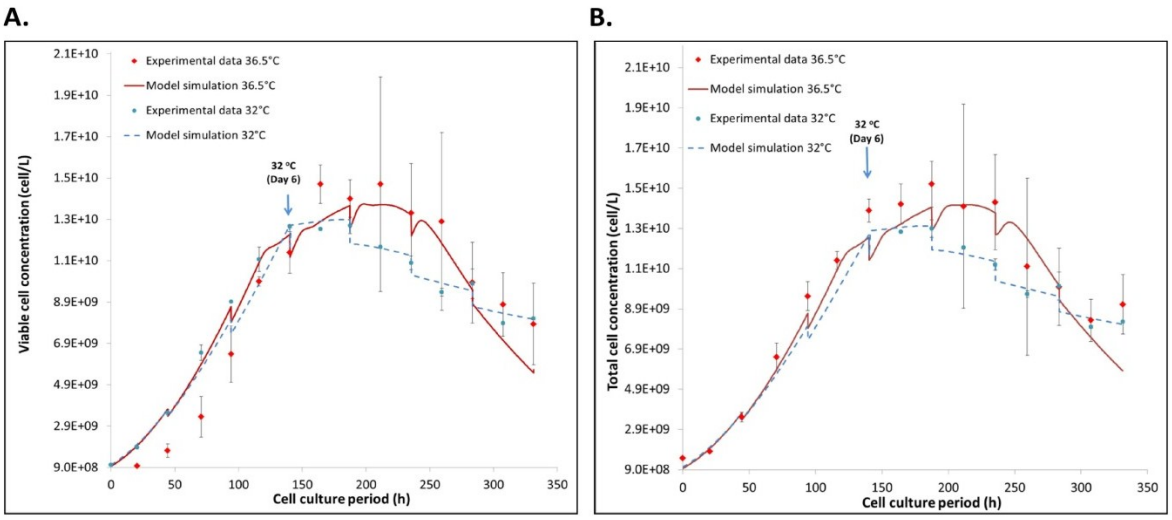

Figure 28. Comparison of model simulation to experimental data for viable (A) and total cell concentrations (B) from fed-batch CHO cell cultures at 36.5°C (red) or at mild hypothermic condition post late exponential growth phase (blue).

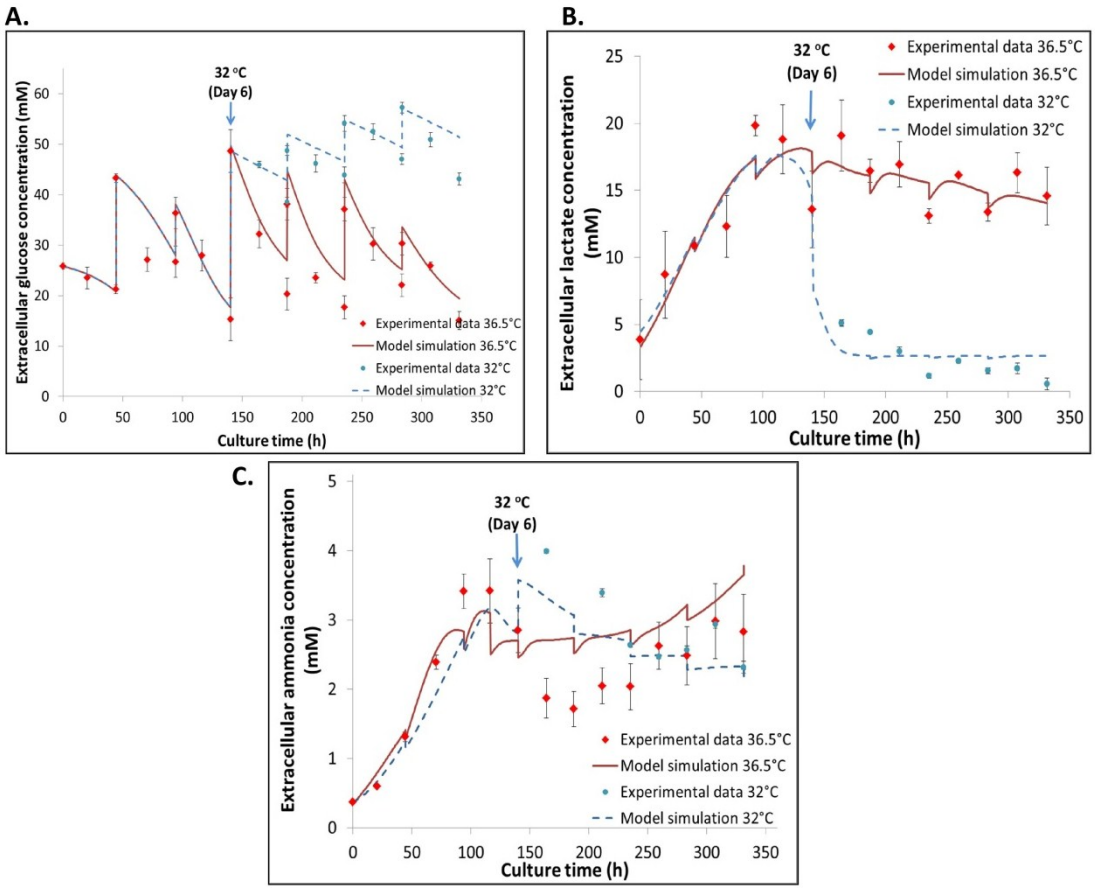

Figure 29. Comparison of model generated fits to experimental data for extracellular glucose (A) extracellular lactate (B) and extracellular ammonia (C) concentrations from fed-batch CHO cell cultures at 36.5°C (red) or at mild hypothermic condition post late exponential growth phase (blue).

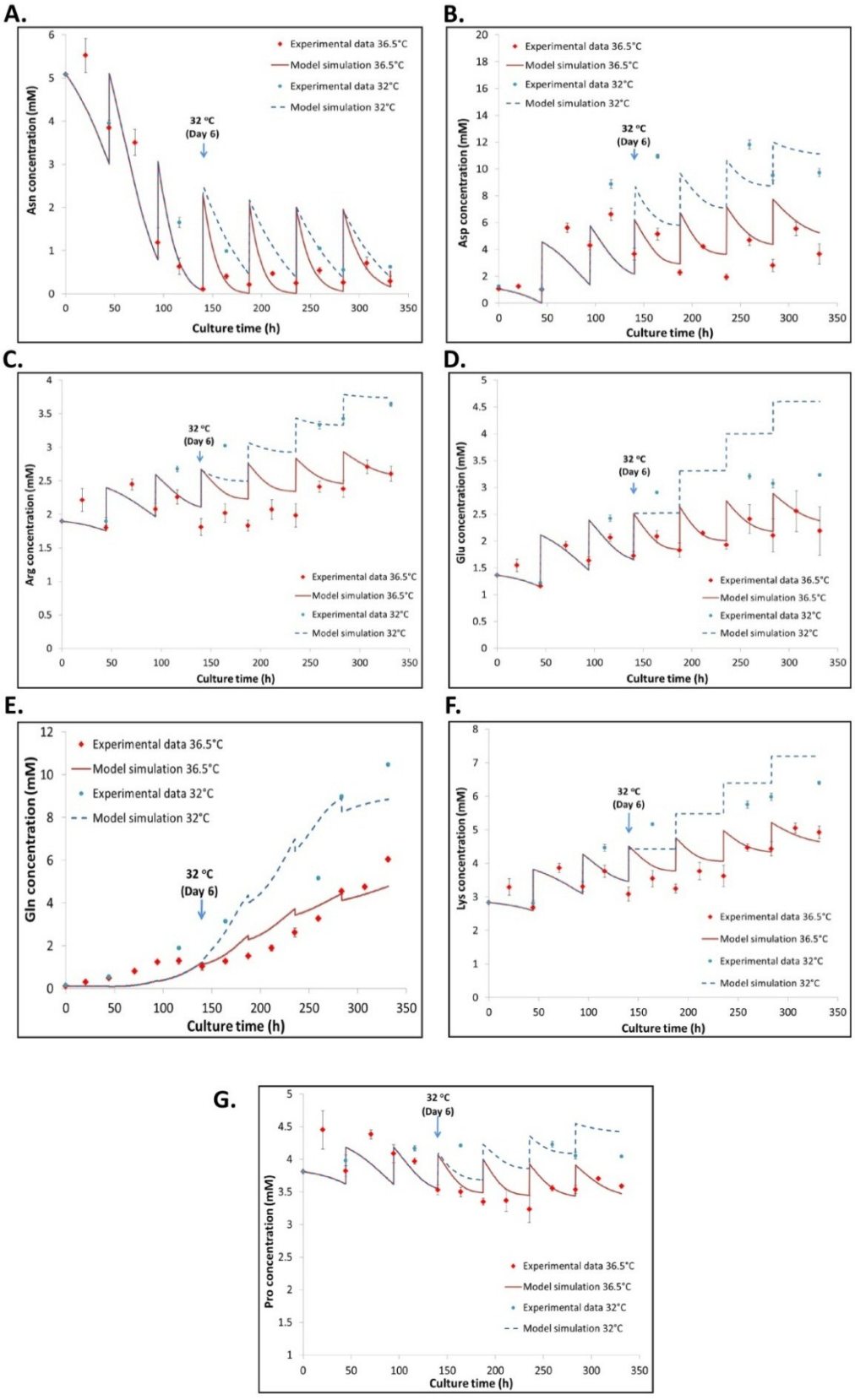

Figure 30. Comparison of model generated fits to experimental data for extracellular asparagine (A), aspartate (B), arginine (C), glutamate (D), glutamine (E), lysine (F) and proline (G) concentrations from fed-batch CHO cell cultures at 36.5°C (red) or at 32°C induced at late exponential growth phase (blue).

Predictions for the process of mAb product synthesis are generated from both parameter sets in the cell dynamic model. Figures 31 A & Figure 31 B illustrate model simulations of HC and LC mRNAs. For the first 150 h before temperature shift, our model over-estimates slightly on the HC mRNA species but provides reasonably good fits for LC mRNA. Upon the introduction of mild hypothermia, simulated results are over-estimated and are not being in complete agreement with each experimental time point, where simulated results reached plateaus instead of gradual decreases that our experiment results suggested. Despite the miss-fittings, our simulated results of HC and LC mRNAs follow the same trend and results are in the same numerical range as the experimental data. Assembly intermediate polypeptides H_2 and H_2L are described well by our models, where the increased net concentrations of both intermediate species under mild hypothermic conditions are well captured. In the case of the secreted mAb product, our model manages to provide good fits to the experimental results, as shown in Figure 32. The total volumetric concentration of mAb is correctly predicted to be higher at the reduced temperature, despite the simulated final value being slightly lower than the experimental results.

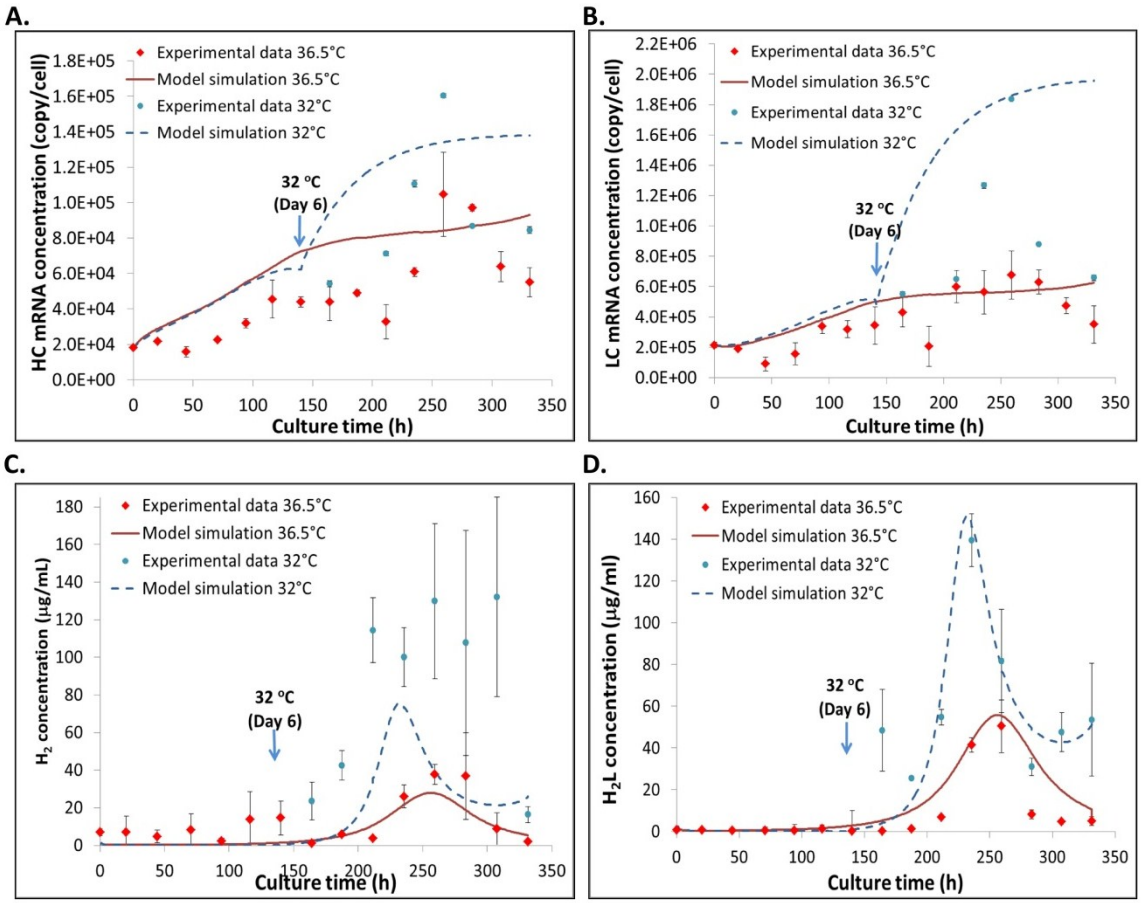

Figure 31. Comparison of model simulation outputs to experimental data for intracellular HC mRNA (A), LC mRNA (B), H2 polypeptide (C) and H2L assembly intermediate (D) concentrations from fed-batch CHO cell cultures at 36.5°C (red) or at 32°C induced at late exponential growth phase (blue).

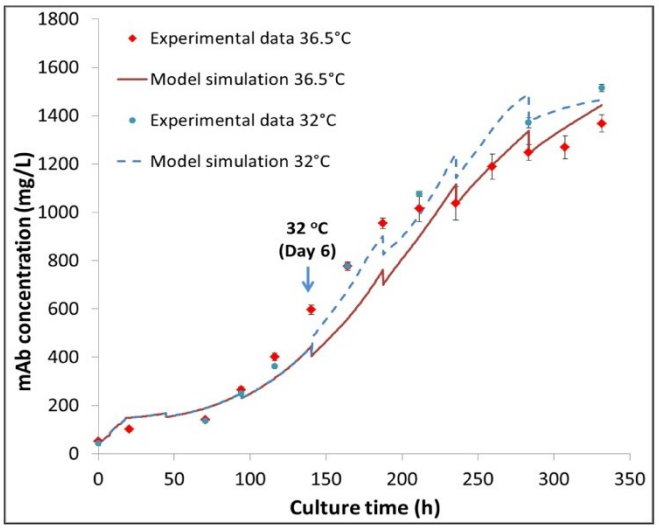

Figure 32. Comparison of model simulation outputs to experimental data for secreted volumetric mAb concentration in fed-batch CHO cell cultures at 36.5°C (red) or at 32°C induced at late exponential growth phase (blue).

By using two different sets of parameter values but the same model structure for the two culture temperatures examined, it becomes possible to understand more on how experimental differences arise between the two conditions, e.g. variations in mAb production, by comparing the two sets of model outputs. Table 12 shows the estimated process parameters for the different culture temperature sets. Under mild hypothermic conditions, rate for the overall maximum cell growth is higher with reduced rate of maximum cell death, in order to sustain prolonged cell growth at 32°C. In accordance with our experimental data, the estimated yield of lactate from glucose is reduced dramatically, which reflects the lactate metabolic shift from production to consumption at 32°C. In the case of mAb synthesis, estimated model outputs indicate that at lower culture temperature, the mRNA decay rates of both HC and LC are expected to be lower; this is in good agreement with experimental results indicated in Chapter 4 and with the studies by O'Callaghan et al. (2010). The polypeptide assembly rate of mAb is estimated to be lower at 32°C, which could suggest a reduced rate of collision between the mAb polypeptide molecules at the lower temperature. Also it correlates well with our experimental analysis in Chapter 4, where reduced assembly rate of mAb and an accumulation of H_2L species were speculated. In addition, rates for HC and LC transcription, mAb polypeptide translate, transport of mAb from ER to Golgi and from Golgi to extracellular matrix (ECM), are all estimated to be higher during mild hypothermia by the model. These support the increased levels of mAb transcription and translation. Estimation of ε_1 and ε_2 is the first attempt to determine the efficiency of product glycosylation with respect to the mAb production; they represent the ER and Golgi glycosylation efficiency factors, respectively. At 32°C, both ε_1 and ε_2 are estimated to be lower and these are first indications from the model that mAb glycosylation could be affected by

changes in culture temperature. The full list of model parameters and variables from both models can be found in the Appendix II Table 2.

Table 12. Comparison of estimated parameters from SGE models between two temperatures. This includes parameter values for cell growth, metabolism and mAb production.

Parameter	36.5 °C	95% conf. internals	32 °C (Day 6)	95% conf. internals	Units
Growth/death related					
μ_{max}	**1.10×10^{-1}**	2.90×10^{-2}	**7.49×10^{-1}**	3.20×10^{-2}	h^{-1}
$\mu_{d,max}$	**9.70×10^{-2}**	1.10×10^{-2}	**3.96×10^{-2}**	2.00×10^{-3}	h^{-1}
K_{lysis}	**4.47×10^{-1}**	1.10×10^{-2}	**2.14×10^{-1}**	5.70×10^{-2}	h^{-1}
Metabolism related					
$Y_{lac,glc}$	**2.00**	2.40×10^{-1}	**5.32×10^{-3}**	1.30×10^{-3}	mmol $mmol^{-1}$
mAb synthesis related					
K_A	**1.38×10^{-1}**	5.82×10^{-2}	**1.94×10^{-3}**	1.80×10^{-4}	molecule $cell^{-1}$ h^{-1}
K_{ER}	**4.56×10^{2}**	3.70×10^{2}	**9.03×10^{2}**	35.10	h^{-1}
K_G	**2.00×10^{3}**	5.73×10^{2}	**2.30×10^{4}**	1.26×10^{2}	h^{-1}
S_H	**15.90**	2.10	**1.11×10^{2}**	7.40	mRNAs $gene^{-1}$ h^{-1}
S_L	**93.10**	15.00	**1.58×10^{2}**	5.30	mRNAs $gene^{-1}$ h^{-1}
T_H	**1.35**	1.20	**2.17**	9.50×10^{-2}	chain $mRNA^{-1}$ h^{-1}
T_L	**3.84×10^{-1}**	1.10×10^{-1}	**5.66×10^{-1}**	2.80×10^{-2}	chain $mRNA^{-1}$ h^{-1}
K_h	**9.77×10^{-3}**	5.90×10^{-5}	**1.68×10^{-3}**	2.30×10^{-4}	h^{-1}
K_I	**1.15×10^{-3}**	4.75×10^{-5}	**1.13×10^{-3}**	3.80×10^{-4}	h^{-1}
mAb post-translational modification related					
ε_2	**11.10**	6.70×10^{-2}	**6.14**	6.00×10^{-2}	n/a

5.4.2. Intracellular nucleotide and NSD model estimation and discussion

This part of the model describes the concentration profiles of nucleotides (ATP, UPT, GTP & CTP) and six NSD species, namely UDP-Glc, UDP-Gal, UDP-GlcNAc, UDP-GalNAc, GDP-Man and GDP-Fuc, where their productions are based on CHO cell behaviour, nutrient and amino acid metabolisms from each condition. To achieve this, CHO cell dynamics and NSD models are linked together, by feeding in model outputs from the cell dynamics module (Appendix II Table 2), into the NSD model. NSD model simulation was performed with gPROMS v.4.0.0. Based on the consumption of nutrients and metabolites of CHO cells from each culture temperature, model simulations are compared to experimentally measured data, while variables that corresponded to the experimental data were estimated from both conditions mentioned in Figure 25 and they are analysed here.

Figures 33 A – I present model simulation results for cell cultures at 36.5°C and 32°C. Nine species are involved in the parameter estimation. The model simulations show that when cells are cultured at mild hypothermic temperature, the net intracellular concentrations of nucleotides, namely ATP, GTP and UTP, are higher. The accumulation in intracellular ATP is related to reduced cell growth and cell metabolism in response to mild hypothermia, where fewer ATP molecules are required as energy source to maintain cellular activities. In addition, fewer ATP molecules are produced when glucose consumption is lower at 32°C. This is supported by the reduced efficiency of lactate production from glucose, estimated by our cell dynamics model. In this case, both sets of parameter values from each condition represent the intracellular mechanisms well and model simulations are in good agreement with experimental data in all species investigated.

In the case of NSD metabolism, our model captures the reduction of intracellular concentrations of UDP-Glc, UDP-Gal, UDP-GlcNAc, UDP-GalNAc and UDP-Fuc, which are determined to be lower experimentally. Despite the good fits of model simulations to experimental measurements, discrepancies are observed in GDP-Fuc and GDP-Man, where the current model fails to predict the peak concentrations of these two species. Since the production of GDP-Fuc is dependent on the concentration of GDP-Man within the synthetic network, the lumped pathway that is used in the NSD model might not be adequate to predict species generated from this pathway. Considering our material balance for GDP-Man does not account of the mannose salvage pathway, one can therefore argue that GDP-Man is predicted to be over-consumed in our model, even though there are experimental reports suggesting that the mannose-salvage pathway reduces net consumption of mannose and its derivatives (Berg et al. 2006).

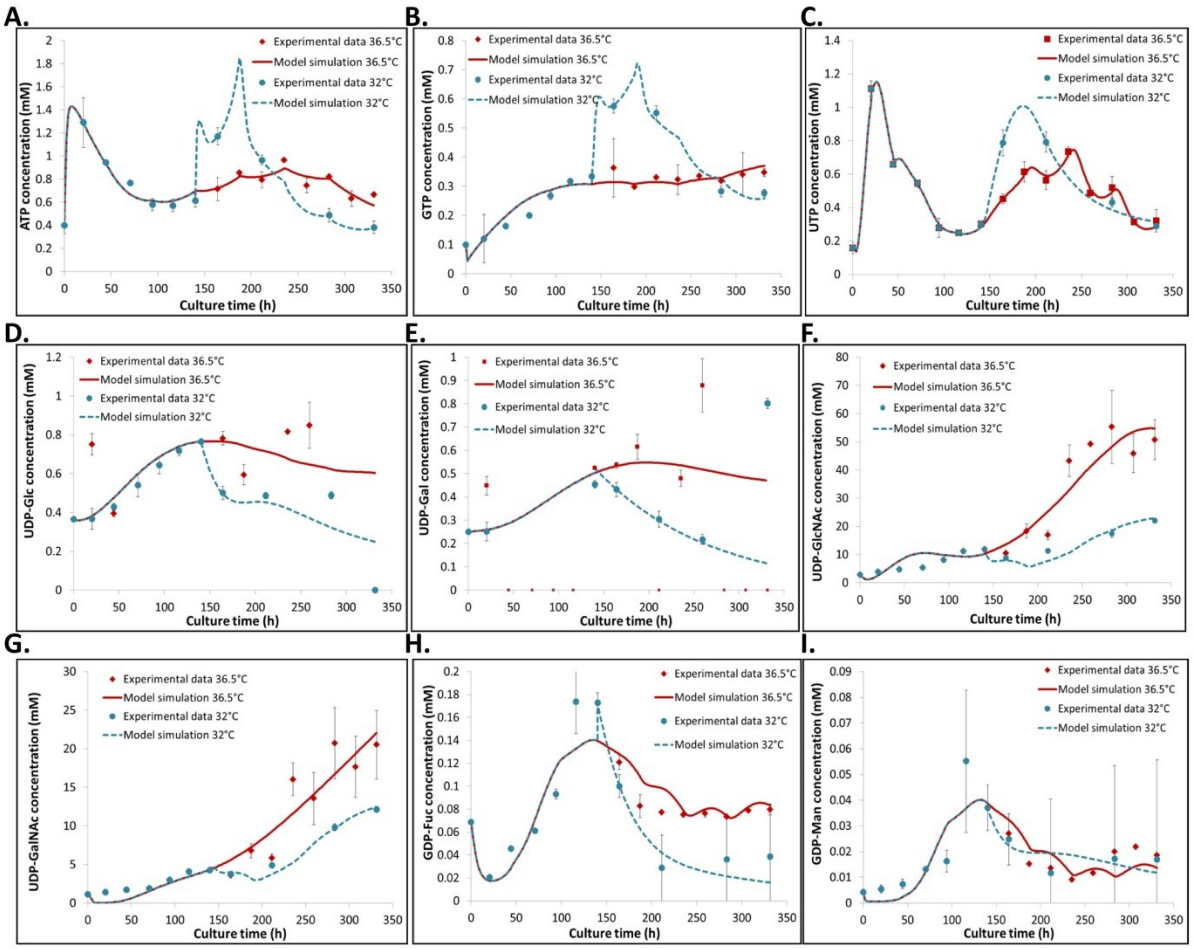

Figure 33. Comparison of nucleotide and NSD profiles from model simulations to experimental data in fed-batch CHO cell cultures at 36.5°C (red) or at 32°C induced at late exponential growth phase (blue). This includes the intracellular concentrations of ATP (A), GTP (B), UTP (C), UDP-Glc (D), UDP-Gal (E), UDP-GlcNAc (F), UDP-GalNAc (G), GDP-Fuc (H) and GDP-Man (I).

Values of V_{max} and K_m for enzymes involved in the NSD synthetic process are estimated in this NSD model. Table 13 shows the estimated set of parameter values when CHO cells are cultured at a sub-physiological temperature. At 32°C, the overall value of V_{max} for enzymes responsible for UDP-Gal synthesis is reduced and its K_m value is higher, which suggest that the reduced concentration of UDP-Gal observed at 32°C could be attributed to the lower estimated efficieny of the UDP-Gal-related enzyme during NSD synthesis (Table 14), and higher amounts of species required for reaction saturation at 32°C. These results agree with literature studies in which researchers showed a positive correlation between K_{cat} and temperature (Thomas and Scopes 1998). A full list of parameter values for the NSD model can be found in Appendix II Table 3.

Table 13. Comparison of estimated parameters from NSD models between two temperatures. This includes parameter values for nucleotide and NSD syntheses.

Parameter	36.5 °C	95% conf. internals	32 °C (Day 6)	95% conf. internals	Units
Nucleotide related					
$V_{max,\ ATP\ synthetic\ pathway}$	**13.70**	2.00×10^{-1}	**2.11**	5.10×10^{-1}	mmol L_{cell}^{-1} h^{-1}
$V_{max,\ GTP\ synthetic\ pathway}$	**44.20**	1.10	**2.68×10^{3}**	4.70	mmol L_{cell}^{-1} h^{-1}
$V_{max,\ UTP\ synthetic\ pathway}$	**34.90**	1.10	**9.26×10^{2}**	21.00	mmol L_{cell}^{-1} h^{-1}
NSD related					
$K_{TP,UDPGlc\ synthetic\ pathway}$	**4.11×10^{-3}**	1.90×10^{-4}	**1.00×10^{-30}**	1.00×10^{-34}	mM
$K_{TP,UDPGal\ synthetic\ pathway}$	**4.68×10^{-2}**	5.40×10^{-3}	**3.47×10^{-4}**	2.49×10^{-5}	mM
$K_{TP,UDPGlcNAc\ synthetic\ pathway}$	**1.00×10^{-30}**	1.00×10^{-34}	**9.76**	4.80×10^{-5}	mM
$K_{TP,GDPMan\ synthetic\ pathway}$	**1.00×10^{-2}**	3.80×10^{-3}	**1.40**	1.27	mM
$K_{TP,GDPFuc\ synthetic\ pathway}$	**1.25×10^{-1}**	4.80×10^{-3}	**7.42×10^{-2}**	1.60×10^{-1}	mM
$V_{max,\ UDPGlc\ synthetic\ pathway}$	**5.00×10^{-1}**	1.25×10^{-3}	**5.84×10^{-1}**	1.70×10^{-2}	mmol L_{cell}^{-1} h^{-1}
$V_{max,\ UDPGal\ synthetic\ pathway}$	**2.26×10^{-3}**	9.20×10^{-4}	**1.00×10^{-30}**	1.00×10^{-34}	mmol L_{cell}^{-1} h^{-1}
$V_{max,\ UDPGlcNAc\ synthetic\ pathway}$	**2.17**	9.00×10^{-2}	**7.66**	1.40×10^{-1}	mmol L_{cell}^{-1} h^{-1}
$V_{max,GDPMan\ synthetic\ pathway}$	**6.57×10^{-1}**	9.53×10^{-3}	**5.28×10^{-1}**	1.96×10^{-3}	mmol L_{cell}^{-1} h^{-1}
$V_{max,GDPFuc\ synthetic\ pathway}$	**11.70**	2.88	**5.37**	4.39×10^{-2}	mmol L_{cell}^{-1} h^{-1}
$K_{UDPGlc,glc\ synthetic\ pathway}$	**6.66×10^{2}**	74.00	**10.50**	12.00	mM
$K_{UDPGal,glc\ synthetic\ pathway}$	**4.73×10^{-1}**	9.10×10^{-3}	**4.40×10^{2}**	4.30×10^{1}	mM
$K_{UDPGlcNAc,glc\ synthetic\ pathway}$	**1.82×10^{-1}**	3.00×10^{-3}	**4.53×10^{-1}**	2.1×10^{-2}	mM
$K_{GDPMan,glc\ synthetic\ pathway}$	**1.71×10^{2}**	1.10	**5.62×10^{3}**	6.50	mM
$K_{GDPFuc,glc\ synthetic\ pathway}$	**8.80×10^{2}**	39.00	**6.19×10^{3}**	1.90×10^{2}	mM

Table 14. Enzymatic efficiencies of NSD synthetic enzymes.

NSD synthetic enzyme catalytic efficiency (h^{-1})		
NSD -related synthetic pathway	**36.5 °C**	**32 °C (Day 6)**
UDPGlc	7.51×10^{-4}	5.56×10^{-2}
UDPGal	4.77×10^{-3}	2.27×10^{-33}
UDPGlcNAc	11.90	16.90
GDPMan	3.85×10^{-3}	9.39×10^{-3}
GDPFuc	1.33×10^{-2}	8.67×10^{-4}

5.4.3. Golgi N-linked glycosylation model estimation and discussion

Model outputs from both cell culture dynamics and the NSD model were incorporated into the Golgi N-linked glycosylation model developed by (Jimenez del Val et al. 2011) and the combined model was simulated in gPROMS version 4.0.0 for both temperatures. Without changing any part of the Golgi model structure, values of key parameters such as dissociation constants and minimal concentrations of various glycosyltransferases were re-estimated for CHO cells that were cultured at 36.5°C and with a shift to 32°C, under the assumption that 100 % of mAb produced are glycosylated and macro-heterogeneity is not considered to be limiting in this model.

Figures 34 A and B show the comparison between experimental and simulated distribution of the cumulative N-linked mAb Fc-glycan structures on days 10, 12 and 14 for culture temperature of 36.5°C and 32°C, respectively. The three chosen time points correspond to late stationary and decline phases, where significant changes in mAb productivity are shown to take place experimentally between the two culture temperatures. Simulation results from both set of parameter values of the model compare well with their respective experimental data and any differences in values are within 3.5% in all cases (Table 15). Intrigued by the experimental variations in transcript expression of glycosyltransferases (Figure 35), K_m values and the concentrations of these enzymes were re-estimated. Our results show that both sets of process variables of the SGE model manage to capture changes in galactosylation in Fc region of our secreted mAb molecules between the two temperatures examined with sufficient accuracy, as well as the slight decreases in Man5 species.

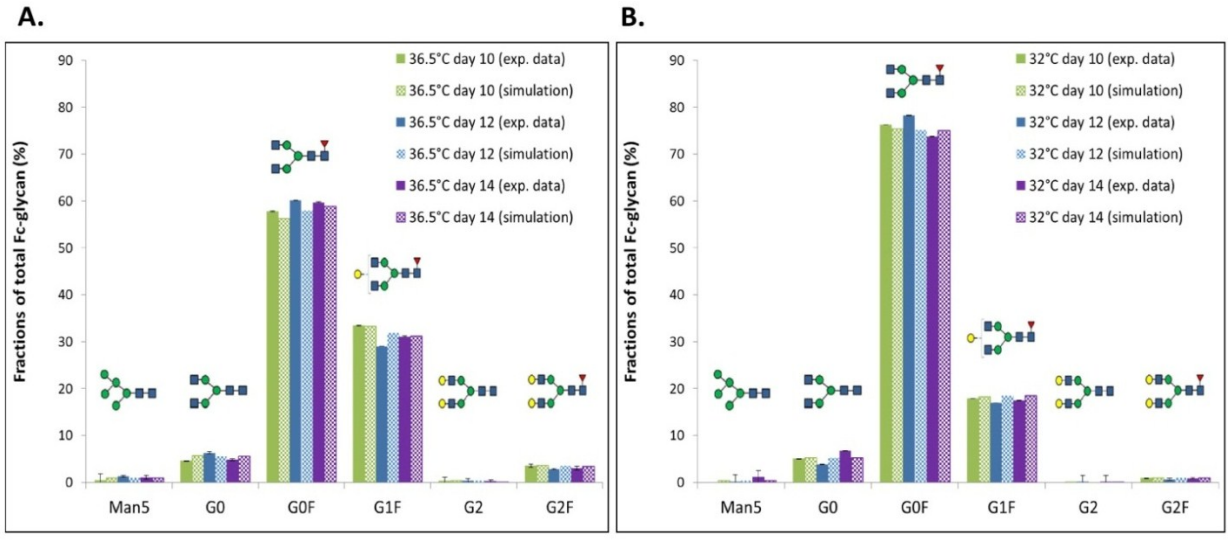

Figure 34. Comparison between experimentally and model simulated determined fractions of the cumulative N-linked glycoforms of secreted mAb for three time points during cell culture, when CHO cells were cultured at 36.5°C (A), or at 32°C (B) when mild hypothermic condition was introduced during late exponential growth phase.

Table 15. Percentage differences between model-simulated and experimentally measured values of N-linked glycan fractions for mAb Fc-regions, for CHO cells that were cultured at 36.5°C and 32°C.

	Deviation from experimental data (%)						
		Man5	G0	G0F	G1F	G2	G2F
36.5°C	Day 10	0.53	1.07	1.58	0.19	0.09	0.07
	Day 12	0.38	0.74	2.26	2.84	0.05	0.60
	Day 14	0.13	0.64	0.88	0.01	0.03	0.34
32°C	Day 10	0.32	0.18	0.89	0.36	0.01	0.02
	Day 12	0.11	1.34	3.16	1.48	0.02	0.24
	Day 14	0.83	1.52	1.28	1.01	0.00	0.07

In addition, parameter estimation was performed for the dissociation constants as well as the enzyme concentrations of Man I & II, GnT I & II, GalT and FucT. Table 16 compares estimated parameter values between the two conditions. Model outputs suggest that the concentrations of mannosidases (Man I & II) and fucosyltransferases (FucT) are comparable in CHO cell cultured at either temperature, but lower levels of galactosyltransferases (GalT) are predicted in order to generate reduced fractions of galactose-bearing glycoforms at 32°C. Despite the comparable concentrations of Man I and Man II suggested by the model, decreases in their respective dissociation constants are estimated, low K_d values suggest a higher affinity of enzyme towards their substrate and it is likely to contribute to an overall drop in Man5 glycan structure at 32°C. Moreover, the concentration of GnT II is estimated to be lower from the set of parameter values at 32°C. This is also accompanied by a significantly higher K_d value, which proposes that UDP-GlcNAc addition is affected by both the kinetics and enzyme concentration. This model estimation correlates well with the reduced transcript expression of GnTII observed experimentally in Chapter 4. Despite the well correlated model outputs to the experimental results, the model here estimated that a higher FucT concentration is required to achieved an increase in G0F profile when the culture temperature is reduced to 32°C, this contradicts with our experimentally measured mRNA level where a decrease in mRNA transcript level is observed under mild hypothermic conditions (Figure 35 A). Without validation of model output with measured concentrations of FucT protein expression, it is hard to conclude whether the conflicting results are owing to a change in enzyme concentration, or other kinetic factors such as k_{cat} or ligand binding affinity in this particular case. Since enzyme concentration and K_d value are highly correlated, it is also possible that another set of parameter values would also generate the same model simulation. But most importantly in the case of GalT, at 32°C, our predicted model output suggests that the concentration of GalT is significantly lower, while its k_d values appear to be higher than the values estimated at 36.5°C. This comparison proposes that, changes in GalT concentration also play a role in limiting product galactosylation, together with the reduced k_{cat} values that one might observed at lower culture temperature.

Lastly we compared the estimated values of glycosyltransferase concentrations from both sets of model inputs, to those that were determined experimentally. Although our experimental results are not quantitative, and only relative differences between conditions are taken into account, variations of parameter values between the two temperatures, however, possess a similar trend to those that are measured through q-rt-PCR studies in Chapter 4. Figure 35 A & Figure 35 B show reduced levels of GalT and FucT mRNA, as well as lowered GalTIII protein expression at 32°C, which correlate well with the estimated decrease in GalT and FucT concentrations by our glycan model. This comparison shows that the proposed model has high capability in representing the biological system in CHO cells, and generates prediction of mAb quality, and its effects in mild hypothermic conditions. This modular model introduces us to the possibility in closing the loop between model simulation and experimental system. To achieve this however, we must next validate the model against an independent set of experimental data to ensure the capability of the model in other data sets.

Table 16. Estimated enzyme concentrations and their respective dissociation constants at both temperatures.

	Parameter	36.5 °C	95% conf. internals	32 °C (Day 6)	95% conf. internals	Units
	Glycosyltransferase concentrations					
	Man I	**9.70×10^{-2}**	1.31×10^{-2}	**1.24×10^{-1}**	8.50×10^{-2}	μM
	Man II	**1.82×10^{-1}**	3.50×10^{-2}	**1.94×10^{-1}**	7.30×10^{-3}	μM
	GnT I	**6.05**	2.10×10^{-1}	**7.69×10^{-1}**	6.80×10^{-4}	μM
	GnT II	**1.14**	2.50×10^{-1}	**7.75×10^{-1}**	1.30×10^{-4}	μM
	GalT	**12.60**	1.70	**6.66**	4.10×10^{-2}	μM
	FucT	**13.30**	8.43	**45.54**	5.96	μM
Substrate	*Enzyme dissociation constants*					
Man_6	$K_{d,Man\ I\ D}$	**4.44×10^{-1}**	1.60×10^{-2}	**2.67×10^{-1}**	3.10×10^{-2}	μM
Man_5	$K_{d,Man\ II\ A}$	**3.45×10^{-5}**	1.84×10^{-6}	**4.44×10^{-5}**	4.71×10^{-9}	μM
$CoreGlcNAc_1$	$K_{d,GnT\ II}$	**5.31**	4.20×10^{-1}	**1.16×10^{2}**	13.00	μM
$CoreGlcNAc_2$ (α-1,3 arm)	$K_{d,GalT\ a1A}$	**3.00×10^{4}**	1.95×10^{3}	**2.29×10^{4}**	3.15×10^{3}	μM
$CoreGlcNAc_2$ (α-1,6 arm)	$K_{d,GalT\ a1B}$	**6.26**	2.73	**11.60**	2.54	μM
$CoreGlcNAc_2Gal_1$ (α-1,6 arm)	$K_{d,GalT\ a2A}$	**2.23×10^{3}**	2.67×10^{2}	**3.38×10^{2}**	4.80×10^{2}	μM
$CoreGlcNAc_2$	$K_{d,Fuc\ A}$	**1.34×10^{4}**	9.34×10^{2}	**1.34×10^{4}**	3.00×10^{2}	μM

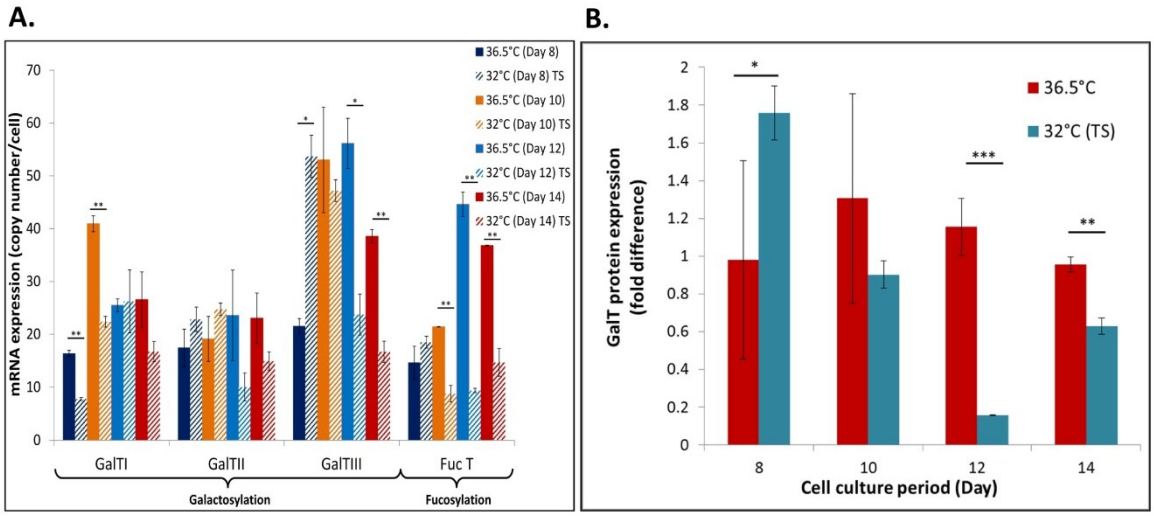

Figure 35. Measured expression levels of glycosyltransferases at physiological temperature or at 32°C. (A). mRNA expression levels of GalTs and FucT. (B). GalTIII protein expression profile.

5.5. Conclusions

This chapter describes the modification and adaptation of a modular model that can successfully replicate the experimental results of CHO cell culture in terms of cell growth, cell metabolism, recombinant mAb production and glycosylation under two culture temperatures, 36.5°C and with a shift to 32°C on day 6. Through model parameter estimation, comparison between the two model outputs becomes possible, enabling us to understand to a greater extent the performance of intracellular mechanisms upon mild hypothermia. Comparison between estimated values by the model for the two conditions show that at a reduced temperature the increase in specific mAb productivity is mostly due to increased rates of transcription, translation and product secretion. Despite changes in cell growth and metabolism observed during experimentation and through FBA studies in Chapter 4, our modelling study suggests that glycosyltransferase levels are the critical factor determining the variation in Fc-glycan profiles between the two culture temperatures. As a result, manipulation of glycosyltransferase expression can be a potential way to attain the Fc-glycan patterns that one would get at physiological temperature, but still retain the advantageous higher q_{prod} of mild hypothermic conditions.

Chapter 6
Differences in recombinant mAb glycosylation between stable and transient gene expression systems

After thorough examination on the impact of mild hypothermia on product glycosylation by both experimental and computational approaches in Chapter 4 and 5, in this chapter the angle of investigation is shifted to the study of an emerging method of rProtein production, the transient gene expression system. This chapter aims to compare the differences in the Fc-glycoforms that are derived from mAbs produced using example industrial stable (SGE) and transient (TGE) gene expression protocols.

6.1. Background and aims

Despite stable gene expression (SGE) being used as the standard manufacturing method of therapeutic recombinant proteins, it remains time-consuming and labour-intensive. These characteristics are unfavourable when fast production of recombinant products is required. On the other hand, transient gene expression (TGE) is well suited for this case. Without the need for clonal selection and repeated cycles of cell expansion, TGE can rapidly deliver recombinant proteins within 10 - 18 days as opposed to traditional SGE systems which can require more than 6 months from transfection to the generation of stable clones (Pham et al. 2006). TGE is especially useful for the rapid provision of materials to support discovery, early stage development and pre-clinical studies. However, the low recombinant protein titre achievable in TGE has been a significant limitation of this method. As a result, there is increased focus on optimising TGE production yields to attain yields

similar to SGE. Through extensive studies on expression vector development (Codamo et al. 2011b), transfection methods and process optimisation (Cain et al. 2013; Codamo et al. 2011a), up to 2 g/L of recombinant protein can now be achieved with Chinese Hamster Ovary (CHO) cells (Cain et al. 2013) and human embryonic kidney 293 (HEK293) cells (Backliwal et al. 2008a).

However, few studies have directly compared the glycosylation profile between monoclonal antibodies (mAbs) produced in stable and transient gene expression systems. Owing to the difference in the nature of the gene materials and the process of gene expression between the two systems (Kim and Eberwine 2010), it is possible that the oligosaccharide content of mAb products varies between the two systems. Under mild hypothermia in TGE, significant changes in galactose abundance were observed (Galbraith et al. 2006), which could lead to differences in the level of mAb galactosylation between the two systems.

Ensuring comparable product characteristics between TGE and SGE systems is clearly of paramount importance, since relatively minor differences between transfection methods can affect cell growth, mAb productivity and glycosylation. Most importantly, it is important to ensure sufficient similarity between end products generated under SGE and TGE, as transiently produced products are often used in pre-clinical studies. Dependent on advances in TGE, if materials generated from transient gene expression are to be used in clinical study in the future, consistency in recombinant product quality achieved with this method is vital. To this end, this chapter aims to compare the Fc-glycosylation of mAbs produced through SGE and TGE using standard industrially-relevant protocols adapted from Daramola et al. (2014). This study compares mAb production in CHO cells cultured at physiological temperature (36.5°C) in SGE and in TGE with and without a shift to mild hypothermia (32°C). The first part of this chapter compares changes in cell metabolic behaviour, mAb productivity and glycosylation between the two systems. Subsequently, we attempt to identify key factors that contributed to these differences through experimental and flux balance analyses, which would be useful for process optimisation.

6.2. Results

Part 1 - Cellular responses to mild hypothermia in TGE

6.2.1. CHO cell growth profile and mAb synthesis in TGE system

With the plasmid transfection method as described in Chapter 3, which was adapted from Daramola et al. (2014), two experiments were carried out: one set of triplicate 14-day fed-batch cultures of the parental CHO cell line at 36.5°C transfected with IgG heavy and light chain plasmid DNA and another set of identical triplicate cultures subjected to a temperature shift from 36.5°C to 32°C 24 h post-transfection. Similar to the effect described in Chapter 4, CHO cells undergoing TGE in mild hypothermic conditions experience a delay in cell growth, where the integral viable cell concentration (IVCC) is lower than those cultured at physiological temperature. Upon DNA transfection, CHO cells at 32°C suffer from a 7% drop in their cell viability in response to the toxicity of the transfection reagent (PEI) and the mild hypothermic temperature. They later recover and exhibit a more prolonged stationary phase with relatively constant viable cell density (Figure 36 A). Despite the reduction in IVCC, cells at 32°C achieved a prolonged higher viability, with 85% viability at harvest vs 70% viability for cells cultured at 36.5°C.

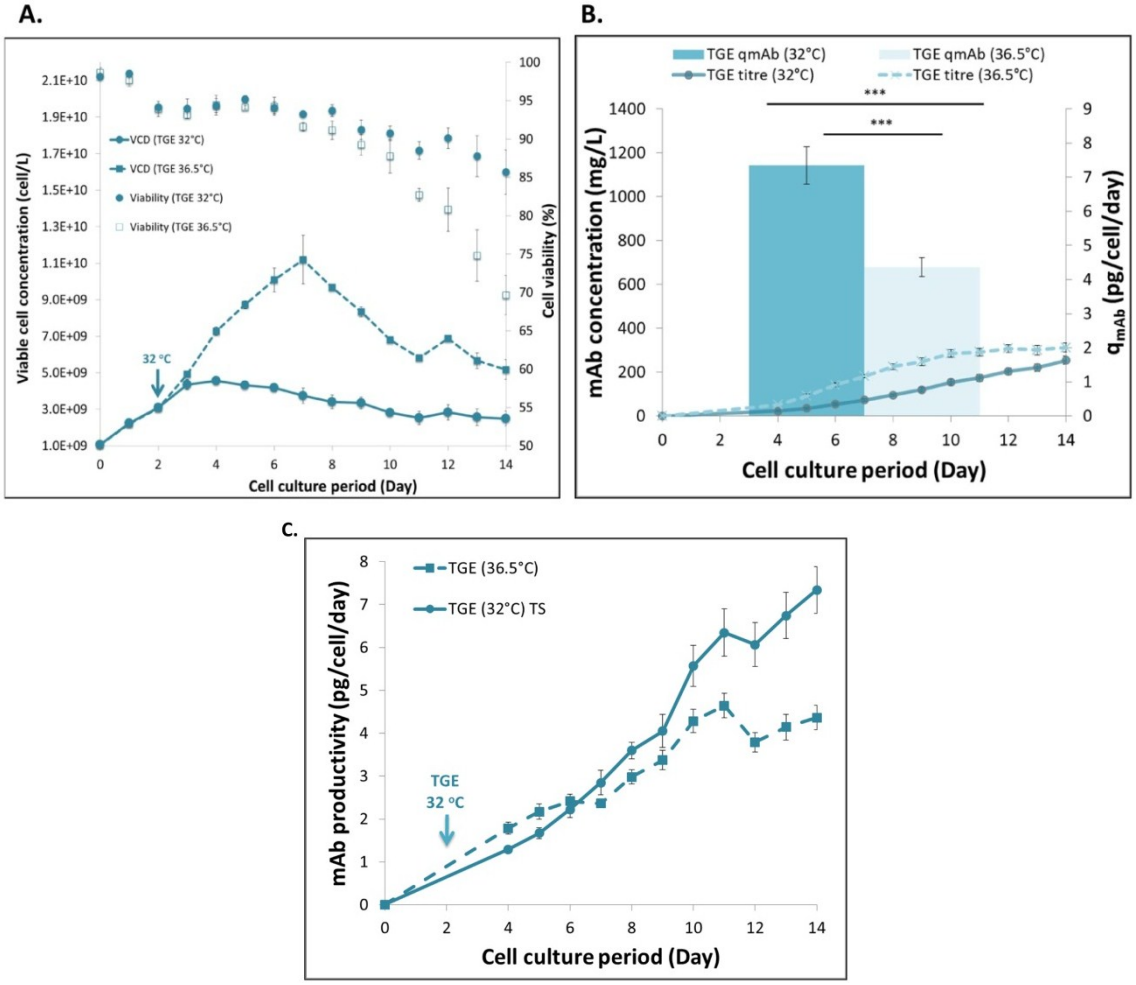

Figure 36. Cell growth, volumetric titre and specific productivity (q_{mAb}) of secreted IgG at 36.5°C and with a temperature shift to 32°C in TGE cells. Viable cell concentration and cell viability profiles were measured along the

period of cell culture (A), together with the q_{mAb} which was calculated based on terminal secreted product and accumulated mAb concentration profile of both temperatures (B). (C). Dynamic q_{mAb} profile of TGE at 36.5°C and at 32°C. Results are average measurements at 36.5°C (n=3) and 32°C (n=3). The error bars represent the standard deviation of the samples.

Figure 36 B shows the volumetric and specific mAb productivities at the two temperatures examined in TGE. Despite a slightly higher volumetric yield observed in TGE system at 36.5°C, our results show that q_{mab} is reduced by 40% in TGE carried out at physiological temperature as compared to TGE with a temperature shift. Specifically, the specific mAb productivity is only 4.1 pg $cell^{-1}$ day^{-1} on harvest day when cells are maintained at 36.5°C, when compared to 7.2 pg $cell^{-1}$ day^{-1} under mild hypothermic conditions. The dynamic profile of q_{mAb} in Figure 36 C shows that higher q_{mAb} is achieved at 32°C from day 10 of cell culture. To investigate the difference in mAb productivity, we examined the DNA copy number, mRNA and polypeptide expression levels at both temperatures. Figure 37 A and Figure 37 B show that upon plasmid transfection, cells in TGE at 32°C exhibit slightly higher transcription efficiency than at 36.5°C. At a transcription level, Figure 37 C and Figure 37 D illustrate that both heavy and light chain mRNA copy numbers are higher at 32°C, with maximum HC and LC mRNA levels observed on day 10. This coincides very well with the dynamic q_{mAb} profile where its rate at 32.5°C is accelerated on day 10. In addition, overall increases in H_2 and H_2L assembly intermediate concentrations are obtained when cells are cultured at 32°C (Figure 37 E and Figure 37 F), with significant increased amount of H_2L species beyond day 10, where q_{mAb} is substantially higher at 32°C. The fact that continuous increase in H_2L concentrations is observed suggests that the addition of LC does not appear to be limiting at 32°C. Our results show that mild hypothermic conditions are beneficial in the TGE in terms of achieving higher q_{mAb} at both transcriptional and translational levels.

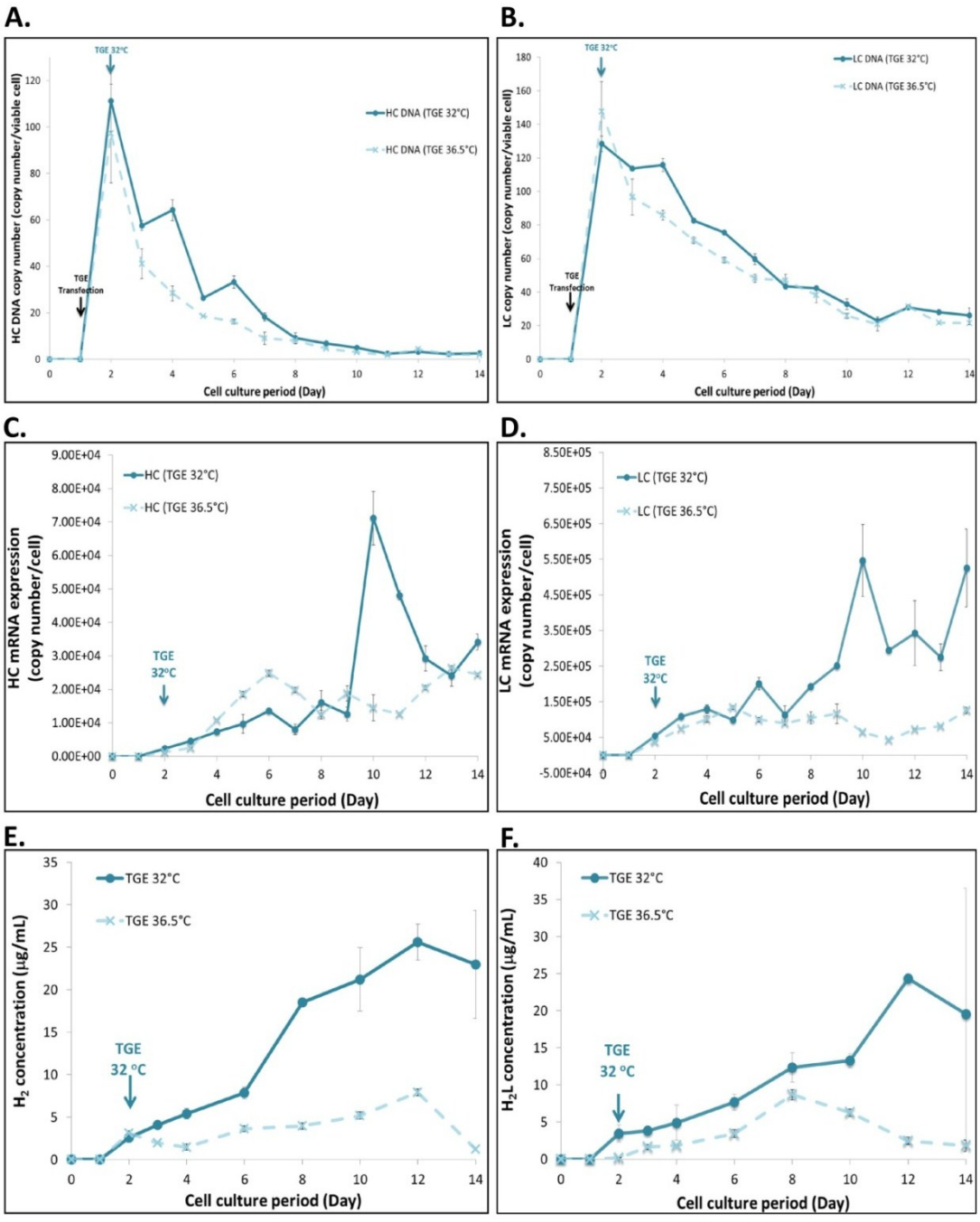

Figure 37. Concentration profiles of heavy and light chain DNA copy number (A & B), heavy and light chain mRNA (C & D), as well as H_2 and H_2L (E & F) intracellular assembly intermediates of IgG molecules in TGE at 36.5°C and TGE at 32°C 24 h post-transfection. Results are averaged measurements at 32°C (n=3) and 36.5°C (n=3) in TGE. The error bars represent the standard deviation of the samples.

6.2.2. The impact of mild hypothermia on NSD metabolism and mAb glycosylation in the TGE system

Firstly, we examined whether product glycosylation was affected by mild hypothermic temperature in the TGE system by comparing the secreted mAb Fc-glycan profiles at 36.5°C and at 32°C on days 10, 12 and 14. When comparing the final quality of our secreted mAb in TGE at the two temperatures chosen, surprisingly and in contrast to the results in Chapter 4 with stable gene expression, the induction of mild hypothermia did not cause many significant changes in the abundance of individual mAb glycan structures at different time points or between the two temperatures examined. The only exceptions are the Man5 and G0 species, in which there were slight increases in cultures conducted under mild hypothermic conditions (Figure 38 A). However, when the rate of mAb galactosylation under each condition was considered, differences between TGE at 36.5°C and 32°C became more pronounced. Results in Figure 38 B suggest that the rate of mAb galactosylation is significantly higher in CHO cells that are cultured at 32°C under TGE. This is also a first indication that CHO cells respond to mild hypothermic temperature differently in different gene expression systems.

A.

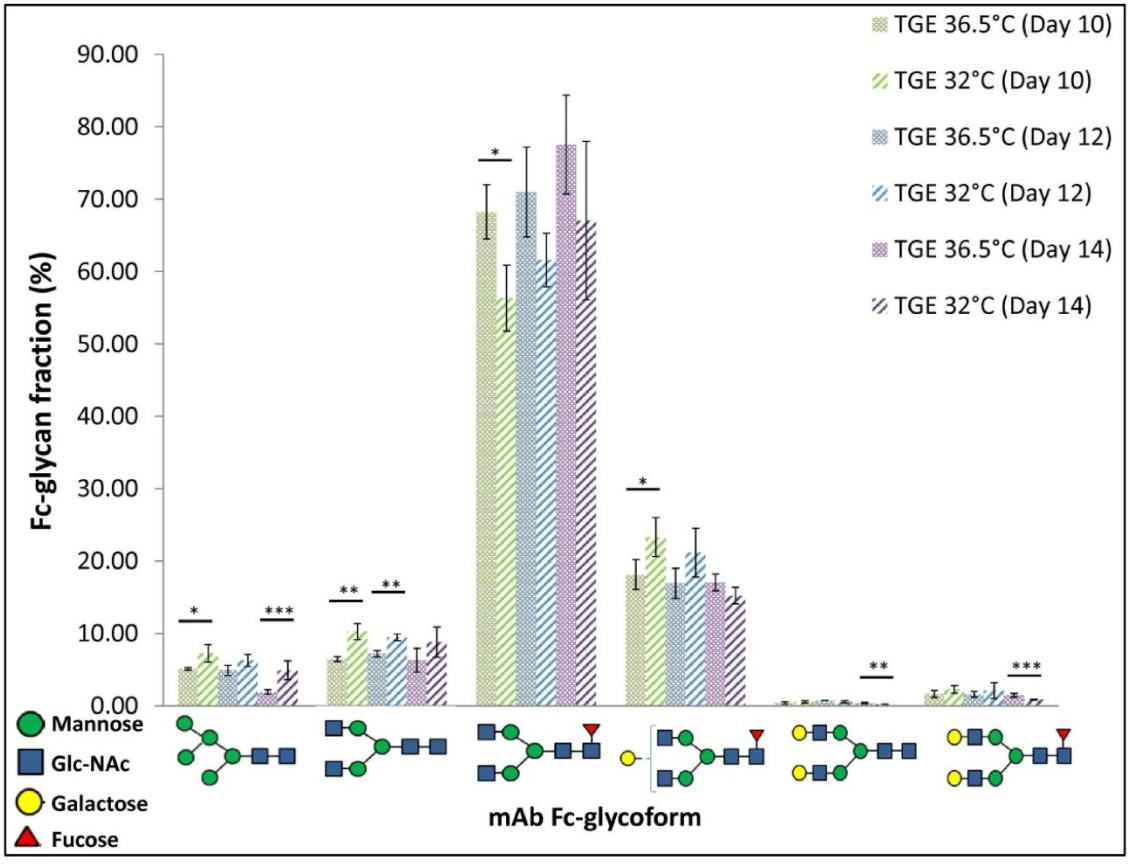

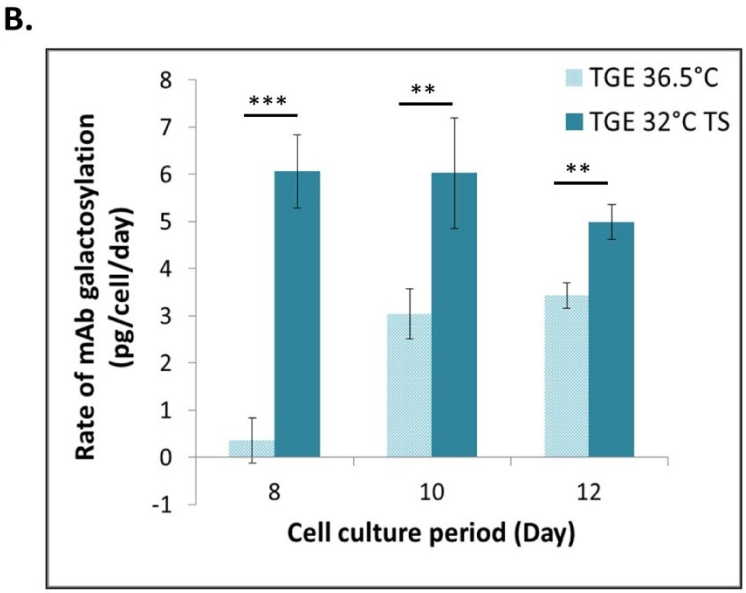

Figure 38. Glycan profile of the secreted IgG. (A). Fractions of 6 glycan structures: Man5, G0, G0F, G1F, G2 and G2F on the secreted IgG products in TGE cells were determined. Results were average measurements at 36.5°C (n=3) and 32°C (n=3). (B). Rate of mAb galactosylation. The error bars represent the standard deviation of the samples. Statistical significance was calculated using a Student's t-test and was represented by: *p≤0.05(*), p≤0.01(**) and p≤0.001(***)*. TS: Temperature shift.

As discussed in Chapter 4, NSD metabolism determines the availability of building components for protein glycosylation. Figure 39 A to Figure 39 C show the net intracellular concentrations of UDP-Glc, UDP-GlcNAc and UDP-Gal in the two temperatures examined. Our results show that UDP-Glc and UDP-Gal levels vary in TGE between 36.5°C and 32°C, with slightly higher concentrations of both species observed at 32°C. These variations could result from the difference in specific glucose uptake rate observed at the later stage of the process in TGE at 32°C (Figures 41 A & B). Similar to Chapter 4, the UDP-Gal profile shown in Figure 39 B contains data points that are under the detection limit of our current HPLC method and they are regarded as value 0.0 pmol/cell on the profile. Owing to this technical limitation, flux balance analysis was being performed to further illustrate the synthesis of NSD species. Despite these increases, comparable levels of UDP-GlcNAc were obtained at both temperatures (Figure 39 C).

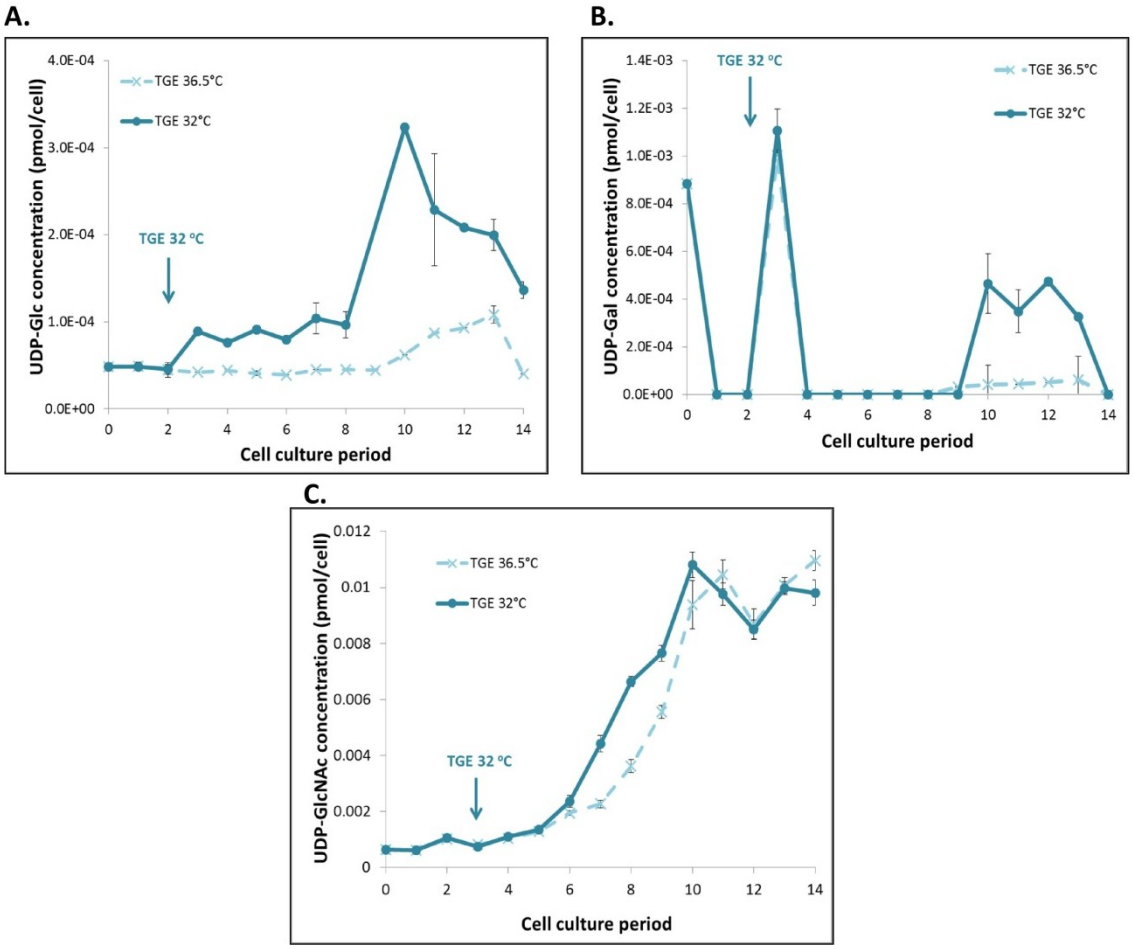

Figure 39. NSD profile of the secreted IgG in TGE. Experimentally determined concentrations of UDP-Glc (A), UDP-Gal (B) and UDP- GlcNAc (C). Results are averaged measurements at 36.5°C (n=3) and 32°C (n=3) in TGE. The error bars represent the standard deviation of the samples.

6.2.3. Expression profile of N-glycosylation related genes in TGE

In addition to the availability of nucleotide sugar donors (NSDs), the other factor that affects glycan processing is the expression and activity of glycosyltransferases and NSD transporters that are involved in N-linked product glycosylation. Given the different concentrations of intracellular UDP-Gal but similar glycan profiles between the two temperatures examined, one must look into the expression level of glycosyltransferases to explain the glycan results. We examined the same sets of glycosyltransferases as in Chapter 4. Figure 40 A shows that the gene expression levels of β-GalTII & III and FucT are higher at 36.5°C than those at 32°C in TGE. Increase in transcription is further accompanied by the higher protein expression level of β-GalTIII at 36.5°C (Figure 40 B). Interestingly we also observed a rise in mRNA expression of GnTII in TGE under mild hypothermic

condition. The fact that GnTII was being massively up-regulated at 32°C in TGE (as observed in this study at transcription level) suggested that the addition of UDP-GlcNAc for bi-antennary glycan structure could also be a crucial factor that promotes mAb glycan processing and provides enough substrate for later mAb galactosylation in the TGE system at 32°C, resulting in increased rate of mAb galactosylation per cell (Figure 38 B). Higher GnTII expression at 32°C could also link to the comparable net concentration of UDP-GlcNAc that was observed between the temperatures in Figure 3 C, where higher consumption of UDP-GlcNAc might be involved.

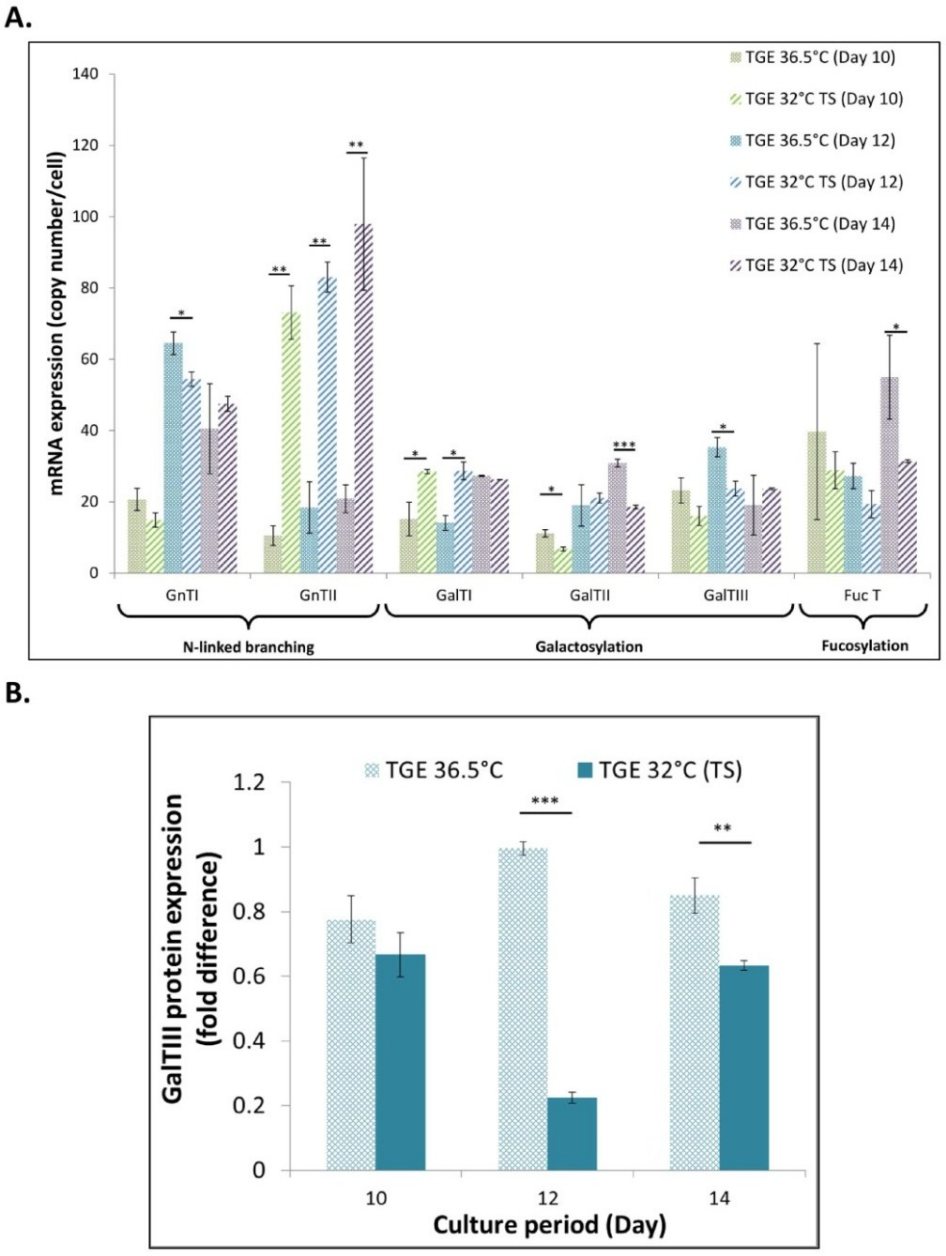

Figure 40. (A) Gene expression profile of N-linked related glycosylation enzymes. mRNA expression levels of 6 glycosyltransferases, namely GnTI, GnTII, GalTI, GalTII, GaTIII and FucT, were determined. (B) Relative difference in galactosyltransferase III (β-GalTIII) protein expression. Results are averaged measurements at 36.5°C

(n=3) and 32°C (n=3) in TGE. The error bars represent the standard deviation of the samples. Statistical significance was calculated using a Student's t-test and was represented by: *p≤0.05(*), p≤0.01(**) and p≤0.001(***).*

6.2.4. Changes in CHO cell metabolism in response to mild hypothermic temperature in the TGE system

To further clarify the difference in rates of mAb galactosylation and NSD profiles between the two chosen temperatures, it is worthwhile looking into the metabolic profile of cells under these conditions. As the main carbon source for CHO cells, glucose consumption profiles shown in Figure 41 A are significantly different between the two temperatures. The overall glucose consumption per cell is around 60% higher in cells undergoing TGE at 32°C than its counterpart at 36.5°C, with a 1.6-fold increase in its peak glucose consumption achieved on day 11 at 32°C. In addition to changes in glucose intake, lactate consumption is high at 32° C, with an average of 74% of the lactate produced during exponential phase being consumed. However, at physiological temperature, lactate consumption is very low with only 12% of lactate being taken up. Cells also produce 1.4-fold more lactate at 36.5°C than the transient transfectants that are cultured at 32°C (Figures 41 B & C). The 60% reduction in glucose demand per cell and 1.4-fold rise in lactate production in CHO cells undergoing TGE at 36.5°C are reflective of the exponential cell death and lowered cell metabolism at 36.5°C. Since NSD metabolism is directly influenced by the availability of the carbon source, changes observed in the intracellular pool of NSD species can be attributed to variation in nutrient metabolism upon different culture temperatures.

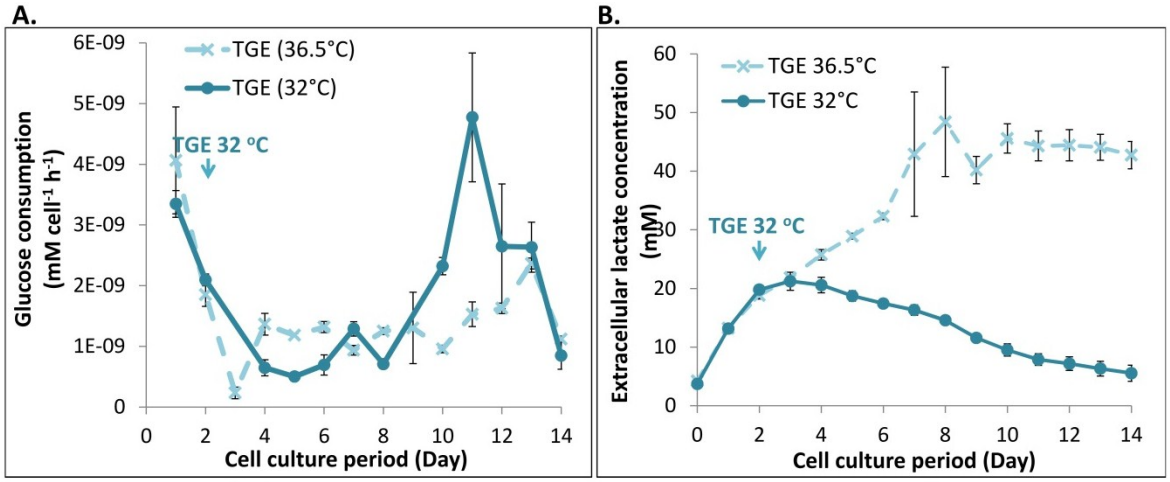

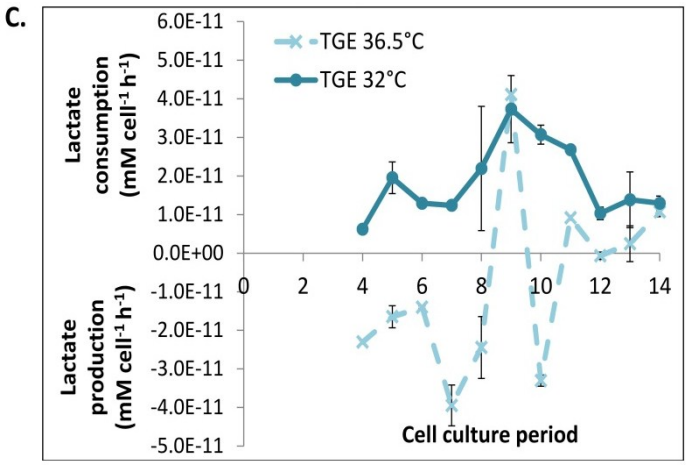

Figure 41. An overview of nutrient utilisation. Concentration profiles of glucose consumption per viable cell (A), the extracellular lactate concentration (B) when CHO cells were expressed in TGE at 36.5°C and at 32°C 24 h post transfection. (C). Lactate consumption/production per viable cell concentration profile in TGE at 36.5°C and at 32°C induced 24 h post-transfection. Results are averaged measurements at 32°C (n=3) and 36.5°C (n=3) in TGE. The error bars represent the standard deviation of the samples.

6.2.5. Examining cell metabolism in TGE at different temperatures through flux balance analysis (FBA)

Despite the usefulness of the NSD study, it can only provide information about the net intracellular concentration of each species, but not distinguishing between over- or under-production and over- or under-consumption of these species. To further elucidate the effect of different temperatures on product glycosylation in TGE, metabolic fluxes were calculated using FBA. From the experimental data, we calculated the consumption and production rates of each measured species using the method presented in Kyriakopoulos (2014). The rates calculated for the stationary phase at both temperatures (Table 17) show that at 36.5°C transient transfectants behave very differently from those at 32°C. In good correlation to experimental results, calculated metabolic rates in Table 17 suggest that cells cultured at 32°C in TGE consume both substantially high levels of glucose and lactate. In the case of amino acids, the consumption of asparagine at 32°C is nearly 3-fold higher, where 1/3 of the Asn consumed is converted into aspartate. But slightly slower consumption of most other amino acids, e.g. isoleucine, lysine, serine, phenylalanine and tyrosine, are observed at 32°C. Most importantly, the rate of mAb synthesis is higher at 32°C, which is in good agreement with the 76% increase in q_{mAb}.

Table 17. Average specific metabolic production and consumption rates for TGE at 36.5°C and with temperature-shifted to 32°C. Results are averaged measurements at 36.5°C (n=3) and 32°C (n=3) in TGE.

	Consumption/production rate (femtomol/cell/day)	
	36.5°C	32°C
	TGE	
Ala	106.8	152.0
Amm	18.0	38.8
Arg	-13.5	5.0
Asn	-118.0	-308.0
Asp	-80.5	159.2
Glc	-346.5	-480.5
Gln	47.5	64.8
Glu	-9.4	2.4
Gly	87.4	72.4
His	-0.5	18.7
Ile	-27.4	-1.9
Lac	481.4	-262.7
Leu	-94.7	-97.5
Lys	-23.6	-1.8
Met	-12.1	-14.2
Phe	-14.2	-7.6
Pro	-25.6	-27.8
Ser	-156.7	-123.5
Thr	-16.8	2.8
Trp	-5.0	-1.6
Tyr	-9.1	6.1
Val	-56.3	-51.4
IgG	0.0	5.8
	Specific growth rate (day^{-1})	
μ	-0.1	0.0

Negative value: consumption. Positive value: pro

The FBA was then constrained with these calculated rates of exometabolites, maximum q_{mAb} and growth rate (μ). Despite not having an obvious stationary phase in the TGE system at 36.5°C, we analysed carbon fluxes in the decline phase and compared them to those at the same time point for the 32°C system, which was still at stationary stage. In line with experimental results, Figure 42 shows that cells at 36.5°C consume less glucose and most carbon fluxes end up in lactate production rather than being utilized in the TCA cycle for cell growth and maintenance. Unlike cells at 32°C, those at 36.5°C experience minimal level of lactate consumption. A higher amount of amino acids are fed back into the TCA cycle and less is available for mAb production, which occurs mostly at exponential growth phase. On the other hand, cells at 32°C consume a much higher amount of asparagine, which

contributes to increased amino acid flux into the TCA cycle, glutamine and aspartate synthesis during the stationary mAb-producing phase. At 36.5°C, the overall carbon and nitrogen fluxes going towards nucleotide, NSD and lipid syntheses are lower (Table 18). Surprisingly, at physiological temperature, we observe an increase in metabolic flux towards UDP-N-acetylhexosamine production. This is reflected by high UDP-GlcNAc levels experimentally (Figure 40 C), where the abundance of nitrogen source could be resulted from a combination of cell death, higher glutamine and ammonia productions (Valley et al. 1999).

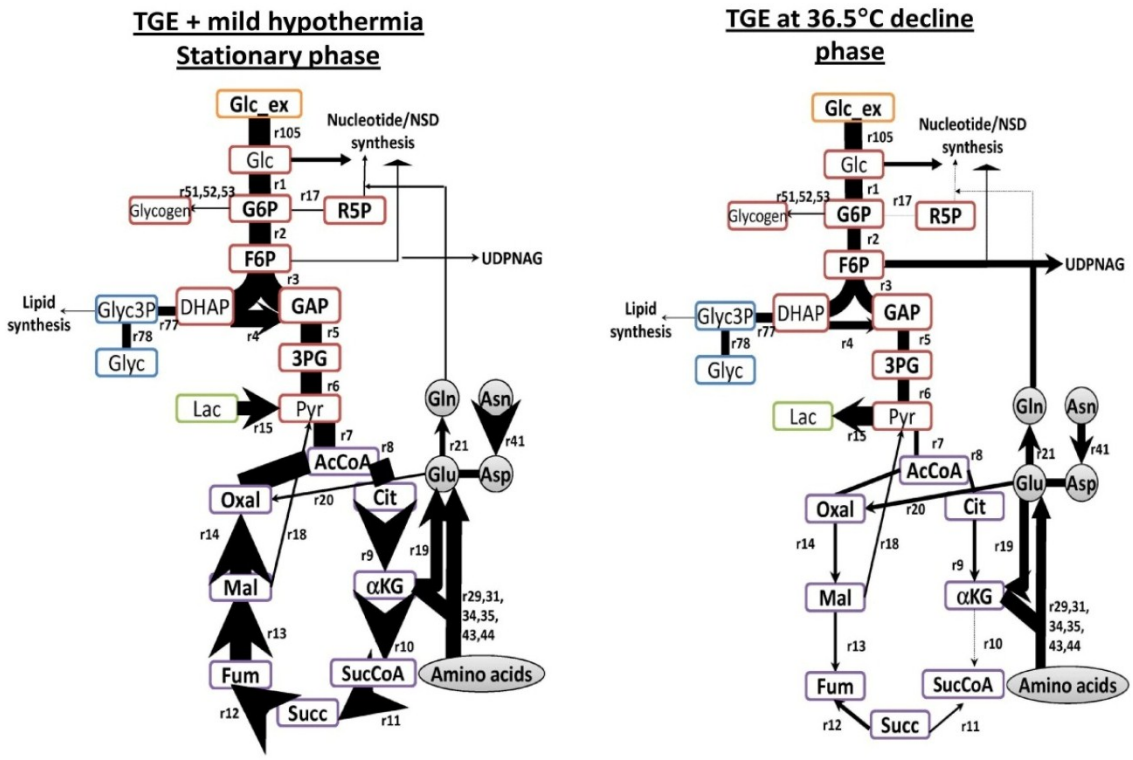

Figure 42. Central carbon metabolism of CHO cells at stationary phase in TGE at 32°C and decline phase at 36.5°C. Thickness of an arrow indicates the relative flow of the carbon source within the system. This figure is simplified to include carbon lost to glycerol, glycogen and lactate production, together nucleotide, NSD, lipid and key amino acid synthesis.

Table 18. FBA estimated flux values in nucleotide synthesis, lipid synthesis and protein glycosylation during stationary phase in TGE at 32°C and decline phase at 36.5°C.

Reaction	Equation		Subsystem	Flux value (femtomol/cell/day)	
				Stationary phase TGE 32°C	Decline phase TGE 36.5°C
54	[c] : R5P + ATP --> PRPP + AMP	Irreversible	Nucleotide	0.07	1.07E-10
55	[c] : PRPP + (2) Gln + Gly + Asp + (5) ATP + CO2 + (2) N10FTHF --> IMP + (2) Glu + Fum + (5) ADP + (2) THF	Irreversible	Nucleotide	0.00	0.00
56	[c] : IMP + Asp + GTP --> AMPRN + Fum + GDP	Irreversible	Nucleotide	0.00	0.00
57	[c] : IMP + Gln + ATP + NAD --> GMPRN + Glu + AMP + NADH	Irreversible	Nucleotide	0.00	0.00
58	[c] : HCO3 + NH4 + Asp + (2) ATP + NAD --> Orotate + (2) ADP + NADH	Irreversible	Nucleotide	0.07	1.07E-10
59	[c] : Orotate + PRPP --> UMPRN + CO2	Irreversible	Nucleotide	0.07	1.07E-10
60	[c] : UMPRN + Gln + ATP --> CMPRN + Glu + ADP	Irreversible	Nucleotide	0.00	0.00
61	[c] : AMPRN --> dAMP	Irreversible	Nucleotide	0.00	0.00
62	[c] : GMPRN --> dGMP	Irreversible	Nucleotide	0.00	0.00
63	[c] : CMPRN --> dCMP	Irreversible	Nucleotide	0.00	0.00
64	[c] : UMPRN --> dTMP	Irreversible	Nucleotide	0.00	0.00
65	[c] : Choline + ATP --> Pcholine + ADP	Irreversible	Lipid	2.63	1.50
66	[c] : Pcholine + (18) AcCoA + Glyc3P + (22) ATP + (33) NADH --> PC + (16) ADP + (6) AMP + (33) NAD + (18) CoASH	Irreversible	Lipid	0.00	0.00
67	[c] : PC + Ser <==> PS + Choline	Reversible	Lipid	0.00	0.00
68	[c] : PS --> PE + CO2	Irreversible	Lipid	0.00	0.00
69	[c] : Choline + Glyc3P <==> Glyc3PC	Reversible	Lipid	3.53	4.67
70	[c] : G6P --> Inositol	Irreversible	Lipid	0.00	0.00
71	[c] : Inositol + (18) AcCoA + Glyc3P + (22) ATP + (33) NADH --> PI + (16) ADP + (6) AMP + (33) NAD + (18) CoASH	Irreversible	Lipid	0.00	0.00
72	[c] : (18) AcCoA + (2) Glyc3P + (22) ATP + (33) NADH --> PG + (16) ADP + (6) AMP + (33) NAD + (18) CoASH	Irreversible	Lipid	0.00	0.00
73	[c] : (2) PG --> DPG + Glyc	Irreversible	Lipid	0.00	0.00
74	[c] : (16) AcCoA + Ser + Choline + (16) ATP + (29) NADPH --> SM + (2) CO2 + (14) ADP + (2) AMP + (29) NADP + (16) CoASH	Irreversible	Lipid	0.00	0.00
75	[c] : (18) AcCoA + (18) ATP + (14) NADPH --> Cholesterol + (9) CO2 + (18) ADP + (14) NADP + (18) CoASH	Irreversible	Lipid	0.00	0.00
79	[c] : UDPG <==> UDPGal	Reversible	Glycosylation	0.07	1.07E-10
80	[c] : Glc + ATP + GTP --> GDPMann + ADP	Irreversible	Glycosylation	0.66	1.08E-09
81	[c] : F6P + Gln + AcCoA + UTP --> UDPNAG + Glu + CoASH	Irreversible	Glycosylation	0.67	44.21
82	[c] : UDPNAG + ATP + 3PG + CTP --> CMPNeu5Ac + UDP + ADP	Irreversible	Glycosylation	0.00	0.00
83	[c] : GDPMann + NADPH --> GDPFuc + NADP	Irreversible	Glycosylation	0.16	2.57E-10
84	[c] : UDPNAG <==> UDP + GlcNAc	Reversible	Glycosylation	0.00	0.00
85	[c] : UDPNAG <==> UDPGalNAc	Reversible	Glycosylation	0.00	0.00
86	[c] : UDPGalNAc <==> GalNAc + UDP	Reversible	Glycosylation	0.00	0.00
87	[c] : GDPMann <==> Mann + GDP	Reversible	Glycosylation	0.00	0.00
88	[c] : UDPGal <==> Gal + UDP	Reversible	Glycosylation	0.00	0.00
89	[c] : CMPNeu5Ac <==> CMP + Neu5Ac	Reversible	Glycosylation	0.00	0.00
90	[c] : GDPFuc <==> GDP + Fuc	Reversible	Glycosylation	0.00	0.00

6.3. Results

Part 2 - Comparing product quality produced under SGE and TGE processes

After examining the impact of mild hypothermia on cell metabolism and mAb glycosylation in the TGE system, in this part of the chapter, we aim to compare the product produced by SGE to that by the TGE system under two conditions for each expression system. These four processes are: a 14-day fed-batch culture of IgG-expressing CHO cells at 36.5°C and the same process with a temperature shift to 32°C during late exponential growth phase in SGE; and 14-day fed-batch culture of the parental CHO cell line with plasmid transfection on day 1 at 36.5°C and the same process with a temperature shift to 32°C 24 h post-transfection. The TGE transfection protocol was adapted from the protocol in Daramola et al. (2014).

6.3.1. CHO cell growth and mAb synthesis in SGE and TGE systems

One of the differences between the two expression systems related to their growth profiles. Stably transfected cells achieve 26% but 3-fold higher in their maximum viable cell concentration than TGE cells cultured at 36.5°C and 32°C, respectively. Despite lower integral of viable cell concentration (IVCC) in the TGE system, cells cultured at 32°C exhibited a more prolonged stationary phase with relatively constant viable cell density after recovery from the toxicity of the transfection reagent and the mild hypothermic temperature (Figure 43 A). On the other hand, cells that undergo TGE at 36.5°C do not achieve the same cell density as those in SGE during exponential growth, but the rate of cell death is higher than the other three conditions, which is reflected by the accelerated drop in cell viability.

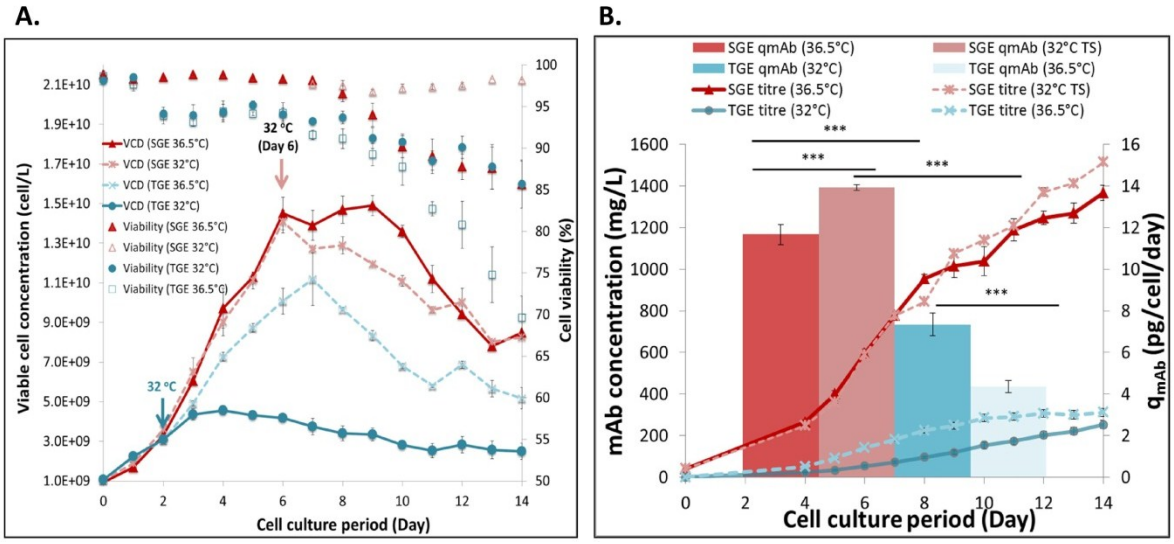

Figure 43. Comparing cell growth profile and secreted IgG productivity between SGE (36.5°C or 32°C TS) and TGE (36.5°C or 32°C TS). (A). Viable cell concentration and cell viability of both expression systems. (B). Volumetric and specific mAb productivity on day 14. Results are averaged measurements at 36.5°C (n=6) and 32°C (n=3) in SGE; 36.5°C (n=3) and 32°C (n=3) in TGE. The error bars represent the standard deviation of the samples. TS: temperature shift.

The low volumetric yield is always the main constraint in transient gene expression (Baldi et al. 2007; Wurm 2004) and we observed the same trend in this work. Specifically, the volumetric product yield in TGE is approximately 4-fold lower than that achieved in the SGE system. In addition, the q_{mAb} in TGE at 32°C in this study is around 40% lower than that of the stably expressing cell line at 36.5°C, and it is half of that of the stable transfectants in mild hypothermic conditions (Figure 43 B). By quantifying the intracellular species produced during mAb synthesis, our results show that, unlike the SGE system, transiently expressing cells do not have a constant DNA copy number of heavy or light chains, as expected. Their DNA copy number peaked within 2 days of transfection, followed by a gradual reduction along the culture period (Figures 44 A & B). In response to the rate of DNA uptake, both heavy and light chain mRNA expression and the concentration of H_2L mAb assembly intermediates are significantly lower under the TGE system, particularly in the system maintained at 36.5°C (Figures 44 C – F). Moreover, different profiles of the assembly intermediates between the two systems suggest that the rate of mAb synthesis varies between exponential and stationary phases. Peaks of H_2 and H_2L concentrations are observed between days 8 to 12 in SGE at both temperatures. In contract, these concentrations rise steadily in TGE at 32°C throughout the culture period. Differences in profile can be the result of reduced mAb assembly rate during TGE which it slows the throughputs of assembled mAb species. Cells undergoing SGE undergo a longer exponential growth phase than their counterpart in TGE at 32°C; transiently transfected cells enter stationary phase 48 h after the induction of mild hypothermia. The prolonged stationary phase in TGE

allowed cells to synthesize mAb at a constant rate, while cells stably expressing mAbs exhibit two stages of production at different rates. Overall, our results show higher transcription, translation and product secretion in SGE at both these stages, contributing to the higher specific mAb productivity in SGE.

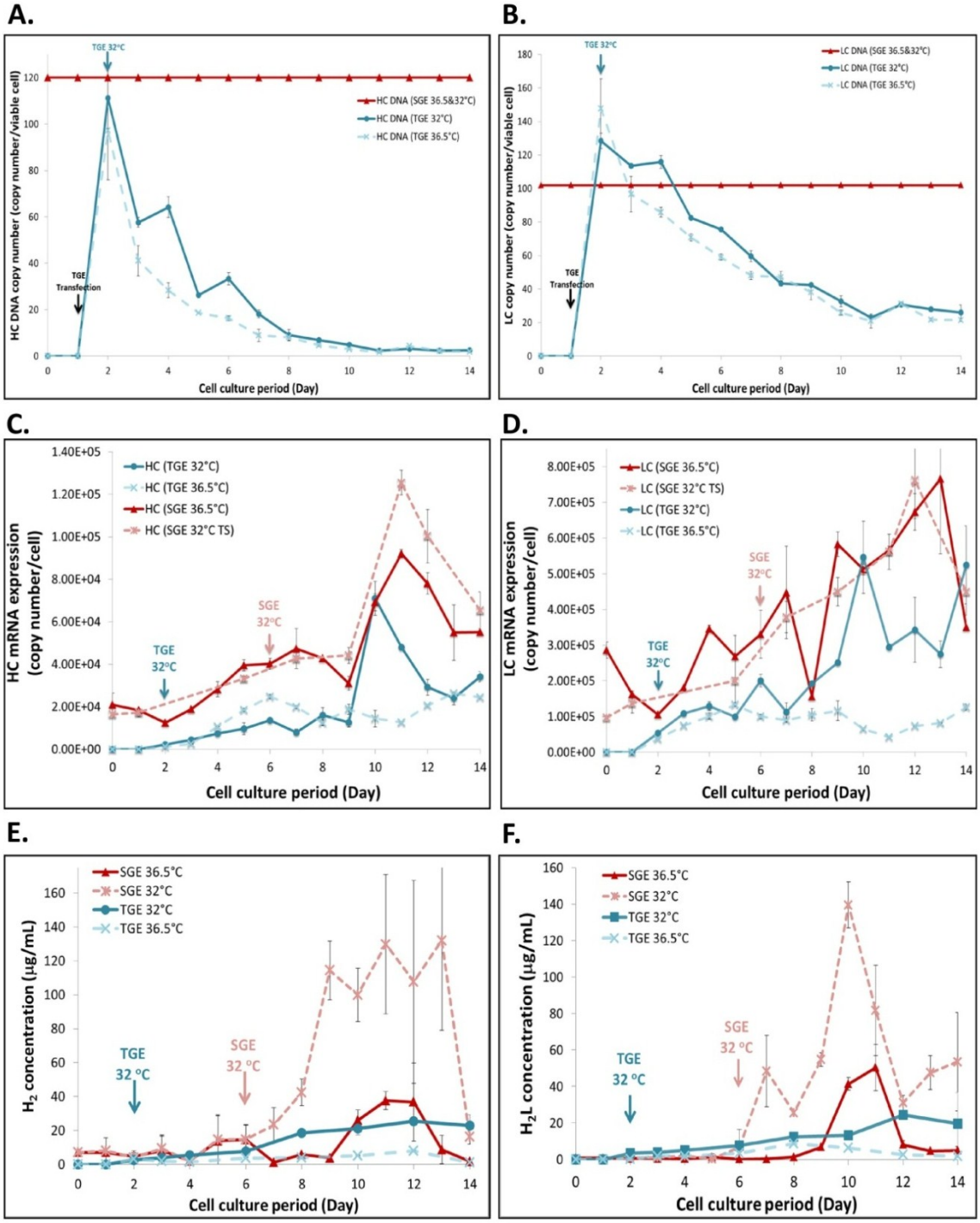

Figure 44. Concentration profiles of heavy and light chain DNA copy number (A & B), heavy and light chain mRNA (C & D), as well as H_2 and H_2L (E & F) intracellular assembly intermediates of IgG molecules in SGE at 36.5°C and 32°C, and TGE at 36.5°C or 32°C 24 h post-transfection. Results are averaged measurements at 36.5°C (n=6) and

32°C (n=3) in SGE; 36.5°C (n=3) and 32°C (n=3) in TGE. The error bars represent the standard deviation of the samples. TS: temperature shift.

6.3.2. Comparing the mAb Fc-glycan profiles and NSD metabolism between SGE and TGE

In addition to the differences in cell growth and mAb productivity, we sought to examine whether there was any variation in glycosylation profiles under TGE. We compared mAb Fc-glycan profiles of both expression systems on days 10, 12 and 14. When examining quality of our secreted mAb products, despite minimal differences in glycan profiles between 36.5°C and 32°C in TGE observed in Part 1, significant changes were found between the SGE and TGE systems. Specifically, in Figure 45 A we observe a decrease in product galactosylation when compared to mAb produced in SGE at 36.5°C, where the proportion of more processed glycoforms namely G1F and G2F, is significantly lower in the mAb produced by the TGE system. In addition, the fraction of Man5 species was approximately 6-fold higher in the TGE experiments. However, when compared to the stable transfectants that undergo mild hypothermia, mAb produced from cells in TGE, at 32°C in particular, achieve a remarkably lower fraction of G0F, higher in Man5, G0 and G2 species (Figure 45 B). Not only does the level of galactosylation is similar in products produced by cells undergoing SGE at 32°C and TGE at 36.5°C, there are very few variations in the mAb glycan profiles produced under these two conditions. However, when rate of galactose addition within a single cell is concerned, there is no doubt that rate of mAb galactosylation is significantly higher in SGE than in TGE in all cases examined in this study (Figure 45C). Our results here clearly indicate that cells are metabolically different under different gene expression systems and cells response to mild hypothermia differently in SGE than in TGE.

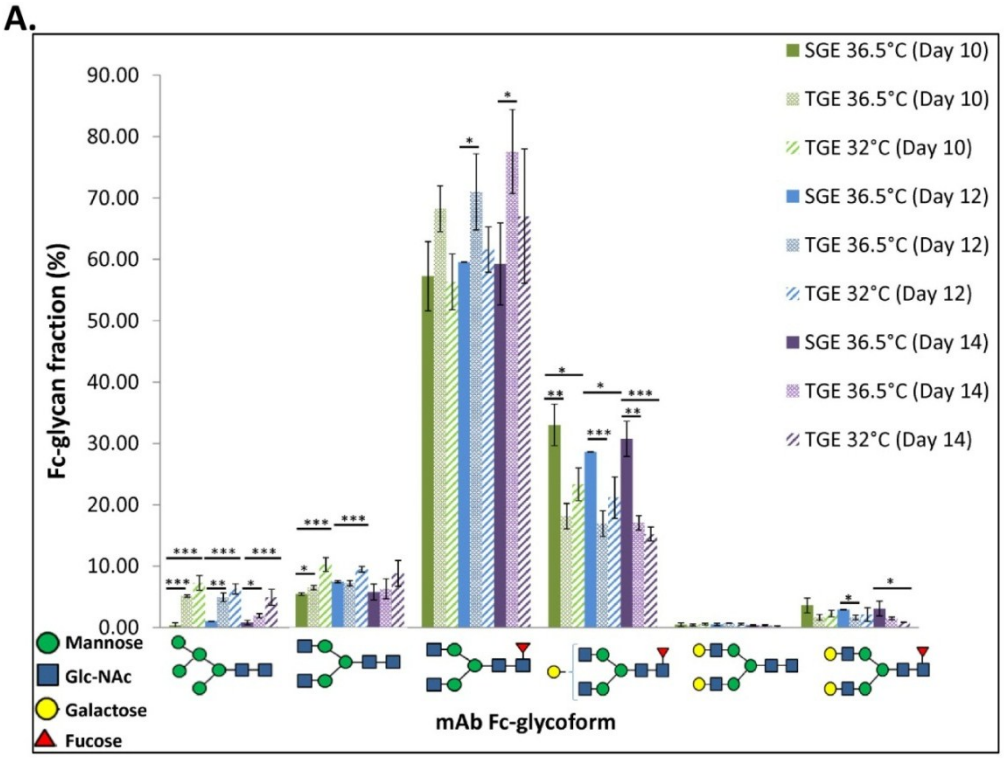
A.
SGE 36.5°C (Day 10)
TGE 36.5°C (Day 10)
TGE 32°C (Day 10)
SGE 36.5°C (Day 12)
TGE 36.5°C (Day 12)
TGE 32°C (Day 12)
SGE 36.5°C (Day 14)
TGE 36.5°C (Day 14)
TGE 32°C (Day 14)
Fc-glycan fraction (%)
90.00
80.00
70.00
60.00
50.00
40.00
30.00
20.00
10.00
0.00
Mannose
Glc-NAc
Galactose
Fucose
mAb Fc-glycoform

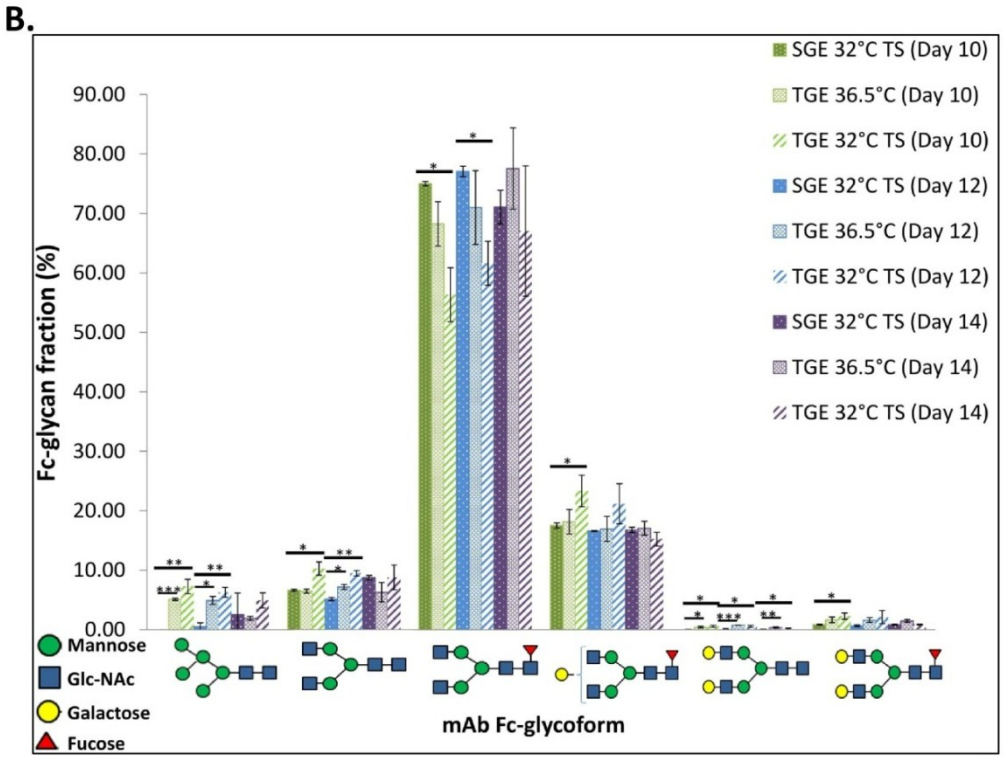
B.
SGE 32°C TS (Day 10)
TGE 36.5°C (Day 10)
TGE 32°C TS (Day 10)
SGE 32°C TS (Day 12)
TGE 36.5°C (Day 12)
TGE 32°C TS (Day 12)
SGE 32°C TS (Day 14)
TGE 36.5°C (Day 14)
TGE 32°C TS (Day 14)
Fc-glycan fraction (%)
90.00
80.00
70.00
60.00
50.00
40.00
30.00
20.00
10.00
0.00
Mannose
Glc-NAc
Galactose
Fucose
mAb Fc-glycoform

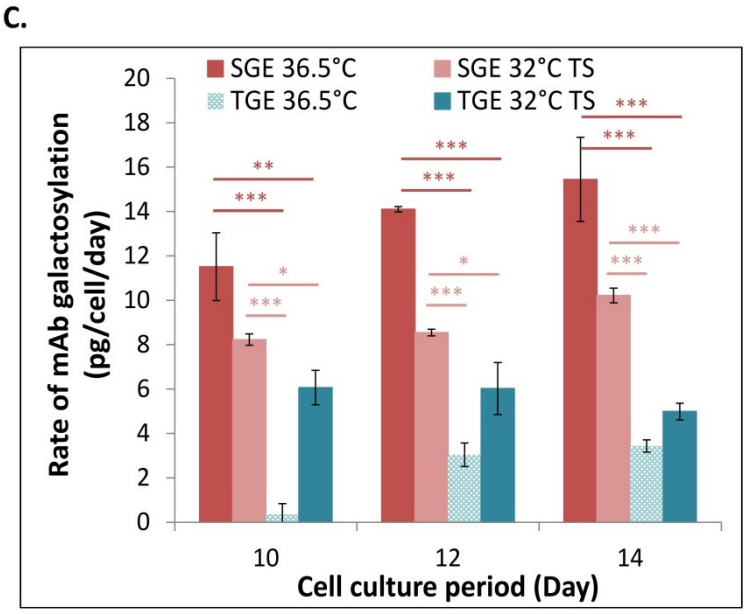

Figure 45. mAb Fc-glycan profile of the secreted IgG. (A). Comparison of mAb Fc glycan profile among SGE at 36.5°C, TGE at 36.5°C and 32°C TS. (B). Comparison of mAb Fc glycan profile among SGE at 32°C TS, TGE at 36.5°C and 32°C TS. Fractions of Man5, G0, G0F, G1F, G2 and G2F were experimentally measured in stably and transiently expressed cell lines. (C). Rate of mAb galactosylation in all four conditions examined (SGE vs. TGE). Results are averaged measurements at 36.5°C (n=6) and 32°C (n=3) in SGE; 36.5°C (n=3) and 32°C (n=3) in TGE. The error bars represent the standard deviation of the samples. Statistical significance was calculated using a Student's t-test and was represented by: *$p \leq 0.05$(*), $p \leq 0.01$(**) and $p \leq 0.001$(***).*

In the case of NSD metabolism, Figures 46 A – C show that the overall concentrations of UDP-Glc, UDP-Gal and UDP-GlcNAc are higher under TGE at 32°C only but not at 36.5°C, when compared to those in SGE at 36.5°C or 32°C. Higher net concentrations of NSDs observed in TGE at 32°C can be a result of increases in specific glucose and lactate uptake rates during stationary phase (see Figures 49 A & B). However, with the exception of UDP-GlcNAc, concentrations of UDP-Glc and UDP-Gal during stationary growth phase in TGE at 36.5°C are similar to those in SGE when cells are cultured at the same temperature. Minimal changes in mAb Fc-glycan observed between SGE at 32°C and TGE at physiological temperature are in this case reflected by the small variations in NSD levels. As mentioned before, UDP-Gal profile shown in Figure 46 B contains data points that are under the detection limit of our current HPLC method and they are regarded as value 0.0 pmol/cell on the profile. This technical limitation indeed reduces the confidence of this data set, and to overcome this issue metabolic distribution of cells was examined later in the chapter.

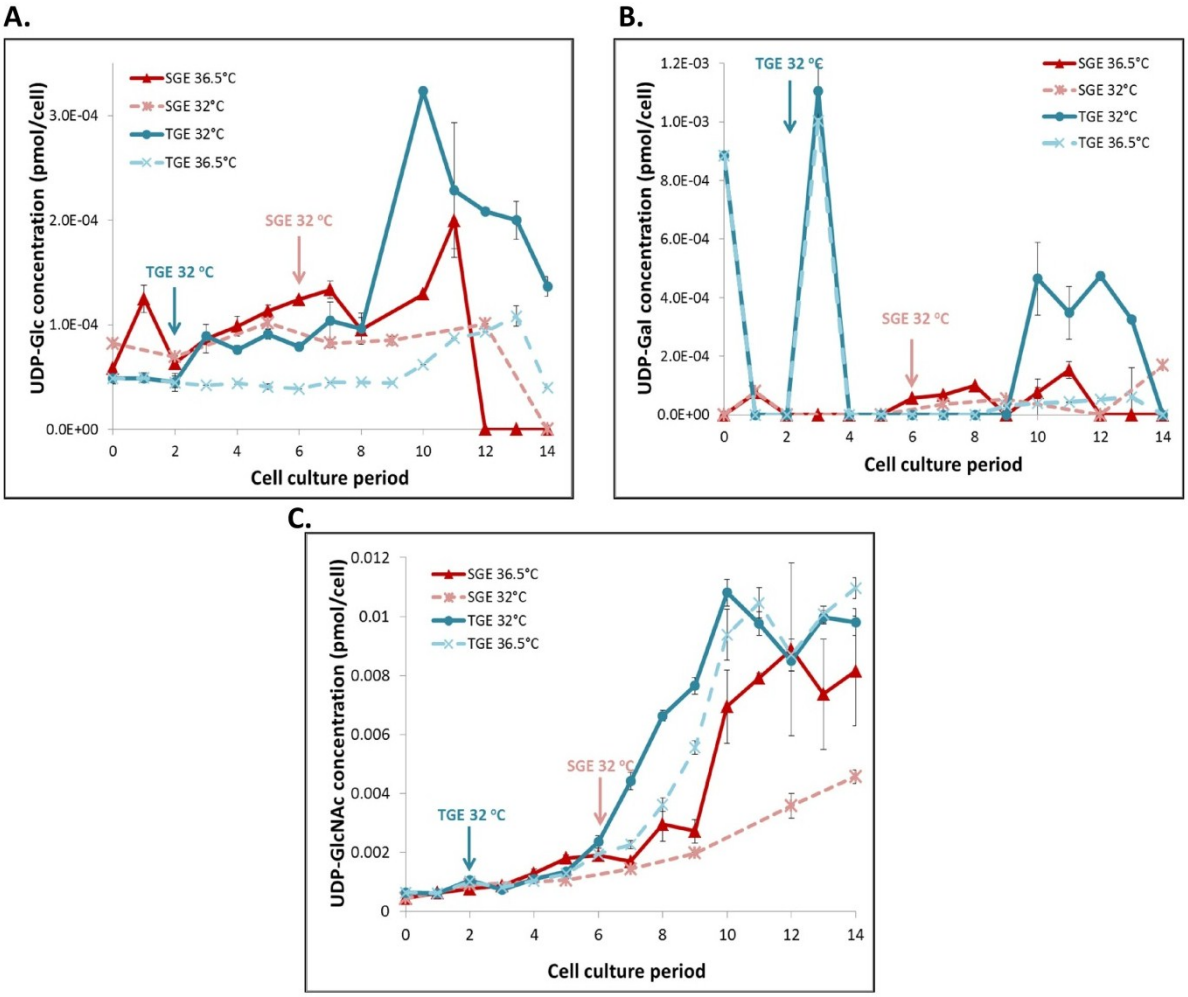

Figure 46. Concentration profiles of NSD species in SGE and TGE cells in physiological and mild hypothermic conditions. Concentrations of UDP-Glc (A), UDP-Gal (B) and UDP-GlcNAc (C) of the four conditions were experimentally determined. Results are averaged measurements at 36.5°C (n=6) and 32°C (n=3) in SGE; 36.5°C (n=3) and 32°C (n=3) in TGE. The error bars represent the standard deviation of the samples.

6.3.3. Differences in N-glycosyltransferase expression between SGE and TGE systems

Given the different profiles of intracellular nucleotide sugar concentrations among all four conditions, we turned to the quantification of glycosyltransferase expression in order to identify the cause of differences in glycan structures between the two systems. Figure 47 A compares gene expression levels of N-linked glycosyltransferases of both temperatures in TGE and SGE at 36.5°C. We observed a significant reduction in GnTI, β- GalTIII and FucT in TGE at 32°C compared to the expression levels of these genes in SGE at 36.5°C. In addition, mRNA level of GnTII were comparable between SGE at 36.5°C and TGE at 32°C, with the exception of TGE at 36.5°C in which its GnTII transcript levels were the lowest among the three conditions. If these are translated into

equivalent changes at protein level, our results suggest that reduction of GnTI at both temperatures in TGE could have contributed to the larger fraction of Man5. The combination of reduced levels in GnTI & II and GalTI & III could in part contribute to the lowest rate of mAb galactosylation observed among the four conditions. While in the case TGE at 32°C, despite the lower level of GnTI, bi-antennary glycan branching of mAb was salvaged by the comparable expression levels of GnTII to some extent, but mAb galactosylation was still affected by the reduced GalTII &III mRNA transcription, resulting in but lower portions of G1F and G2F in TGE at 32°C. Limited mAb galactosylation at 32°C is further explained by the reduced protein expression of galactosyltransferase (Figure 48 A). On the other hand, the transcript level of FucT is significantly higher in TGE at 36.5°C compared to its level at SGE at 36.5°C and TGE at 32°C. This might explain the increase in G0F levels in mAb produced under TGE at 36.5°C. Despite observing a decrease in protein galactosylation in TGE compared to SGE at 36.5°C, protein expression of β-GalTIII is shown to be at similar levels in both systems at 36.5°C. The results here suggest that galactosylation is not limited by the expression of galactosyltransferase in TGE at 36.5°C, but by the expression of GnTI & II, or other potential factors such as the availability of UDP-Gal. .

Comparing now the enzyme expression profiles from TGE at both temperatures to those of SGE at 32°C, Figure 47 B shows that apart from day 10 where the expression of GnTI in TGE were lower than that of SGE at 32°C, comparable results among all three conditions were observed for the rest of the time points. This piece of result correlates well with the gradual decrease of Man5 level from day 10 to 14 in mAbs produced under TGE. Also while similar mRNA levels of GnTII were obtained between SGE at 32°C and TGE at 36.5°C, the up-regulation in GnTII mRNA expression in TGE at 32°C was believed to contribute to the increased fractions of G0 in mAbs secreted at 32°C in TGE. However, fluctuation among the expression of the three GalT species is observed, showing no specific general trend; This is in line with the glycan results which showed no significant variation in galactosylation between TGE and SGE at 32°C. In addition, Figure 48 B suggests similarity in β-GalTIII protein expression levels between SGE and TGE at 32°C. Our results show that enzyme expression in our case is only subjected to changes upon temperature shift and that the expression of β-GalTIII in TGE at 36.5° is comparable to that in SGE at the same temperature.

The fact that rates of mAb galactosylation in cells cultured under TGE remained lower than their counterparts in SGE, there are several hypothesis for this. Firstly when 1. the availability of UDP-Gal is limited (in the case of TGE at 36.5°C); or 2. Lower expression levels of GnTI and FucT could be limiting the amount of substrate for GalT to work on (TGE at both 36.5°C and 32°C). 3. In

the case of TGE at 32°C, increased expression of GnTII could have resulted in more G0F species for mAb galactosylation. But the expression level of the GalT enzymes (GalT expression was down-regulated in SGE and TGE at 32°C) still remained as an important factor that limit galactose addition.

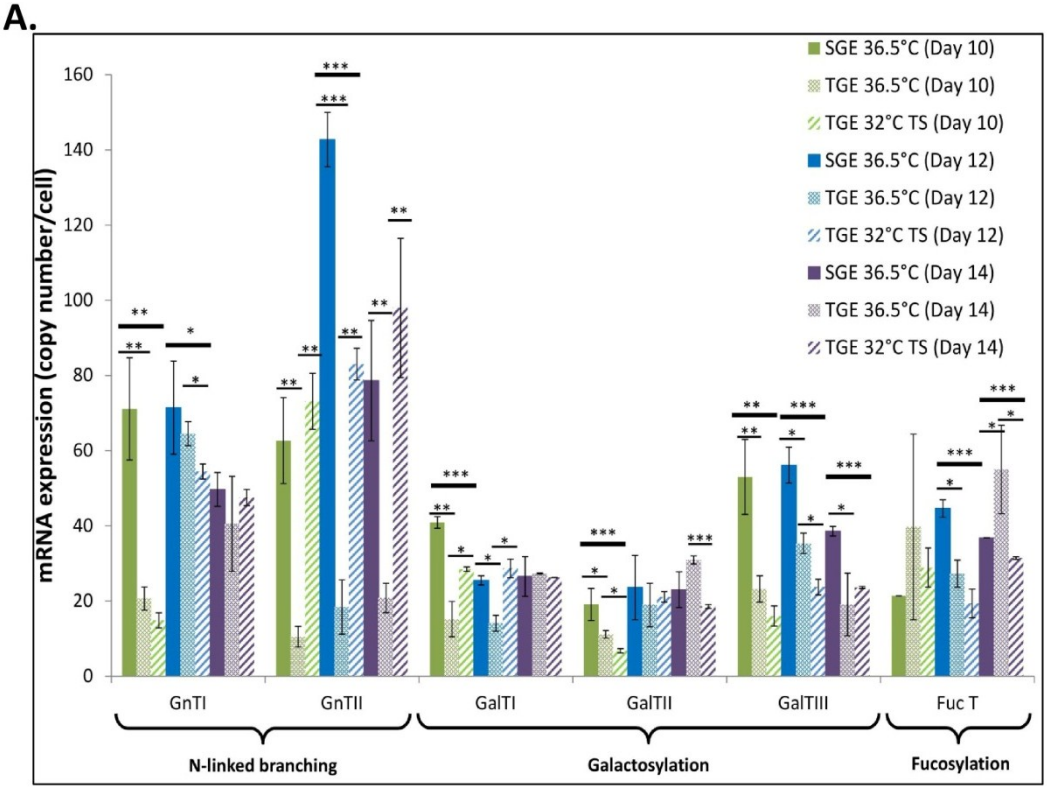

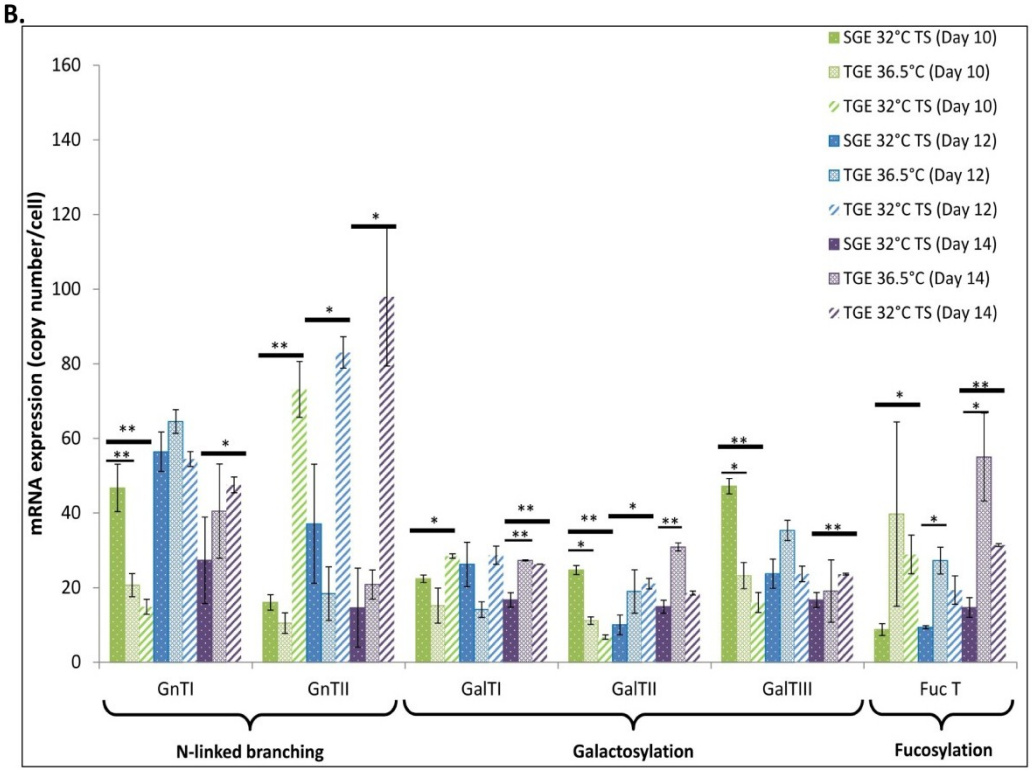

Figure 47. Comparison of gene expression profile of N-linked related glycosylation enzymes among all conditions. (A) mRNA expression levels of 6 glycosyltransferases, namely GnTI, GnTII, GalTI, GalTII, GaTIII and FucT, were measured and species from both temperature in TGE are compared to those in SGE at 36.5°C. (B) Difference in glycosyltransferase gene expression among TGE at 36.5°C and 32°C to SGE at 32°C TS. Results are averaged measurements at 36.5°C (n=6) and 32°C (n=3) in SGE; 36.5°C (n=3) and 32°C (n=3) in TGE.The error bars represent the standard deviation of the samples. Statistical significance was calculated using a Student's t-test and was represented by: *p≤0.05(*), p≤0.01(**) and p≤0.001(***).*

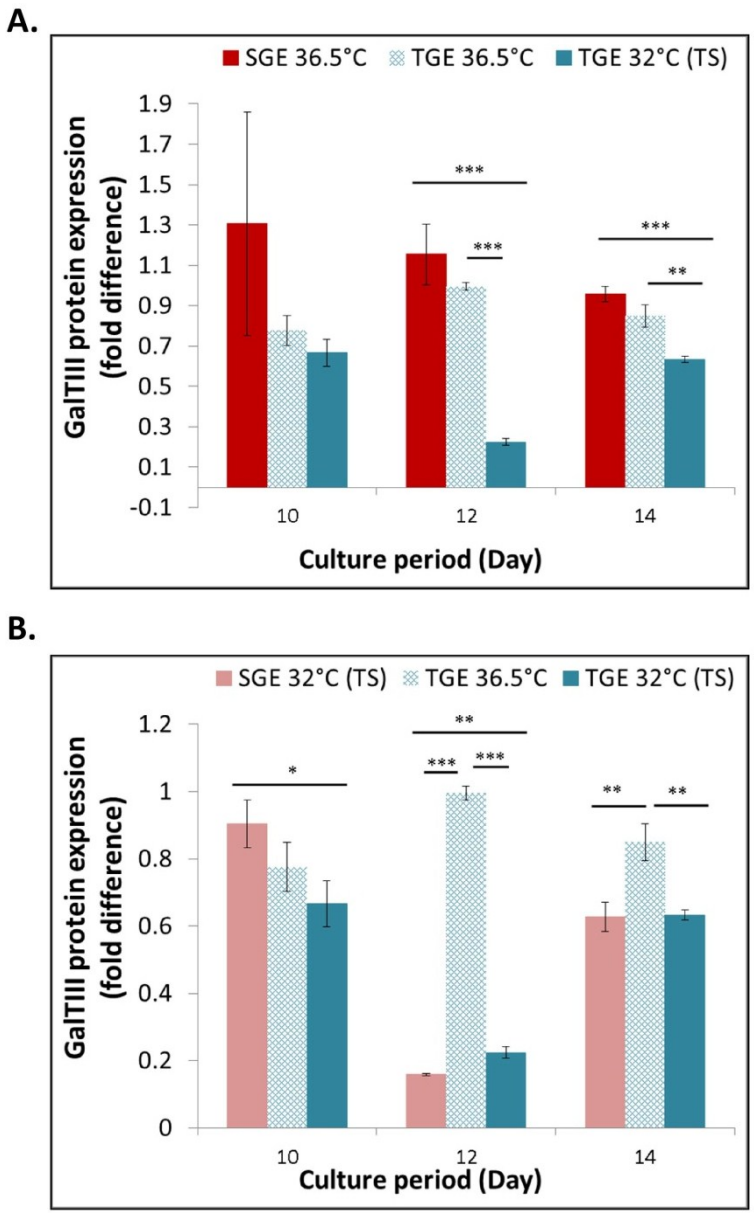

Figure 48. β-GalTIII protein expression profiles. (A) Comparison of species among both temperature in TGE and that in SGE at 36.5°C. (B) Difference in β-GalTIII protein expression among TGE at 36.5°C and 32°C and SGE at 32°C TS. Results are averaged measurements at 36.5°C (n=6) and 32°C (n=3) in SGE; 36.5°C (n=3) and 32°C (n=3) in TGE.The error bars represent the standard deviation of the samples. Statistical significance was calculated using a Student's t-test and was represented by: *p≤0.05(*), p≤0.01(**) and p≤0.001(***)*

6.3.4. Experimental analysis of cell metabolism in SGE and TGE

To further clarify the reason for differences arise in mAb Fc-glycan patterns between products from SGE and TGE systems, the metabolic profile of cells cultured under these processes were experimentally examined. Figure 49 A illustrates the overall glucose consumption per cell in the four conditions. Our results show that glucose consumption rates are very comparable among cells undergoing SGE at both temperatures and TGE at 36.5°C. However in the TGE system at 32°C, the specific glucose consumption during stationary growth phase is 2.7-fold higher compared to that in SGE. In addition, CHO cells produced and consumed lactate differently between the two expression systems at different temperatures. Lactate production occurs in exponential phase of both systems, however only cells that are cultured in mild hypothermic conditions experience a metabolic shift from lactate production to lactate consumption. TGE cells cultured at 32°C consume 74% of the total amount of lactate produced, while cells undergoing SGE at 32°C utilise 97% of the peak amount produced (Figure 49 B). At 32°C, cells undergoing TGE consume glucose and lactate at a ratio of 1.78:1, while in the case of SGE at 32°C the ratio is 0.96:1. Despite the higher consumption of glucose in SGE at 32°C, the overall consumption of sugar in TGE is higher in mild hypothermic conditions, in order to fuel cell maintenance and protein production during stationary growth.

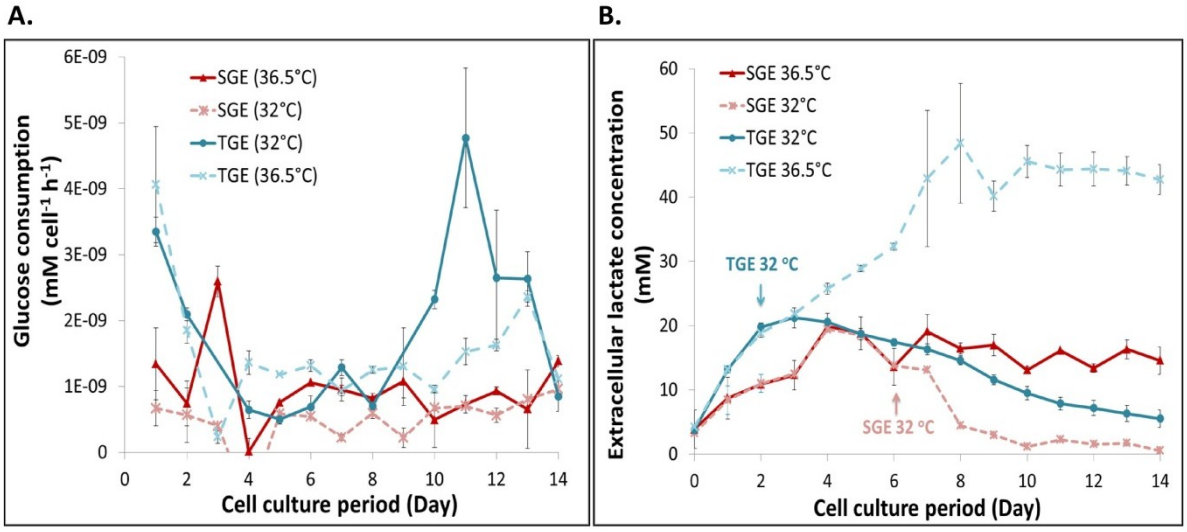

Figure 49. Glucose consumption and lactate concentration profiles. Concentration profiles of glucose consumption per viable cell (A) and extracellular lactate (B) when CHO cells were expressed in SGE at 36.5°C or at 32°C, and in TGE at 36.5°C or at 32°C 24 h post transfection. Results are averaged measurements at 36.5°C (n=6) and 32°C (n=3) in SGE; 36.5°C (n=3) and 32°C (n=3) in TGE. The error bars represent the standard deviation of the samples.

6.3.5. Flux balance analysis studies

The FBA studies in Part 1 showed that carbon fluxes towards nucleotide and NSD syntheses were minimal in TGE cells regardless of temperature changes. Part 2 focuses on comparing the calculated carbon fluxes between the SGE and TGE cells at exponential and stationary phases. From the results we aimed to identify the contributing factors that affect product glycosylation.

The FBA was constrained with the calculated production and consumption rates during exponential and stationary phases for both expression systems in all conditions in Tables 19 A & B. Our results show that at exponential phase, consistent with the difference in cell growth profiles between the two systems, the specific consumption of glucose and amino acids and the specific IgG production rate are lower in TGE than in SGE. The only exception is asparagine, the consumption of which is 78% higher in cells undergoing TGE, together with almost 100% increase in glutamine production. In line with the experimental data, the carbon flux going towards lactate production is significantly higher under TGE during exponential growth phase. The calculated fluxes suggest a different carbon intake and distribution within the TGE system before the induction of mild hypothermia.

In contrast, Table 19 B shows the calculated fluxes at stationary phase for all four conditions. Our results show that the specific glucose consumption rate is higher in the TGE system at stationary phase. When compared to both temperatures in SGE, the consumption of most amino acids, such as asparagine, glycine, leucine, methionine, proline and serine is higher in transiently transfected cells. The calculated flux for glutamine production, however, is higher in TGE only when compared to SGE at physiological temperature, but remains lower when compared to the flux in stable transfectants at 32°C. With robust amino acid metabolism, ammonia production in cells cultured under TGE is higher than both SGE conditions. Lactate consumption is low in TGE at 36.5°C, with cells consuming higher amount of lactate in TGE at 32°C. Cells undergoing SGE at 32°C achieved the highest rate of lactate consumption out of all conditions examined. In the case of mAb productivity, the specific IgG productivity is higher in SGE at stationary phase at both temperatures; it is in agreement with our experimental results where the q_{mab} in TGE is often lower.

Table 19 A. Average specific metabolic production and consumption rates for SGE at 36.5°C and at 32°C T\S, and TGE at 36.5°C and 32°C TS, at exponential phase. Results are averaged measurements at 36.5°C (n=6) and 32°C (n=3) in SGE; 36.5°C (n=3) and 32°C (n=3) in TGE.

	Consumption/production rate (femtomol/cell/day) Exponential phase			
	36.5°/32°C		36.5°/32°C	
	SGE		TGE	
	VALUE	STDEV	VALUE	STDEV
Ala	**196.2**	12.2	**55.7**	6.9
Amm	**-8.5**	9.9	**146.4**	9.6
Arg	**-38.9**	5.1	**-14.9**	3.1
Asn	**-175.9**	10.2	**-313.9**	14.7
Asp	**-186.8**	18.1	**139.4**	12.4
Glc	**-696.0**	245.4	**-362.5**	126.2
Gln	**17.5**	5.6	**35.7**	2.4
Glu	**-33.5**	3.7	**-3.8**	3.3
Gly	**29.8**	7.5	**22.6**	3.1
His	**-14.3**	3.0	**0.7**	2.7
Ile	**-53.9**	8.1	**-15.1**	5.7
Lac	**82.2**	76.5	**1461.6**	188.1
Leu	**-117.9**	14.8	**-75.2**	6.9
Lys	**-59.6**	8.7	**-24.9**	5.7
Met	**-15.9**	2.3	**-14.4**	2.7
Phe	**-26.1**	3.6	**-12.4**	2.8
Pro	**-43.5**	4.6	**-43.6**	5.4
Ser	**-162.2**	14.8	**-81.8**	9.2
Thr	**-42.5**	6.1	**-14.3**	5.5
Trp	**-9.2**	2.0	**-7.0**	2.6
Tyr	**-34.0**	3.8	**-7.1**	3.1
Val	**-74.6**	9.1	**-46.6**	6.0
IgG	**15.5**	0.7	**1.9**	0.1
	Specific growth rate (day^{-1})			
μ	**0.3**	0.0	**0.3**	0.0

Negative value: consumption. Positive value: production.

Table 19 B. Average specific metabolic production and consumption rates for SGE at 36.5°C and at 32°C T\S, and TGE at 36.5°C and 32°C TS, at stationary phase. Results are averaged measurements at 36.5°C (n=6) and 32°C (n=3) in SGE; 36.5°C (n=3) and 32°C (n=3) in TGE.

	Consumption/production rate (femtomol/cell/day) Stationary phase							
	36.5°C		32°C		36.5°C		32°C	
	SGE				TGE			
	VALUE	STDEV	VALUE	STDEV	VALUE	STDEV	VALUE	STDEV
Ala	**134.0**	18.8	**15.1**	3.1	**106.8**	24.0	**152.0**	20.0
Amm	**-17.4**	6.3	**-60.3**	1.4	**18.0**	13.0	**38.8**	26.0
Arg	**-19.5**	3.2	**-20.9**	2.4	**-13.5**	3.0	**5.0**	7.0
Asn	**-63.9**	3.2	**-72.6**	4.1	**-118.0**	4.0	**-308.0**	18.0
Asp	**-171.0**	7.3	**-122.9**	6.8	**-80.5**	21.0	**159.2**	21.0
Glc	**-412.0**	74.7	**-268.9**	49.0	**-346.5**	91.0	**-480.5**	222.0
Gln	**30.6**	3.6	**149.0**	1.4	**47.5**	2.0	**64.8**	5.0
Glu	**-24.3**	1.6	**-11.8**	1.8	**-9.4**	4.0	**2.4**	4.0
Gly	**23.5**	4.1	**22.5**	0.8	**87.4**	3.0	**72.4**	2.0
His	**-6.2**	2.3	**-5.4**	2.2	**-0.5**	2.0	**18.7**	5.0
Ile	**-39.5**	5.0	**-13.3**	5.4	**-27.4**	8.0	**-1.9**	14.0
Lac	**-45.5**	11.0	**-321.6**	7.9	**481.4**	91.0	**-262.7**	132.0
Leu	**-89.1**	8.0	**-33.0**	6.3	**-94.7**	14.0	**-97.5**	21.0
Lys	**-30.6**	6.0	**-36.4**	5.3	**-23.6**	5.0	**-1.8**	11.0
Met	**-8.5**	1.0	**-4.9**	2.0	**-12.1**	2.0	**-14.2**	4.0
Phe	**-14.4**	2.0	**-8.4**	2.2	**-14.2**	3.0	**-7.6**	5.0
Pro	**-25.0**	4.0	**-21.3**	4.1	**-25.6**	4.0	**-27.8**	10.0
Ser	**-78.2**	9.0	**-63.4**	5.7	**-156.7**	10.0	**-123.5**	21.0
Thr	**-24.2**	4.0	**-11.1**	4.0	**-16.8**	5.0	**2.8**	11.0
Trp	**-5.1**	1.0	**-2.6**	2.0	**-5.0**	2.0	**-1.6**	4.0
Tyr	**-18.4**	1.0	**-8.3**	2.1	**-9.1**	2.0	**6.1**	6.0
Val	**-53.5**	6.0	**-26.5**	4.9	**-56.3**	8.0	**-51.4**	14.0
IgG	**10.7**	1.0	**12.8**	1.0	**0.0**	0.0	**5.8**	1.0
	Specific growth rate (day^{-1})							
μ	**0.1**	0.0	**0.0**	0.01	**-0.1**	0.03	**0.0**	0.01

Negative value: consumption. Positive value: production.

Figures 50 A - C show the metabolic fluxes of stably (36.5°C & 32°C) and transiently (36.5°C & 32°C) transfected CHO cells at exponential and stationary phases, respectively. During exponential growth, almost all pyruvate is converted into lactate and little went into the TCA cycle for energy production in the TGE system. In contrast, the glucose is utilised more efficiently by CHO by

channelling it through the TCA cycle in stable transfectants. The overall flux towards ATP and NADH generation in the TGE system is around half of that in the SGE system. In addition, fluxes towards nucleotide, nucleotide sugar and lipid syntheses are marginally lower in TGE at exponential phase.

During stationary phase, Figures 50 A and B illustrate that glucose metabolism in glycolysis and TCA cycle in TGE at 32°C are twice as efficient as that in SGE at either 36.5°C or 32°C. This does not apply, however, to cells in TGE at 36.5°C where cells enter exponential decline. As a result of mild hypothermia, lactate acted as an additional carbon source in both SGE and TGE systems (Ivarsson et al. 2014). Cells cultured at 32°C in both systems show higher fluxes of lactate entering the TCA cycle than those that are cultured at physiological temperature. Changes in lactate metabolism in mild hypothermic conditions are also reflected by reduced extracellular lactate concentrations that are experimentally observed. Fluxes from various amino acids that enter the TCA cycle for glutamine synthesis and energy generation are higher within TGE at 32°C in order to attain its robust TCA cycle, sustain the prolonged cell growth in TGE at 32°C, as well as contribute to mAb synthesis. However, in the case of TGE at 32°C, despite the higher overall carbon fluxes entering the cell, the carbon flux distribution towards mAb synthesis is around 50% lower than those in SGE at both temperatures. In addition, glucose metabolism towards nucleotide, NSD and lipid syntheses is low in transiently transfected cells. Cells in the TGE system only exhibited approximately 20% of the corresponding flux of stable transfectants towards protein glycosylation (Tables 20 A and B). The only exception is UDPNAG in TGE at 36.5°C: the flux towards this species is comparable to that in SGE at physiological temperature and this is reflected by the similar net concentration of UDP-GlcNAc in these two conditions (Figure 46 C). In addition, glutamine is a crucial component for UDP-N-acetyl-hexosamine synthesis (UDP-GlcNAc, UDP-GalNAc). Carbon and nitrogen fluxes towards UDPNAG synthesis are high in TGE at 36.5°C, while those at 32°C are comparatively low and indeed lower than those in SGE. The reduction in nucleotide/NSD synthesis in TGE at 32°C is further emphasized by the reduced flux of glutamine into these synthetic pathways suggested by the FBA.

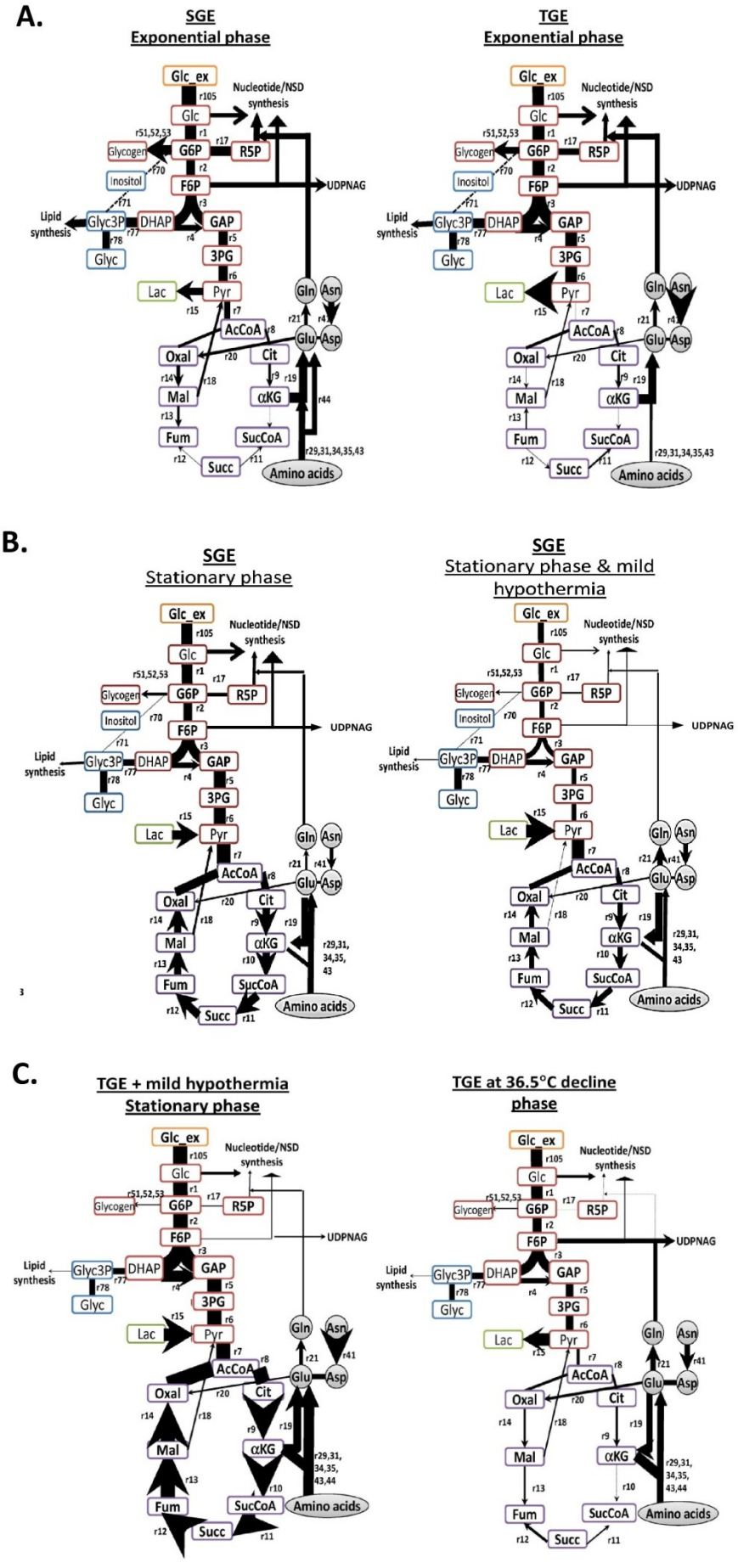
A.
SGE
Exponential phase
TGE
Exponential phase
B.
SGE
Stationary phase
SGE
Stationary phase & mild hypothermia
C.
TGE + mild hypothermia
Stationary phase
TGE at 36.5°C decline phase
Glc_ex
Nucleotide/NSD synthesis
Glc
Glycogen
G6P
R5P
Inositol
F6P
UDPNAG
Lipid synthesis
Glyc3P
DHAP
GAP
Glyc
3PG
Lac
Pyr
Gln
Asn
AcCoA
Glu
Asp
Oxal
Cit
Mal
αKG
Fum
SucCoA
Succ
Amino acids

Figure 50. Central carbon metabolism of CHO cells at exponential growth (A) in SGE and TGE at both temperatures, (B) stationary growth phase in SGE at 36.5°C and 32°C TS and (C) stationary phase in TGE at 36.5°C and 32°C TS. Thickness of an arrow indicates the relative flow of the carbon source within the system. This figure is simplified to include carbon lost to glycerol, glycogen and lactate production, together nucleotide, NSD, lipid and key amino acid synthesis.

Table 20 A. FBA estimated flux values in nucleotide synthesis, lipid synthesis and protein glycosylation during exponential phase in SGE and TGE.

Reaction	Equation		Subsystem	Flux value (femtomol/cell/day) Exponential phase	
				SGE 36.5°C	TGE 32°C
54	[c] : R5P + ATP --> PRPP + AMP	Irreversible	Nucleotide	50.34	20.24
55	[c] : PRPP + (2) Gln + Gly + Asp + (5) ATP + CO2 + (2) N10FTHF --> IMP + (2) Glu + Fum + (5) ADP + (2) THF	Irreversible	Nucleotide	8.00	7.28
56	[c] : IMP + Asp + GTP --> AMPRN + Fum + GDP	Irreversible	Nucleotide	4.72	4.30
57	[c] : IMP + Gln + ATP + NAD --> GMPRN + Glu + AMP + NADH	Irreversible	Nucleotide	3.27	2.98
58	[c] : HCO3 + NH4 + Asp + (2) ATP + NAD --> Orotate + (2) ADP + NADH	Irreversible	Nucleotide	42.34	12.95
59	[c] : Orotate + PRPP --> UMPRN + CO2	Irreversible	Nucleotide	42.34	12.95
60	[c] : UMPRN + Gln + ATP --> CMPRN + Glu + ADP	Irreversible	Nucleotide	3.43	3.12
61	[c] : AMPRN --> dAMP	Irreversible	Nucleotide	1.19	1.08
62	[c] : GMPRN --> dGMP	Irreversible	Nucleotide	0.84	0.81
63	[c] : CMPRN --> dCMP	Irreversible	Nucleotide	0.85	0.78
64	[c] : UMPRN --> dTMP	Irreversible	Nucleotide	1.18	1.08
65	[c] : Choline + ATP --> Pcholine + ADP	Irreversible	Lipid	6.77	1.50
66	[c] : Pcholine + (18) AcCoA + Glyc3P + (22) ATP + (33) NADH --> PC + (16) ADP + (6) AMP + (33) NAD + (18) CoASH	Irreversible	Lipid	5.27	0.00
67	[c] : PC + Ser <==> PS + Choline	Reversible	Lipid	1.55	-3.39
68	[c] : PS --> PE + CO2	Irreversible	Lipid	1.41	0.00
69	[c] : Choline + Glyc3P <==> Glyc3PC	Reversible	Lipid	3.53	3.53
70	[c] : G6P --> Inositol	Irreversible	Lipid	0.51	0.47
71	[c] : Inositol + (18) AcCoA + Glyc3P + (22) ATP + (33) NADH --> PI + (16) ADP + (6) AMP + (33) NAD + (18) CoASH	Irreversible	Lipid	0.51	0.47
72	[c] : (18) AcCoA + (2) Glyc3P + (22) ATP + (33) NADH --> PG + (16) ADP + (6) AMP + (33) NAD + (18) CoASH	Irreversible	Lipid	0.45	0.41
73	[c] : (2) PG --> DPG + Glyc	Irreversible	Lipid	0.19	0.17
74	[c] : (16) AcCoA + Ser + Choline + (16) ATP + (29) NADPH --> SM + (2) CO2 + (14) ADP + (2) AMP + (29) NADP + (16) CoASH	Irreversible	Lipid	0.44	0.00
75	[c] : (18) AcCoA + (18) ATP + (14) NADPH --> Cholesterol + (9) CO2 + (18) ADP + (14) NADP + (18) CoASH	Irreversible	Lipid	0.98	0.00
79	[c] : UDPG <==> UDPGal	Reversible	Glycosylation	3.93	-22.01
80	[c] : Glc + ATP + GTP --> GDPMann + ADP	Irreversible	Glycosylation	8.45	0.00
81	[c] : F6P + Gln + AcCoA + UTP --> UDPNAG + Glu + CoASH	Irreversible	Glycosylation	8.29	6.62
82	[c] : UDPNAG + ATP + 3PG + CTP --> CMPNeu5Ac + UDP + ADP	Irreversible	Glycosylation	0.98	0.57
83	[c] : GDPMann + NADPH --> GDPFuc + NADP	Irreversible	Glycosylation	0.79	0.00
84	[c] : UDPNAG <==> UDP + GlcNAc	Reversible	Glycosylation	5.00	4.55
85	[c] : UDPNAG <==> UDPGalNAc	Reversible	Glycosylation	1.42	1.29
86	[c] : UDPGalNAc <==> GalNAc + UDP	Reversible	Glycosylation	1.42	1.29
87	[c] : GDPMann <==> Mann + GDP	Reversible	Glycosylation	7.13	-0.15
88	[c] : UDPGal <==> Gal + UDP	Reversible	Glycosylation	3.58	-22.03
89	[c] : CMPNeu5Ac <==> CMP + Neu5Ac	Reversible	Glycosylation	0.60	0.54
90	[c] : GDPFuc <==> GDP + Fuc	Reversible	Glycosylation	0.61	-0.05

Table 20 B. FBA estimated flux values in nucleotide synthesis, lipid synthesis and protein glycosylation during stationary phase in SGE (36.5°C) and TGE (32°C).

Reaction	Equation		Subsystem	Flux value (femtomol/cell/day)			
				Stationary phase			Decline phase
				SGE 36.5°C	SGE 32°C	TGE 32°C	TGE 36.5°C
54	[c] : R5P + ATP --> PRPP + AMP	Irreversible	Nucleotide	11.06	0.30	0.07	1.07E-10
55	[c] : PRPP + (2) Gln + Gly + Asp + (5) ATP + CO2 + (2) N10FTHF --> IMP + (2) Glu + Fum + (5) ADP + (2) THF	Irreversible	Nucleotide	1.75	0.00	0.00	0.00
56	[c] : IMP + Asp + GTP --> AMPRN + Fum + GDP	Irreversible	Nucleotide	1.03	0.00	0.00	0.00
57	[c] : IMP + Gln + ATP + NAD --> GMPRN + Glu + AMP + NADH	Irreversible	Nucleotide	0.72	0.00	0.00	0.00
58	[c] : HCO3 + NH4 + Asp + (2) ATP + NAD --> Orotate + (2) ADP + NADH	Irreversible	Nucleotide	9.31	0.30	0.07	1.07E-10
59	[c] : Orotate + PRPP --> UMPRN + CO2	Irreversible	Nucleotide	9.31	0.30	0.07	1.07E-10
60	[c] : UMPRN + Gln + ATP --> CMPRN + Glu + ADP	Irreversible	Nucleotide	0.75	0.00	0.00	0.00
61	[c] : AMPRN --> dAMP	Irreversible	Nucleotide	0.26	0.00	0.00	0.00
62	[c] : GMPRN --> dGMP	Irreversible	Nucleotide	0.20	0.00	0.00	0.00
63	[c] : CMPRN --> dCMP	Irreversible	Nucleotide	0.19	0.00	0.00	0.00
64	[c] : UMPRN --> dTMP	Irreversible	Nucleotide	0.56	0.00	0.00	0.00
65	[c] : Choline + ATP --> Pcholine + ADP	Irreversible	Lipid	2.88	2.63	2.63	1.50
66	[c] : Pcholine + (18) AcCoA + Glyc3P + (22) ATP + (33) NADH --> PC + (16) ADP + (6) AMP + (33) NAD + (18) CoASH	Irreversible	Lipid	1.15	0.00	0.00	0.00
67	[c] : PC + Ser <==> PS + Choline	Reversible	Lipid	0.34	0.00	0.00	0.00
68	[c] : PS --> PE + CO2	Irreversible	Lipid	0.31	0.00	0.00	0.00
69	[c] : Choline + Glyc3P <==> Glyc3PC	Reversible	Lipid	0.53	3.53	3.53	4.67
70	[c] : G6P --> Inositol	Irreversible	Lipid	0.11	0.00	0.00	0.00
71	[c] : Inositol + (18) AcCoA + Glyc3P + (22) ATP + (33) NADH --> PI + (16) ADP + (6) AMP + (33) NAD + (18) CoASH	Irreversible	Lipid	0.11	0.00	0.00	0.00
72	[c] : (18) AcCoA + (2) Glyc3P + (22) ATP + (33) NADH --> PG + (16) ADP + (6) AMP + (33) NAD + (18) CoASH	Irreversible	Lipid	0.10	0.00	0.00	0.00
73	[c] : (2) PG --> DPG + Glyc	Irreversible	Lipid	0.04	0.00	0.00	0.00
74	[c] : (16) AcCoA + Ser + Choline + (16) ATP + (29) NADPH --> SM + (2) CO2 + (14) ADP + (2) AMP + (29) NADP + (16) CoASH	Irreversible	Lipid	0.10	0.00	0.00	0.00
75	[c] : (18) AcCoA + (18) ATP + (14) NADPH --> Cholesterol + (9) CO2 + (18) ADP + (14) NADP + (18) CoASH	Irreversible	Lipid	0.21	0.00	0.00	0.00
79	[c] : UDPG <==> UDPGal	Reversible	Glycosylation	0.90	0.30	0.07	1.07E-10
80	[c] : Glc + ATP + GTP --> GDPMann + ADP	Irreversible	Glycosylation	2.90	0.61	0.66	1.08E-09
81	[c] : F6P + Gln + AcCoA + UTP --> UDPNAG + Glu + CoASH	Irreversible	Glycosylation	2.76	0.76	0.67	44.21
82	[c] : UDPNAG + ATP + 3PG + CTP --> CMPNeu5Ac + UDP + ADP	Irreversible	Glycosylation	0.14	0.00	0.00	0.00
83	[c] : GDPMann + NADPH --> GDPFuc + NADP	Irreversible	Glycosylation	0.42	0.15	0.16	2.57E-10
84	[c] : UDPNAG <==> UDP + GlcNAc	Reversible	Glycosylation	1.09	0.00	0.00	0.00
85	[c] : UDPNAG <==> UDPGalNAc	Reversible	Glycosylation	0.31	0.00	0.00	0.00
86	[c] : UDPGalNAc <==> GalNAc + UDP	Reversible	Glycosylation	0.31	0.00	0.00	0.00
87	[c] : GDPMann <==> Mann + GDP	Reversible	Glycosylation	1.56	0.00	0.00	0.00
88	[c] : UDPGal <==> Gal + UDP	Reversible	Glycosylation	0.78	0.00	0.00	0.00
89	[c] : CMPNeu5Ac <==> CMP + Neu5Ac	Reversible	Glycosylation	0.13	0.00	0.00	0.00
90	[c] : GDPFuc <==> GDP + Fuc	Reversible	Glycosylation	0.13	0.00	0.00	0.00

6.4. Discussion

Variation in IgG gene expression levels between the stable and transient systems has led to significant differences, not only with respect to specific IgG productivity, but it also partially contributes to changes within cell metabolism, the timeframe for mAb production and the product glycoforms. Cells in the TGE system were exposed to PEI, a cytotoxic transfection reagent, at the start of cell culture. Its negative impact was reflected in the drop in cell viability at early exponential phase but cells later recovered from the stress imposed by the transfection reagent. At the same time, cells displayed high levels of lactate production and comparatively lower flux entering the TCA cycle during exponential phase as suggested by the FBA study. This was in contrast to SGE cells where the gene of interest was already incorporated into the host genome and cells had re-established a new steady state, in which most glucose was converted into useful metabolites. With the introduction of mild hypothermia 24 h post-transfection, instead of rapid cell division, cell growth in TGE at 32°C was maintained at a relatively constant level and cells experienced a longer stationary phase than those that were stably transfected at both temperatures examined. However, cell viability was higher in the SGE system than in the TGE system at 36.5°C. The prolonged cell viability had a direct positive impact on specific mAb productivity in TGE and is beneficial during bioprocessing. Despite the different cell growth profile due to the early temperature shift in TGE, both cells undergoing SGE and TGE at 32°C exhibited prolonged cell viability and reduced rate of cell death. It would be interesting to examine how the timing of the temperature shift can affect cell metabolism and mAb production.

When examining the impact of transient gene expression on cell metabolism, in contrast to the exponential phase of TGE where most of the pyruvate was converted to lactate, the TCA cycle in transiently transfected cells at 32°C was heavily fuelled by glucose and lactate together at stationary phase. This is different from cells in SGE at 32°C where the flux from lactate to the TCA cycle was higher than that from glucose. On the other hand, cells undergoing TGE at physiological temperature consumed a similar amount of glucose during stationary phase but most of it was being converted into lactate. Fluxes of amino acids, asparagine in particular, into the system during stationary phase were also very high in TGE at both temperatures examined. Carbon backbones of most amino acids were fed back into the TCA cycle to prolong stationary growth phase in TGE at 32°C, while most amino acids were converted into glutamine in TGE at 36.5°C, according to the flux balance analysis carried out. In addition, metabolic rates calculated as shown in Tables 19 A and 19 B suggest that mAb productivity was higher during stationary phase in TGE cells at 32°C, while in SGE mAb production was higher in exponential phase. The increased amino acid consumption and energy generated from

the TCA cycle, together with the reduced need of cells to divert energy towards cell growth, fuelled product synthesis in TGE. Our previous study on mild hypothermia in SGE presented in Chapter 4 has suggested that more energy was likely to have been channelled towards protein production (Sou et al. 2014). The same impact was observed in the TGE system at 32°C, in which around 40% rise in protein productivity was achieved compared to that in TGE cells at 36.5°C. As opposed to the results for 32°C, cells in the TGE system at 36.5°C did not exhibit a stationary phase.

The glycan pattern of the secreted mAb also showed variations between the two expression systems. Despite increased glucose metabolism in TGE at 32°C during stationary phase, results from the FBA showed that overall fluxes towards nucleotide and NSD syntheses were dramatically reduced (Tables 18 and 20 B). With a closer examination, metabolic rates for UDP-Gal and UDP-NAG (N-acetylhexosamines) were 13- and 4- times lower in transient transfectants at 32°C respectively, and significantly lower at 36.5°C, when compared to those in stable transfectants at 36.5°C. However, metabolic fluxes towards NSD synthesis were comparable among TGE at both temperatures and SGE at 32°C; this is in agreement with the similar glycan profiles achieved in these three conditions.

Analysis of experimental NSD data, N-linked glycosyltransferase expression levels, flux balance analysis and secreted mAb glycosylation profile provide a thorough picture of the impact of TGE at different temperatures on the process of glycosylation. The limitation in protein galactosylation observed in TGE when compared to SGE at 36.5°C, and variations in the intracellular concentration of UDP-Gal in TGE between the two temperatures, suggest that the decreased G1F/G2F fractions in TGE at different temperatures can be contributed from different factors. When cells in TGE at both temperatures experienced reduced metabolic fluxes towards NSD synthesis, only those at 32°C have their GalT expression downregulated. We can therefore conclude that limited mAb galactosylation arise in TGE at 36.5°C is mainly due to reduced production of NSDs, while reduced expression of glycosyltransferases is the main contributor in reduced product galactosylation in TGE cells at 32°C. This is further confirmed by the accumulation of UDP-Gal resulting from under-consumption of the species at this temperature. Despite changes observed in mAb glycosylation between the two systems, one can argue that they are within similar magnitude to those observed as a result of other cellular (e.g. clonal variation) or environmental perturbations (van Berkel et al. 2009). In addition to GalT enzymes, one also has to take into consideration of GnTI and GnTII expression in cells cultured under TGE, where their levels of expression also place a crucial impact on generating bi-antennary glycan structures. Without these, further mAb processing, to be more specific, mAb galactosylation cannot take place. Also, the fact that within the TGE system CHO cells cultured at

32°C was more capable of galactose addition and expressed more GnTII than at 36.5°C, again stresses the importance of GnTII in aiding mAb galactosylation during N-linked mAb glycosylation.

In addition to protein glycosylation, lipids play a significant role in protein transport and retention of glycosyltransferases in the Golgi apparatus (Banfield 2011). Reduced metabolic rates towards lipid synthesis could affect membrane formation, which, in turn, can impact cell growth and product glycosylation.

Table 21 summarises the differences between the stable and transient gene expression systems with and without mild hypothermia. In brief, transiently transfected cells are less metabolically robust in early exponential phase owing to their gradual recovery from stresses imposed by both the transfection reagent and/or mild hypothermia. During stationary phase, cells in TGE at 32°C concentrated more on energy and recombinant protein production, in contrast to stable transfectants at 36.5°C where more energy was spent on protein glycosylation. However, cells from both expression systems have low carbon fluxes towards NSD synthesis, similar levels of GalT expression and, as a result, similar mAb glycan profiles at 32°C. On the other hand, despite similar glycan profiles in the TGE system at both temperatures, lack of NSD production appeared to be the main factor of reduced galactosylation at 36.5°C, while decrease in β-GalT expression resulted in reduced consumption of NSD for mAb glycosylation at 32°C and different supplementations showed minimal effects.

Table 21. Summary table describing differences between stable and transient gene expression systems, in terms of rProtein production, cell metabolism and Fc-glycan profile.

	SGE (36.5°C)	SGE (32°C TS)	TGE (36.5°C)	TGE (32°C TS)
Time frame required for product synthesis	≥ 6 months		~ 10 - 14 days	
Gene selection	Yes		No	
mAb productivity	~ 11.9 pg cell^{-1} day^{-1}	~ 14.0 pg cell^{-1} day^{-2}	~ 4.2 pg cell^{-1} day^{-2}	~ 7.4 pg cell^{-1} day^{-1}
Cell metabolism	Moderate glucose consumption per cell	Moderate glucose consumption per cell	Moderate glucose consumption per cell	Higher glucose consumption
	Higher NSD consumption	Reduced NSD consumption	Reduced NSD consumption	Reduced NSD consumption
Metabolic flux	Moderately robust glycolysis & TCA	Reduced robustness in glycolysis & TCA	Non robust glycolysis & TCA	More robust glycolysis & TCA
	Higher metabolic flux into NSD, nucleotide & lipid synthesis	Reduced metabolic flux into NSD, nucleotide & lipid synthesis	Minimal metabolic flux into NSD, nucleotide & lipid synthesis	Reduced metabolic flux into NSD, nucleotide & lipid synthesis
NSD consumption	High	Low	Low	
GnTI mRNA expression	High	High	Low	Low
GnTII mRNA expression	High	Low	Low	High
GalT expression	High	Low	High	Low
Secreted mAb Fc-glycosylation	More G1F, G2F species	Fewer G1F, G2F species	More Man5 but fewer G1F, G2F species	
Rate of mAb galactosylation	Highest	Medium	Lowest	Medium

6.5. Concluding remarks

In this chapter we analysed the differences in cell culture behaviour between model SGE and TGE processes in terms of cell profile, cell metabolism, recombinant protein synthesis, as well as the Fc-glycan pattern of the secreted mAb. Our results showed that CHO cell behaviour varied in response to a change in DNA transfection and expression pattern. Firstly CHO cell growth was shown to be affected by the addition of mild-toxic transfection chemicals as well as the timing of temperature shift. In contrast integrating target DNA into the host cell genome during stable gene expression, the expression of mAb as a foreign protein in TGE placed a burden on protein glycosylation and reduced availability of NSD species and limited expressions of glycosyltransferases. Among all conditions examined in this chapter, the two expression systems that resemble industrial practices the most are: IgG-expressing CHO cells cultured at 36.5°C in SGE and its parental CHO cell line at 36.5°C with plasmid transfection on day 1 and with a temperature shift to 32°C 24 h post-transfection in TGE. By comparing these two model industrial processes, it is evident that there are differences in mAb glycoforms between the two conditions. In order to use TGE materials for early stage pre-clinical studies or to even replace materials produced through SGE in the future, process optimisation will definitely be necessary to attain similar product quantity and quality. Our study identified factors that influence product glycosylation in TGE and provides a platform for bioprocess optimisation and development. This could involve feeding essential nucleotides or other carbon sources such as galactose, lactate or pyruvate, or manipulating glycosyltransferases through cell line engineering. Despite the changes observed between the two systems in this chapter, one has to bear in mind that changes in protein glycosylation in this study can be cell- or transfection protocol-specific. Our study only provides a first-hand comparison between the two expression systems but more investigations on different cell culture conditions as well as transient transfection protocols are necessary to draw a more concrete conclusion on the differences in mAb glycosylation between SGE and TGE expression systems.

Chapter 7
Comparison of recombinant monoclonal antibody glycosylation between SGE and TGE systems through computational studies

In Chapter 6 we compared conditions in the SGE and the TGE systems experimentally, with respect to cell growth, cell metabolism and mAb glycosylation. Despite serving as a useful start in understanding the difference between the two expression systems, our experimental data alone was not sufficient to draw a more meaningful insight into why transient transfectants behaved very differently from their stably transfected counterparts. Although the use of flux balance analysis shed more light into the metabolic distribution of glucose and amino acid feeds within the cells under the four different conditions, it still remains difficult to speculate on the reasons behind the experimentally observed differences. As a result, a mathematical model was constructed for the TGE system to describe cellular behaviour at physiological and mild hypothermic conditions. The model followed same structure as that for the SGE described in Chapter 5 and was adapted to the particularities of the TGE system.

7.1. TGE model structure

The TGE model described in this chapter retains the modular characteristics of that presented in Chapter 5 and includes descriptions for cell dynamics, NSD metabolism and mAb N-linked glycosylation in the Golgi apparatus. Most parts of the model remain the same as that for the SGE system, with two changes made introduced in the cell dynamics section. They are:

- The incorporation of the transfection reagent 25kDa linear polyethylenimine (PEI) into the cell growth limitation term f_{inh}.

$$f_{inh} = \left(\frac{KI_{amm}}{KI_{amm} + [Amm]}\right)\left(\frac{KI_{lac}}{KI_{lac} + [Lac]}\right)\left(\frac{[PEI]}{K_{PEI} + [PEI]}\right) \quad \text{...Eq. 63}$$

PEI has been shown to have a toxic effect on cell cultures (Kafil and Omidi 2011) and it affects cell growth. The level of PEI and the timing of its addition are controlled by a feeding schedule, in which PEI is only introduced once to the model 24 h post transfection. .

- Unlike stable gene expression where constant DNA copy number of target gene is achieved, the DNA levels of heavy and light chains increase upon DNA transfection and their levels change along the cell culture period. Such changes are captured and controlled by a feeding sequence described in Appendix III Table 1. The copy numbers of heavy and light chains indicated in the feeding schedule were experimentally determined through qrt-PCR.

With the availability of experimental data for HC and LC DNA copy numbers, it is easier to incorporate their respective DNA copy numbers in a schedule in gPROMS, most importantly because we do not have enough information to predict the transfection efficiency of target genes, but also to minimise changes in the model structure that would otherwise be necessary. By keeping the model structure of the TGE model similar to that of the SGE model, a more valid comparison between the two model outputs is enabled.

7.2. Comparing model simulation results between SGE and TGE systems

By incorporating the modifications discussed above, the TGE model was simulated in gPROMS v.4.0.0 (Process System Enterprise, 1997-2015) using two sets of parameter values estimated separately for each of the two conditions examined in the TGE system: fed-batch TGE at 36.5°C or with a temperature shift to 32°C 24 h post DNA transfection, with HC and LC DNA transfection taking place on day 1. In this section, model simulations are first compared to the experimental data from triplicate experiments under each condition to evaluate the capability of the model to represent the TGE system. Estimation of model parameter is perform in gPROMS v.4.0.0, in which unknown parameter values in both physical and variance models are simultaneously predicted by the maximum likelihood formulation. It maximizes the chance of the model fitting parameter values to the experimental data, and provides statistical analysis that indicates the level of uncertainty in the estimated values (Process System Enterprise, 1997-2015) . Estimated parameter values for the two conditions are then carried followed by a comparison to the CHO cells cultured in the SGE system at 36.5°C, with an aim to understand how differences in cellular behaviour and product quality arise between expression systems.

7.2.1. Discussion of CHO cell culture dynamics and mAb production model

Figures 51 A - D show simulated viable and total cell growth profiles from our transient model against the respective experimental data at different temperatures, as well as comparison of model simulations between stable and transient gene expression. By incorporating the inhibitory effect of transfection reagent PEI on cell growth, simulated results for both temperatures examined are in good agreements with their respective experimental data points. Our TGE model is capable of differentiating cell growth at 36.5°C from that at 32°C: the prolonged stationary growth phase that occurred at 32°C is also well captured. Despite the reduced viable cell density achieved in cells undergoing TGE, the general cell growth profile in TGE at 36.5°C is very similar to that in SGE at mild hypothermic temperature.

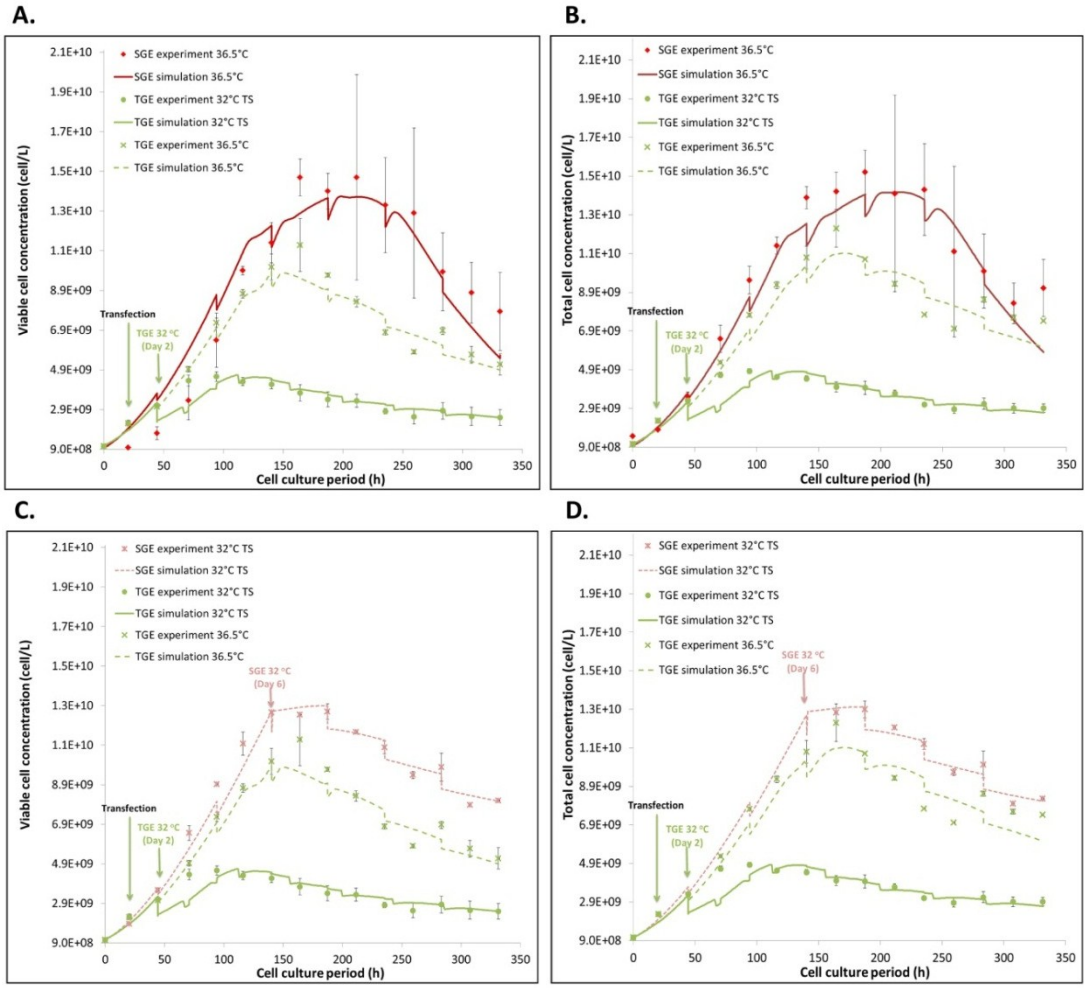

Figure 51. Comparison of model simulation to experimental data for viable (A & C) and total cell concentrations (B & D) from fed-batch CHO cell cultures in SGE at 36.5°C or at 32°C TS, and in TGE at 36.5°C or at 32°C TS.

In addition, simulation results from the transient model generate good fits to experimental inputs for nutrient and amino acid metabolism at both temperatures. Glucose consumption is suggested to be temperature dependent. The extracellular glucose profile of cells in TGE at 36.5°C is comparable to that in SGE at 36.5°C, while the profile of glucose in TGE transfectants cultured at 32°C also resembles that of SGE culture with mild hypothermia (Figure 52 A). Despite the similar glucose profiles between the SGE and TGE at 32°C, their distinctive difference in cell growth, however, results in higher consumption of glucose in cells undergoing TGE at 32°C (Chapter 6, Figure 49). Moreover, lactate and ammonia concentration profiles are described effectively (Figures 52 B & C), with the model describing well the high lactate production of cells in TGE at 36.5°C. In addition, simulations from the transient model for amino acid metabolism are in good agreements with those that are measured experimentally (Figures 53 A – F), apart from arginine where our model under-estimates its consumption under TGE. Other amino acids, namely asparagine, glutamate, glutamine, lysine and proline, are correctly described by the model for both temperatures. Our results

show that for some amino acids such as Arg and Lys, the concentration profiles are similar between expression systems at the same temperature. On the other hand, the concentration profiles of Asn and Pro in TGE at 36.5°C are comparable to those in SGE regardless of temperatures. It is hard to conclude the consumption rate of each amino acid based on their concentration profiles alone. However the fold difference between cell growth profile in TGE at 32°C and the other three conditions examined are always higher, when compared to differences observed in amino acid metabolism. Our results suggest that rates of amino acid consumption in cells undergoing TGE at 32°C is therefore higher. With similar trends as those in mAb production (Figure 55), glutamine concentration profiles in TGE are lower when compared to those in SGE.

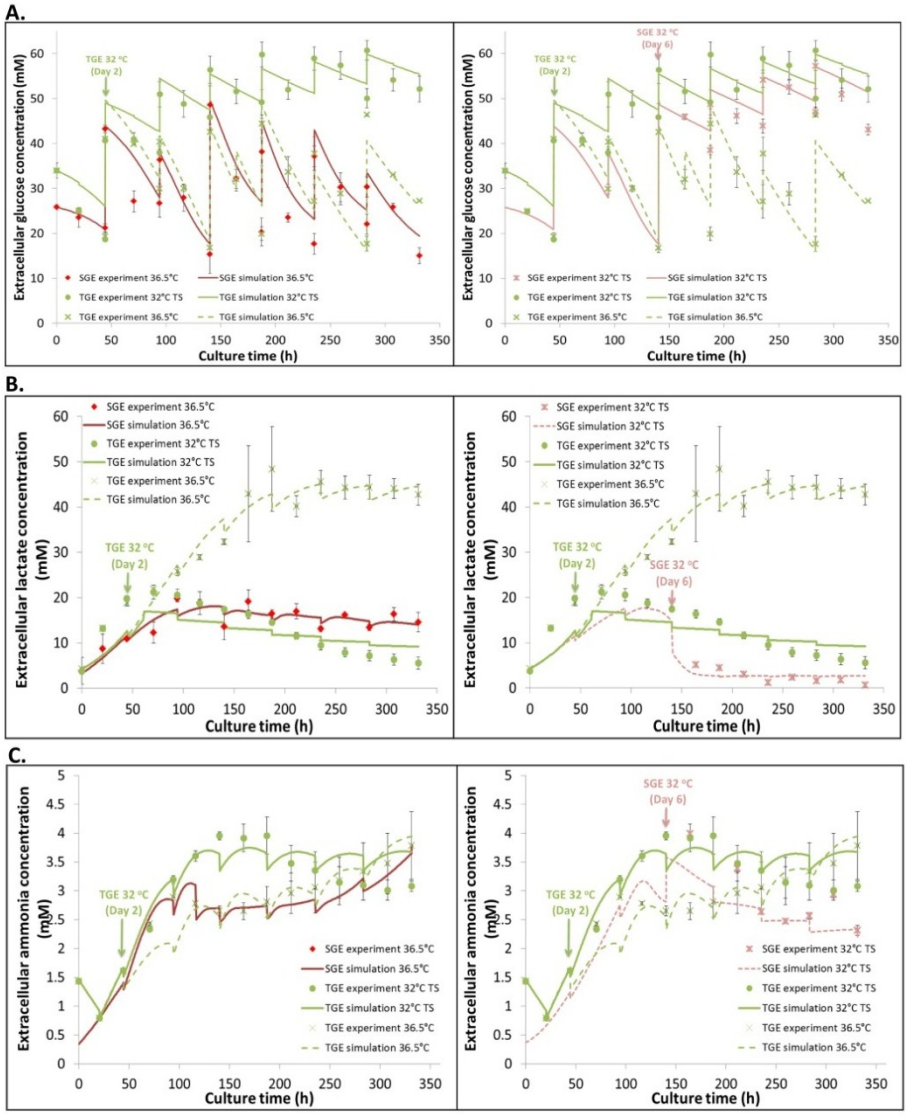

Figure 52. Comparison of model generated fits to experimental data for extracellular glucose (A) extracellular lactate (B) and extracellular ammonia (C) concentrations from fed-batch CHO cell cultures in SGE at 36.5°C or at 32°C TS, and in TGE at 36.5°C or at 32°C TS.

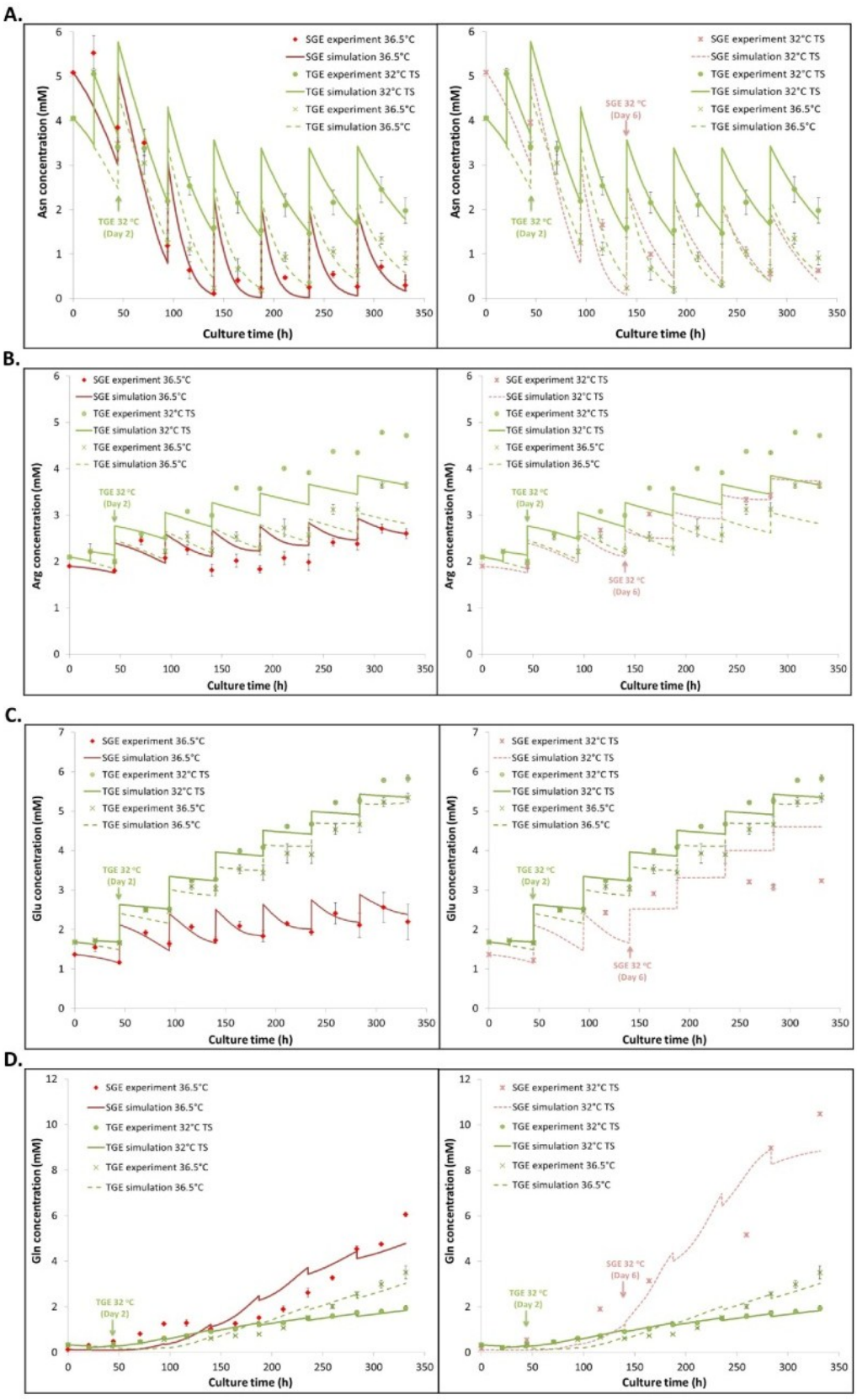
A.
Asn concentration (mM)
Culture time (h)
SGE experiment 36.5°C
SGE simulation 36.5°C
TGE experiment 32°C TS
TGE simulation 32°C TS
TGE experiment 36.5°C
TGE simulation 36.5°C
SGE experiment 32°C TS
SGE simulation 32°C TS
TGE 32 °C (Day 2)
SGE 32 °C (Day 6)
B.
Arg concentration (mM)
C.
Glu concentration (mM)
D.
Gln concentration (mM)

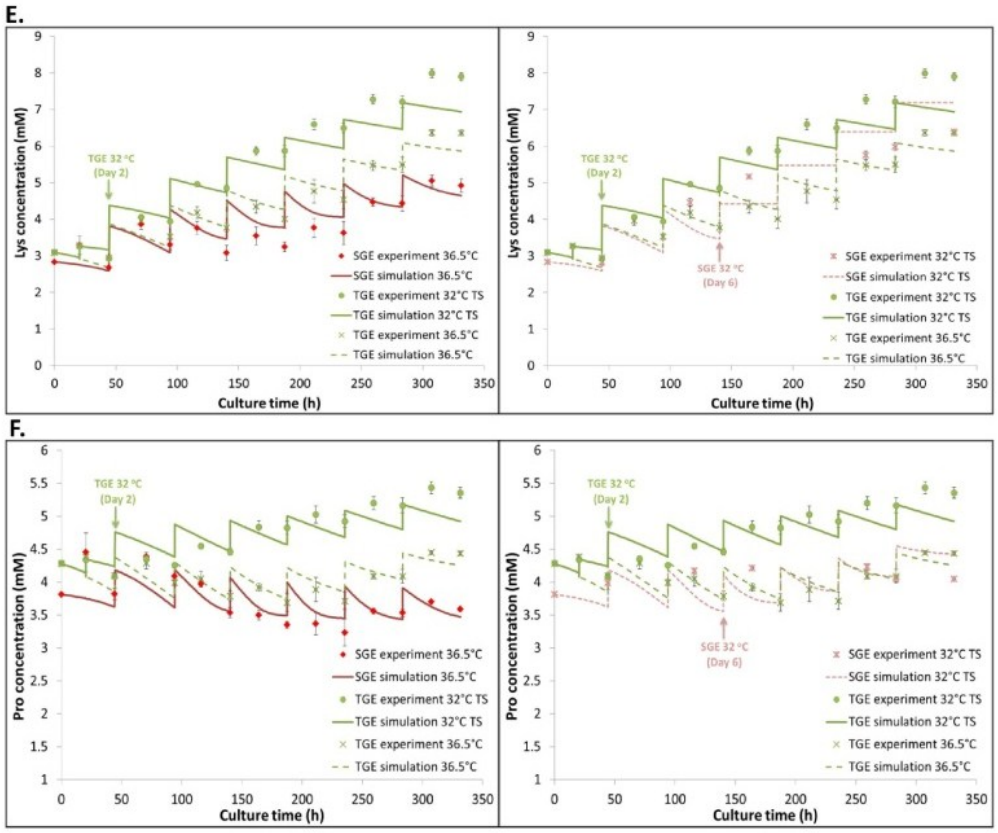

Figure 53. Comparison of model generated fits to experimental data for extracellular asparagine (A), arginine (B), glutamate (C), glutamine (D), lysine (E) and proline (F) concentrations from fed-batch CHO cell cultures in SGE at 36.5°C or at 32°C TS, and in TGE at 36.5°C or at 32°C TS.

In the case of mAb synthesis, a different parameter set was required to describe system behaviour under the two different temperatures in TGE. Similar to SGE, simulated results of HC mRNA expression in TGE are not in complete agreement with experimental data, failing to replicate peak expression on days 10 and 11 in TGE at 32°C. However, generated results are of the same magnitude as our experimental data (Figure 54 A). LC mRNA expression in TGE at both temperatures, on the other hand, is well described by our cell dynamics model (Figure 54 B). Transcription levels of both HC and LC are pronouncedly reduced in TGE. The same applies to the mAb assembly intermediate species: Figure 54 C illustrates that the intracellular H_2L_2 concentration is lower in TGE regardless of culture temperature and the TGE model correctly describes this reduction, which is also reflected in decreases in mAb transcription and translation rates. Finally, the TGE model accurately simulates the volumetric mAb yield in TGE (Figure 55), which is approximately 5-fold lower than that produced in SGE systems.

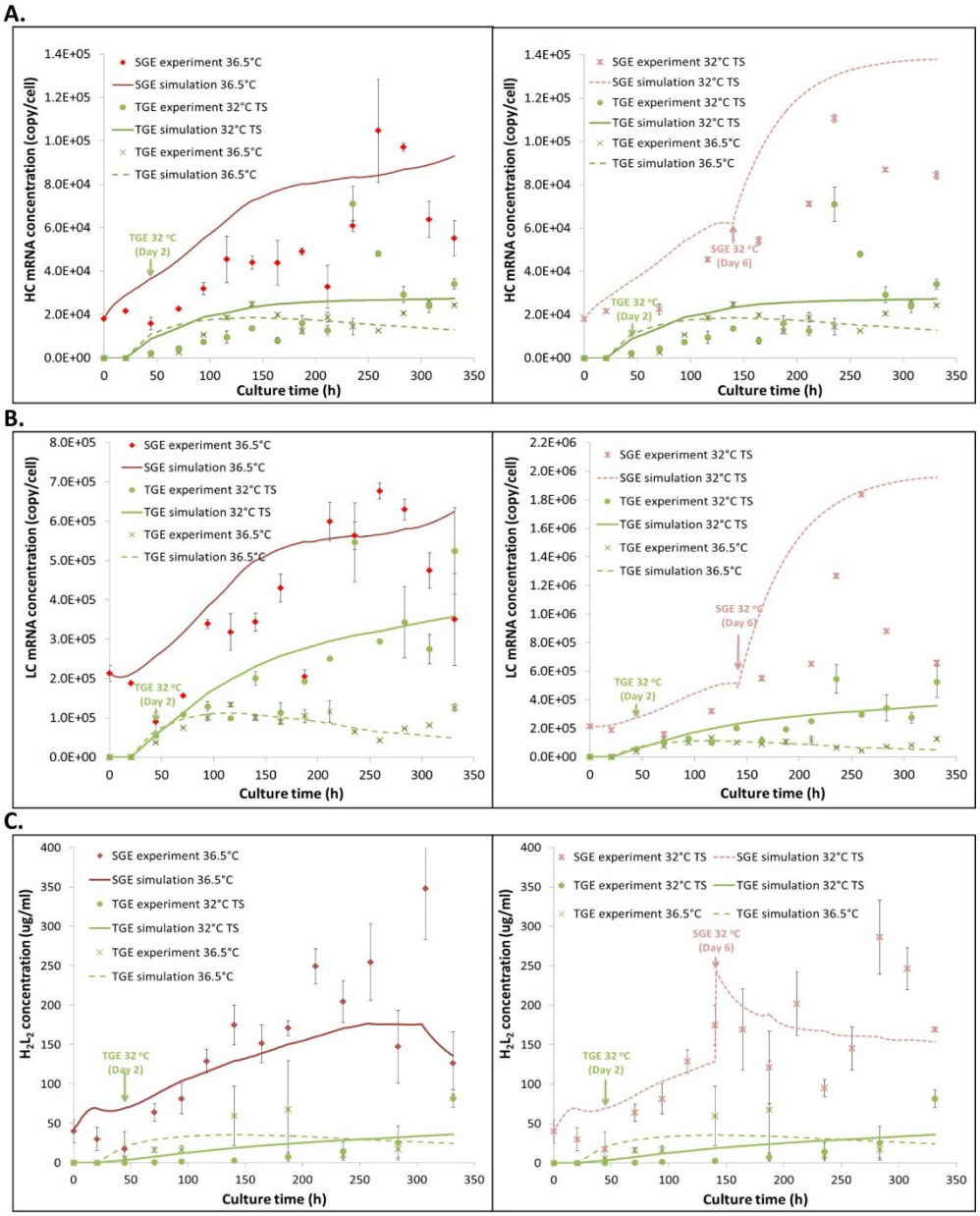

Figure 54. Comparison of model simulation outputs to experimental data for intracellular HC mRNA (A), LC mRNA (B), H_2L_2 polypeptide (C) assembly intermediate concentrations from fed-batch CHO cell cultures in SGE at 36.5°C or at 32°C TS, and in TGE at 36.5°C or at 32°C TS.

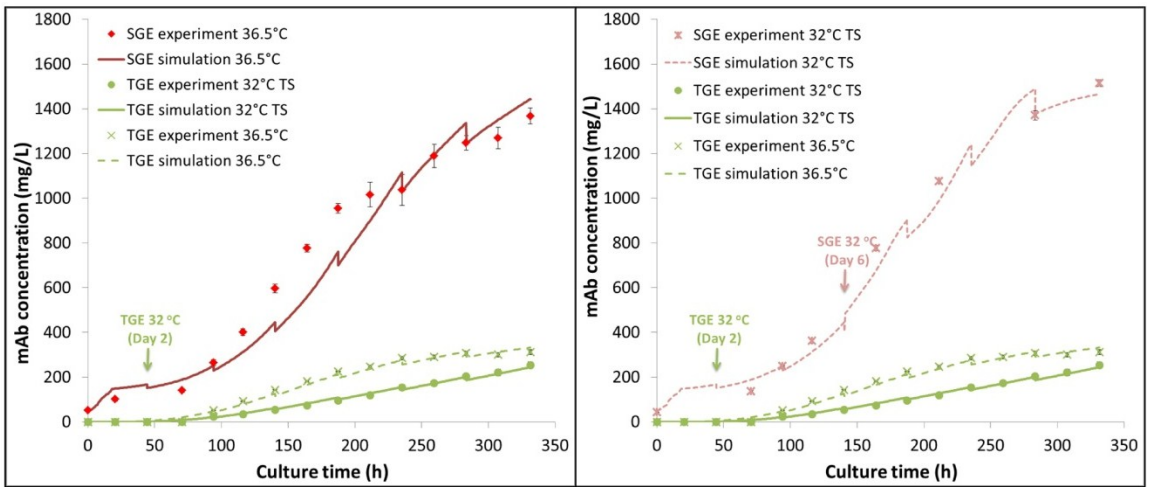

Figure 55. Comparison of model simulation outputs to experimental data for secreted volumetric mAb concentration in fed-batch CHO cell cultures in SGE at 36.5°C or at 32°C TS, and in TGE at 36.5°C or at 32°C TS.

Tables 22 and 23 compare estimated parameters for the cell dynamics model in TGE at both temperatures to those in SGE at 36.5°C or at 32°C, respectively. The comparison shows that values of μ_{max} at both temperatures in TGE are higher, with cells in TGE requiring higher growth rates to overcome the inhibitory effect of PEI. In line with experimental results, μ_{max} of cells that undergo TGE at 32°C is lower than that at 36.5°C, which, together with a reduced value of $\mu_{d,max}$ to generate a steady and prolonged stationary growth phase. Among all four conditions examined, the rate of cell lysis is generally estimated to be lower at 32°C in both SGE and TGE where their cell membranes are suggested to be more rigid at reduced temperatures. This correlates well with the findings of Tait et al. (2013) where cells are suggested to be less shear sensitive at high cell viability.

On the other hand, estimated synthetic rates of mAb are different among all four conditions. mAb assembly rates are estimated to be lower in TGE when compared to cells in SGE at 36.5°C, but are comparable to that of SGE at 32°C. Despite decreases in K_A values, estimated rates of transcription in TGE at both temperatures are at similar magnitude as those in SGE at 36.5°C, but relatively lower when compared to those in SGE at 32°C. The rates of decay for heavy and light chain mRNA are estimated to be lower in the TGE systems. Moreover, translation rates of both heavy and light chains are estimated to be higher in all TGE conditions than in the SGE system. When compared within TGE systems, the rate of translation at 32°C is higher than at 36.5°C, which might have enhanced the specific mAb productivity in cells undergoing TGE at mild hypothermic temperature. Our model outputs demonstrate mAb production in TGE is not highly affected by their transcriptional and translational machinery. Reduced levels of HC and LC mRNA and their assembly intermediates observed experimentally in TGE illustrated in Figure 44 could be a result of the lower and

inconsistent HC and LC DNA copy numbers during TGE culture; or the reduced mAb assembly rates under the TGE system.

Also, the rate of mAb transport from ER to Golgi apparatus in cells undergoing TGE is higher, which suggests a higher throughput of mAb species entering the Golgi apparatus during TGE. However, mAb molecules appear to be retained longer within this organelle as reflected by decreased values in the secretion rate of assembled mAb product from the Golgi apparatus to the extracellular matrix (K_G) in TGE when compared to those in SGE. The model proposes low secretion rate to be the main bottleneck in TGE mAb production. A full list of parameter values for the NSD model can be found in Appendix III Table 2.

Table 22. Comparison of estimated parameters between models of SGE at 36.5°C and TGE at 36.5°C or 32°C TS. This includes parameter values for cell growth, metabolism and mAb production.

	Values						
Parameter	**SGE 36.5 °C**	**95% conf. internals**	**TGE 36.5 °C**	**95% conf. internals**	**TGE 32 °C**	**95% conf. internals**	**Units**
Growth/death related							
μ_{max}	**1.10×10^{-1}**	2.90×10^{-2}	**1.12**	1.10×10^{-2}	**1.58×10^{-1}**	2.10×10^{-3}	h^{-1}
$\mu_{d,max}$	**9.70×10^{-2}**	1.10×10^{-2}	**2.88×10^{-2}**	3.30×10^{-4}	**2.66×10^{-2}**	1.90×10^{-4}	h^{-1}
K_{lysis}	**4.47×10^{-1}**	1.10×10^{-2}	**2.94×10^{-1}**	1.10×10^{-2}	**1.39×10^{-1}**	8.50×10^{-2}	h^{-1}
Metabolism related							
$Y_{lac,glc}$	**2.00**	2.40×10^{-1}	**2.00**	1.20	**1.11×10^{-15}**	3.30×10^{-16}	mmol $mmol^{-1}$
mAb synthesis related							
K_A	**1.38×10^{-1}**	5.82×10^{-2}	**4.15×10^{-2}**	1.50×10^{-2}	**1.87×10^{-3}**	3.00×10^{-4}	molecule $cell^{-1}$ h^{-1}
K_{ER}	**4.56×10^{2}**	3.70×10^{2}	**2.79×10^{3}**	1.10×10^{3}	**3.00×10^{3}**	6.20×10^{2}	h^{-1}
K_G	**2.00×10^{3}**	5.73×10^{2}	**1.35×10^{-3}**	2.00×10^{-3}	**7.22×10^{-3}**	2.20×10^{-3}	h^{-1}
S_H	**15.90**	2.10	**14.00**	1.80	**7.52**	5.70×10^{-1}	mRNAs $gene^{-1}$ h^{-1}
S_L	**93.10**	15.00	**2.33×10^{2}**	38.00	**46.40**	1.60	mRNAs $gene^{-1}$ h^{-1}
T_H	**1.35**	1.20	**4.90**	3.50×10^{-1}	**4.71×10^{2}**	1.30×10^{-2}	chain $mRNA^{-1}$ h^{-1}
T_L	**3.84×10^{-1}**	1.10×10^{-1}	**1.36**	3.40×10^{-1}	**4.70**	2.70×10^{-2}	chain $mRNA^{-1}$ h^{-1}
K_h	**9.77×10^{-3}**	5.90×10^{-5}	**1.00×10^{-30}**	1.00×10^{-34}	**1.00×10^{-30}**	1.00×10^{-34}	h^{-1}
K_I	**1.15×10^{-3}**	4.75×10^{-5}	**65.00**	32.00	**9.61×10^{-1}**	6.40×10^{-1}	h^{-1}

Table 23. Comparison of estimated parameters between models of SGE at 32°C TS and TGE at 36.5°C or 32°C TS. This includes parameter values for cell growth, metabolism and mAb production.

Parameter	SGE 32°C	95% conf. internals	TGE 36.5°C	95% conf. internals	TGE 32°C	95% conf. internals	Units
Growth/death related							
μ_{max}	**7.49×10^{-1}**	3.20×10^{-2}	**1.12**	1.10×10^{-2}	**1.58×10^{-1}**	2.10×10^{-3}	h^{-1}
$\mu_{d,max}$	**3.96×10^{-2}**	2.00×10^{-3}	**2.88×10^{-2}**	3.30×10^{-4}	**2.66×10^{-2}**	1.90×10^{-4}	h^{-1}
K_{lysis}	**2.14×10^{-1}**	5.70×10^{-2}	**2.94×10^{-1}**	1.10×10^{-2}	**1.39×10^{-1}**	8.50×10^{-2}	h^{-1}
Metabolism related							
$Y_{lac,glc}$	**5.32×10^{-3}**	1.30×10^{-3}	2.00	1.20	1.11×10^{-15}	3.30×10^{-16}	mmol $mmol^{-1}$
mAb synthesis related							
K_A	**1.94×10^{-3}**	1.80×10^{-4}	**4.15×10^{-2}**	1.50×10^{-2}	**1.87×10^{-3}**	3.00×10^{-4}	molecule $cell^{-1}$ h^{-1}
K_{ER}	**9.03×10^{2}**	35.10	**2.79×10^{3}**	1.10×10^{3}	**3.00×10^{3}**	6.20×10^{2}	h^{-1}
K_G	**2.30×10^{4}**	1.26×10^{2}	**1.35×10^{-3}**	2.00×10^{-3}	**7.22×10^{-3}**	2.20×10^{-3}	h^{-1}
S_H	**1.11×10^{2}**	7.40	**14.00**	1.80	**7.52**	5.70×10^{-1}	mRNAs $gene^{-1}$ h^{-1}
S_L	**1.58×10^{2}**	5.30	**2.33×10^{2}**	38.00	**46.40**	1.60	mRNAs $gene^{-1}$ h^{-1}
T_H	**2.17**	9.50×10^{-2}	**4.90**	3.50×10^{-1}	**4.71×10^{2}**	1.30×10^{-2}	chain $mRNA^{-1}$ h^{-1}
T_L	**5.66×10^{-1}**	2.80×10^{-2}	**1.36**	3.40×10^{-1}	**4.70**	2.70×10^{-2}	chain $mRNA^{-1}$ h^{-1}
K_h	**1.68×10^{-3}**	2.30×10^{-4}	**1.00×10^{-30}**	1.00×10^{-34}	**1.00×10^{-30}**	1.00×10^{-34}	h^{-1}
K_I	**1.13×10^{-3}**	3.80×10^{-4}	**65.00**	32.00	**9.61×10^{-1}**	6.40×10^{-1}	h^{-1}

7.2.2. Discussion of model results for intracellular nucleotide and NSD metabolism

Despite the longer retention time of mAb within the Golgi apparatus estimated by the cell dynamics model, it is rather interesting to observe through experiments limited galactosylation on the secreted product generated from the TGE processes (Chapter 6, Figure 45). By using the same nucleotide and NSD model as for SGE to describe the behaviour of the TGE system, parameter estimation NSD model was performed using the maximum likelihood formulation in gPROMS v.4.0.0. and the corresponding model simulations were compared to our measured data.

The nucleotide and NSD concentration profiles from cells undergoing TGE are pronouncedly different from their profiles in SGE at either temperature. Figures 56 and 57 show good alignments between model simulations and experimental results for 9 different nucleotides and NSD species in

TGE at both temperatures. When compared to species in SGE, our results show that net concentrations of ATP in TGE are higher; this could be a result of the combination of lower viable cell density and a more robust citric acid cycle in cells undergoing TGE, especially at 32°C. GTP concentrations, however, are significantly lower in the TGE system. Since GTP molecules can be readily converted into ATP, our results suggest that the yield of ATP from GTP is probably higher than in cells cultured in TGE than in SGE (Figures 56 A & B). Moreover, UTP concentration profiles are comparable among all conditions examined.

In the case of NSD metabolism, our model suggests that the net concentration of UDP-Glc is lower in TGE conditions than in SGE at 36.5°C. Despite the reduced concentrations of UDP-Glc species, comparable levels of UDP-GlcNAc and UDP-GalNAc are observed in cells undergoing TGE at physiological temperature, but significantly reduced amounts in TGE at 32°C, when compared to concentration profiles from SGE at 36.5°C. The simulated results are in good agreement with those from our FBA studies in Chapter 6, where higher carbon flux is channelled only towards UDP-HexNAc in cells cultured in TGE at physiological temperature. However when compared to levels in SGE at 32°C, UDP-Glc concentration is comparative higher in both conditions of TGE, and both UDP-HexNAc species possess higher net concentrations in TGE (Figures 57 D, F & G). Despite good fits generated from both sets of parameter values in the TGE model, they fail to represent the fluctuations of the experimental data points between days 4 to 9, when the levels of UDP-Gal are below the detection limit of our HPLC method. Apart from these points, the high level of UDP-Gal at lag growth phase and the higher net concentration in TGE at 32°C are generally well described by the model.

In addition, the model provides estimates of intracellular glucose and glutamine levels, which are essential inputs to NSD synthesis. Simulation results for intracellular glucose in the TGE model provide good fits to the experimental data. In line with the increased glucose flux entering the cells in TGE at 32°C, intracellular glucose concentration is higher in TGE than in SGE (Figure 56 H & Figure 57 H). However, our model fails to describe the exact concentration profile of intracellular glutamine in TGE at 32°C, underestimating its peak intracellular concentration on day 12.

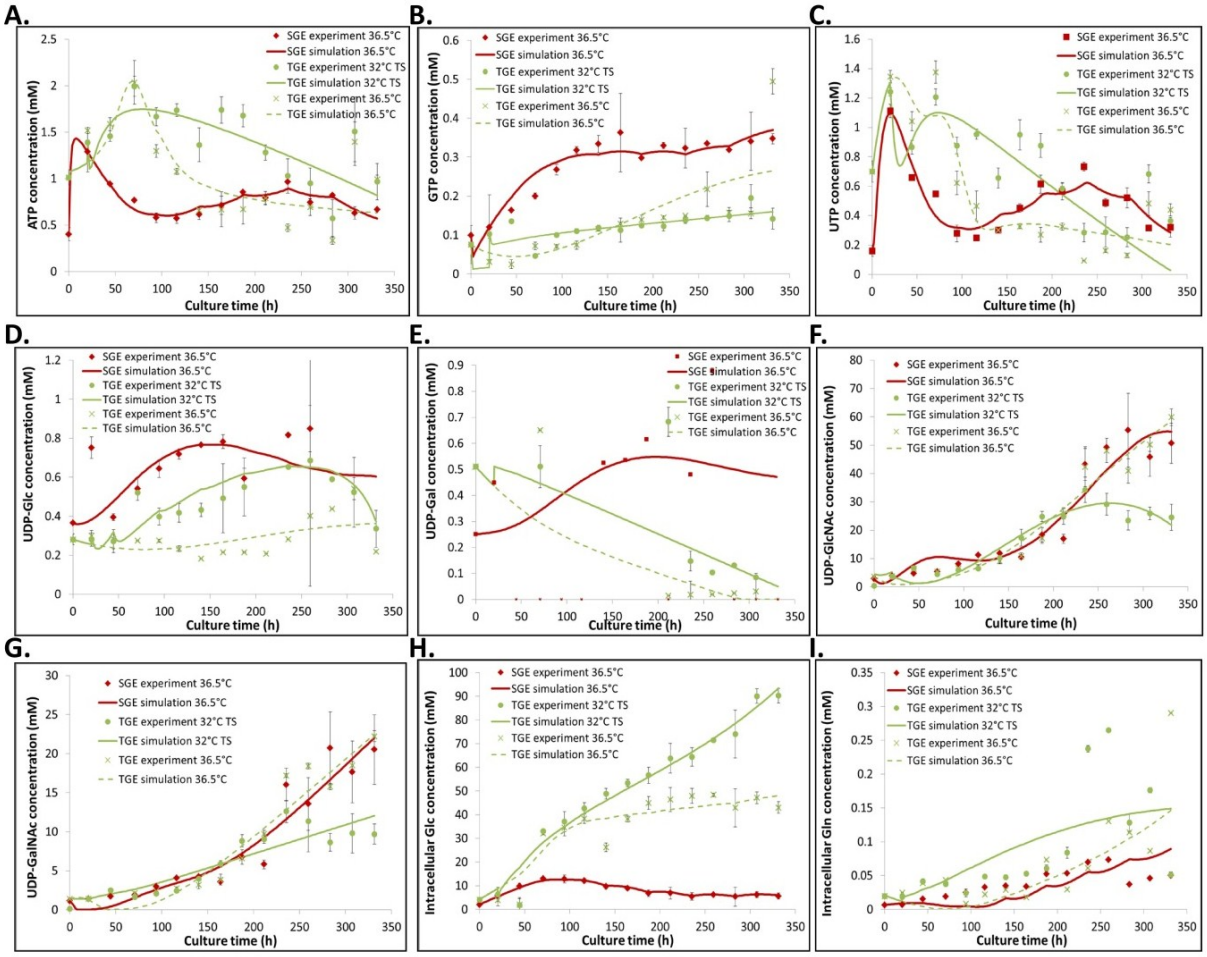

Figure 56. Comparison of nucleotide and NSD profiles from model simulations to experimental data in fed-batch CHO cell cultures in SGE at 36.5°C (red), and in TGE at 36.5°C or at 32°C TS (green). This includes the intracellular concentrations of ATP (A), GTP (B), UTP (C), UDP-Glc (D), UDP-Gal (E), UDP-GlcNAc (F), UDP-GalNAc (G), Int-Glc (H) and Int-Gln (I).

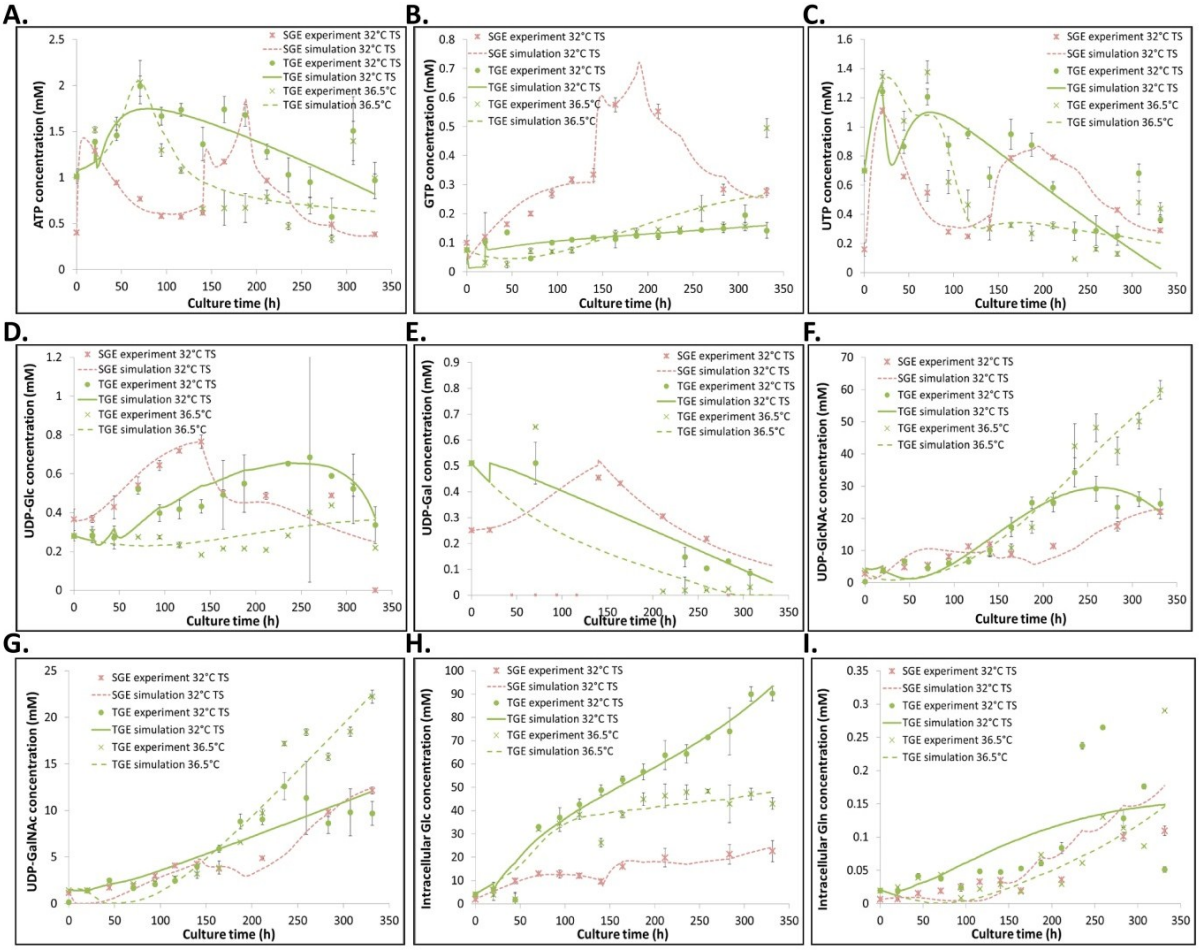

Figure 57. Comparison of nucleotide and NSD profiles from model simulations to experimental data in fed-batch CHO cell cultures in SGE at 32°C TS (pink), and in TGE at 36.5°C or at 32°C TS (green). This includes the intracellular concentrations of ATP (A), GTP (B), UTP (C), UDP-Glc (D), UDP-Gal (E), UDP-GlcNAc (F), UDP-GalNAc (G), Int-Glc (H) and Int-Gln (I).

Estimation of the V_{max} and K_m values for enzymes that are involved in the biosynthesis of nucleotides and NSDs are indeed useful in understanding this part of metabolism and comparing the synthetic rate of each species when changes in bioprocess conditions are introduced. Tables 24 and 25 compare the estimated parameter values for the NSD model in TGE at both temperatures, to those estimated for the SGE models at 36.5°C or 32°C, respectively. In line with the measured ATP concentrations, the TGE model suggests higher V_{max} values in cells that are cultured in TGE. On the other hand, GTP species is particularly interesting, as the estimated V_{max} values for GTP related enzymes from the TGE model are higher than that estimated by the SGE model, despite the lower net concentration profile observed experimentally. These estimated V_{max} values seem to support our initial hypothesis, that the rate of conversion from GTP to ATP is high in TGE; as a result increased enzyme efficiency is required to synthesize GTP.

As for NSD synthesis, estimated V_{max} and K_m values of NSD-synthetic enzymes are reflective of the concentration profiles of their respective output species. V_{max} values of most NSD-related enzymes are lower in TGE when compared to those estimated in SGE at 36.5°C, with the exception of enzymes responsible for UDP-Gal synthetic pathway (Chapter 4, Figure 27) where their V_{max} values of which in TGE at both 36.5°C and 32°C are similar to that predicted in SGE at 36.5°C. That is also in line with their comparable net concentrations of UDP-Gal as discussed above. When compared to parameters estimated from the SGE model at 32°C, estimated V_{max} values of other NSD-related enzymes in TGE are mostly slightly lower or similar, and these are well reflected by the comparable concentration profiles illustrated in Figure 57. Our experimental results are therefore well represented by the TGE model. In addition to enzyme kinetics, the TGE model suggests higher transport rates of NSD species entering the ER and Golgi apparatus only at 36.5°C. This correlates well with the increased levels of mRNA expression of transporters for UDP-Gal and UDP-GlcNAc in TGE at 36.5°C that could have assisted NSD transport (Figure 58), especially when compared to expression in SGE at 32°C. A full list of parameter values for the NSD model can be found in Appendix III Table 3.

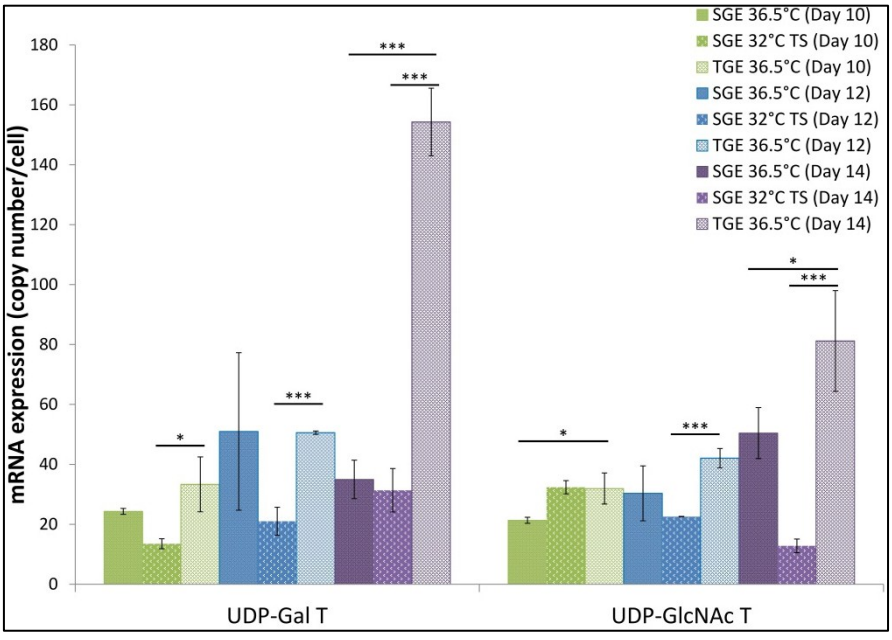

Figure 58. mRNA expression levels of transporters of UDP-Gal and UDP-GlcNAc, in SGE at 36.5°C and 32°C TS, and in TGE at 36.5°C. Results are averaged measurements at 36.5°C (n=6) and 32°C (n=3) in SGE; 36.5°C (n=3) in TGE. The error bars represent the standard deviation of the samples. Statistical significance was calculated using a Student's t-test and was represented by: *$p \leq 0.05$(*), $p \leq 0.01$(**) and $p \leq 0.001$(***).*

Table 24. Comparison of estimated parameters from NSD models between two expression systems, among SGE at 36.5°C, and in TGE at 36.5°C or at 32°C TS. This includes parameter values for nucleotide and NSD syntheses.

	Values						
Parameter	**SGE 36.5°C**	**95% conf. internals**	**TGE 36.5°C**	**95% conf. internals**	**TGE 32°C**	**95% conf. internals**	**Units**
Nucleotide related							
$V_{max,\ ATP\ synthetic\ pathway}$	**13.70**	2.00×10^{-1}	**54.60**	26.00	**3.20**	6.00×10^{-1}	mmol L_{cell}^{-1} h^{-1}
$V_{max,\ GTP\ synthetic\ pathway}$	**44.20**	1.10	**2.31×10^{2}**	23.00	**28.50**	3.90	mmol L_{cell}^{-1} h^{-1}
$V_{max,\ UTP\ synthetic\ pathway}$	**34.90**	1.10	**4.74×10^{2}**	1.20	**2.46**	5.40×10^{-1}	mmol L_{cell}^{-1} h^{-1}
NSD related							
$K_{TP,UDPGlc\ synthetic\ pathway}$	**4.11×10^{-3}**	1.90×10^{-4}	**1.00**	4.30×10^{-2}	**4.89×10^{-1}**	2.00×10^{-2}	mM
$K_{TP,UDPGal\ synthetic\ pathway}$	**4.68×10^{-2}**	5.40×10^{-3}	**1.26×10^{-2}**	4.80×10^{-3}	**1.00×10^{-30}**	1.00×10^{-34}	mM
$K_{TP,UDPGlcNAc\ synthetic\ pathway}$	**1.00×10^{-30}**	1.00×10^{-34}	**61.40**	8.10×10^{-5}	**5.02**	7.70×10^{-2}	mM
$V_{max,\ UDPGlc\ synthetic\ pathway}$	**5.00×10^{-1}**	1.25×10^{-3}	**4.86**	8.70×10^{-1}	**7.17×10^{-4}**	1.50×10^{-4}	mmol L_{cell}^{-1} h^{-1}
$V_{max,\ UDPGal\ synthetic\ pathway}$	**2.26×10^{-3}**	9.20×10^{-4}	**2.06×10^{-3}**	6.70×10^{-4}	**5.76×10^{-2}**	2.20×10^{-7}	mmol L_{cell}^{-1} h^{-1}
$V_{max,\ UDPGlcNAc\ synthetic\ pathway}$	**2.17**	9.00×10^{-2}	**1.00**	1.28×10^{-1}	**4.95×10^{-1}**	1.40×10^{-2}	mmol L_{cell}^{-1} h^{-1}
$K_{UDPGlc,Glc\ synthetic\ pathway}$	**6.66×10^{2}**	74.00	**9.67×10^{2}**	8.70×10^{-5}	**1.00×10^{-30}**	1.00×10^{-34}	mM
$K_{UDPGal,Gal\ synthetic\ pathway}$	**4.73×10^{-1}**	9.10×10^{-3}	**5.00×10^{-1}**	4.30×10^{-2}	**2.00×10^{2}**	2.20×10^{-7}	mM
$K_{UDPGlcNAc,GlcNAc\ synthetic\ pathway}$	**1.82×10^{-1}**	3.00×10^{-3}	**22.20**	5.40	**1.00×10^{-30}**	1.00×10^{-34}	mM

Table 25. Comparison of estimated parameters from NSD models between two expression systems, among SGE at 32°C TS, and in TGE at 36.5°C or at 32°C TS. This includes parameter values for nucleotide and NSD syntheses.

	Values						
Parameter	**SGE 32°C**	**95% conf. internals**	**TGE 36.5°C**	**95% conf. internals**	**TGE 32°C**	**95% conf. internals**	**Units**
Nucleotide related							
$V_{max,\ ATP\ synthetic\ pathway}$	**2.11**	5.10×10^{-1}	**54.60**	26.00	**3.20**	6.00×10^{-1}	mmol L_{cell}^{-1} h^{-1}
$V_{max,\ GTP\ synthetic\ pathway}$	**2.68×10^{3}**	4.70	**2.31×10^{2}**	23.00	**28.50**	3.90	mmol L_{cell}^{-1} h^{-1}
$V_{max,\ UTP\ synthetic\ pathway}$	**9.26×10^{2}**	21.00	**4.74×10^{2}**	1.20	**2.46**	5.40×10^{-1}	mmol L_{cell}^{-1} h^{-1}
NSD related							
$K_{TP,UDPGlc\ synthetic\ pathway}$	**1.00×10^{-30}**	1.00×10^{-34}	**1.00**	4.30×10^{-2}	**4.89×10^{-1}**	2.00×10^{-2}	mM
$K_{TP,UDPGal\ synthetic\ pathway}$	**3.47×10^{-4}**	2.49×10^{-19}	**1.26×10^{-2}**	4.80×10^{-3}	**1.00×10^{-30}**	1.00×10^{-34}	mM
$K_{TP,UDPGlcNAc\ synthetic\ pathway}$	**9.76**	4.80×10^{-5}	**61.40**	8.10×10^{-5}	**5.02**	7.70×10^{-2}	mM
$V_{max,\ UDPGlc\ synthetic\ pathway}$	**5.84×10^{-1}**	1.70×10^{-2}	**4.86**	8.70×10^{-1}	**7.17×10^{-4}**	1.50×10^{-4}	mmol L_{cell}^{-1} h^{-1}
$V_{max,\ UDPGal\ synthetic\ pathway}$	**1.00×10^{-30}**	1.00×10^{-34}	**2.06×10^{-3}**	6.70×10^{-4}	**5.76×10^{-2}**	2.20×10^{-7}	mmol L_{cell}^{-1} h^{-1}
$V_{max,\ UDPGlcNAc\ synthetic\ pathway}$	**7.66**	1.40×10^{-1}	**1.00**	1.28×10^{-1}	**4.95×10^{-1}**	1.40×10^{-2}	mmol L_{cell}^{-1} h^{-1}
$K_{UDPGlc,Glc\ synthetic\ pathway}$	**10.50**	12.00	**9.67×10^{2}**	8.70×10^{-5}	**1.00×10^{-30}**	1.00×10^{-34}	mM
$K_{UDPGal,Gal\ synthetic\ pathway}$	**4.40×10^{2}**	43.00	**5.00×10^{-1}**	4.30×10^{-2}	**2.00×10^{2}**	2.20×10^{-7}	mM
$K_{UDPGlcNAc,GlcNAc\ synthetic\ pathway}$	**4.53×10^{-1}**	21.00	**22.20**	5.40	**1.00×10^{-30}**	1.00×10^{-34}	mM

7.2.3. Discussion of Golgi N-linked glycosylation model in TGE system

The third part of the TGE model describes the process of mAb N-linked glycosylation within the Golgi apparatus, which is the same as for the SGE system. Model outputs from both cell culture dynamics and the NSD model were input into the Golgi N-linked glycosylation model developed by Jimenez del Val et al. (2011), and simulation was performed in gPROMS version 4.0.0. The resulting model outputs were compared to their respective sets of measured glycan data. We sought to investigate the reason of the glycoform difference between SGE and TGE systems, through re-estimating and comparing key parameters such as enzyme dissociation constants and concentrations of glycosyltransferases involved in product glycosylation between the two expression systems.

Figures 59 A and B show the comparison between experimental and simulated distribution of the cumulative N-linked mAb Fc-glycan structure on day 10, 12 and 14 in TGE at 36.5°C and 32°C, respectively. Owing to the low mAb titre in TGE, sufficient amounts of mAb for analysis were only obtained beyond day 10 of the culture period. To aid comparison between SGE and TGE, results for days 10, 12 and 14 were therefore chosen. The model outputs show that the TGE model describes the experimental data equally well as the SGE model does, where differences between estimated and measured values in both SGE and TGE models are within 3.5% in most species. Moreover, simulation results from both sets of parameter values in the TGE model compare reasonably very well to their respective experimental inputs. Table 26 shows that the average difference between experimental and computational values is around 0.9% and they all lay within/below the limit of 3.5%, with two exceptions with discrepancies of 3.7% and 6.1%. Despite the higher percentage differences observed, they are both overlapping with error-bars of their respective experimental data. TGE model simulations are therefore still within the measured data range. Model simulations of the mAb glycan profile between the two conditions in TGE are indeed very comparable and in good agreement with our experimental analysis in Chapter 6.

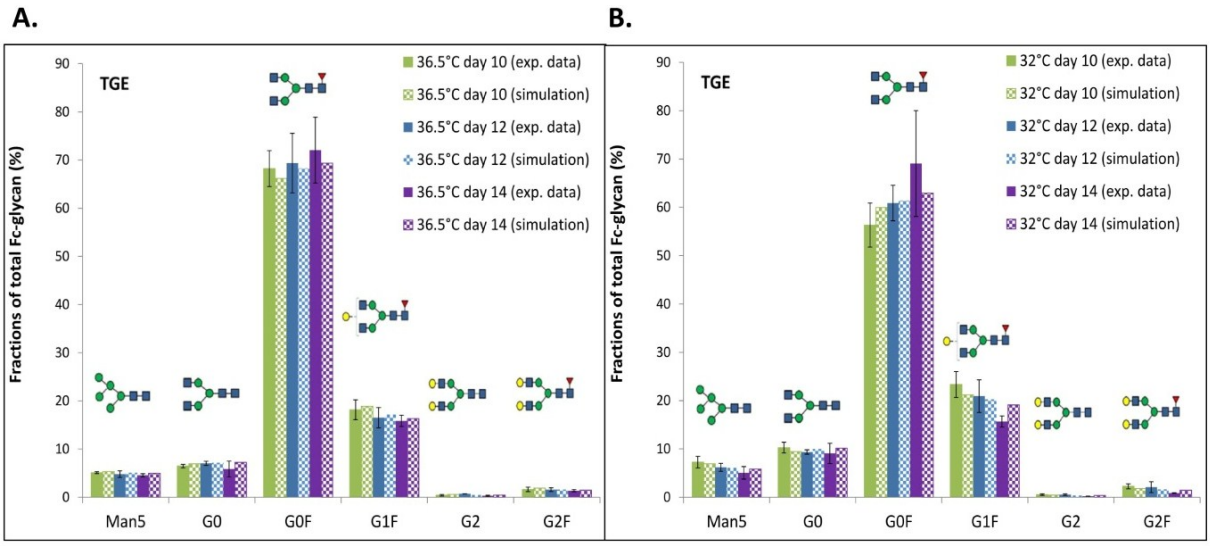

Figure 59. Comparison between experimentally and model simulated determined fractions of the cumulative N-linked glycoforms of secreted mAb for three time points during cell culture, when CHO cells were cultured in TGE at 36.5°C (A), or at 32°C (B) when mild hypothermic condition was introduced 24 h post-transfection.

Table 26. Percentage differences between model-simulated and experimentally measured values of N-linked glycan fractions for mAb Fc-regions, for CHO cells that were cultured at 36.5°C and 32°C in TGE.

	Deviation from experimental data (%)						
		Man5	G0	G0F	G1F	G2	G2F
36.5°C	Day 10	0.26	0.52	2.02	0.77	0.19	0.29
	Day 12	0.32	0.16	1.03	0.69	0.21	0.06
	Day 14	0.44	1.44	2.65	0.51	0.14	0.12
32°C	Day 10	0.29	0.79	3.66	2.08	0.07	0.42
	Day 12	0.07	0.65	0.58	0.62	0.11	0.43
	Day 14	0.81	1.11	6.12	3.45	0.15	0.61

To achieve the above results, we re-estimated the K_m values and glycosyltransferase concentrations in the TGE model. The results can help us shed more light onto the differences in mAb N-linked glycan profiles that arise among the four conditions examined in SGE and TGE systems (Table 27 & 28). Despite minimal variations in secreted mAb glycosylation in TGE between the two temperatures, increased fractions of G0 species and a slight reduction in G0F portion are observed in cells undergoing TGE at 32°C (Chapter 6, Figure 38). By comparing outputs from the TGE model at different temperatures, Man II enzyme concentration is in TGE at 32°C suggested to be 7 times higher than that at 36.5°C, it is also accompanied by significant reduction in the K_m value of this enzyme; as a result it flavours activity by manosidases, providing more substrates for GnTI and II to act on and therefore encourages higher levels of G0 species at 32°C. In addition, FucT concentration is also suggested to be lower in this condition; the reduced FucT enzyme level at 32°C may prevent the conversion of G0F and other fucose-bearing-species, G0 profile therefore remains higher.

When comparing parameter values for both conditions in the TGE system to the set of estimated values for the SGE model at 36.5°C, parameter values in TGE at 32°C suggest that the limitation observed experimentally on mAb galactosylation at 32°C (Chapter 6, Figure 45 A) could be a result of a combination of the reduced GalT enzyme expression and increased values in its K_m values. However in the case of TGE at 36.5°C, the model suggests that the amount of GalT enzyme required for mAb galactosylation is of similar level as that in SGE at 36.5°C, and reduced availability of UDP-Gal species appears more as the key factor that affect mAb galactosylation instead. The computational outputs coincide with our experimental results (Chapter 6, Figure 48 A) and distinguish reasons for limiting mAb galactosylation in TGE at different temperatures. In addition, the level of GnTII is estimated to be higher in TGE at 32°C than that in SGE at 36.5°C. Despite not exactly coordinating with what was observed experimentally (where GnTII mRNA expression levels were

comparable), the higher GnTII enzyme concentration estimated here in the model suggested that there could be a high possibility that GnTII assisted mAb galactosylation by providing increased number of bi-antennary structures for the limited amount of GalT enzymes to work on, so as to achieve a rate of mAb galactosylation higher than that of TGE at 36.5°C but still remained lower than SGE at 36.5°C.

When comparing mAb glycosylation of TGE to that in SGE at 32°C, estimated parameter values from the TGE model indicate that the higher Man_5 levels observed in Chapter 6 (Figure 45 B), is a result of increased Man I enzyme level which converts Man_6 to Man_5, together with a reduced k_d value of Man II enzyme at 32°C (TGE), meaning that fewer Man_5 species are being processed (Table 28). The comparable level of mAb galactosylation between molecules produced under SGE at 32°C and TGE at 36.5°C appears to be attributed to the comparable amount of GalT enzyme that is estimated to exist under both conditions. The increased fractions of G0 and G2 observed in TGE at 32°C, in contrast to those generated in SGE at 32°C, correlate well to the lower concentration of the FucT enzyme which limits the activity of FucT for mAb fucosylation; this at the same time limits the level of G0F species in TGE at 32°C.

In both comparisons drawn above, it is quite interesting how there are conflicting results suggested between model estimation and experimental transcript analysis of GnTI and II. However one has to bear in mind that these estimated values has not yet been validated. They only give an idea about the kinetics of glycosyltransferase involved but not necessarily 100% reliable. As a result, to improve the quality of this work, model validation is indeed extremely important and will be included as one of the main future studies.

Table 27. Estimated enzyme concentrations and their respective dissociation constants in SGE at 36.5°C, and in TGE at 36.5°C or at 32°C TS.

	Parameter	SGE 36.5°C	95% conf. internals	TGE 36.5°C	95% conf. internals	TGE 32°C	95% conf. internals	Units
	Glycosyltransferase concentrations							
	Man I	**9.70×10^{-2}**	1.31×10^{-2}	**12.60**	1.80×10^{-1}	**7.59**	4.40×10^{-1}	µM
	Man II	**1.82×10^{-1}**	3.50×10^{-2}	**3.20×10^{-1}**	4.50×10^{-2}	**2.32**	1.70×10^{-1}	µM
	GnT I	**6.05**	2.10×10^{-1}	**3.73**	8.5×10^{-2}	**5.24**	4.60×10^{-2}	µM
	GnT II	**1.14**	2.50×10^{-1}	**2.94**	9.70×10^{-5}	**2.79**	4.40×10^{-4}	µM
	GalT	**12.60**	1.70	**13.00**	6.00×10^{-2}	**3.21**	5.40×10^{-1}	µM
	FucT	**13.30**	8.43	**8.54**	1.00×10^{-2}	**5.49**	4.30×10^{-1}	µM
Substrate	*Enzyme dissociation constants*							
Man_6	$K_{d,Man\ I\ D}$	**4.44×10^{-1}**	1.60×10^{-2}	**3.93×10^{2}**	3.10×10^{-2}	**64.90**	3.10×10^{-2}	µM

Man_5	$K_{d,Man\ II\ A}$	**3.45×10^{-5}**	1.84×10^{-6}	**5.91×10^{2}**	6.40×10^{-7}	**6.75×10^{-8}**	2.50×10^{-10}	μM
$CoreGlcNAc_1$	$K_{d,GnT\ II}$	**5.31**	4.20×10^{-1}	**1.40×10^{3}**	46.00	**1.08×10^{4}**	4.40×10^{-4}	μM
$CoreGlcNAc_2$ (α-1,3 arm)	$K_{d,GalT\ a1A}$	**3.00×10^{4}**	1.95×10^{3}	**5.18×10^{3}**	1.50×10^{-5}	**4.60×10^{3}**	1.10×10^{-3}	μM
$CoreGlcNAc_2$ (α-1,6 arm)	$K_{d,GalT\ a1B}$	**6.26**	2.73	**9.69×10^{3}**	3.10×10^{-6}	**4.19×10^{3}**	2.40×10^{3}	μM
$CoreGlcNAc_2$ Gal_1 (α-1,6 arm)	$K_{d,GalT\ a2A}$	**2.23×10^{3}**	2.67×10^{2}	**3.98×10^{2}**	2.00×10^{-4}	**6.98×10^{3}**	7.10×10^{-4}	μM
$CoreGlcNAc_2$	$K_{d,Fuc\ A}$	**1.34×10^{4}**	9.34×10^{2}	**1.24×10^{2}**	5.30×10^{-4}	**2.05**	3.90×10^{-2}	μM

Table 28. Estimated enzyme concentrations and their respective dissociation constants in SGE at 32°C TS, and in TGE at 36.5°C or at 32°C TS.

	Parameter	SGE 32°C	95% conf. internals	TGE 36.5°C	95% conf. internals	TGE 32°C	95% conf. internals	Units
	Glycosyltransferase concentrations							
	Man I	**1.24×10^{-1}**	8.50×10^{-2}	**12.60**	1.80×10^{-1}	**7.59**	4.40×10^{-1}	μM
	Man II	**1.94×10^{-1}**	7.30×10^{-3}	**3.20×10^{-1}**	4.50×10^{-2}	**2.32**	1.70×10^{-1}	μM
	GnT I	**7.69×10^{-1}**	6.80×10^{-4}	**3.73**	8.5×10^{-2}	**5.24**	4.60×10^{-2}	μM
	GnT II	**7.75×10^{-1}**	1.30×10^{-4}	**2.94**	9.70×10^{-5}	**2.79**	4.40×10^{-4}	μM
	GalT	**6.66**	4.10×10^{-2}	**13.00**	6.00×10^{-2}	**3.21**	5.40×10^{-1}	μM
	FucT	**45.54**	5.96	**8.54**	1.00×10^{-2}	**5.49**	4.30×10^{-1}	μM
Substrate	*Enzyme dissociation constants*							
Man_6	$K_{d,Man\ I\ D}$	**2.67×10^{-1}**	3.10×10^{-2}	**3.93×10^{2}**	3.10×10^{-2}	**64.90**	3.10×10^{-2}	μM
Man_5	$K_{d,Man\ II\ A}$	**4.44×10^{-5}**	4.71×10^{-9}	**5.91×10^{2}**	6.40×10^{-7}	**6.75×10^{-8}**	2.50×10^{-10}	μM
$CoreGlcNAc_1$	$K_{d,GnT\ II}$	**1.16×10^{2}**	13.00	**1.40×10^{3}**	46.00	**1.08×10^{4}**	4.40×10^{-4}	μM
$CoreGlcNAc_2$ (α-1,3 arm)	$K_{d,GalT\ a1A}$	**2.29×10^{4}**	3.15×10^{3}	**5.18×10^{3}**	1.50×10^{-5}	**4.60×10^{3}**	1.10×10^{-3}	μM
$CoreGlcNAc_2$ (α-1,6 arm)	$K_{d,GalT\ a1B}$	**11.60**	2.54	**9.69×10^{3}**	3.10×10^{-6}	**4.19×10^{3}**	2.40×10^{3}	μM
$CoreGlcNAc_2$ Gal_1 (α-1,6 arm)	$K_{d,GalT\ a2A}$	**3.38×10^{2}**	4.80×10^{2}	**3.98×10^{2}**	2.00×10^{-4}	**6.98×10^{3}**	7.10×10^{-4}	μM
$CoreGlcNAc_2$	$K_{d,Fuc\ A}$	**1.34×10^{4}**	3.00×10^{2}	**1.24×10^{2}**	5.30×10^{-4}	**2.05**	3.90×10^{-2}	μM

Despite providing more information about the kinetics properties of enzymes involved in protein glycosylation, estimated parameters such as enzyme concentration, k_{cat} and K_m values are correlated. As a result, it is difficult to provide unique estimates of either of these parameters. Since galactosylation is important in mAb production, there is a high potential for glyco-engineering. It is therefore essential to test the reliability of the sets of estimated parameters describing enzyme kinetics and to identify if variation in GalT enzymatic activity is solely contributed from changes in k_{cat} value, or from a combinatorial effect by the protein expression of GalT. To test the hypothesis, a comparison in glycosyltransferase concentrations between model outputs and measured concentrations were performed. Protein expression of galactosyltransferase (GalT) is experimentally determined in Chapter 6 (Figure 48 A & B). Firstly, outputs from the TGE model propose that GalT concentration in

TGE at 32°C to be around 39% lower than that at 36.5°C; this correlates reasonably well with our experimentally measured results where the average GalT protein expression is approximately 31% lower at 32°C. Tables 29 A and 29 B compare the average percentage difference of GalT enzyme concentration among all four conditions examined in this chapter, through experimentally analysis and model estimation, respectively. Our results show that variations between experimentally measured data and estimated model outputs are indeed very marginal, where differences between most values in the Tables 29 A and 29 B are within 8%, with the exception of a 20% difference between SGE at 2°C and TGE at 36.5°C. Despite that fact that both models are not validated by separate sets of experiment data, the comparability between the estimated and measured values suggested in Tables 29 A and 29 B already demonstrates the high capability of both models in representing the underlying biological systems.

Table 29. Percentage difference of GalT enzyme concentration among all four conditions examined, that are (A) experimentally measured, or (B) estimated by the SGE and TGE models.

A.

Average percentage difference of experimentally determined GalT protein expression among all conditions (%)			
	SGE 36.5°C	SGE 32°C	TGE 32°C
TGE 36.5°C	17.7%	48.2%	30.5%
TGE 32°C	42.7%	14.3%	-

B.

Average percentage difference of model estimated GalT protein concentration among all conditions (%)			
	SGE 36.5°C	SGE 32°C	TGE 32°C
TGE 36.5°C	16.6%	68.0%	38.7%
TGE 32°C	48.9%	3.0%	-

Comparison of N-linked Golgi model outputs between the two expression systems suggests that the reduced levels of mAb galactosylation in TGE when compared to those in SGE, are mainly due to reduced expression of GalT enzymes. Our model suggests that enzyme concentrations and kinetics properties of other glycosyltransferases also play a role in altering the mAb glycan structures, such as mAb core-fucose and high mannose structures. Despite such findings, it can always be argued that decreases in the expression of glycosyltransferases might only be a result of reduced mAb

volumetric yield in the TGE system; however the comparable concentrations of GalT between SGE at 36.5°C and TGE at 36.5°C for instance, show that the concentration profiles of these enzymes are not entirely dependent on the amount of mAb molecules produced, but more expression system and temperature dependent. Therefore, in addition to feedings of NSD precursors and amino acids, one can attempt to manipulate the expression of different glycosyltransferases to improve both the quality of the secreted mAb products. Since the expression of GnTI and GnTII are shown in previous chapters to be important enzymes that determine the branching of mAb N-linked, and we are experiencing conflicting results between model estimation of GnTII expression and experimentally determined mRNA expression, it is therefore necessary to validate these estimations from the model by analysing the protein expression of glycosyltransferases, preferably GnTI and II.

7.3. Conclusions

The first part of this chapter analysed CHO cell performance in terms of cell metabolisms and mAb Fc N-linked glycosylation in cultures that undergo transient gene expression at physiological temperature or with a temperature shift to 32°C 24 hours post DNA plasmid transfection through a mechanistic mathematical model. The latter was based on the SGE model presented in Chapter 5 with slight modifications in the cell dynamics model and re-estimated key parameter sets for each temperature examined in the TGE system. Our results showed that our TGE model is capable of describing experimental results well in all aspects under both conditions. The second part of the chapter compared model outputs between the SGE and the TGE models, with an aim to identify differences in mAb productivity and glycan profiles between the two expression systems. The tremendous difference in mAb productivity between SGE and TGE was not only a consequence of the lower IVCC; the cell dynamics model proposed that reduced transcription rates of both heavy and light chains were the bottlenecks for mAb production in the TGE system. On the other hand, major variations in mAb Fc-glycosylation appear between products that were produced in cells undergoing SGE at 36.5°C and at both temperatures examined in TGE. Most enzymes that were involved in NSD synthesis, their enzymatic efficiencies, GalT in particular, were suggested by the NSD model to be lower. This correlated well with the reduced metabolic fluxes for nucleotide and NSD production calculated for TGE in Chapter 7. In addition, the N-linked Golgi glycosylation module of the model identified that the enzyme concentrations of GalT, FucT and GnTI were lower and their kinetics slower. The combination of the less efficient NSD synthetic network and reduced expression of key glycosyltransferases, such as GnTI, II and GalTs contributed to limiting bi-antennary structures of mAb, which are required for further N-linked glycan processing including mAb galactosylation.

Based on the comparison of model outputs between SGE and TGE, rather than modifying the bioprocess through a “Quality by Testing” approach, one can now target a specific area through tailored feeds, cell line modification, or altering other bioprocess conditions, according to the outputs of the model. Not only does it aim to improve the production yield or product quality, such an approach also enables the application of Quality by Design (QbD) in pharmaceuticals.

Chapter 8
Manipulating expression of N-linked galactosyltransferases to improve monoclonal antibody galactosylation

Both experimental and computational studies on mAb glycosylation in mild hypothermic conditions in Chapter 4 - 7 suggest that expression levels of glycosyltransferases, galactosyltransferases in particular, are contributing factors that lead to variations in mAb glycan profiles. To improve mAb galactosylation in these conditions, manipulating expression levels of enzymes related to N-linked glycosylation can be an approach. This chapter attempts to manipulate the expression level of galactosyltransferase, through increasing the level of three micro-RNAs (miRNAs) that were reported to regulate expression of β-1,4 galactosyltransferases.

8.1. Background and aim

When it comes to process optimisation to improve mAb glycosylation, there are a number of possible approaches; these include feeding with nutrients such as glucose, glutamine or galactose (Grainger and James 2013; Gramer et al. 2011; Kim do et al. 2013; Seo et al. 2014), nucleotide or NSD precursor supplementation (Bergfeld et al. 2012; Gramer et al. 2011; Gu and Wang 1998; Wong et al. 2010), or other chemical supplements such as manganese chloride (Gramer et al. 2011) or butyrate (Lee et al. 2014). N-linked enzyme manipulation through cell-line engineering, including the gene knockout (Malphettes et al. 2010; Sealover et al. 2013) or overexpression (Onitsuka et al. 2012; Zhang et al. 2010a). The latter option appears to be favourable, especially in bulk rProtein production when large volumes of external feedings can be costly and extensive dilution can be an issue.

Glyco-engineering in different host cell lines is an advent approach to produce humanised antibodies. mAb fucosylation and bisecting GlcNAc addition are often targets in glycoengineering, to increase binding affinity between mAb Fc region and their activating receptors. An overexpression of *N*-acetylglucosaminyltransferase III (GnT III) in eukaryotes was firstly introduced in 1999 to include bisecting GlcNAc in the secreted product, but the results of it had greatly impeded cell growth (Umana et al. 1999a). With advances in protein engineering, Roche GlycArt AG had successfully generated a genetically modified host cell that altered expression levels of enzymes including β(1,4)-N-acetylglucosaminyltransferase III, β(1,4)-N-acetylglucosaminyltransferase V, β(1,4)-galactosyltransferase, α-mannosidase II, and core α-1,6-fucosyltransferase (Pablo Umaña and Jean-Mairet 2012), which was shown to enhance antibody-dependent cellular cytotoxicity with no significant negative impacts on cell growth. In addition, this technology is widely employed in other host cells such as yeast that are incapable of performing human-like glycosylation (Potgieter et al. 2009), and overexpression of manosidases are necessary to prevent hypermannosylation.

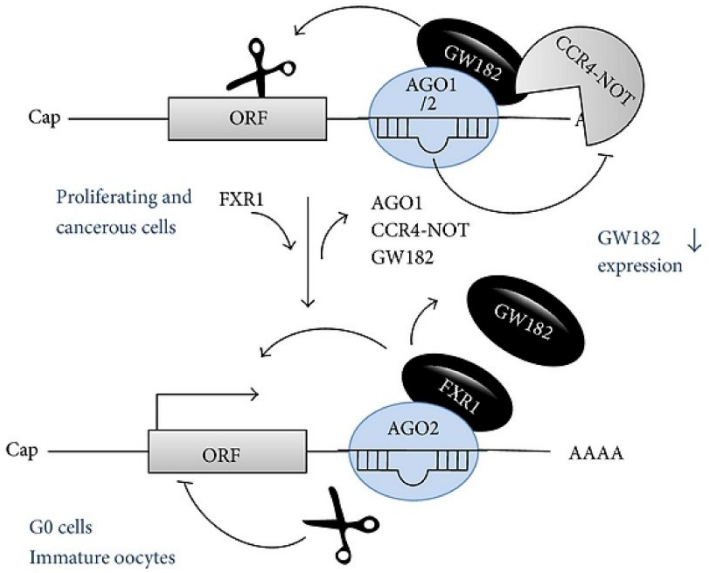

Figure 60. Regulation of miRNA mediated suppression and activation in different cell cycle stages. Figure is adopted from Valinezhad Orang et al. (2014). In brief, protein GW182 is the key regulator cells, where binding to Ago in proliferating cells encourages the slicing of ORF of target gene and suppresses gene expression. While the release of GW182 from the Ago complex in G0 cell cycle stage, especially when cells are undergoing cell cycle arrest, attracts a different protein Fxr1 and prevents the slicing of the open reading frame, resulting in the activation of target gene.

On the other hand an emerging candidate, miRNA, was proven to be useful for pharmaceutical bioprocessing. miRNAs are short non-coding RNA molecules (~ 20 to 25 nts) that are processed by the RNase III endonuclease Dicer complex in the nucleus and are coupled to RNA-induced silencing complex (RICS) to form mi-RISCs. They possess a degree of complementarity to their target mRNAs and bind to the 3'-UTR (untranslated region) of their target sequences, recruiting an Argonaute (Ago) protein to modulate transcriptional expression. The traditional role of miRNAs involves gene silencing and repression through mRNA promoter attenuation. However recent studies show the ability of miRNAs is not only limited to gene suppression, but they can also activate gene translation during specific cell conditions or with or without certain stimulators (Vasudevan et al. 2007). The most investigated case involves cell quiescence. It was reported and Figure 60 illustrates that when cells were arrested in G1/G0 state, miRNA binds to target mRNA and recruited argonaute RISC catalytic component 2 (Ago2) and fragile X mental retardation-related protein 1 (Fxr1), this inhibited the interaction between Ago2 and GW182, an important candidate that mediates gene-repression, and thus promoted activation of gene translation (Valinezhad Orang et al. 2014).

Within the past two decades, a vast number of studies showed the application of miRNAs in cellular processes, ranged from cell growth and cell development (Chen et al. 2006; Cheng et al. 2005; Croce and Calin 2005; Johnston and Hobert 2003; Matsushima et al. 2011), to modulation of cell metabolism and protein secretion (Filipowicz 2005; Poy et al. 2004). Recently the understanding of the CHO cell genome has enabled scientists to extend the ability of miRNA to improvement in recombinant protein bioprocessing. Jadhav et al. (2014b) demonstrated that stable overexpression of miR-17 increased the Erythropoietin-Fc fusion protein (EpoFc) titre by 3-fold and also enhanced CHO cell growth. Site-specific miRNA editing is evolutionarily conserved among species (Warnefors et al. 2014) and through lectin microarrays experiments, Agrawal et al. (2014) identified miRNAs or a combination of different miRNA that related to specific glycan biosynthetic enzymes, specifically miRNAs cgr-miR-500, cgr-miR-501-5p and cgr-miR-181d which are shown to be related to and regulate β(1,4)-galactose addition during protein glycosylation. By incorporating each of the three pre-miRNA in separate mammalian expression vector that functions with a CMV promoter, and co-transfecting these three pre-miRNAs into an IgG expressing CHO cell line, in this chapter we have decided to make use of the regulatory mechanisms of miRNA between gene activation and repression during cell cycle arrest, and investigated two aspects here: the effect of co-overexpressing that combination of three miRNAs that were suggested to relate β(1,4)-galactosylation on galactosyltransferase expression; and whether they imposed any changes in mAb glycosylation.

8.2. Results

8.2.1. CHO cell culture behaviour upon miRNA overexpression

In this chapter we examined four sets of experimental conditions: 1. CHO cell fed-batch culture at 36.5°C (Control 36.5°C), or 2. with a temperature shift from 36.5°C to 32°C on day 6 during late exponential phase (Control 32°C TS); 3. miRNA combination transfected - CHO cell fed-batch culture with a temperature shift to 32°C (miRNA 32°C TS), or 4. empty vector transfected-cell culture with a temperature shift to 32°C (null-vector 32°C TS). Firstly, we examined differences in CHO cell growth among all conditions. Figures 61 A and B show the viable cell concentration and viability, and total cell density of CHO cell cultures in all conditions, respectively. As suggested in Chapter 4, CHO cells possess prolonged cell viability when cultured at 32°C. A similar cell growth profile is observed when a null-vector is transfected and mild hypothermia was introduced. Conversely, viable cell density increases upon the co-transfection of the three pre-miRNA vectors at 32°C, but with cell viability above 75%, which is similar to their non-transfected counterparts at 32°C. Increased in time-course viable cell density is also reflected by a 18% rise in the IVCC of miRNA-transfected species when compared to that of the non-transfected species at 32°C; at the same time the IVCC of pre-miRNA transfected cells is very comparable to that of the control cells cultured at 36.5°C (Figure 61 C).

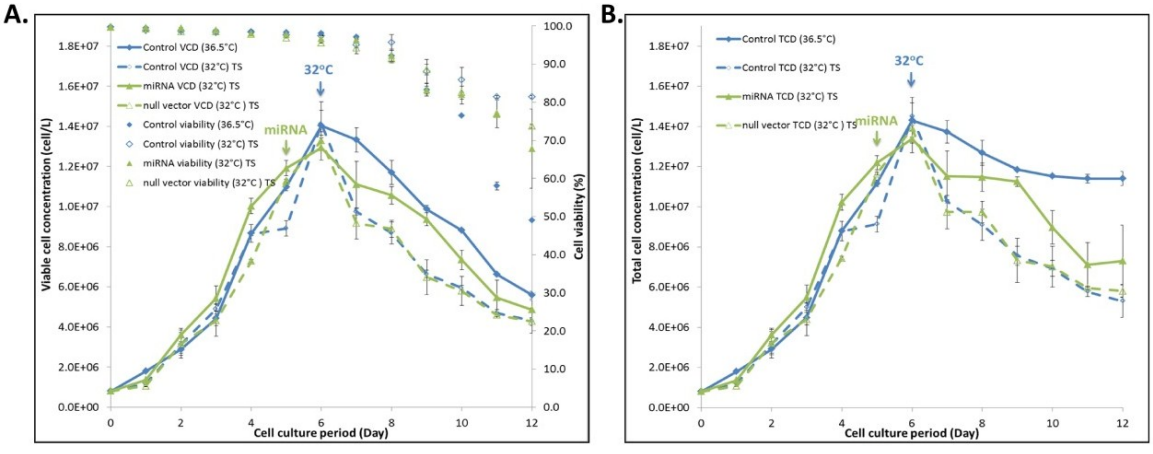

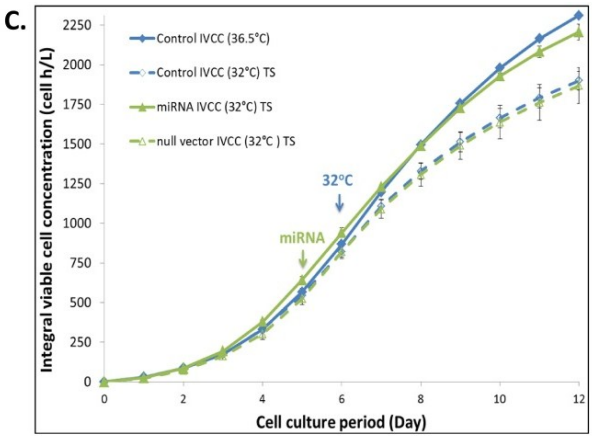

Figure 61. Cell growth profiles of control cells at 36.5°C and with a temperature shift to 32°C, together with miRNA or null-vector transfected CHO cell culture under mild hypothermic conditions. (A). Viable cell concentration and cell viability profiles were measured along the period of cell culture in all conditions examined, together with the total cell concentration profile in (B). IVCC profiles of respective conditions (C). Results are average measurements control cells at 36.5°C (n=2) and 32°C (n=2), or miRNA-transfection (n=2) and null-vector transfected (n=2) at 32°C. The error bars represent the standard deviation of the samples. TS: Temperature shift.

8.2.2. mAb production in miRNA-transfectants

Accompanied by the variation in CHO cell growth profile, the volumetric and specific mAb productivities in miRNA transfected cells are shown to be higher (Figure 62 A). Correlated well with previous results observed in Chapter 4, higher specific mAb productivity (q_{mab}) is achieved when biphasic culture temperatures are introduced during cell culture process (Figure 62 B). Upon co-transfection of pre-miRNAs, q_{mAb} value of mAb molecules generated from miRNA transfectants is comparable to that of the control species cultured at 32°C (Figure 62 C). At the same time, the miRNA-transfected species show a 7.8% increase in its q_{mAb} when compared to cells transfected with a null-vector (Figure 62 D). The increase in mAb production appears to be related to the improved cell growth and cell viability upon the miRNA transfection. However further investigation into CHO cell metabolism is required to identify the underlying factors for improved mAb production.

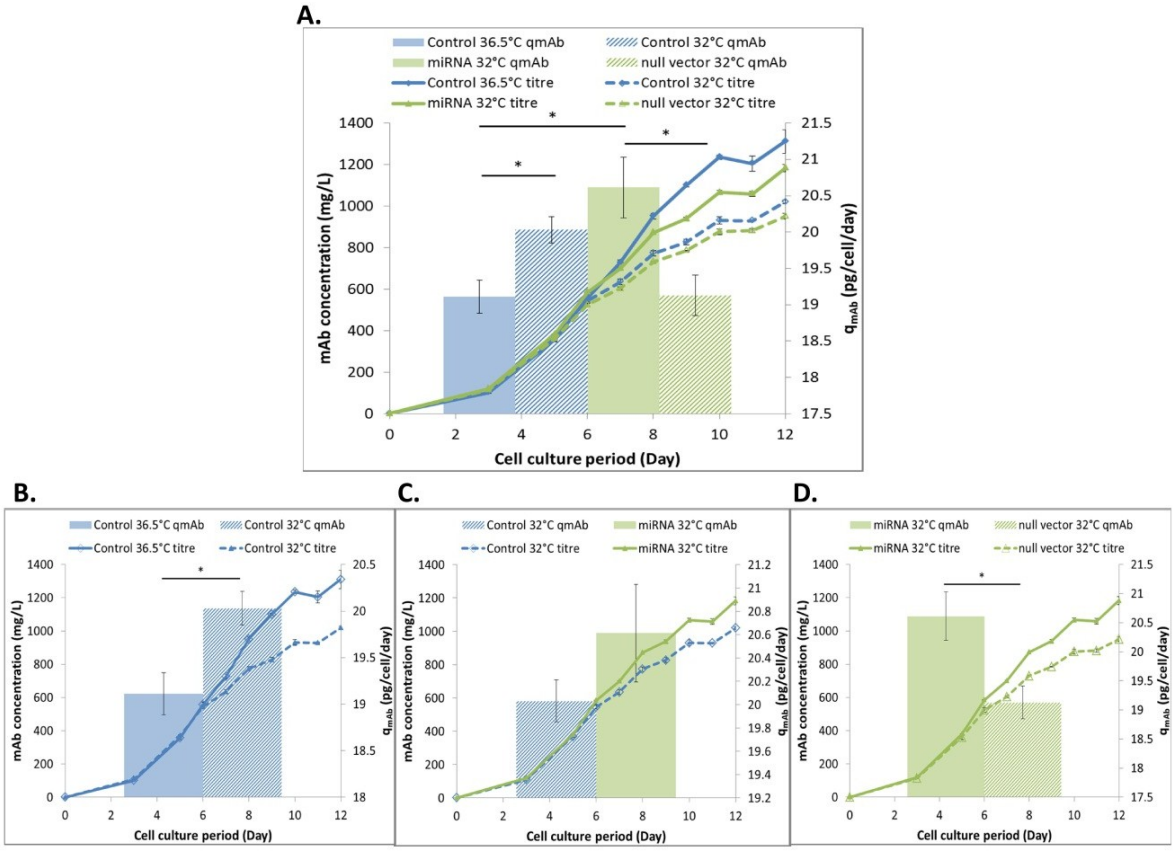

Figure 62. (A). Volumetric and specific mAb productivities when control cells are culture under all four conditions examined, including a comparison between control cells at both temperatures (B), between control cells and miRNA-transfectants at 32°C (C), and between miRNA- and null-vector- transfected cells at 32°C (D). Results were average measurements at 36.5°C (n=2) and 32°C TS (n=2) in control cells, miRNA and null-vector transfectants. The error bars represent the standard deviation of the samples. TS: Temperature shift.

8.2.3. The impact of miRNA overexpression on CHO cell metabolism

Firstly we examined changes in nutrient metabolism upon miRNA transfection. As a result of increase in viable cell density in miRNA-transfectants, transfected cultures consumed a higher amount of glucose than the control and the null-vector transfected cultures at 32°C, and the rate of consumption in miRNA transfectants was comparable to that of the control cells at 36.5°C (Figures 63 A & D). On the other hand, Figure 63 B shows that lactate metabolism shifts from predominantly lactate production to lactate consumption upon the induction of mild hypothermia during cell culture in control cells, with a 53% increase in lactate consumption on day 6 which correlates well with previous results demonstrated in Chapter 4. A similar concentration profile is observed when a null-vector is transfected to CHO cells at 32°C. Interestingly, lactate concentration profile of miRNA transfectants at 32°C resembles that of the control cells at 36.5°C on day 6 and day 7 shortly after the reduction of culture temperature to 32°C. Lactate production is reduced from day 8 (stationary growth

phase) of cell culture in miRNA transfectants. Figure 63 C shows that the rate of lactate consumption is high between day 9 and day 11. The final net concentration of lactate in miRNA transfected cells on day 12 is comparable to those in control cells at 32°C, which is 44% lower than that in control cells at 36.5°C. Unlike control cells at 36.5°C which utilise predominantly glucose, the behaviour of miRNA-transfected cells towards lactate metabolism sits between control cells cultured at 36.5°C and 32°C: they consume a higher level of glucose but at the same time the uptake rate of lactate increases. Our results suggest that the amount of carbon required increases upon the co-transfection of pre-miRNA vectors to fuel cellular activities such as glycolysis and the TCA cycle. However, it still remains difficult to speculate whether these extra carbon molecules are consumed towards protein synthesis or glycosylation.

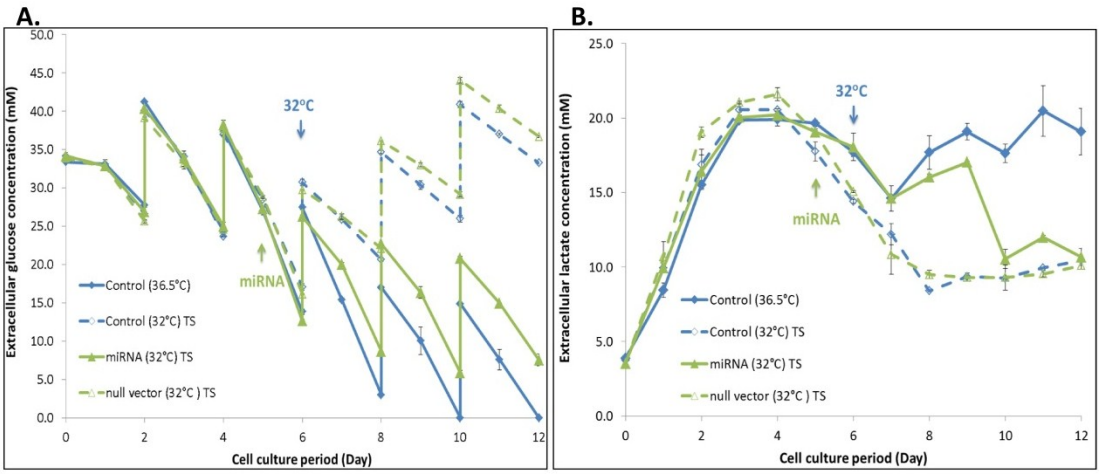

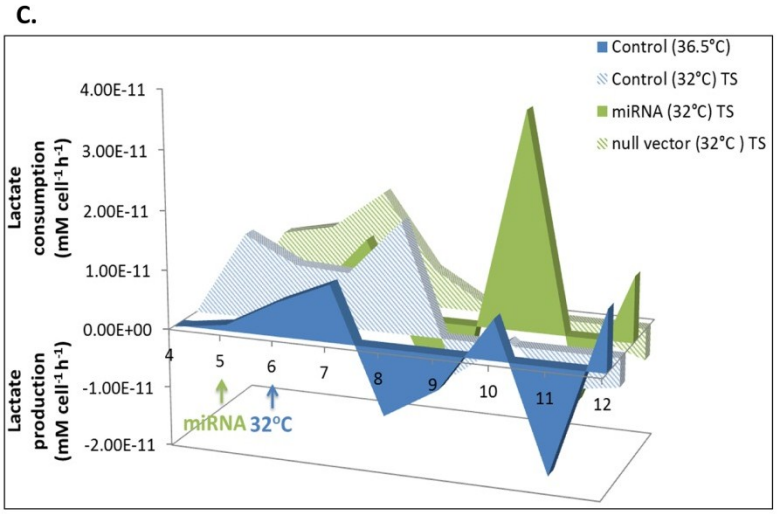

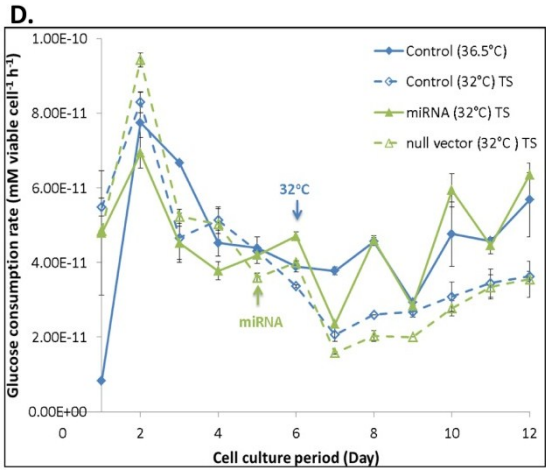

Figure 63. Nutrient metabolism in CHO cells under all four conditions examined. (A). Concentration profile of extracellular glucose. (B). Concentration profile of extracellular lactate. (C). Rate of lactate production/consumption per viable cell under all four conditions. (D). Rate of glucose production/consumption per viable cell. Results were average measurements at 36.5°C (n=2) and 32°C TS (n=2) in control cells, miRNA and null-vector transfectants. The error bars represent the standard deviation of the samples. TS: Temperature shift.

In addition to increased glucose and lactate uptakes, amino acid utilization was also examined in miRNA transfectants. Figures 64 A – F show the concentration profiles and consumption rates of six amino acids that contribute 5 - 9% and above of the total mAb peptide sequence, namely valine, threonine, leucine, proline, lysine and glutamate. Their amino acid concentration profiles resemble that of glucose, where in most cases the extracellular concentrations of control cells at 32°C and null-vector transfectants are higher than those observed in control cells at 36.5°C and in miRNA transfectants. Variations in extracellular concentration are without doubt related to changes in viable cell density among the four conditions, rates of amino acid consumption per viable cell are therefore considered. In most cases, rates of consumption of the six amino acids are higher in miRNA transfectants than in control cells that are cultured under mild hypothermic temperature, with percentage increase ranges from 24% to 70%. Not only do these amino acids fuel the TCA cycle for energy generation, they also account for at least 40% of the mAb peptide sequence; increased rates of consumption in these amino acids upon miRNA transfection have a positive effect on mAb synthesis.

A.

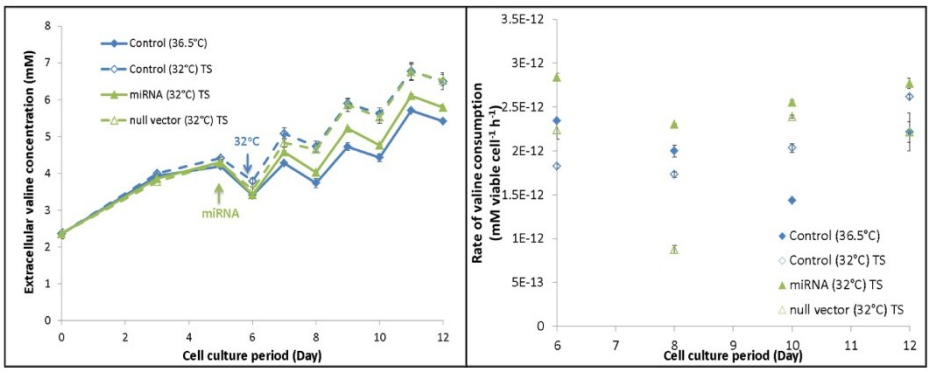
Extracellular valine concentration (mM)
Control (36.5°C)
Control (32°C) TS
miRNA (32°C) TS
null vector (32°C) TS
32°C
miRNA
Cell culture period (Day)
Rate of valine consumption (mM viable cell⁻¹ h⁻¹)
Control (36.5°C)
Control (32°C) TS
miRNA (32°C) TS
null vector (32°C) TS
Cell culture period (Day)

B.

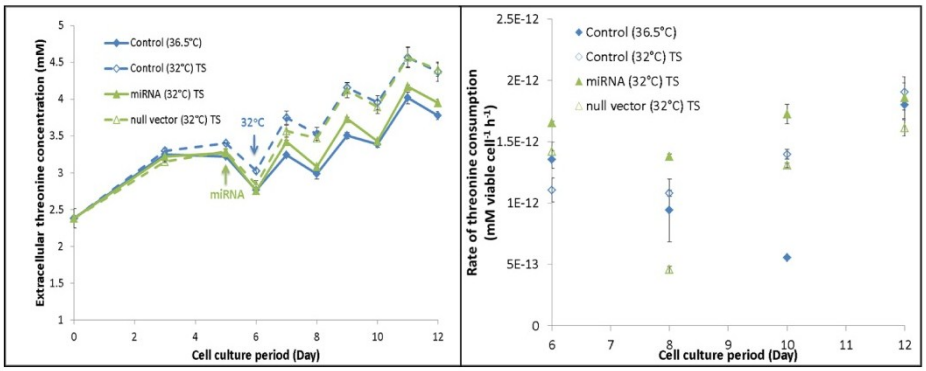
Extracellular threonine concentration (mM)
Control (36.5°C)
Control (32°C) TS
miRNA (32°C) TS
null vector (32°C) TS
32°C
miRNA
Cell culture period (Day)
Rate of threonine consumption (mM viable cell⁻¹ h⁻¹)
Control (36.5°C)
Control (32°C) TS
miRNA (32°C) TS
null vector (32°C) TS
Cell culture period (Day)

C.

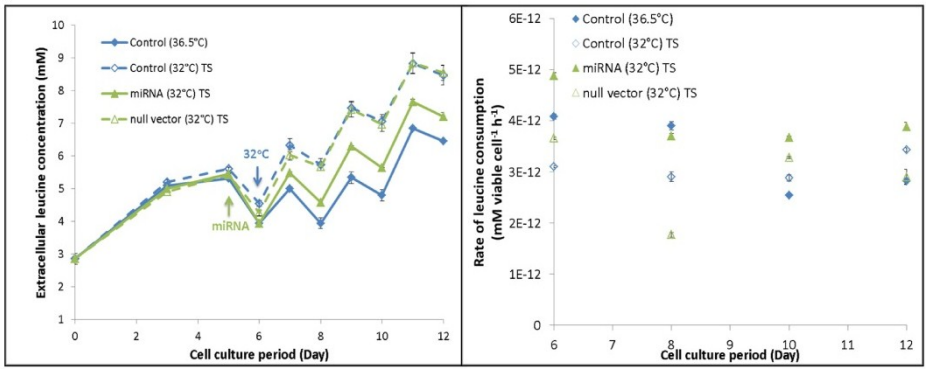
Extracellular leucine concentration (mM)
Control (36.5°C)
Control (32°C) TS
miRNA (32°C) TS
null vector (32°C) TS
32°C
miRNA
Cell culture period (Day)
Rate of leucine consumption (mM viable cell⁻¹ h⁻¹)
Control (36.5°C)
Control (32°C) TS
miRNA (32°C) TS
null vector (32°C) TS
Cell culture period (Day)

D.

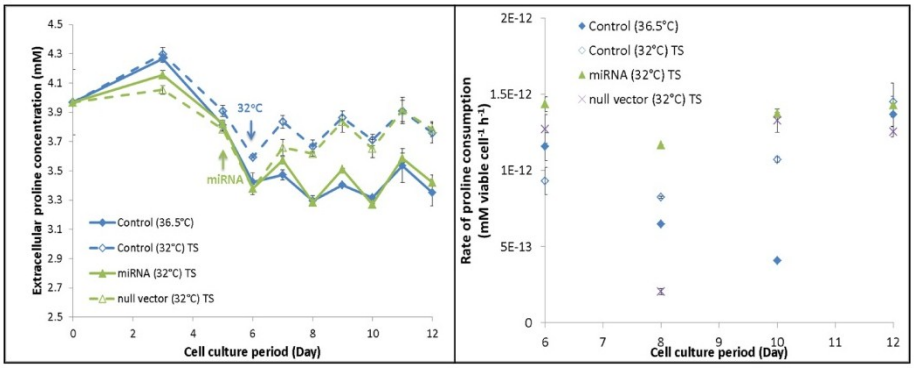
Extracellular proline concentration (mM)
Control (36.5°C)
Control (32°C) TS
miRNA (32°C) TS
null vector (32°C) TS
32°C
miRNA
Cell culture period (Day)
Rate of proline consumption (mM viable cell⁻¹ h⁻¹)
Control (36.5°C)
Control (32°C) TS
miRNA (32°C) TS
null vector (32°C) TS
Cell culture period (Day)

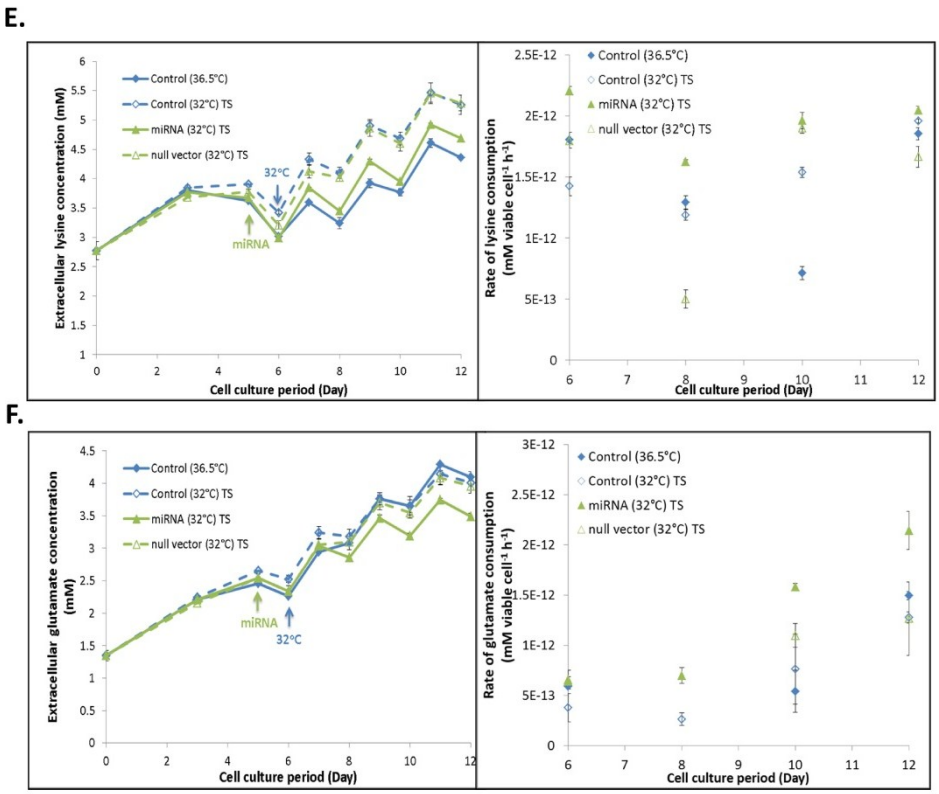

Figure 64. Amino acid metabolism in CHO cells under all four conditions examined. Extracellular concentration and consumption rate profiles of (A). valine, (B). threonine, (C). leucine, (D). proline, (E). lysine and (F). glutamate. Results were average measurements at 36.5°C (n=2) and 32°C TS (n=2) in control cells, miRNA and null-vector transfectants. The error bars represent the standard deviation of the samples. TS: Temperature shift.

NSD synthesis is directly impacted by changes in carbon and amino acid metabolism. Figures 65 A – F show net concentration profiles of five NSD species, including UDP-Glc, UDP-Gal, UDP-GlcNAc, GDP-Man and GDP-Fuc. Our results suggest that by co-transfecting vectors bearing pre-miRNAs into cells that are cultured under mild hypothermic conditions, significant reduction in the net concentration of UDP-Glc, UDP-Gal and GDP-Man are observed when compared to the control cells at 32°C (Figures 65 A, B & D); while comparable levels of UDP-GlcNAc and GDP-Fuc are achieved in all conditions examined (Figures 65 C & E). Again, one has to bear in mind that zero values of GDP-Man on Figure 65 E represent results that are under the detection limit of the current HPLC method. On the other hand, flux balance analysis results suggests that the difference in carbon flux towards NSD between miRNA transfected cells and control cells at 32°C is only 5%. The tiny difference in NSD metabolic flux between the two conditions demonstrates that differences observed in experimentally measured NSD concentrations are more likely due to the consumption instead of extra production of the NSD species in miRNA transfected CHO cells.

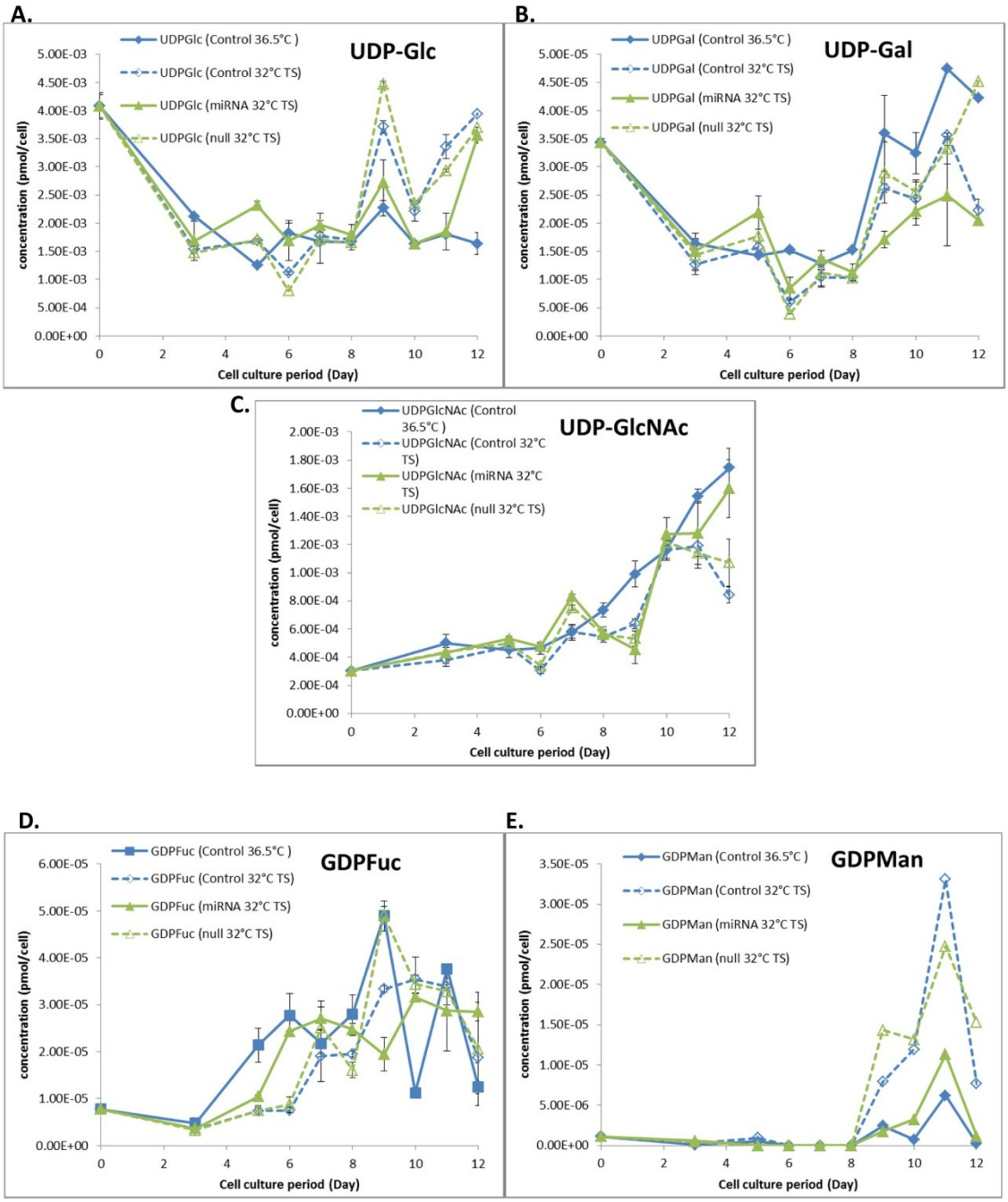

Figure 65. Net concentration profiles of five NSD species under all conditions examined. Concentrations of UDP-Glc (A), UDP-Gal (B), UDP-GlcNAc (C), GDP-Fuc (D) and GDP-Man (E) are measured experimentally. Results were average measurements at 36.5°C (n=2) and 32°C TS (n=2) in control cells, miRNA and null-vector transfectants. The error bars represent the standard deviation of the samples. TS: Temperature shift.

8.2.4. Impact of miRNA transfection on expression of N-glycosylation related genes

The aim of co-transfection of three pre-miRNAs was to indirectly manipulate the expression of galactosyltransferases in CHO cells that are cultured at 32°C. Both mRNA and protein expression of the enzyme were experimentally quantified and results of the miRNA transfectants were compared to those in the non-transfected species. Figures 66 A – G examine transcript levels of six glycosyltransferases and one NSD transporter in N-linked protein glycosylation. As expected, not all enzymes are affected upon pre-miRNA co-transfections. Our results show that mRNA expression levels of GalT I, GalT II and GalT III are higher in miRNA transfectants than in control cells at 32°C, with an average increase of 46% (Figures 66 E – G). In fact, mRNA expression levels are comparable to those observed in control cells cultured at 36.5°C. Although miRNA vectors were co-transfected on day 5 during cell culture, significant increases in GalT transcript levels were only observed beyond day 6, when the temperature was shifted from 36.5°C to 32°C. This temperature-dependent increase in GalT mRNA levels coincides with research carried out by Vasudevan et al. (2007), which suggested a switch of miRNA regulation from transcription repression to expression when cells were arrested in G_1/G_0 state, which is common in mild hypothermic conditions (Marchant et al. 2008).

Despite higher UDP-Gal transporter mRNA level observed in miRNA transfected cells (Figure 66 C), the increase was only significant on one incident (on day 8 of cell culture). There is no evidence in this study which suggests that the co-transfected miRNAs impact on the expression of UDP-GalT transporter. Surprisingly, the transcript level of GnT I was also shown to increase in miRNA transfected species (Figure 66 A), while the mRNA expression of other enzymes including GnT II and FucT, did not show significant variation in miRNA transfected CHO cells (Figures 66 B & D).

Protein expression level of GalT III was further quantified through Western blotting and fold difference of its expression levels was compared among all conditions examined (Figure 67). Despite significant increases in mRNA expression levels of GalTIII, time-course increases in protein expression of GalT III were not as pronounced. Figure 67 shows that significant changes in GalTIII protein expression between miRNA transfected and non-transfected cells at 32°C are only observed on day 8 and 9, where their relative differences only vary by 13% and 18%, respectively. Minor increases in GalT protein expression might minimize the impact of miRNA overexpression on Fc-glycosylation of the secreted product.

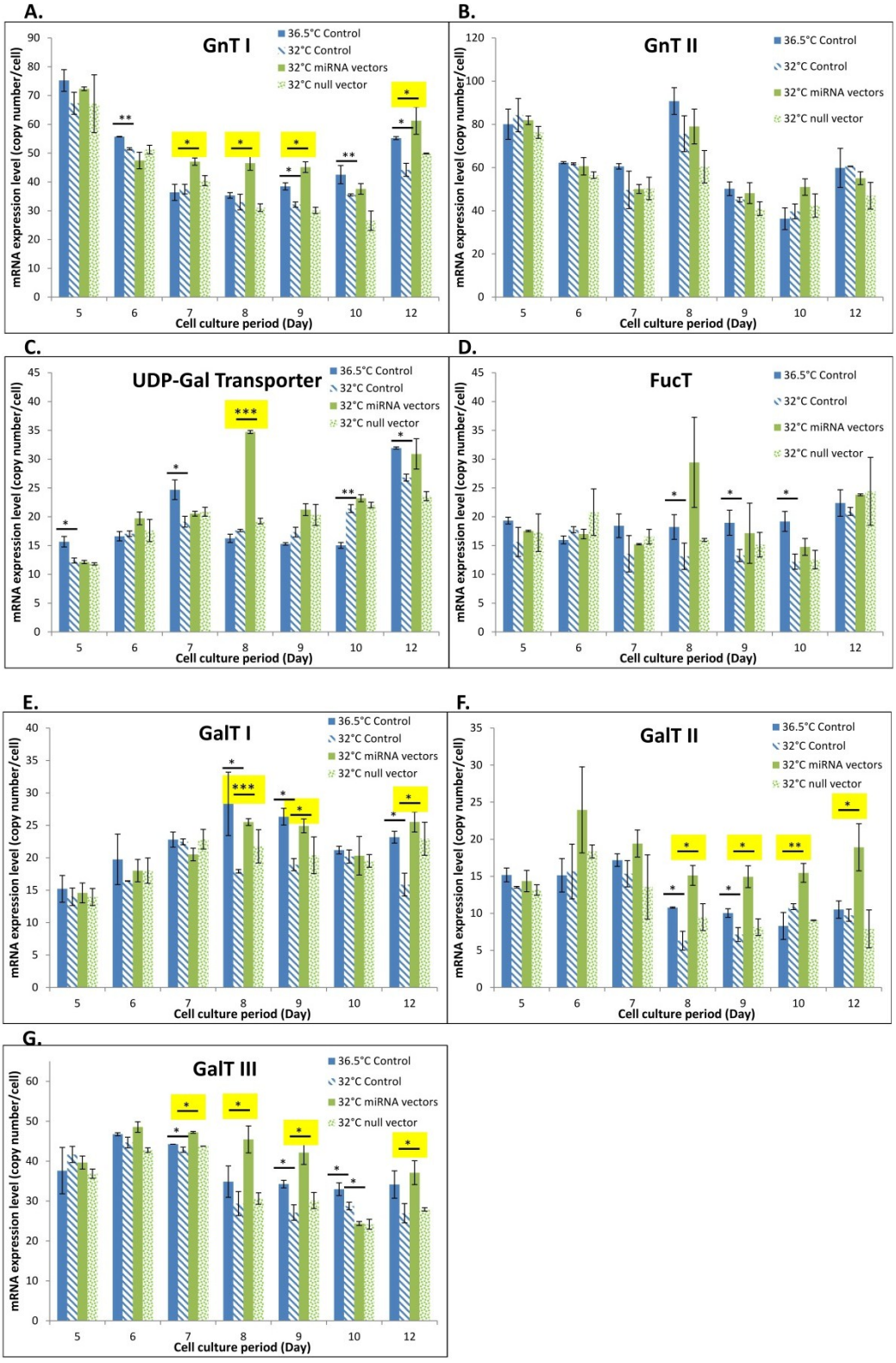

Figure 66. mRNA Expression profile of the enzymes involved in N-linked glycosylation under 4 conditions. Transcript levels of (A). GnT I, (B). GnT II, (C). UDP-Gal transporter, (D). FucT, (E). GalT I, (F). GalT II and (G). GalT III. Results were average measurements at 36.5°C (n=2) and 32°C TS (n=2) in control cells, miRNA and null-vector transfectants. The error bars represent the standard deviation of the samples. TS: Temperature shift. Statistical significance was calculated using a Student's t-test and was represented by: *$p \leq 0.05$(*), $p \leq 0.01$(**) and $p \leq 0.001$(***)*.TS: Temperature shift.

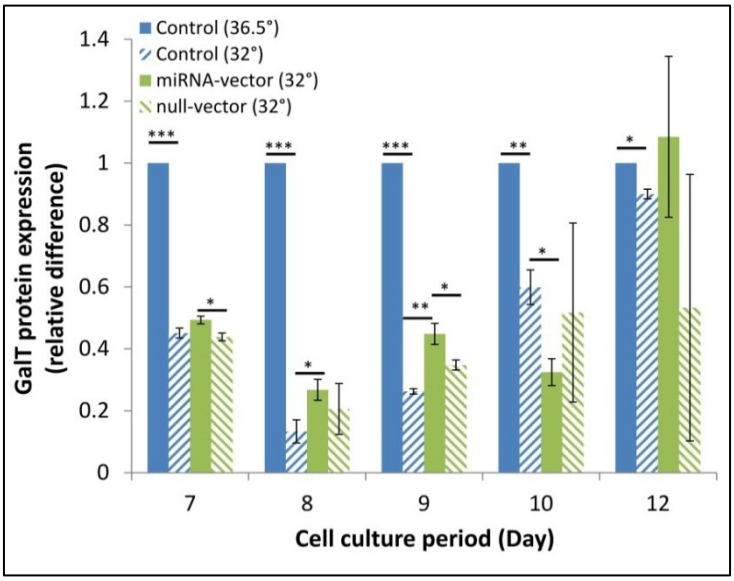

Figure 67. The relative difference in galactosyltransferase III (β-GalTIII) protein expression under all conditions examined. Results were average measurements at 36.5°C (n=2) and 32°C TS (n=2) in control cells, miRNA and null-vector transfectants. The error bars represent the standard deviation of the samples. TS: Temperature shift. Statistical significance was calculated using a Student's t-test and was represented by: *p≤0.05(*), p≤0.01(**) and p≤0.001(***)*.TS: Temperature shift.

8.2.5. The impact of overexpressing miRNAs on mAb Fc-glycosylation

Despite higher mRNA expression of galactosyltransferases and increased consumption of UDP-Gal in miRNA transfectants, only negligible changes of mAb Fc-galactosylation were observed. Figures 68 A – F show profiles of six glycoforms, including Man5, G0, G0F, G1F, G2 and G2F. Firstly, no significant changes are observed in the amount of G0 species between miRNA-transfected and control cells at 32°C (Figures 68 A & B). In addition, fractions of Man5 are higher in cells undergoing mild hypothermia than those that are cultured at 36.5°C, which correlates well with the study on mild hypothermic conditions in Chapter 4. When comparing glycan patterns achieved in mAb generated in miRNA transfected and control cells under mild hypothermic conditions, the proportions of G0F glycoforms are reduced by approximately 2% to 3% on day 8, 10 and 11 (Figure 68 C). On the other hand, galactose-bearing species G1F, G2 and G2F, their glycan fractions increased upon the miRNA transfection, but only by minimal fractions of roughly 3% increase. There is some confidence in our results of the miRNA experiment that the amount of non-galactosylated mAb, when compared to mAb of control cells at 32°C, is lower (Figure 69 C). However when compared to control at 36.5°C, the rate of mAb galactosylation still remains lower, improvement in galactosylation is indeed very small, and we fail to attain similar rate of mAb galactosylation as of the control cells at 36.5°C, and the amount of non-galactosylated species still remains higher under

miRNA-treated condition (Figure 69 B & D). One hypothesis is generated according to our analyses, that despite observing comparable levels of G0F in our secreted mAb between control 36.5°C and miRNA treated conditions (Figure 68 C), it appears that the drop on G0F level is not entirely attributed by higher galactosylation but by higher level of Man5 species that are not being further processed (Figure 69 E). This questions our current experimental strategy and suggests the manipulation of GnTs.

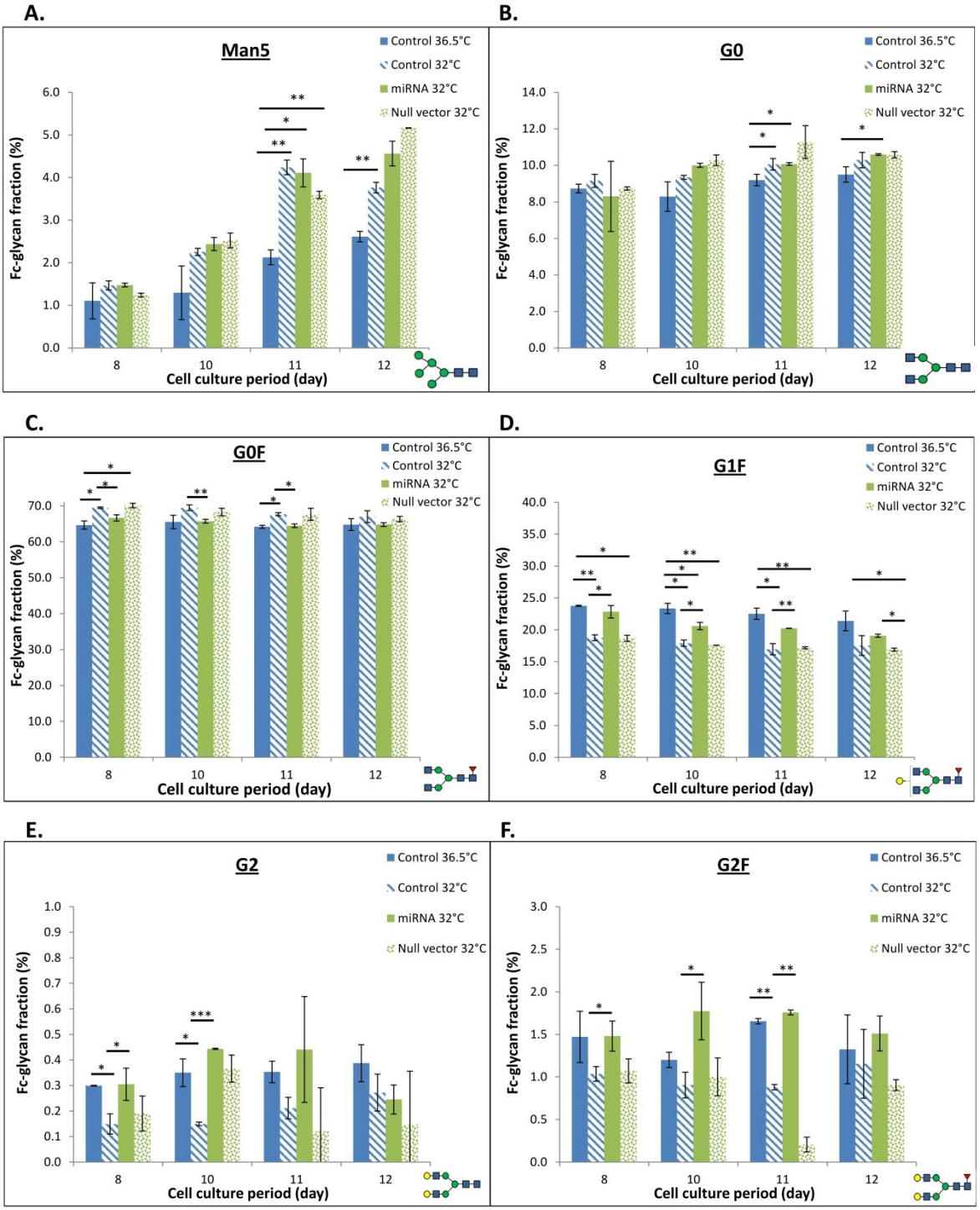

Figure 68. Glycan profile of the secreted IgG under four conditions examined. Fractions of 6 glycan structures: (A). Man5, (B). G0, (C). G0F, (D). G1F, (E). G2 and (F). G2F on the secreted IgG products were determined under each

condition on day 8, 10, 11 and 12 along the 12-day cell culture period. Results were average measurements at 36.5°C (n=2) and 32°C TS (n=2) in control cells, miRNA and null-vector transfectants. The error bars represent the standard deviation of the samples. TS: Temperature shift. Statistical significance was calculated using a Student's t-test and was represented by: *p≤0.05(*), p≤0.01(**) and p≤0.001(***)*.TS: Temperature shift.

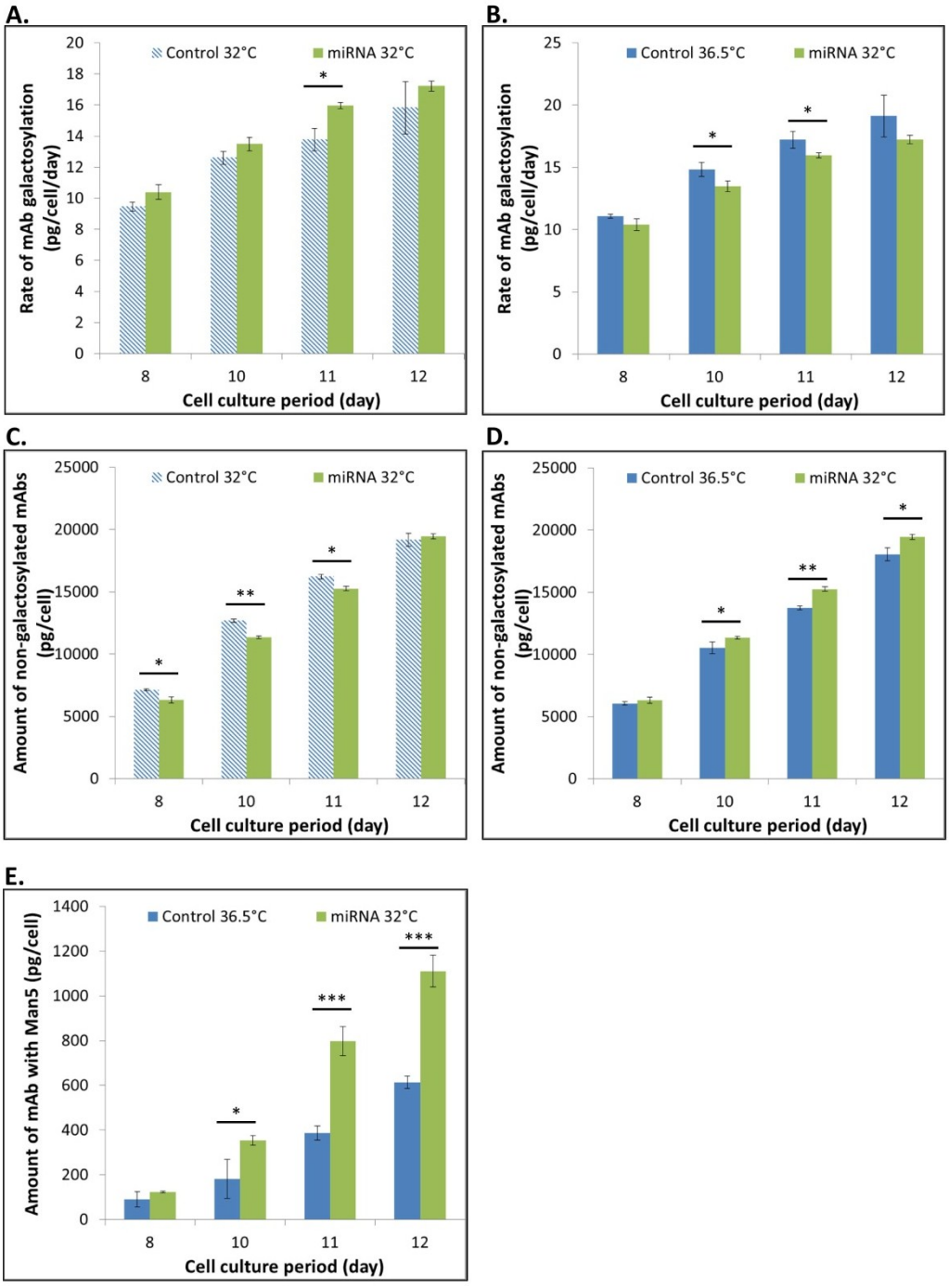

Figure 69. Calculated rate of mAb galactosylation. Comparison between (A). miRNA transfected cells and control cells at 32°C; or (B). between miRNA transfected cells under mild hypothermic temperature and control cells cultured at 36.5°C. Amount of mAb that are not galactosylated. Comparison between (C). Control vs. miRNA transfection at 32°C; or (D). Control at 36.5°C vs. miRNA transfection at 32°C. (E). Quantity of mAb bearing Man5 structure between Control cells 36.5°C and miRNA transfection at 32°C. Results were average measurements at

36.5°C (n=2) and 32°C TS (n=2) in control cells, miRNA and null-vector transfectants. The error bars represent the standard deviation of the samples. TS: Temperature shift. Statistical significance was calculated using a Student's t-test and was represented by: *p≤0.05(*), p≤0.01(**) and p≤0.001(***)*.TS: Temperature shift.

To further clarify if the failure in increasing Fc-galactosylation in the miRNA experiment is related to the amount of miRNAs transfected, we increased the concentration of the each transfected miRNA from 5 μM to 10, 25 and 50 μM. Table 30 shows the Fc-galactosylation index of mAb under different concentrations of miRNAs examined. Our results show that increase in the concentration of transfected miRNAs (above 5 μM) did not provide further significant increase in Fc-galactosylation in the mAb product. Their galactosylation levels remain 3% – 4% higher than control condition at 32°C.

Table 30. Calculated Fc-galactosylation index in conditions with increased concentrations of miRNA.

	Fc-galactosylation index				
	Control (32°C)	5 μM miRNA (32°C)	10 μM miRNA (32°C)	25 μM miRNA (32°C)	50 μM miRNA (32°C)
Day 10	0.21	0.24 *	0.24 *	0.24 *	0.23 *
Day 12	0.21	0.23 *	0.24 *	0.23 *	0.22
Day 14	0.18	0.21 *	0.22 *	0.21 *	0.20

* Statistical significance of $p \leq 0.05$, when calculated using a Student's t-test. Comparison was drawn between each miRNA-transfected species and non-transfected control species.

8.3. Discussion

This proof-of-concept study attempts to increase the expression of galactosyltransferases through manipulating endogenous amounts of miRNAs that are related to GalT enzyme expression. Despite not achieving huge success in elevating the amount of protein galactosylation in the secreted products, overexpressing three miRNAs that impose effects on CHO cell growth, cell metabolism and product generation.

Increase in cell growth in miRNA transfected cells was one of the first changes that we experimentally observed. This also served as an indication of changes in CHO cell metabolism. The variation observed in cell growth was most likely independent from the increase in culture osmolarity induced by NaCl used during transfection, since CHO cell growth was not observed to be uplifted in null-vector transfected species in which the same amount of NaCl was added to the culture. Increase in cell growth was therefore a consequence of the overexpression of the miRNAs cgr-miR-500, cgr-

miR-501-5p and cgr-miR-181d bundle. One can speculate that this combination of miRNAs is not restricted to a single target and it might have encouraged the translation of host cell proteins that promoted cell growth, such as the expression of anti-apoptotic proteins or other chaperone proteins, but host cell proteomic analysis is needed to support this hypothesis.

On the other hand, metabolic changes that were imposed by the transfection of this miRNA bundle occurred partially to maintain the increased viable cell growth, as well as to increase the specific productivity of the recombinant product. Not only did the higher rates of glucose and lactate uptake in miRNA transfected CHO cells generate more energy to sustain cell growth and cellular activities, increased carbon pool within a cell could encourage DNA and RNA syntheses that were advantageous in recombinant mAb production. In addition, a higher amount of amino acids were consumed and catabolized into pyruvate or other TCA cycle intermediates in order to fuel and to maintain the efficiency of the TCA cycle. Moreover, new amino acids generated were also utilized in host cell and recombinant protein synthesis. Therefore, increased rates of consumption of various amino acids definitely imposed a positive effect in protein production. Despite higher uptake rates of glucose, lactate and amino acids, NSD synthesis in miRNA transfectants remained comparable to that of control cells at 32°C, where only 5% increase in carbon fluxes towards NSD synthesis was suggested by the FBA study. This further confirmed that most nutrients were utilized towards cell growth and energy production.

Despite the little success in rescuing mAb terminal galactosylation through overexpressing of miRNAs that regulate β-1,4galactosyltransferase expression, our results demonstrated uplifting of the transfected species in GalT expression at transcriptional level, and at translational level to a certain extent. There are three possible hypotheses behind these changes. Firstly, the natural gene repression capability of miRNA could have been inhibited and encouraged translational activation by the induction of mild hypothermia, in which cells were most likely to be arrested at G_0/G_1 stages of cell cycle (Vasudevan et al. 2007). Moreover, the complementary sequences between the double stranded miRNA and the promoter region of the targeted GalT could have led to RNA activation, which increased gene induction of the target gene (Place et al. 2008). The fact that terminal galactosylation was only improved by a very tiny fraction (which was even smaller than changes observed within cell line variations might be owing to the very small differences detected in GalTIII protein expression. In addition, failure to further increase Fc-galactosylation when miRNA concentrations were raised to a maximum level of 50 μM suggests either the amount of miRNA expressed is limited by the low transfection efficiency of the non-optimised transient transfection protocol, or the partial cell-cycle arrest was not sufficient enough to completely avert the mechanism of miRNA overexpression from

translation inhibition to up-regulation. With higher levels of non-galactosylated mAbs, particularly in the amount of Man5 structures, and the fact that rate of mAb galactosylation still remains lower than that of the control at 36.5°C, all together suggest that in addition to raising the expression level of GalT, we might want to extend our focus further and also increase the expression of GnT enzymes, so as to ensure sufficient amount of bi-antennary glycan profiles for GalT enzymes to work on in the later stage of N-linked glycan processing. Of course, future investigation is necessary to test these hypotheses. Despite the lack of evidence, potential co-localisation of GalT with other glycosyltransferase may affect the potency to overexpress GalT, if overexpression of all co-localised enzymes would be required for effective result.

8.4. Concluding remarks

In this study, we demonstrated that the overexpression of the miRNAs cgr-miR-500, cgr-miR-501-5p and cgr-miR-181d bundle imposed changes to cell growth, cell metabolism, GalTIII expression and mAb Fc-glycosylation by a very small level. Upon the transfection of the miRNA bundle, cells remodeled their carbon and nitrogen metabolism to sustain cell growth and increase protein production. Despite the common nature of miRNA in gene translation repression, our study showed that mRNA and protein expression of target gene could be improved through overexpressing miRNAs that had high complementary to the target gene promoter. Hence, our study here confirm that the concept of increasing GalT expression through miRNA manipulation under mild hypothermia is possible, but the transfection method will have to be optimized in order to increase the protein expression level of the target gene and to elevate product galactosylation under mild hypothermia.

Chapter 9
Concluding Remarks and future studies

9.1. Summary of results

This thesis has examined the impact of two chosen bioprocess conditions on recombinant mAb productivity and the resulting Fc N-linked glycosylation, namely mild hypothermia and transient gene expression. It was done through detailed examination of changes in cell metabolism as well as intracellular protein processing machinery in each condition by both experimental and computational approaches.

The thesis first presented the current situation in biopharmaceutical production. This was followed by a thorough review of relevant existing literature that discussed about the relationship between bioprocess conditions and mAb production, and to a lesser extent, mAb Fc-glycosylation. From the background research, limitations in the current drug manufacturing processes were identified and the employment of the Quality by Design paradigm was discussed as necessary to improve the efficiency of the bioproduction process. Within this, the mild hypothermic culture temperature and transient gene expression system became the main focus in this research work. A brief review on potential experimental and computational analytic approaches that could be used to examine CHO cell metabolism and characterise the N-linked glycan profiles of the secreted mAb molecules were also discussed in the thesis.

Following that, we commenced our research study with examining the impact of mild hypothermia on the Fc-glycosylation of mAb molecules that were stably expressed in CHO cells with respect to both experimental findings and modelling approaches. Our results showed that a 25%

increase in mAb productivity was achieved in mild hypothermic conditions, but significant limitation in Fc-terminal galactosylation was observed in the glycan profile of mAb produced at 32°C. Contributing factors for changes observed in mAb Fc-galactosylation were identified through flux balance analysis and computational studies. Results from the FBA demonstrated changes in cellular carbon distribution upon the introduction of mild hypothermic culture temperature, where a reduced flux of carbon was channelled towards NSD synthesis and mAb glycosylation to compensate for the increase in energy and carbon consumption towards mAb synthesis for a higher q_{mAb}. The modular mathematical model estimated reduced rates of NSD production and galactosyltransferase (GalT) expression in CHO cells during mild hypothermia. Both findings have successfully established the impact of mild hypothermia on mAb Fc-glycosylation for the cell line under study. In addition, the modular mathematical model represented the time-course data well in all aspects, including cell growth, cell metabolism, mAb synthesis, as well as reproducing the N-linked glycosylation profiles of mAb produced under mild hypothermia. Model estimation of reduced GalT concentration expression was then confirmed by the experimental measurements of GalT expression levels, thus show the capability of our model in representing the biological system. However, parameter re-estimation will be necessary when the model is performed on a different cell line.

On the other hand, the experimental and model comparison drawn between SGE and TGE processes with respect to their cellular behaviour, recombinant protein synthesis and the Fc-glycan pattern of the secreted mAb showed evident variations in all aspects mentioned above between the two expression systems. The expression of mAb as a foreign protein in TGE placed a burden on protein glycosylation. The combination of lowered carbon flux towards NSD production observed in the FBS study, and the less efficient NSD synthetic network in terms of reduced carbon flux and activities of enzymes in the NSD synthetic pathway, as well as the limited expression of glycosyltransferases suggested by the TGE mathematical model, served as contributing factors for changes in mAb Fc-glycan pattern observed between the two expression systems. By adapting the modular model entity of SGE to the particularities of the TGE system, the TGE model was capable of describing experimental results well in all aspect under all conditions examined in TGE, with discrepancies of 5% or less between experimentally measured and estimated N-linked glycan profiles of mAb molecules. Moreover, enzymatic properties estimated by the TGE model were in good correlation with our experimentally quantified data.

Based on the experimental results and model outputs in this work, expression of galactosyltransferase was suggested to be the key contributing factor to changes in glycan profiles under the mild hypothermic conditions in this cell line. We attempted to manipulate the expression of

the GalT enzyme by exploiting the level of a group of GalT-related miRNAs. Despite showing little success in increasing the level of terminal galactosylation in the secreted mAb products in this proof-of-concept study, results showed a slight increase in GalT expression, which might indicate the potential of employing this strategy in enzyme manipulation if the method is to be optimised, or when it is incorporated with the expression of other glycosyltransferase, e.g. GnTs.

9.2. Main conclusions

The followings are conclusions that can be drawn from the above findings:

1. As shown through literature, following the Quality by Design paradigm is certainly a way to improve the overall yield and the quality of the recombinant protein. To do so, it is of paramount importance to understand fully the influence of each bioprocess condition on host cell metabolic pathways and relevant cellular activities that would pose an impact on product production.

2. Experimentation on its own is useful in identifying variations among different process conditions, but it can reveal more information regarding intracellular behaviour and activities when experimental data is coupled with computational tools, namely flux balance analysis and quantitative mechanistic models. While FBA studies allows the exploitation of intracellular carbon and nitrogen distributions under each condition examined, the mathematical model is particularly important in providing information on changes in cellular activities, which aids our understanding on fundamental mechanisms that impact mAb glycosylation. Moreover, the modelling approach will allow the implementation of quality control throughout the fermentation process if the model is validated, which satisfies the Quality by Design paradigm.

3. Galactosyltranferase (GalT) expression was identified in our work by both experimentation and mathematical model as one of the main contributing factors for reduced terminal galactosylation in mAb products under mild hypothermia in this cell line, regardless of the expression system. However, our work also indicated that GnTs can also be a high potential target for glycol-engineering, given that their transcript expressions are quite different even within the TGE, or between SGE and TGE systems.

4. The availability of nucleotide sugar donors especially UDP-Gal species was suggested in this work to be critical in mAb Fc-terminal galactosylation in the TGE, but not in the SGE system.

5. In this study, heavy and light chain mRNA transcription was demonstrated to be the bottleneck in TGE during mAb protein synthesis.

6. Adapted and modified from models developed by Kontoravdi et al. (2005) and Jimenez del Val (2013), modular mathematical models presented in this work mechanistically relates much information on the external variation and nutrient availability during the process of cell culture to mAb synthesis and N-linked glycosylation, through cell metabolism, this includes amino acid, nucleotide and NSD metabolism.

7. Modular mathematical models developed in this work have high capability in representing biological processes under mild hypothermia or under different gene expression scenarios, with respect to cellular behaviour, mAb synthesis, NSD metabolism and N-linked Fc glycosylation. The developed models also possess high fidelity in estimating unknown parameters within the system under conditions mentioned above. When fully validated, these models will be of great help in predicting cell behaviour and mAb N-linked glycan patterns of a given species and generating estimation on possible ranges of process inputs that will be necessary for optimal mAb production.

8. The proof-of-concept study conducted in this work shows some potential of indirect manipulation of β-1,4 galactosyltransferase expression through control of endogenous levels of GalT related miRNAs. However, a more optimised transfection protocol is required in order to improve its efficiency towards N-linked glycan editing. And potential co-overexpression with GnT enzymes will ensure enough bi-antennary glycan substrates for GalT to work on.

9.3. Main contributions

1. Instead of looking at the impact of different bioprocess conditions on Fc-glycosylation through “black-box” or “trial-and-error” approaches, in this thesis we employed a combination of experimentation, flux balance analysis and mathematical modelling to systematically identify contributing factors of each condition examined on the host cell dynamics, which subsequently affect the process of Fc-glycosylation. This approach identifies

major variations within the metabolic pathway in each bioprocess condition which aids future process optimisation.

2. More importantly, the mathematical model developed in this study allows the identification of bottlenecks within cellular processes for a specific quality attribute of the secreted product, by estimating a range of model parameters that satisfy specific conditions. By incorporating measures specific for increasing the capacity of the identified bottlenecks, process optimisation and improvements in product quality can therefore be achieved. This approaches aims to satisfy both the QbD paradigm proposed by the FDA, as well as providing the industry with a more efficient and effective way in running their manufacturing processes.

3. By extending existing models to include and link external factors (e.g. changes in nutrient availability) during the process of cell culture to mAb synthesis and N-linked glycosylation for CHO cells through cellular metabolic pathway, our model encourages the possibility of *in silico* experiments prior to any laboratorial experiments, where the model aims to generate an estimated range of product quality based on model inputs of the experiment.

4. With promising results generated from the model in this thesis, there is a high potential to refine our model and apply it onto industrially relevant projects, which can be mAb-based processes or extend our model application to other protein production lines.

9.4. Suggestions for future studies

Based on the results and conclusions of work conducted in this thesis, the following are suggestions of future work that can be carried to improve current research:

9.4.1. Consideration of other cell lines

Examination carried out in the thesis regarding the impact of mild hypothermia on mAb glycosylation in SGE were based on one single high producing cell line, conclusions drawn in this study may only be relevant to this particular cell clone. With research suggesting changes in cell metabolism among high, medium and low producing cell lines (Chusainow et al. 2009), it is therefore worthwhile to investigate if the impact of mild hypothermia on cell metabolism and mAb

glycosylation that we observed on the high producer will vary on the medium and the low producers. Moreover, comparative results between the SGE and the TGE systems might change if compared to a different stable cell line. Moreover, results that we observed in this study could be product specific. In addition to examining different cell lines, it will be worthwhile to also investigate in cell line expressing a different product.

9.4.2. Examination with optimised transfection protocols

Despite revealing significant differences between SGE and TGE systems with a non-optimised transfection protocol, one could argue that a set of results could be achieved if transfection method used was optimised. Analysing mAb Fc glycan patterns from transient transfectants generated from different transfection protocols (e.g. different transfection reagents, transfection density, gene to reagent ratio, electroporation) will widen our knowledge on mAb glycosylation in TGE system; it also allows generating a clearer vision of how different approaches within the TGE system contribute to changes in their cell metabolism and mAb glycosylation. By comparing different transient transfection protocols, we can examine the relationship among transfection efficiency, q_P and the Fc-glycoforms on the product.

9.4.3. Importance of vector construction

In addition, the actual vector construction is also a crucial element that places a big impact especially on the target gene expression. For instance, if the vector expresses a viral element of Epstein-Barr virus (EBV) nuclear antigen-1 (EBNA-1), it is a vector that controls gene replication and transcription activity. In the case, changes in host cell growth induced by different bioprocess conditions will therefore affect the expression of recombinant genes that are expressed in the same vector as EBNA-1 element, thus affecting q_P. As a result, it is important to take into account elements involved in the vectors used in this thesis.

9.4.4. Strategies to improve protein galactosylation

Results in our work suggested two ways in which product galactosylation can be improved: by increasing expression levels of GalTs, or by tailoring culture feeds by including specific NSD

precursors for UDP-Gal synthesis. Firstly, GalT expression levels can be increased by traditional overexpression of the enzyme through cell line engineering (Pablo Umaña and Jean-Mairet 2012).

Manipulation of GalT expression through miRNA exploitation was attempted in this work, but results were not promising even when higher miRNA concentrations were attempted. Instead of manipulating miRNA levels in a transient manner in which its transfection efficiency is limited, one can try overexpressing these miRNAs stably and have it controlled by a temperature sensitive promoter such as CHO S100a6 promoter in mild hypothermic conditions to control the timing of overexpression (Thaisuchat et al. 2011).

In addition to focusing on GalT overexpression, in the case of IgG one has to remember that GalT enzyme cannot perform galactose addition without sufficient quantity of bi-antennary glycan structures as substrates. Co-expression of both GnTs and GalT will be a more ideal experimental strategy to improve mAb galactosylation.

In addition to overexpressing GalT enzyme, one can also couple this strategy with tailored feeding of uridine, magnesium and galactose to increase the intracellular amount of UDP-Gal level as suggested in Gramer et al. (2011). As our model outputs suggested reduced enzymatic activities of enzymes related to UDP-Gal synthesis during mild hypothermia and in TGE experiments, one can try to overexpress these enzymes during cell culture (Fridovich-Keil and Jinks-Robertson 1993; Heidenreich 1995).

9.4.5. Improvement in modular mathematical models

The current modular mathematical model certainly has space for improvement. Firstly, the current model (SGE or TGE) describes each module in mild hypothermic condition with a separate set of parameter values. The model is applicable to mild hypothermic temperature at 32°C, but a different set of parameter values will have to be used to represent conditions at a different temperature. The fidelity of the model can be improved and to truly represent the impact on culture temperature if mass balances within the model are constructed as a function of temperature rather than relying on distinctive sets of parameter values. To do so, experimental data at different temperatures will be necessary to train the model with all sets of experimental data to estimate a common set of parameter value.

In addition, the current nucleotide and NSD part of the model was constructed based on a simplified NSD synthetic network, by merging all sequential reactions along one given NSD branch into a single reaction. Other intermediate reactions along a NSD branch might impose regulatory effects and therefore if possible, the model should be expanded to include relevant species.

Data analysis using FBA and mathematical approaches in this work identified contributing factors of bioprocess conditions on mAb glycosylation, but they were not able to distinguish which of the two is dominant, lowered GalT enzymatic activity or reduced NSD synthesis. It will be of more use if the flux distribution can be implemented into the current model to identify the dominating factor. In addition, radioactive labelling experiments can be carried out to validate results obtained from the FBA study. This way instead of constraining the model through experimental data, data of real-time intracellular metabolites can be used to increase the fidelity of the model.

9.4.6. Model validation

Not all parameter values estimated our models in this work were validated. Since the comparisons drawn between different bioprocess conditions are based on parameter estimation, model validation with a separate set of experimental data is therefore necessary to test the model fidelity and to improve the confidence of parameter values estimated by our models. For instance, we can validate the model by carrying out a separate set of experiment using a different mAb product with or without mild hypothermia. If the model is valid, it should be able to capture any change in consumption rate of nutrients and metabolites in response to the change of environment (in our case mild hypothermia and gene expression system), as well as relating this change to product yield and Fc-glycosylation.

9.5. Closing remarks

Our work in this thesis managed to bring us one step closer to better but cheaper production of drugs, through understanding the effect of each bioprocess condition on the fundamental cellular activities and the relationship among each individual cellular network. By identifying bottlenecks within cellular processes, more efficient processes with better quality control on the end products can be achieved at reduced manufacturing costs, which will definitely be beneficial to all sectors including the manufactures, the drug control authorities as well as the patients.

List of publications

1. Sou SN, Sellick C, Lee K, Mason A, Kyriakopoulos S, Polizzi KM, Kontoravdi C. (2015). Understanding the impact of different bioprocess conditions on monoclonal antibody glycosylation in CHO cell culture through experimental and computational analyses. Paper presented at 2015 European Society for Animal Cell Technology (ESACT) meeting. Barcelona, Spain. *BMC Proceedings*. Submitted.

2. Sou SN, Sellick C, Lee K, Mason A, Kyriakopoulos S, Polizzi KM, Kontoravdi C. (2015). How does mild hypothermia affect monoclonal antibody glycosylation?. *Biotechnol. Bioeng.,* 112: 1165–1176.

3. Sou SN, Sellick C, Lee K, Mason A, Polizzi KM, Kontoravdi C. (2014). Differences in Recombinant Monoclonal Antibody Glycosylation between Stable and Transient Gene Expression Systems. Paper presented at Food, Pharmaceutical & Bioengineering Division – Cell Culture I: Process and Media Design (52d), 2014 American Institute of Chemical Engineers Annual Meeting. Atlanta, Georgia, U.S.A. *AIChE Conference Proceedings*.

4. Sou SN, Sellick C, Lee K, Mason A, Kyriakopoulos S, Polizzi KM, Kontoravdi C. (2014). Understanding the Effect of Mild Hypothermia on Monoclonal Antibody Glycosylation through Flux Balance Analysis and Mechanistic Modelling. Paper presented at Food, Pharmaceutical & Bioengineering Division – Cell Culture III: Metabolic Flux Analysis and Modelling (173f), 2014 American Institute of Chemical Engineers Annual Meeting. Atlanta, Georgia, U.S.A. *AIChE Conference Proceedings*.

5. Sou SN, Sellick C, Lee K, Mason A, Polizzi KM, Kontoravdi C. (2013). Experimental and Computational Analysis of Chinese Hamster Ovary Stable Transfectants Grown in Fed-Batch Culture. Paper presented at Food, Pharmaceutical & Bioengineering Division – Cell Culture I: Process and Media Design (597a), 2013 American Institute of Chemical Engineers Annual Meeting. San Francisco, CA, U.S.A. *AIChE Conference Proceedings*.

6. Sou SN, Kontoravdi C, Polizzi KM. (2013). Evaluation of transfection methods for transient gene expression in Chinese hamster ovary cells. *Adv Bios Biotech.* 4(12): 1013 – 1019.

7. Jimenez del Val I, Jedrzejewski PM, Exley K, Sou SN, Kyriakopoulos S, Polizzi KM, Kontoravdi C (2012). Application of Quality by Design Paradigm to the Manufacture of Protein Therapeutics, Glycosylation, Dr. Stefana Petrescu (Ed.), ISBN: 978-953-51-0771-2, InTech, DOI: 10.5772/50261.

References

Abbott BJ, Clamen A. 1973. The relationship of substrate, growth rate, and maintenance coefficient to single cell protein production. Biotechnol Bioeng 15(1):117-27.

Agrawal P, Kurcon T, Pilobello KT, Rakus JF, Koppolu S, Liu Z, Batista BS, Eng WS, Hsu K-L, Liang Y and others. 2014. Mapping posttranscriptional regulation of the human glycome uncovers microRNA defining the glycocode. Proceedings of the National Academy of Sciences 111(11):4338-4343.

Ahn WS, Antoniewicz MR. 2012. Towards dynamic metabolic flux analysis in CHO cell cultures. Biotechnology Journal 7(1):61-74.

Ahn WS, Jeon JJ, Jeong YR, Lee SJ, Yoon SK. 2008. Effect of culture temperature on erythropoietin production and glycosylation in a perfusion culture of recombinant CHO cells. Biotechnol Bioeng 101(6):1234-44.

Allen AC, Harper SJ, Feehally J. 1995. Galactosylation of N- and O-linked carbohydrate moieties of IgA1 and IgG in IgA nephropathy. Clinical and Experimental Immunology 100(3):470-474.

Antoniewicz MR. 2015. Methods and advances in metabolic flux analysis: a mini-review. J Ind Microbiol Biotechnol 42(3):317-25.

Apweiler R, Hermjakob H, Sharon N. 1999. On the frequency of protein glycosylation, as deduced from analysis of the SWISS-PROT database. Biochim Biophys Acta 1473(1):4-8.

Avezov E, Frenkel Z, Ehrlich M, Herscovics A, Lederkremer GZ. 2008. Endoplasmic Reticulum (ER) Mannosidase I Is Compartmentalized and Required for N-Glycan Trimming to Man(5–6)GlcNAc(2) in Glycoprotein ER-associated Degradation. Molecular Biology of the Cell 19(1):216-225.

Backliwal G, Hildinger M, Chenuet S, Dejesus M, Wurm FM. 2008a. Coexpression of acidic fibroblast growth factor enhances specific productivity and antibody titers in transiently transfected HEK293 cells. N Biotechnol 25(2-3):162-6.

Backliwal G, Hildinger M, Chenuet S, Wulhfard S, De Jesus M, Wurm FM. 2008b. Rational vector design and multi-pathway modulation of HEK 293E cells yield recombinant antibody titers exceeding 1 g/l by transient transfection under serum-free conditions. Nucleic Acids Research 36(15).

Backliwal G, Hildinger M, Kuettel I, Delegrange F, Hacker DL, Wurm FM. 2008c. Valproic acid: a viable alternative to sodium butyrate for enhancing protein expression in mammalian cell cultures. Biotechnol Bioeng 101(1):182-9.

Bacon CL, O'Driscoll E, Regan CM. 1997. Valproic acid suppresses G1 phase-dependent sialylation of a 65kDa glycoprotein in the C6 glioma cell cycle. Int J Dev Neurosci 15(6):777-84.

Baik JY, Lee MS, An SR, Yoon SK, Joo EJ, Kim YH, Park HW, Lee GM. 2006. Initial transcriptome and proteome analyses of low culture temperature-induced expression in CHO cells producing erythropoietin. Biotechnol Bioeng 93(2):361-71.

Baldi L, Hacker DL, Adam M, Wurm FM. 2007. Recombinant protein production by large-scale transient gene expression in mammalian cells: state of the art and future perspectives. Biotechnol Lett 29(5):677-84.

Banfield DK. 2011. Mechanisms of protein retention in the Golgi. Cold Spring Harb Perspect Biol 3(8):a005264.

Barb AW, Prestegard JH. 2011. NMR analysis demonstrates immunoglobulin G N-glycans are accessible and dynamic. Nat Chem Biol 7(3):147-53.

Barron N, Kumar N, Sanchez N, Doolan P, Clarke C, Meleady P, O'Sullivan F, Clynes M. 2011. Engineering CHO cell growth and recombinant protein productivity by overexpression of miR-7. J Biotechnol 151(2):204-11.

Bartel DP. 2004. MicroRNAs: genomics, biogenesis, mechanism, and function. Cell 116(2):281-97.

Bebbington CR, Renner G, Thomson S, King D, Abrams D, Yarranton GT. 1992. High-level expression of a recombinant antibody from myeloma cells using a glutamine synthetase gene as an amplifiable selectable marker. Biotechnology (N Y) 10(2):169-75.

Becerra S, Berrios J, Osses N, Altamirano C. 2012. Exploring the effect of mild hypothermia on CHO cell productivity. Biochemical Engineering Journal 60:1-8.

Becerra S, Vergara M, González R, Osses N, Altamirano C. 2011. Condition of mild hypothermia does not promote an increase in specific productivity of recombinant protein at high specific growth rate. Current Opinion in Biotechnology 22, Supplement 1(0):S35-S36.

Berg JM, Tymoczko JL, Stryer L. 2006. Biochemistry: International Edition. New York: W.H. Freeman and Company.

Bergfeld AK, Pearce OM, Diaz SL, Lawrence R, Vocadlo DJ, Choudhury B, Esko JD, Varki A. 2012. Metabolism of vertebrate amino sugars with N-glycolyl groups: incorporation of N-glycolylhexosamines into mammalian glycans by feeding N-glycolylgalactosamine. J Biol Chem 287(34):28898-916.

Bibila T, Flickinger MC. 1991. A structured model for monoclonal antibody synthesis in exponentially growing and stationary phase hybridoma cells. Biotechnol Bioeng 37(3):210-26.

Bollati-Fogolin M, Forno G, Nimtz M, Conradt HS, Etcheverrigaray M, Kratje R. 2005. Temperature reduction in cultures of hGM-CSF-expressing CHO cells: effect on productivity and product quality. Biotechnol Prog 21(1):17-21.

Boulianne GL, Hozumi N, Shulman MJ. 1984. Production of functional chimaeric mouse/human antibody. Nature 312(5995):643-6.

Brezinsky SC, Chiang GG, Szilvasi A, Mohan S, Shapiro RI, MacLean A, Sisk W, Thill G. 2003. A simple method for enriching populations of transfected CHO cells for cells of higher specific productivity. J Immunol Methods 277(1-2):141-55.

Butler M. 2006. Optimisation of the cellular metabolism of glycosylation for recombinant proteins produced by Mammalian cell systems. Cytotechnology 50(1-3):57-76.

Cain K, Peters S, Hailu H, Sweeney B, Stephens P, Heads J, Sarkar K, Ventom A, Page C, Dickson A. 2013. A CHO cell line engineered to express XBP1 and ERO1-Lalpha has increased levels of transient protein expression. Biotechnol Prog 29(3):697-706.

Carinhas N, Duarte TM, Barreiro LC, Carrondo MJ, Alves PM, Teixeira AP. 2013. Metabolic signatures of GS-CHO cell clones associated with butyrate treatment and culture phase transition. Biotechnology and Bioengineering 110(12):3244-57.

Castilho A, Gattinger P, Grass J, Jez J, Pabst M, Altmann F, Gorfer M, Strasser R, Steinkellner H. 2011. N-glycosylation engineering of plants for the biosynthesis of glycoproteins with bisected and branched complex N-glycans. Glycobiology 21(6):813-23.

Chee Furng Wong D, Tin Kam Wong K, Tang Goh L, Kiat Heng C, Gek Sim Yap M. 2005. Impact of dynamic online fed-batch strategies on metabolism, productivity and N-glycosylation quality in CHO cell cultures. Biotechnol Bioeng 89(2):164-77.

Chen JF, Mandel EM, Thomson JM, Wu Q, Callis TE, Hammond SM, Conlon FL, Wang DZ. 2006. The role of microRNA-1 and microRNA-133 in skeletal muscle proliferation and differentiation. Nat Genet 38(2):228-33.

Chen X, Alonso AP, Allen DK, Reed JL, Shachar-Hill Y. 2011. Synergy between (13)C-metabolic flux analysis and flux balance analysis for understanding metabolic adaptation to anaerobiosis in E. coli. Metab Eng 13(1):38-48.

Cheng AM, Byrom MW, Shelton J, Ford LP. 2005. Antisense inhibition of human miRNAs and indications for an involvement of miRNA in cell growth and apoptosis. Nucleic Acids Res 33(4):1290-7.

Chotigeat W, Watanapokasin Y, Mahler S, Gray PP. 1994. Role of environmental conditions on the expression levels, glycoform pattern and levels of sialyltransferase for hFSH produced by recombinant CHO cells. Cytotechnology 15(1-3):217-21.

Chuppa S, Tsai YS, Yoon S, Shackleford S, Rozales C, Bhat R, Tsay G, Matanguihan C, Konstantinov K, Naveh D. 1997. Fermentor temperature as a tool for control of high-density perfusion cultures of mammalian cells. Biotechnol Bioeng 55(2):328-38.

Chusainow J, Yang YS, Yeo JH, Toh PC, Asvadi P, Wong NS, Yap MG. 2009. A study of monoclonal antibody-producing CHO cell lines: what makes a stable high producer? Biotechnol Bioeng 102(4):1182-96.

Clementi N, Mancini N, Solforosi L, Castelli M, Clementi M, Burioni R. 2012. Phage Display-based Strategies for Cloning and Optimization of Monoclonal Antibodies Directed against Human Pathogens. International Journal of Molecular Sciences 13(7):8273-8292.

Codamo J, Hou JJC, Hughes BS, Gray PP, Munro TP. 2011a. Efficient mAb production in CHO cells incorporating PEI-mediated transfection, mild hypothermia and the co-expression of XBP-1. Journal of Chemical Technology and Biotechnology 86(7):923-934.

Codamo J, Munro TP, Hughes BS, Song M, Gray PP. 2011b. Enhanced CHO Cell-Based Transient Gene Expression with the Epi-CHO Expression System. Molecular biotechnology 48(2):109-115.

Courtete J, Guehenneux F, ROPART A. 2012. Recombinant protein production system. Google Patents.

Croce CM, Calin GA. 2005. miRNAs, cancer, and stem cell division. Cell 122(1):6-7.

Daramola O, Stevenson J, Dean G, Hatton D, Pettman G, Holmes W, Field R. 2014. A high-yielding CHO transient system: coexpression of genes encoding EBNA-1 and GS enhances transient protein expression. Biotechnol Prog 30(1):132-41.

del Val IJ, Kontoravdi C, Nagy JM. 2010. Towards the implementation of quality by design to the production of therapeutic monoclonal antibodies with desired glycosylation patterns. Biotechnol Prog 26(6):1505-27.

del Val IJ, Kyriakopoulos S, Polizzi KM, Kontoravdi C. 2013. An optimized method for extraction and quantification of nucleotides and nucleotide sugars from mammalian cells. Anal Biochem 443(2):172-80.

Dietmair S, Hodson MP, Quek L-E, Timmins NE, Gray P, Nielsen LK. 2012. A Multi-Omics Analysis of Recombinant Protein Production in Hek293 Cells. PLoS ONE 7(8):e43394.

Dietmair S, Timmins NE, Gray PP, Nielsen LK, Kroemer JO. 2010. Towards quantitative metabolomics of mammalian cells: Development of a metabolite extraction protocol. Analytical Biochemistry 404(2):155-164.

Ecker DM, Jones SD, Levine HL. 2015. The therapeutic monoclonal antibody market. MAbs 7(1):9-14.

Ehrhardt C, Schmolke M, Matzke A, Knoblauch A, Will C, Wixler V, Ludwig S. 2006. Polyethylenimine, a cost-effective transfection reagent. Signal transduction 6:179 – 184.

Ellgaard L, Helenius A. 2003. Quality control in the endoplasmic reticulum. Nat Rev Mol Cell Biol 4(3):181-191.

EvaluatePharma. 2014. World preview 2014, Outlook to 2020. EvaluatePharma.

Fan Y, Del Val IJ, Müller C, Lund AM, Sen JW, Rasmussen SK, Kontoravdi C, Baycin-Hizal D, Betenbaugh MJ, Weilguny D and others. 2015. A multi-pronged investigation into the effect of glucose starvation and culture duration on fed-batch CHO cell culture. Biotechnology and Bioengineering:n/a-n/a.

Ferrara C, Grau S, Jager C, Sondermann P, Brunker P, Waldhauer I, Hennig M, Ruf A, Rufer AC, Stihle M and others. 2011. Unique carbohydrate-carbohydrate interactions are required for high affinity binding between FcgammaRIII and antibodies lacking core fucose. Proc Natl Acad Sci U S A 108(31):12669-74.

Filipowicz W. 2005. RNAi: the nuts and bolts of the RISC machine. Cell 122(1):17-20.

Fox SR, Patel UA, Yap MG, Wang DI. 2004. Maximizing interferon-gamma production by Chinese hamster ovary cells through temperature shift optimization: experimental and modeling. Biotechnol Bioeng 85(2):177-84.

Fox SR, Tan HK, Tan MC, Wong SC, Yap MG, Wang DI. 2005. A detailed understanding of the enhanced hypothermic productivity of interferon-gamma by Chinese-hamster ovary cells. Biotechnol Appl Biochem 41(Pt 3):255-64.

Fridovich-Keil JL, Jinks-Robertson S. 1993. A yeast expression system for human galactose-1-phosphate uridylyltransferase. Proceedings of the National Academy of Sciences of the United States of America 90(2):398-402.

Galbraith DJ, Tait AS, Racher AJ, Birch JR, James DC. 2006. Control of culture environment for improved polyethylenimine-mediated transient production of recombinant monoclonal antibodies by CHO cells. Biotechnology Progress 22(3):753-762.

Gelius-Dietrich G, Desouki AA, Fritzemeier CJ, Lercher MJ. 2013. sybil - Efficient constraint-based modelling in R. BMC Syst Biol 7(1):125.

Goetze AM, Liu YD, Zhang Z, Shah B, Lee E, Bondarenko PV, Flynn GC. 2011. High-mannose glycans on the Fc region of therapeutic IgG antibodies increase serum clearance in humans. Glycobiology 21(7):949-59.

Gouveia R, Kandzia S, Conradt HS, Costa J. 2010. Production and N-glycosylation of recombinant human cell adhesion molecule L1 from insect cells using the stable expression system. Effect of dimethyl sulfoxide. J Biotechnol 145(2):130-8.

Grainger RK, James DC. 2013. CHO cell line specific prediction and control of recombinant monoclonal antibody N-glycosylation. Biotechnol Bioeng 110(11):2970-83.

Gramer MJ, Eckblad JJ, Donahue R, Brown J, Shultz C, Vickerman K, Priem P, van den Bremer ET, Gerritsen J, van Berkel PH. 2011. Modulation of antibody galactosylation through feeding of uridine, manganese chloride, and galactose. Biotechnol Bioeng 108(7):1591-602.

Green LL, Hardy MC, Maynard-Currie CE, Tsuda H, Louie DM, Mendez MJ, Abderrahim H, Noguchi M, Smith DH, Zeng Y and others. 1994. Antigen-specific human monoclonal antibodies from mice engineered with human Ig heavy and light chain YACs. Nat Genet 7(1):13-21.

Gu X, Wang DI. 1998. Improvement of interferon-gamma sialylation in Chinese hamster ovary cell culture by feeding of N-acetylmannosamine. Biotechnol Bioeng 58(6):642-8.

Harrison PM, Kumar A, Lang N, Snyder M, Gerstein M. 2002. A question of size: the eukaryotic proteome and the problems in defining it. Nucleic Acids Research 30(5):1083-1090.

Heidenreich RA. 1995. Regulation of galactose-1-phosphate uridyltransferase gene expression. Eur J Pediatr 154(7 Suppl 2):S28-32.

Hills AE, Patel A, Boyd P, James DC. 2001a. Metabolic control of recombinant monoclonal antibody N-glycosylation in GS-NS0 cells. Biotechnol Bioeng 75(2):239-51.

Hills AE, Patel A, Boyd P, James DC. 2001b. Metabolic control of recombinant monoclonal antibody N-glycosylation in GS-NS0 cells. Biotechnology and Bioengineering 75(2):239-251.

Ho SC, Bardor M, Feng H, Mariati, Tong YW, Song Z, Yap MG, Yang Y. 2012a. IRES-mediated Tricistronic vectors for enhancing generation of high monoclonal antibody expressing CHO cell lines. J Biotechnol 157(1):130-9.

Ho Y, Kiparissides A, Pistikopoulos EN, Mantalaris A. 2012b. Computational approach for understanding and improving GS-NS0 antibody production under hyperosmotic conditions. J Biosci Bioeng 113(1):88-98.

Hodoniczky J, Zheng YZ, James DC. 2005. Control of recombinant monoclonal antibody effector functions by Fc N-glycan remodeling in vitro. Biotechnol Prog 21(6):1644-52.

Hossler P, Khattak SF, Li ZJ. 2009. Optimal and consistent protein glycosylation in mammalian cell culture. Glycobiology 19(9):936-49.

Hossler P, Mulukutla BC, Hu WS. 2007. Systems Analysis of N-Glycan Processing in Mammalian Cells. Plos One 2(8).

Houde D, Peng Y, Berkowitz SA, Engen JR. 2010. Post-translational modifications differentially affect IgG1 conformation and receptor binding. Mol Cell Proteomics 9(8):1716-28.

Hubert C, Lebrun P, Houari S, Ziemons E, Rozet E, Hubert P. 2014. Improvement of a stability-indicating method by Quality-by-Design versus Quality-by-Testing: A case of a learning process. Journal of Pharmaceutical and Biomedical Analysis 88(0):401-409.

Ivarsson M, Villiger TK, Morbidelli M, Soos M. 2014. Evaluating the impact of cell culture process parameters on monoclonal antibody N-glycosylation. Journal of Biotechnology 188(0):88-96.

Jadhav V, Hackl M, Klanert G, Hernandez Bort JA, Kunert R, Grillari J, Borth N. 2014a. Stable overexpression of miR-17 enhances recombinant protein production of CHO cells. Journal of Biotechnology 175(0):38-44.

Jadhav V, Hackl M, Klanert G, Hernandez Bort JA, Kunert R, Grillari J, Borth N. 2014b. Stable overexpression of miR-17 enhances recombinant protein production of CHO cells. J Biotechnol 175:38-44.

Janeway C. 2005. Immunobiology : the immune system in health and disease. 6th ed. ed. New York :: Garland Science.

Jang JD, Barford JP. 2000. An unstructured kinetic model of macromolecular metabolism in batch and fed-batch cultures of hybridoma cells producing monoclonal antibody. Biochemical Engineering Journal 4(2):153-168.

Jedrzejewski PM, del Val IJ, Constantinou A, Dell A, Haslam SM, Polizzi KM, Kontoravdi C. 2014. Towards controlling the glycoform: a model framework linking extracellular metabolites to antibody glycosylation. Int J Mol Sci 15(3):4492-522.

Jenkins N, Parekh RB, James DC. 1996. Getting the glycosylation right: Implications for the biotechnology industry. Nat Biotech 14(8):975-981.

Jimenez del Val I. 2013. Assessment of the interactions between bioprocess conditions and protein glycosylation in antibody- producing mammalian cell cultures [PhD thesis]. London, United Kingdoms: Imperial College London. 183 p.

Jimenez del Val I, Nagy JM, Kontoravdi C. 2011. A dynamic mathematical model for monoclonal antibody N-linked glycosylation and nucleotide sugar donor transport within a maturing Golgi apparatus. Biotechnology Progress 27(6):1730-43.

Joao HC, Scragg IG, Dwek RA. 1992. Effects of glycosylation on protein conformation and amide proton exchange rates in RNase B. FEBS Lett 307(3):343-6.

Johnston RJ, Hobert O. 2003. A microRNA controlling left/right neuronal asymmetry in Caenorhabditis elegans. Nature 426(6968):845-9.

Josse L, Smales CM, Tuite MF. 2010. Transient expression of human TorsinA enhances secretion of two functionally distinct proteins in cultured Chinese hamster ovary (CHO) cells. Biotechnol Bioeng 105(3):556-66.

Kafil V, Omidi Y. 2011. Cytotoxic Impacts of Linear and Branched Polyethylenimine Nanostructures in A431 Cells. BioImpacts : BI 1(1):23-30.

Kaneko Y, Nimmerjahn F, Ravetch JV. 2006. Anti-inflammatory activity of immunoglobulin G resulting from Fc sialylation. Science 313(5787):670-3.

Kantardjieff A, Jacob NM, Yee JC, Epstein E, Kok YJ, Philp R, Betenbaugh M, Hu WS. 2010. Transcriptome and proteome analysis of Chinese hamster ovary cells under low temperature and butyrate treatment. J Biotechnol 145(2):143-59.

Kaufman RJ. 2000. Overview of vector design for mammalian gene expression. Mol Biotechnol 16(2):151-60.

Kaveh O, Hengameh A, Johannes G, Legge M, Jeno S, Hector B. 2013. Novel dynamic model to predict the glycosylation pattern of monoclonal antibodies from extracellular cell culture conditions. 12th IFAC Symposium on Computer Applications in Biotechnology. Mumbal, India: 12th IFAC Symposium on Computer Applications in Biotechnology.

Kim AJ, Shi Y, Austin RC, Werstuck GH. 2005. Valproate protects cells from ER stress-induced lipid accumulation and apoptosis by inhibiting glycogen synthase kinase-3. J Cell Sci 118(Pt 1):89-99.

Kim do Y, Chaudhry MA, Kennard ML, Jardon MA, Braasch K, Dionne B, Butler M, Piret JM. 2013. Fed-batch CHO cell t-PA production and feed glutamine replacement to reduce ammonia production. Biotechnol Prog 29(1):165-75.

Kim TK, Eberwine JH. 2010. Mammalian cell transfection: the present and the future. Analytical and Bioanalytical Chemistry 397(8):3173-3178.

Kobata A. 2000. A journey to the world of glycobiology. Glycoconj J 17(7-9):443-64.

Kohler G, Milstein C. 1975. Continuous cultures of fused cells secreting antibody of predefined specificity. Nature 256(5517):495-497.

Kontoravdi C, Asprey SP, Pistikopoulos EN, Mantalaris A. 2007. Development of a dynamic model of monoclonal antibody production and glycosylation for product quality monitoring. Computers & Chemical Engineering 31(5-6):392-400.

Kontoravdi C, Asprey SP, Pistikopoulos S, Mantalaris A. 2005. Dynamic model of MAb production and glycosylation for the purpose of product quality control. In: Puigjaner LEA, editor. European Symposium on Computer-Aided Process Engineering-15, 20A and 20B. p 307-312.

Kontoravdi C, Pistikopoulos EN, Mantalaris A. 2010a. Systematic development of predictive mathematical models for animal cell cultures. Computers & Chemical Engineering 34:1192-1198.

Kontoravdi C, Pistikopoulos EN, Mantalaris A. 2010b. Systematic development of predictive mathematical models for animal cell cultures. Computers & Chemical Engineering 34(8):1192-1198.

Kozlowski S, Swann P. 2006. Current and future issues in the manufacturing and development of monoclonal antibodies. Adv Drug Deliv Rev 58(5-6):707-22.

Krambeck FJ, Bennun SV, Narang S, Choi S, Yarema KJ, Betenbaugh MJ. 2009. A mathematical model to derive N-glycan structures and cellular enzyme activities from mass spectrometric data. Glycobiology 19(11):1163-1175.

Krambeck FJ, Betenbaugh MJ. 2005. A mathematical model of N-linked glycosylation. Biotechnology and Bioengineering 92(6):711-728.

Krapp S, Mimura Y, Jefferis R, Huber R, Sondermann P. 2003. Structural analysis of human IgG-Fc glycoforms reveals a correlation between glycosylation and structural integrity. J Mol Biol 325(5):979-89.

Krichevsky AM, Gabriely G. 2009. miR-21: a small multi-faceted RNA. J Cell Mol Med 13(1):39-53.

Kukrer B, Filipe V, van Duijn E, Kasper PT, Vreeken RJ, Heck AJ, Jiskoot W. 2010. Mass spectrometric analysis of intact human monoclonal antibody aggregates fractionated by size-exclusion chromatography. Pharm Res 27(10):2197-204.

Kumar N, Gammell P, Meleady P, Henry M, Clynes M. 2008. Differential protein expression following low temperature culture of suspension CHO-K1 cells. BMC Biotechnol 8:42.

Kunaparaju R, Liao M, Sunstrom NA. 2005. Epi-CHO, an episomal expression system for recombinant protein production in CHO cells. Biotechnol Bioeng 91(6):670-7.

Kunkel JP, Jan DC, Jamieson JC, Butler M. 1998. Dissolved oxygen concentration in serum-free continuous culture affects N-linked glycosylation of a monoclonal antibody. J Biotechnol 62(1):55-71.

Kyriakopoulos S. 2014. Amino acid metabolism in Chinese hamster ovary cell culture [PhD]. London, U.K.: Imperial College London.

Kyriakopoulos S, Kontoravdi C. 2014a. A framework for the systematic design of fed-batch strategies in mammalian cell culture. Biotechnol Bioeng.

Kyriakopoulos S, Kontoravdi C. 2014b. A framework for the systematic design of fed-batch strategies in mammalian cell culture. Biotechnology and Bioengineering 111(12):2466-2476.

Kyriakopoulos S, Polizzi KM, Kontoravdi C. 2013. Comparative analysis of amino acid metabolism and transport in CHO variants with different levels of productivity. Journal of Biotechnology(0).

Lamotte D, Buckberry L, Monaco L, Soria M, Jenkins N, Engasser J-M, Marc A. 1999. Na-butyrate increases the production and α2,6-sialylation of recombinant interferon-γ expressed by α2,6- sialyltransferase engineered CHO cells. Cytotechnology 29(1):55-64.

Lee AH, Iwakoshi NN, Glimcher LH. 2003. XBP-1 regulates a subset of endoplasmic reticulum resident chaperone genes in the unfolded protein response. Mol Cell Biol 23(21):7448-59.

Lee MS, Lee GM. 2001. Effect of hypoosmotic pressure on cell growth and antibody production in recombinant Chinese hamster ovary cell culture. Cytotechnology 36(1-3):61-69.

Lee SM, Kim YG, Lee EG, Lee GM. 2014. Digital mRNA profiling of N-glycosylation gene expression in recombinant Chinese hamster ovary cells treated with sodium butyrate. J Biotechnol 171:56-60.

Lehninger A, Nelson D, Cox M. 2008. Lehninger Principles of Biochemistry: W. H. Freeman.

Lin J, Takagi M, Qu Y, Gao P, Yoshida T. 1999. Enhanced monoclonal antibody production by gradual increase of osmotic pressure. Cytotechnology 29(1):27-33.

Lin J, Teo S, Lam DH, Jeyaseelan K, Wang S. 2012. MicroRNA-10b pleiotropically regulates invasion, angiogenicity and apoptosis of tumor cells resembling mesenchymal subtype of glioblastoma multiforme. Cell Death Dis 3:e398.

Lin N, Davis A, Bahr S, Borgschulte T, Achtien K, Kayser K. 2011. Profiling highly conserved microrna expression in recombinant IgG-producing and parental Chinese hamster ovary cells. Biotechnol Prog 27(4):1163-71.

Linton D, Allan E, Karlyshev AV, Cronshaw AD, Wren BW. 2002. Identification of N-acetylgalactosamine-containing glycoproteins PEB3 and CgpA in Campylobacter jejuni. Molecular Microbiology 43(2):497-508.

Liu L, Stadheim A, Hamuro L, Pittman T, Wang W, Zha D, Hochman J, Prueksaritanont T. 2011. Pharmacokinetics of IgG1 monoclonal antibodies produced in humanized Pichia pastoris with specific glycoforms: a comparative study with CHO produced materials. Biologicals 39(4):205-10.

Maccani A, Hackl M, Leitner C, Steinfellner W, Graf AB, Tatto NE, Karbiener M, Scheideler M, Grillari J, Mattanovich D and others. 2014. Identification of microRNAs specific for high producer CHO cell lines using steady-state cultivation. Appl Microbiol Biotechnol 98(17):7535-48.

Malphettes L, Freyvert Y, Chang J, Liu PQ, Chan E, Miller JC, Zhou Z, Nguyen T, Tsai C, Snowden AW and others. 2010. Highly efficient deletion of FUT8 in CHO cell lines using zinc-finger nucleases yields cells that produce completely nonfucosylated antibodies. Biotechnol Bioeng 106(5):774-83.

Man Sung C, Scheinberg DA, Avdalovic NM, McGraw K, Vasquez M, Caron PC, Queen C. 1993. Genetically engineered deglycosylation of the variable domain increases the affinity of an anti-CD33 monoclonal antibody. Molecular Immunology 30(15):1361-1367.

Marchant RJ, Al-Fageeh MB, Underhill MF, Racher AJ, Smales CM. 2008. Metabolic rates, growth phase, and mRNA levels influence cell-specific antibody production levels from in vitro-cultured mammalian cells at sub-physiological temperatures. Molecular biotechnology 39(1):69-77.

Matsushima K, Isomoto H, Yamaguchi N, Inoue N, Machida H, Nakayama T, Hayashi T, Kunizaki M, Hidaka S, Nagayasu T and others. 2011. MiRNA-205 modulates cellular invasion and migration via regulating zinc finger E-box binding homeobox 2 expression in esophageal squamous cell carcinoma cells. J Transl Med 9:30.

Maurisse R, De Semir D, Emamekhoo H, Bedayat B, Abdolmohammadi A, Parsi H, Gruenert DC. 2010. Comparative transfection of DNA into primary and transformed mammalian cells from different lineages. BMC Biotechnol 10:9.

McLeod J, O'Callaghan PM, Pybus LP, Wilkinson SJ, Root T, Racher AJ, James DC. 2011. An empirical modeling platform to evaluate the relative control discrete CHO cell synthetic

processes exert over recombinant monoclonal antibody production process titer. Biotechnol Bioeng 108(9):2193-204.

Mohan C, Lee GM. 2010. Effect of inducible co-overexpression of protein disulfide isomerase and endoplasmic reticulum oxidoreductase on the specific antibody productivity of recombinant Chinese hamster ovary cells. Biotechnol Bioeng 107(2):337-46.

Moore A, Donahue CJ, Hooley J, Stocks DL, Bauer KD, Mather JP. 1995. Apoptosis in CHO cell batch cultures: examination by flow cytometry. Cytotechnology 17(1):1-11.

Moore A, Mercer J, Dutina G, Donahue CJ, Bauer KD, Mather JP, Etcheverry T, Ryll T. 1997. Effects of temperature shift on cell cycle, apoptosis and nucleotide pools in CHO cell batch cultues. Cytotechnology 23(1-3):47-54.

Mori K, Kuni-Kamochi R, Yamane-Ohnuki N, Wakitani M, Yamano K, Imai H, Kanda Y, Niwa R, Iida S, Uchida K and others. 2004. Engineering Chinese hamster ovary cells to maximize effector function of produced antibodies using FUT8 siRNA. Biotechnol Bioeng 88(7):901-8.

Morrow KJ. 2008. Optimizing transient gene expression. Genetic Engineering & Biotechnology News 28(5):54-59.

Mullard A. 2012. Can next-generation antibodies offset biosimilar competition? Nat Rev Drug Discov 11(6):426-8.

Munzer DGG, Ivarsson M, Usaku C, Habicher T, Soos M, Morbidelli M, Pistikopoulos EN, Mantalaris A. 2015. An unstructured model of metabolic and temperature dependent cell cycle arrest in hybridoma batch and fed-batch cultures. Biochemical Engineering Journal 93:260-273.

Murrell MP, Yarema KJ, Levchenko A. 2004. The systems biology of glycosylation. Chembiochem 5(10):1334-47.

Muthing J, Kemminer SE, Conradt HS, Sagi D, Nimtz M, Karst U, Peter-Katalinic J. 2003. Effects of buffering conditions and culture pH on production rates and glycosylation of clinical phase I anti-melanoma mouse IgG3 monoclonal antibody R24. Biotechnol Bioeng 83(3):321-34.

Nam JH, Zhang F, Ermonval M, Linhardt RJ, Sharfstein ST. 2008. The effects of culture conditions on the glycosylation of secreted human placental alkaline phosphatase produced in Chinese hamster ovary cells. Biotechnol Bioeng 100(6):1178-92.

North SJ, Huang HH, Sundaram S, Jang-Lee J, Etienne AT, Trollope A, Chalabi S, Dell A, Stanley P, Haslam SM. 2010. Glycomics profiling of Chinese hamster ovary cell glycosylation mutants reveals N-glycans of a novel size and complexity. J Biol Chem 285(8):5759-75.

Nyberg GB, Balcarcel RR, Follstad BD, Stephanopoulos G, Wang DI. 1999. Metabolic effects on recombinant interferon-gamma glycosylation in continuous culture of Chinese hamster ovary cells. Biotechnol Bioeng 62(3):336-47.

O'Callaghan PM, McLeod J, Pybus LP, Lovelady CS, Wilkinson SJ, Racher AJ, Porter A, James DC. 2010. Cell line-specific control of recombinant monoclonal antibody production by CHO cells. Biotechnol Bioeng 106(6):938-51.

Oliveira CC, McCarthy JEG. 1995. The relationship between eukaryotic translation and mRNA stability: A short upstream open reading frame strongly inhibits translational initiation

and greatly accelerates mRNA degradation in yeast saccharomyces cerevisiae. Journal of Biological Chemistry 270(15):8936-8943.

Onitsuka M, Kim WD, Ozaki H, Kawaguchi A, Honda K, Kajiura H, Fujiyama K, Asano R, Kumagai I, Ohtake H and others. 2012. Enhancement of sialylation on humanized IgG-like bispecific antibody by overexpression of alpha2,6-sialyltransferase derived from Chinese hamster ovary cells. Appl Microbiol Biotechnol 94(1):69-80.

Oyaas K, Ellingsen TE, Dyrset N, Levine DW. 1995. Transport of osmoprotective compounds in hybridoma cells exposed to hyperosmotic stress. Cytotechnology 17(3):143-51.

Pablo Umaña, Jean-Mairet J; Roche GlycArt AG, assignee. 2012 2012-05-17 Glycosylation Engineering of Antibodies for Improving Antibody-Dependent Cellular Cytotoxicity.

Parekh RB, Dwek RA, Sutton BJ, Fernandes DL, Leung A, Stanworth D, Rademacher TW, Mizuochi T, Taniguchi T, Matsuta K and others. 1985. Association of rheumatoid arthritis and primary osteoarthritis with changes in the glycosylation pattern of total serum IgG. Nature 316(6027):452-457.

Pels Rijcken WR, Overdijk B, Van den Eijnden DH, Ferwerda W. 1995. The effect of increasing nucleotide-sugar concentrations on the incorporation of sugars into glycoconjugates in rat hepatocytes. Biochemical Journal 305(Pt 3):865-870.

Percy JR, Percy ME, Dorrington KJ. 1975. A theoretical model for the covalent assembly of immunoglobulins. Application to the assembly of human immunoglobulin G in vitro. J Biol Chem 250(6):2398-400.

Pham PL, Kamen A, Durocher Y. 2006. Large-scale transfection of mammalian cells for the fast production of recombinant protein. Mol Biotechnol 34(2):225-37.

Pichler J, Galosy S, Mott J, Borth N. 2011. Selection of CHO Host Cell Subclones With Increased Specific Antibody Production Rates by Repeated Cycles of Transient Transfection and Cell Sorting. Biotechnology and Bioengineering 108(2):386-394.

Place RF, Li L-C, Pookot D, Noonan EJ, Dahiya R. 2008. MicroRNA-373 induces expression of genes with complementary promoter sequences. Proceedings of the National Academy of Sciences 105(5):1608-1613.

Potgieter TI, Cukan M, Drummond JE, Houston-Cummings NR, Jiang YW, Li F, Lynaugh H, Mallem M, McKelvey TW, Mitchell T and others. 2009. Production of monoclonal antibodies by glycoengineered Pichia pastoris. Journal of Biotechnology 139(4):318-325.

Poy MN, Eliasson L, Krutzfeldt J, Kuwajima S, Ma X, Macdonald PE, Pfeffer S, Tuschl T, Rajewsky N, Rorsman P and others. 2004. A pancreatic islet-specific microRNA regulates insulin secretion. Nature 432(7014):226-30.

PSE. 1997-2015. gPROMS, www.psenterprise.com/gproms. Version v.4.0.0: Process Systems Enterprise.

Pybus LP, Dean G, West NR, Smith A, Daramola O, Field R, Wilkinson SJ, James DC. 2014a. Model-directed engineering of "difficult-to-express" monoclonal antibody production by Chinese hamster ovary cells. Biotechnol Bioeng 111(2):372-85.

Pybus LP, James DC, Dean G, Slidel T, Hardman C, Smith A, Daramola O, Field R. 2014b. Predicting the expression of recombinant monoclonal antibodies in Chinese hamster ovary cells based on sequence features of the CDR3 domain. Biotechnol Prog 30(1):188-97.

R Development Core Team. 2010. R: A language and environment for statistical computing. Austria.

Rabouille C, Hui N, Hunte F, Kieckbusch R, Berger EG, Warren G, Nilsson T. 1995. Mapping the distribution of Golgi enzymes involved in the construction of complex oligosaccharides. J Cell Sci 108 (Pt 4):1617-27.

Rajendra Y, Kiseljak D, Baldi L, Hacker DL, Wurm FM. 2011a. A simple high-yielding process for transient gene expression in CHO cells. J Biotechnol 153(1-2):22-6.

Rajendra Y, Kiseljak D, Baldi L, Hacker DL, Wurm FM. 2011b. A simple high-yielding process for transient gene expression in CHO cells. Journal of Biotechnology 153(1-2):22-26.

Raju TS. 2008. Terminal sugars of Fc glycans influence antibody effector functions of IgGs. Current Opinion in Immunology 20(4):471-478.

Raju TS, Briggs JB, Borge SM, Jones AJ. 2000. Species-specific variation in glycosylation of IgG: evidence for the species-specific sialylation and branch-specific galactosylation and importance for engineering recombinant glycoprotein therapeutics. Glycobiology 10(5):477-86.

Raman R, Venkataraman M, Ramakrishnan S, Lang W, Raguram S, Sasisekharan R. 2006. Advancing glycomics: implementation strategies at the consortium for functional glycomics. Glycobiology 16(5):82r-90r.

Rathore AS, Winkle H. 2009. Quality by design for biopharmaceuticals. Nat Biotech 27(1):26-34.

Reddy S, Miller WM. 1994. Effects of abrupt and gradual osmotic stress on antibody production and content in hybridoma cells that differ in production kinetics. Biotechnol Prog 10(2):165-73.

Richter A, Sanford KK, Evans VJ. 1972. Influence of oxygen and culture media on plating efficiency of some mammalian tissue cells. J Natl Cancer Inst 49(6):1705-12.

Rothman RJ, Warren L, Vliegenthart JFG, Hard KJ. 1989. Clonal analysis of the glycosylation of immunoglobulin G secreted by murine hybridomas. Biochemistry 28(3):1377-1384.

Rupp O, Becker J, Brinkrolf K, Timmermann C, Borth N, Pühler A, Noll T, Goesmann A. 2014. Construction of a Public CHO Cell Line Transcript Database Using Versatile Bioinformatics Analysis Pipelines. PLoS ONE 9(1):e85568.

Ryu JS, Kim TK, Chung JY, Lee GM. 2000. Osmoprotective effect of glycine betaine on foreign protein production in hyperosmotic recombinant chinese hamster ovary cell cultures differs among cell lines. Biotechnol Bioeng 70(2):167-75.

Schmelzer AE, Miller WM. 2002. Hyperosmotic stress and elevated pCO2 alter monoclonal antibody charge distribution and monosaccharide content. Biotechnol Prog 18(2):346-53.

Schwarz F, Huang W, Li C, Schulz BL, Lizak C, Palumbo A, Numao S, Neri D, Aebi M, Wang L-X. 2010. A combined method for producing homogeneous glycoproteins with eukaryotic N-glycosylation. Nat Chem Biol 6(4):264-266.

Sealover NR, Davis AM, Brooks JK, George HJ, Kayser KJ, Lin N. 2013. Engineering Chinese hamster ovary (CHO) cells for producing recombinant proteins with simple glycoforms by zinc-finger nuclease (ZFN)-mediated gene knockout of mannosyl (alpha-1,3-)-

glycoprotein beta-1,2-N-acetylglucosaminyltransferase (Mgat1). J Biotechnol 167(1):24-32.

Selman MH, Niks EH, Titulaer MJ, Verschuuren JJ, Wuhrer M, Deelder AM. 2011. IgG fc N-glycosylation changes in Lambert-Eaton myasthenic syndrome and myasthenia gravis. J Proteome Res 10(1):143-52.

Selvarasu S, Ho YS, Chong WPK, Wong NSC, Yusufi FNK, Lee YY, Yap MGS, Lee DY. 2012. Combined in silico modeling and metabolomics analysis to characterize fed-batch CHO cell culture. Biotechnology and Bioengineering 109(6):1415-1429.

Senger RS, Karim MN. 2005. Variable site-occupancy classification of N-linked glycosylation using artificial neural networks. Biotechnol Prog 21(6):1653-62.

Seo JS, Min BS, Kim YJ, Cho JM, Baek E, Cho MS, Lee GM. 2014. Effect of glucose feeding on the glycosylation quality of antibody produced by a human cell line, F2N78, in fed-batch culture. Appl Microbiol Biotechnol 98(8):3509-15.

Serrato JA, Palomares LA, Meneses-Acosta A, Ramirez OT. 2004. Heterogeneous conditions in dissolved oxygen affect N-glycosylation but not productivity of a monoclonal antibody in hybridoma cultures. Biotechnol Bioeng 88(2):176-88.

Sevier CS, Kaiser CA. 2006. Disulfide Transfer between Two Conserved Cysteine Pairs Imparts Selectivity to Protein Oxidation by Ero1. Molecular Biology of the Cell 17(5):2256-2266.

Shelikoff M, Sinskey AJ, Stephanopoulos G. 1996. A modeling framework for the study of protein glycosylation. Biotechnology and Bioengineering 50(1):73-90.

Shen D, Kiehl TR, Khattak SF, Li ZJ, He A, Kayne PS, Patel V, Neuhaus IM, Sharfstein ST. 2010. Transcriptomic responses to sodium chloride-induced osmotic stress: a study of industrial fed-batch CHO cell cultures. Biotechnol Prog 26(4):1104-15.

Shinkawa T, Nakamura K, Yamane N, Shoji-Hosaka E, Kanda Y, Sakurada M, Uchida K, Anazawa H, Satoh M, Yamasaki M and others. 2003. The absence of fucose but not the presence of galactose or bisecting N-acetylglucosamine of human IgG1 complex-type oligosaccharides shows the critical role of enhancing antibody-dependent cellular cytotoxicity. J Biol Chem 278(5):3466-73.

Sidoli FR, Asprey SP, Mantalaris A. 2006. A Coupled Single Cell-Population-Balance Model for Mammalian Cell Cultures. Industrial & Engineering Chemistry Research 45(16):5801-5811.

Slikker W, 3rd, Desai VG, Duhart H, Feuers R, Imam SZ. 2001. Hypothermia enhances bcl-2 expression and protects against oxidative stress-induced cell death in Chinese hamster ovary cells. Free Radic Biol Med 31(3):405-11.

Sou SN, Polizzi KM, Kontoravdi C. 2013. Evaluation of transfection methods for transient gene expression in Chinese hamster ovary cells. ABB 4:7.

Sou SN, Sellick C, Lee K, Mason A, Kyriakopoulos S, Polizzi KM, Kontoravdi C. 2014. How does mild hypothermia affect monoclonal antibody glycosylation? Biotechnology and Bioengineering:n/a-n/a.

Srour O, Young JD, Eldar YC. 2011. Fluxomers: a new approach for (13)C metabolic flux analysis. BMC Systems Biology 5:129-129.

Sunley K, Tharmalingam T, Butler M. 2008. CHO cells adapted to hypothermic growth produce high yields of recombinant beta-interferon. Biotechnol Prog 24(4):898-906.

Tait AS, Tarrant RDR, Velez-Suberbie ML, Spencer DIR, Bracewell DG. 2013. Differential response in downstream processing of CHO cells grown under mild hypothermic conditions. Biotechnology Progress 29(3):688-696.

Tatiraju S, Soroush M, Mutharasan R. 1999. Multi-rate nonlinear state and parameter estimation in a bioreactor. Biotechnol Bioeng 63(1):22-32.

Taylor ME, Drickamer K. 2003. Introduction to Glycobiology: Oxford University Press.

Tekoah Y, Ko K, Koprowski H, Harvey DJ, Wormald MR, Dwek RA, Rudd PM. 2004. Controlled glycosylation of therapeutic antibodies in plants. Arch Biochem Biophys 426(2):266-78.

Thaisuchat H, Baumann M, Pontiller J, Hesse F, Ernst W. 2011. Identification of a novel temperature sensitive promoter in CHO cells. BMC Biotechnol 11:51.

Thomas TM, Scopes RK. 1998. The effects of temperature on the kinetics and stability of mesophilic and thermophilic 3-phosphoglycerate kinases. Biochem J 330 (Pt 3):1087-95.

Umana P, Bailey JE. 1997. A mathematical model of N-linked glycoform biosynthesis. Biotechnology and Bioengineering 55(6):890-908.

Umana P, Jean-Mairet J, Bailey JE. 1999a. Tetracycline-regulated overexpression of glycosyltransferases in Chinese hamster ovary cells. Biotechnol Bioeng 65(5):542-9.

Umana P, Jean-Mairet J, Moudry R, Amstutz H, Bailey JE. 1999b. Engineered glycoforms of an antineuroblastoma IgG1 with optimized antibody-dependent cellular cytotoxic activity. Nat Biotechnol 17(2):176-80.

Underhill MF, Smales CM. 2007. The cold-shock response in mammalian cells: investigating the HeLa cell cold-shock proteome. Cytotechnology 53(1-3):47-53.

Valinezhad Orang A, Safaralizadeh R, Kazemzadeh-Bavili M. 2014. Mechanisms of miRNA-Mediated Gene Regulation from Common Downregulation to mRNA-Specific Upregulation. International Journal of Genomics 2014:15.

Valley U, Nimtz M, Conradt HS, Wagner R. 1999. Incorporation of ammonium into intracellular UDP-activated N-acetylhexosamines and into carbohydrate structures in glycoproteins. Biotechnology and Bioengineering 64(4):401-417.

van Berkel PH, Gerritsen J, Perdok G, Valbjorn J, Vink T, van de Winkel JG, Parren PW. 2009. N-linked glycosylation is an important parameter for optimal selection of cell lines producing biopharmaceutical human IgG. Biotechnol Prog 25(1):244-51.

Vasudevan S, Tong Y, Steitz JA. 2007. Switching from Repression to Activation: MicroRNAs Can Up-Regulate Translation. Science 318(5858):1931-1934.

Viant M, Bundy J, Pincetich C, de Ropp J, Tjeerdema R. 2005. NMR-derived developmental metabolic trajectories: an approach for visualizing the toxic actions of trichloroethylene during embryogenesis. Metabolomics 1(2):149-158.

Wacker M, Feldman MF, Callewaert N, Kowarik M, Clarke BR, Pohl NL, Hernandez M, Vines ED, Valvano MA, Whitfield C and others. 2006. Substrate specificity of bacterial

oligosaccharyltransferase suggests a common transfer mechanism for the bacterial and eukaryotic systems. Proc Natl Acad Sci U S A 103(18):7088-93.

Wacker M, Linton D, Hitchen PG, Nita-Lazar M, Haslam SM, North SJ, Panico M, Morris HR, Dell A, Wren BW and others. 2002. N-linked glycosylation in Campylobacter jejuni and its functional transfer into E. coli. Science 298(5599):1790-3.

Warnefors M, Liechti A, Halbert J, Valloton D, Kaessmann H. 2014. Conserved microRNA editing in mammalian evolution, development and disease. Genome Biology 15(6):R83.

Weikert S, Papac D, Briggs J, Cowfer D, Tom S, Gawlitzek M, Lofgren J, Mehta S, Chisholm V, Modi N and others. 1999. Engineering Chinese hamster ovary cells to maximize sialic acid content of recombinant glycoproteins. Nat Biotechnol 17(11):1116-21.

Wingens M, Gätgens J, Schmidt A, Albaum SP, Büntemeyer H, Noll T, Hoffrogge R. 2015. 2D-DIGE screening of high-productive CHO cells under glucose limitation—Basic changes in the proteome equipment and hints for epigenetic effects. Journal of Biotechnology 201:86-97.

Wong NSC, Wati L, Nissom PM, Feng HT, Lee MM, Yap MGS. 2010. An Investigation of Intracellular Glycosylation Activities in CHO Cells: Effects of Nucleotide Sugar Precursor Feeding. Biotechnology and Bioengineering 107(2):321-336.

Wulhfard S, Baldi L, Hacker DL, Wurm F. 2010. Valproic acid enhances recombinant mRNA and protein levels in transiently transfected Chinese hamster ovary cells. J Biotechnol 148(2-3):128-32.

Wulhfard S, Tissot S, Bouchet S, Cevey J, De Jesus M, Hacker DL, Wurm FM. 2008. Mild hypothermia improves transient gene expression yields several fold in chinese hamster ovary cells. Biotechnology Progress 24(2):458-465.

Wurm FM. 2004. Production of recombinant protein therapeutics in cultivated mammalian cells. Nat Biotechnol 22(11):1393-8.

Xia W, Bringmann P, McClary J, Jones PP, Manzana W, Zhu Y, Wang S, Liu Y, Harvey S, Madlansacay MR and others. 2006. High levels of protein expression using different mammalian CMV promoters in several cell lines. Protein Expr Purif 45(1):115-24.

Xu X, Nagarajan H, Lewis NE, Pan S, Cai Z, Liu X, Chen W, Xie M, Wang W, Hammond S and others. 2011. The genomic sequence of the Chinese hamster ovary (CHO)-K1 cell line. Nat Biotech 29(8):735-741.

Ye J, Kober V, Tellers M, Naji Z, Salmon P, Markusen JF. 2009. High-level protein expression in scalable CHO transient transfection. Biotechnol Bioeng 103(3):542-51.

Yee JC, Gerdtzen ZP, Hu WS. 2009. Comparative transcriptome analysis to unveil genes affecting recombinant protein productivity in mammalian cells. Biotechnol Bioeng 102(1):246-63.

Yoon SK, Kim SH, Song JY, Lee GM. 2006. Biphasic culture strategy for enhancing volumetric erythropoietin productivity of Chinese hamster ovary cells. Enzyme and Microbial Technology 39(3):362-365.

Yoon SK, Song JY, Lee GM. 2003. Effect of low culture temperature on specific productivity, transcription level, and heterogeneity of erythropoietin in Chinese hamster ovary cells. Biotechnol Bioeng 82(3):289-98.

Zhang P, Tan DL, Heng D, Wang T, Mariati, Yang Y, Song Z. 2010a. A functional analysis of N-glycosylation-related genes on sialylation of recombinant erythropoietin in six commonly used mammalian cell lines. Metab Eng 12(6):526-36.

Zhang X, Garcia IF, Baldi L, Hacker DL, Wurm FM. 2010b. Hyperosmolarity enhances transient recombinant protein yield in Chinese hamster ovary cells. Biotechnol Lett 32(11):1587-92.

Zhu J. 2012. Mammalian cell protein expression for biopharmaceutical production. Biotechnol Adv 30(5):1158-70.

Zou G, Ochiai H, Huang W, Yang Q, Li C, Wang LX. 2011. Chemoenzymatic synthesis and Fcgamma receptor binding of homogeneous glycoforms of antibody Fc domain. Presence of a bisecting sugar moiety enhances the affinity of Fc to FcgammaIIIa receptor. J Am Chem Soc 133(46):18975-91.

Zustiak MP, Jose L, Xie Y, Zhu J, Betenbaugh MJ. 2014. Enhanced transient recombinant protein production in CHO cells through the co-transfection of the product gene with Bcl-xL. Biotechnol J 9(9):1164-74.

Appendix I

Chapter 3 supplementary materials

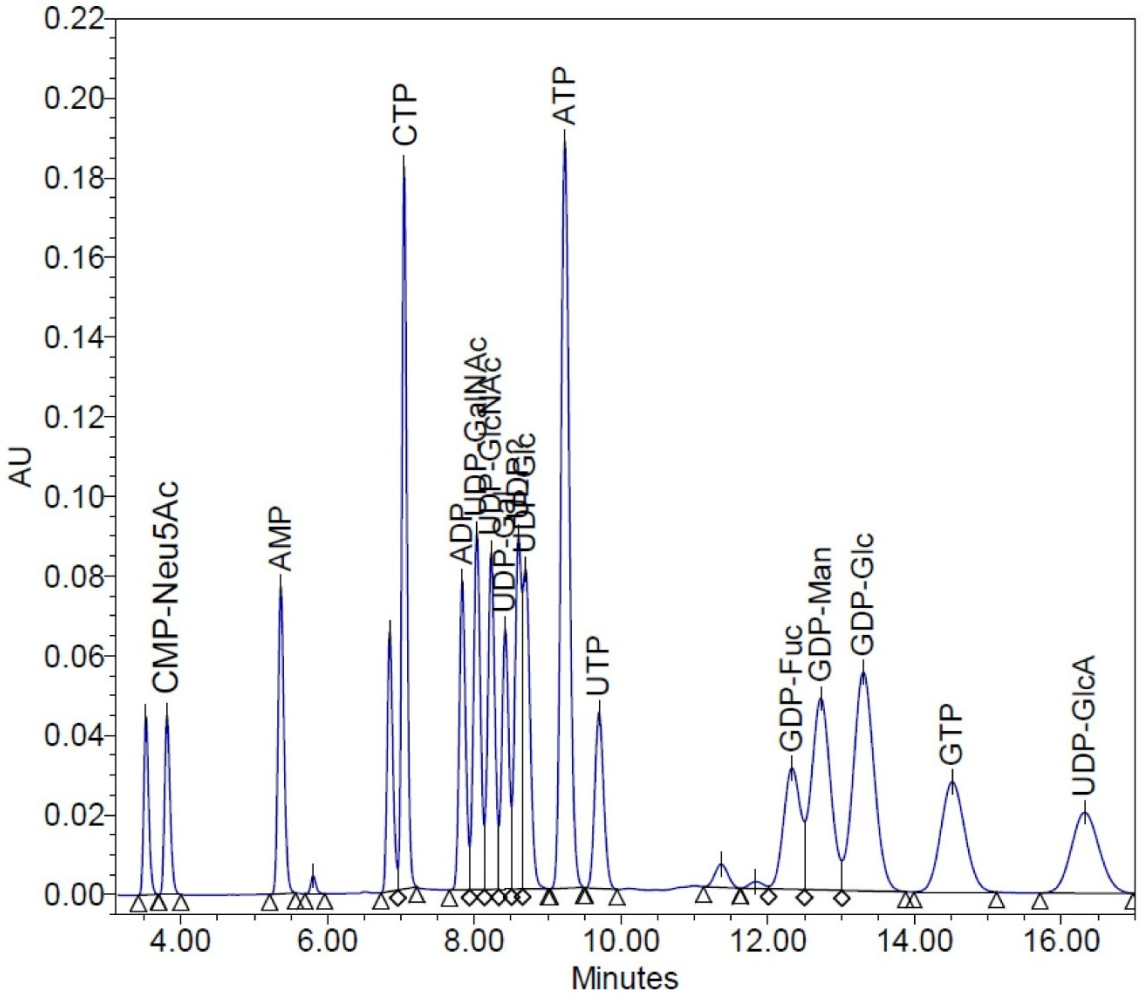

Appendix Figure 1. Typical HPAEC chromatogram of intracellular nucleotide and NSD species. The chromatogram shows the elution profile of nucleotide AMP, CTP, ADP, ATP, UTP and GTP and NSD CMA-Neu5Ac, UDP-GalNAc, UDP-GlcNAc, UDP-Gal, UDP-Glc, GDP-Fuc, GDP-Man, GDP-Glc and UDP-GlcA.

Appendix Table 1. FBA reactions of CHO cells included in the model.

#	Reaction	Reversibility
	Glycolysis	
1	[c] : Glc + ATP --> G6P + ADP	Irreversible
2	[c] : G6P <==> F6P	Reversible
3	[c] : F6P + ATP --> DHAP + GAP + ADP	Irreversible
4	[c] : DHAP <==> GAP	Reversible
5	[c] : GAP + NAD + ADP <==> 3PG + NADH + ATP	Reversible
6	[c] : 3PG + ADP --> Pyr + ATP	Irreversible
	TCA cycle	
7	[c] : Pyr + NAD + CoASH --> AcCoA + CO2 + NADH	Irreversible
8	[c] : AcCoA + Oxal --> Cit + CoASH	Irreversible
9	[c] : Cit + NADP --> αKG + CO2 + NADPH	Irreversible
10	[c] : αKG + CoASH + NAD --> SucCoA + CO2 + NADH	Irreversible
11	[c] : SucCoA + GDP <==> Succ + GTP + CoASH	Reversible
12	[c] : Succ + FAD <==> Fum + FADH2	Reversible
13	[c] : Fum <==> Mal	Reversible
14	[c] : Mal + NAD <==> Oxal + NADH	Reversible
	Pyruvate fates	
15	[c] : Pyr + NADH <==> Lac + NAD	Reversible
16	[c] : Pyr + Glu <==> Ala + αKG	Reversible
	Pentose Phosphate Pathway	
17	[c] : (3) G6P + (6) NADP --> (3) CO2 + (3) R5P + (6) NADPH	Irreversible
	Anaplerotic Reaction	
18	[c] : Mal + NADP <==> Pyr + HCO3 + NADPH	Reversible
	Amino Acid Metabolism	
19	[c] : Glu + NADP <==> αKG + NH4 + NADPH	Reversible
20	[c] : Oxal + Glu <==> Asp + αKG	Reversible
21	[c] : Gln + ADP <==> Glu + ATP + NH4	Reversible
22	[c] : Thr + NAD + CoASH --> Gly + NADH + AcCoA	Irreversible
23	[c] : Ser + THF + NADP <==> Gly + NADPH + N10FTHF	Reversible
24	[c] : N10FTHF + ADP <==> ATP + Formate + THF	Reversible
25	[c] : Ser --> Pyr + NH4	Irreversible
26	[c] : Thr --> αKb + NH4	Irreversible
27	[c] : αKb + CoASH + NAD + HCO3 + ATP --> SucCoA + ADP + NADH + CO2	Irreversible
28	[c] : Trp --> Ala + (2) CO2 + αKa	Irreversible
29	[c] : Lys + (2) αKG + (3) NADP + FAD --> αKa + (2) Glu + (3) NADPH + FADH2	Irreversible
30	[c] : αKa + (2) CoASH + (2) NAD --> (2) AcCoA + (2) NADH + (2) CO2	Irreversible
31	[c] : Val + αKG + CoASH + NAD --> IsobutCoA + Glu + CO2 + NADH	Irreversible
32	[c] : IsobutCoA + FAD + (2) NAD + HCO3 + ATP --> SucCoA + ADP + FADH2 + (2) NADH + CO2	Irreversible
33	[c] : IsobutCoA --> Isobut	Irreversible
34	[c] : Ile + αKG + (2) CoASH + (2) NAD + FAD + HCO3 + ATP --> AcCoA + SucCoA + ADP + Glu + CO2 + (2) NADH + FADH2	Irreversible
35	[c] : Leu + αKG + CoASH + NAD --> IsovalCoA + Glu + CO2 + NADH	Irreversible
36	[c] : IsovalCoA + FAD + ATP + CO2 + SucCoA + CoASH --> (3) AcCoA + Succ + FADH2 + ADP	Irreversible
37	[c] : IsovalCoA --> Isoval	Irreversible
38	[c] : Phe + NADH --> Tyr + NAD	Irreversible
39	[c] : Tyr + αKG + SucCoA + CoASH --> Fum + (2) AcCoA + Succ + Glu + CO2	Irreversible
40	[c] : Met + Ser + ATP --> αKb + NH4 + AMP	Irreversible
41	[c] : Asn <==> Asp + NH4	Reversible
42	[c] : Pro + NADP <==> Glu + NADPH	Reversible
43	[c] : Arg + αKG + NADP --> (2) Glu + NADPH + Urea	Irreversible
44	[c] : His --> Glu + NH4	Irreversible
45	[c] : Arg --> Orn + Urea	Irreversible
46	[c] : Orn --> PTRSC + CO2	Irreversible
47	[c] : Met + ATP --> SAM	Irreversible
48	[c] : SAM --> DSAM + CO2	Irreversible

49	[c] : DSAM + PTRSC --> 5MTA + SPRMD	Irreversible
50	[c] : 5MTA + SPRM --> DSAM + SPRMD	Irreversible
	Glycogen Synthesis	
51	[c] : G6P --> G1P	Irreversible
52	[c] : G1P + UMPRN + (2) ATP --> UDPG + (2) ADP	Irreversible
53	[c] : UDPG --> Glycogen + UDP	Irreversible
	Nucleotide Synthesis	
54	[c] : R5P + ATP --> PRPP + AMP	Irreversible
55	[c] : PRPP + (2) Gln + Gly + Asp + (5) ATP + CO2 + (2) N10FTHF --> IMP + (2) Glu + Fum + (5) ADP + (2) THF	Irreversible
56	[c] : IMP + Asp + GTP --> AMPRN + Fum + GDP	Irreversible
57	[c] : IMP + Gln + ATP + NAD --> GMPRN + Glu + AMP + NADH	Irreversible
58	[c] : HCO3 + NH4 + Asp + (2) ATP + NAD --> Orotate + (2) ADP + NADH	Irreversible
59	[c] : Orotate + PRPP --> UMPRN + CO2	Irreversible
60	[c] : UMPRN + Gln + ATP --> CMPRN + Glu + ADP	Irreversible
61	[c] : AMPRN --> dAMP	Irreversible
62	[c] : GMPRN --> dGMP	Irreversible
63	[c] : CMPRN --> dCMP	Irreversible
64	[c] : UMPRN --> dTMP	Irreversible
	Lipid Synthesis	
65	[c] : Choline + ATP --> Pcholine + ADP	Irreversible
66	[c] : Pcholine + (18) AcCoA + Glyc3P + (22) ATP + (33) NADH --> PC + (16) ADP + (6) AMP + (33) NAD + (18) CoASH	Irreversible
67	[c] : PC + Ser <==> PS + Choline	Reversible
68	[c] : PS --> PE + CO2	Irreversible
69	[c] : Choline + Glyc3P <==> Glyc3PC	Reversible
70	[c] : G6P --> Inositol	Irreversible
71	[c] : Inositol + (18) AcCoA + Glyc3P + (22) ATP + (33) NADH --> PI + (16) ADP + (6) AMP + (33) NAD + (18) CoASH	Irreversible
72	[c] : (18) AcCoA + (2) Glyc3P + (22) ATP + (33) NADH --> PG + (16) ADP + (6) AMP + (33) NAD + (18) CoASH	Irreversible
73	[c] : (2) PG --> DPG + Glyc	Irreversible
74	[c] : (16) AcCoA + Ser + Choline + (16) ATP + (29) NADPH --> SM + (2) CO2 + (14) ADP + (2) AMP + (29) NADP + (16) CoASH	Irreversible
75	[c] : (18) AcCoA + (18) ATP + (14) NADPH --> Cholesterol + (9) CO2 + (18) ADP + (14) NADP + (18) CoASH	Irreversible
	Biomass Formation	
76	For 36.5°C [c] : (88.038) Ala + (54.1149) Arg + (54.6624) Asn + (101.835) Asp + (60.4002) Gln + (143.2041) Glu + (90.2061) Gly + (15.1986) His + (44.8731) Ile + (91.3887) Leu + (103.7403) Lys + (23.0388) Met + (41.61) Phe + (51.8592) Pro + (66.6198) Ser + (54.6843) Thr + (7.01895) Trp + (22.8855) Tyr + (65.3934) Val + (9450.507) ATP + (11.043513) AMPRN + (3.055269) Cholesterol + (8.038614) CMPRN + (3.721686) dAMP + (2.665668) dCMP + (2.79444) dGMP + (0.5913) DPG + (3.696063) dTMP + (94.6299) Glycogen + (7.437459) GMPRN + (11.622111) PC + (4.407156) PE + (0.22119) PG + (1.59651) PI + (0.438) PS + (1.382985) SM + (11.006064) UMPRN + (0.47085) NAD + (0.02847) NADP + (0.00219) FAD + (0.01095) NADH + (0.0876) NADPH + (0.001314) SucCoA + (0.01095) AcCoA + (0.012264) CoASH + (10.95) MTHF + (7.665) PTRSC + (1.533) SPRMD + (1.8615) Neu5Ac + (19.1596666087446) GlcNAc + (4.43910147525) GalNAc + (14.3965857576054) Mann + (6.32724069101717) Gal + (4.52592703789134) Fuc --> (1) Biomass + (9450.507) ADP For 32°C TS [c] : (88.038) Ala + (54.1149) Arg + (54.6624) Asn + (101.835) Asp + (60.4002) Gln + (143.2041) Glu + (90.2061) Gly + (15.1986) His + (44.8731) Ile + (91.3887) Leu + (103.7403) Lys + (23.0388) Met + (41.61) Phe + (51.8592) Pro + (66.6198) Ser + (54.6843) Thr + (7.01895) Trp + (22.8855) Tyr + (65.3934) Val + (9450.507) ATP + (11.043513) AMPRN + (3.055269) Cholesterol + (8.038614) CMPRN + (3.721686) dAMP + (2.665668) dCMP + (2.79444) dGMP + (0.5913) DPG + (3.696063) dTMP + (94.6299) Glycogen + (7.437459) GMPRN + (11.622111) PC + (4.407156) PE + (0.22119) PG + (1.59651) PI + (0.438) PS + (1.382985) SM + (11.006064) UMPRN + (0.47085) NAD + (0.02847) NADP + (0.00219) FAD + (0.01095) NADH + (0.0876) NADPH + (0.001314) SucCoA + (0.01095) AcCoA + (0.012264) CoASH + (10.95) MTHF + (7.665) PTRSC + (1.533) SPRMD + (1.8615) Neu5Ac + (19.1750013522) GlcNAc + (4.43910147525) GalNAc + (14.38125101415) Mann + (5.40043757441596) Gal + (4.48368385448878) Fuc --> (1) Biomass + (9450.507) ADP	Irreversible
	Other by-products	
77	[c] : AcCoA + AMP <==> Acetate + CoASH + ATP	Reversible

78	[c] : DHAP + NADH <==> Glyc3P + NAD	Reversible
79	[c] : Glyc3P <==> Glyc	Reversible
	Glycosylation	
80	[c] : UDPG <==> UDPGal	Reversible
81	[c] : Glc + ATP + GTP --> GDPMann + ADP	Irreversible
82	[c] : F6P + Gln + AcCoA + UTP --> UDPNAG + Glu + CoASH	Irreversible
83	[c] : UDPNAG + ATP + 3PG + CTP --> CMPNeu5Ac + UDP + ADP	Irreversible
84	[c] : GDPMann + NADPH --> GDPFuc + NADP	Irreversible
85	[c] : UDPNAG <==> UDP + GlcNAc	Reversible
86	[c] : UDPNAG <==> UDPGalNAc	Reversible
87	[c] : UDPGalNAc <==> GalNAc + UDP	Reversible
88	[c] : GDPMann <==> Mann + GDP	Reversible
89	[c] : UDPGal <==> Gal + UDP	Reversible
90	[c] : CMPNeu5Ac <==> CMP + Neu5Ac	Reversible
91	[c] : GDPFuc <==> GDP + Fuc	Reversible
92	[c] : CMPNeu5Ac <==> CMPNeu5Gc	Reversible
93	[c] : CMPNeu5Gc <==> CMP + Neu5Gc	Reversible
	Vitamin metabolism	
94	[c] : Fol + NADH --> THF + NAD	Reversible
95	[c] : Gly + THF + NAD <==> METTHF + NH4 + CO2 + NADH	Reversible
96	[c] : MTHF + NADP <==> METTHF + NADPH	Reversible
	IgG Formation	
97	[c] : (423.795512610944) Ala + (266.385750784022) Arg + (314.819523653844) Asn + (302.711080436388) Asp + (363.253296523666) Gln + (363.253296523666) Glu + (581.205274437866) Gly + (133.192875392011) His + (605.422160872777) Leu + (520.663058350588) Lys + (72.6506593047332) Met + (266.385750784022) Phe + (532.771501568043) Pro + (1138.19366244082) Ser + (593.313717655321) Thr + (121.084432174555) Trp + (387.470182958577) Tyr + (690.181263394965) Val + (10.992) GDPFuc + (54.962) UDPNAG + (32.977) GDPMann + (21.985) UDPGal + (21.985) CMPNeu5Ac --> (32.977) GDP + (21.985) UDP + (21.985) CMP + (1) IgG	Irreversible
	Transport Reactions	
98	Acetate[e] <==>	Reversible
99	ADP[e] <==>	Reversible
100	Ala[e] <==>	Reversible
101	AMP[e] <==>	Reversible
102	Arg[e] <==>	Reversible
103	Asn[e] <==>	Reversible
104	Asp[e] <==>	Reversible
105	ATP[e] <==>	Reversible
106	Biomass[e] <==>	Reversible
107	Choline[e] <==>	Reversible
108	Cit[e] <==>	Reversible
109	CMP[e] <==>	Reversible
110	CO2[e] <==>	Reversible
111	CoASH[e] <==>	Reversible
112	CTP[e] <==>	Reversible
113	FAD[e] <==>	Reversible
114	FADH2[e] <==>	Reversible
115	Fol[e] <==>	Reversible
116	Formate[e] <==>	Reversible
117	Fum[e] <==>	Reversible
118	GDP[e] <==>	Reversible
119	Glc[e] <==>	Reversible
120	Gln[e] <==>	Reversible
121	Glu[e] <==>	Reversible
122	Gly[e] <==>	Reversible
123	Glyc[e] <==>	Reversible
124	Glyc3PC[e] <==>	Reversible
125	GTP[e] <==>	Reversible

126	His[e] <==>	Reversible
127	IgG[e] <==>	Reversible
128	Ile[e] <==>	Reversible
129	Isobut[e] <==>	Reversible
130	Isoval[e] <==>	Reversible
131	Lac[e] <==>	Reversible
132	Leu[e] <==>	Reversible
133	Lys[e] <==>	Reversible
134	Mal[e] <==>	Reversible
135	Met[e] <==>	Reversible
136	NAD[e] <==>	Reversible
137	NADH[e] <==>	Reversible
138	NADP[e] <==>	Reversible
139	NADPH[e] <==>	Reversible
140	NH4[e] <==>	Reversible
141	Pcholine[e] <==>	Reversible
142	Phe[e] <==>	Reversible
143	Pro[e] <==>	Reversible
144	Pyr[e] <==>	Reversible
145	Ser[e] <==>	Reversible
146	SPRM[e] <==>	Reversible
147	Succ[e] <==>	Reversible
148	Thr[e] <==>	Reversible
149	Trp[e] <==>	Reversible
150	Tyr[e] <==>	Reversible
151	UDP[e] <==>	Reversible
152	Urea[e] <==>	Reversible
153	UTP[e] <==>	Reversible
154	Val[e] <==>	Reversible

Appendix II

Chapter 5 supplementary materials

Appendix Table 1. Feeding schedules used in gPROMS for both conditions.

SCHEDULE (SGE 36.5°C)	SCHEDULE (SGE 32°C)
From Day 0	From Day 6
SEQUENCE	SEQUENCE
RESET	RESET
CELL.F_in_feed := 0;	CELL.F_in_feed := 0;
CELL.F_out:= 0;	CELL.F_out:= 0;
CELL.F_in_glc := 0;	CELL.F_in_glc := 0;
END	END
CONTINUE FOR 20.42	CONTINUE FOR 24.0
RESET	RESET
CELL.F_in_feed := 0;	CELL.F_in_feed := 0;
CELL.F_out:= 0.25;	CELL.F_out:= 0.15;
CELL.F_in_glc := 0;	CELL.F_in_glc := 0;
END	END
CONTINUE FOR 0.1	CONTINUE FOR 0.1
RESET	RESET
CELL.F_in_feed := 0;	CELL.F_in_feed := 0;
CELL.F_out := 0;	CELL.F_out := 0;
CELL.F_in_glc := 0;	CELL.F_in_glc := 0;
END	END
CONTINUE FOR 23.90	CONTINUE FOR 23.15
RESET	RESET
CELL.F_in_feed := 0.8;	CELL.F_in_feed := 0.8;
CELL.F_out:= 1.0;	CELL.F_out:= 0.15;
CELL.F_in_glc := 0.04;	CELL.F_in_glc := 0.0;
END	END
CONTINUE FOR 0.1	CONTINUE FOR 0.1
RESET	RESET
CELL.F_in_feed := 0;	CELL.F_in_feed := 0;
CELL.F_out:= 0;	CELL.F_out:= 0;
CELL.F_in_glc := 0;	CELL.F_in_glc := 0;
END	END
CONTINUE FOR 26.15	CONTINUE FOR 23.9
RESET	RESET
CELL.F_in_feed := 0;	CELL.F_in_feed := 0;
CELL.F_out:= 0.15;	CELL.F_out:= 0.15;
CELL.F_in_glc := 0;	CELL.F_in_glc := 0;
END	END
CONTINUE FOR 0.1	CONTINUE FOR 0.1
RESET	RESET
CELL.F_in_feed := 0;	CELL.F_in_feed := 0;
CELL.F_out:= 0;	CELL.F_out:= 0;
CELL.F_in_glc := 0;	CELL.F_in_glc := 0;
END	END
CONTINUE FOR 23.40	CONTINUE FOR 23.90
RESET	RESET
CELL.F_in_feed := 0.8;	CELL.F_in_feed := 0.8;
CELL.F_out:= 0.15;	CELL.F_out:= 0.15;
CELL.F_in_glc := 0;	CELL.F_in_glc := 0;
END	END
CONTINUE FOR 0.1	CONTINUE FOR 0.1
RESET	RESET
CELL.F_in_feed := 0;	CELL.F_in_feed := 0;
CELL.F_out:= 0;	CELL.F_out:= 0;
CELL.F_in_glc := 0;	CELL.F_in_glc := 0;
END	END
CONTINUE FOR 21.90	CONTINUE FOR 23.90
RESET	RESET
CELL.F_in_feed := 0;	CELL.F_in_feed := 0;
CELL.F_out:= 0.15;	CELL.F_out:= 0.15;
CELL.F_in_glc := 0;	CELL.F_in_glc := 0;
END	END
CONTINUE FOR 0.1	CONTINUE FOR 0.1

RESET	RESET
CELL.F_in_feed := 0;	CELL.F_in_feed := 0;
CELL.F_out:= 0;	CELL.F_out:= 0;
CELL.F_in_glc := 0;	CELL.F_in_glc := 0;
END	END
CONTINUE FOR 23.90	CONTINUE FOR 23.90
RESET	RESET
CELL.F_in_feed := 0.8;	CELL.F_in_feed := 0.8;
CELL.F_out:= 0.15;	CELL.F_out:= 0.15;
CELL.F_in_glc := 0.0767;	CELL.F_in_glc := 0.0;
END	END
CONTINUE FOR 0.1	CONTINUE FOR 0.1
RESET	RESET
CELL.F_in_feed := 0;	CELL.F_in_feed := 0;
CELL.F_out:= 0;	CELL.F_out:= 0;
CELL.F_in_glc := 0;	CELL.F_in_glc := 0;
END	END
CONTINUE FOR 23.9	CONTINUE FOR 23.9
RESET	RESET
CELL.F_in_feed := 0;	CELL.F_in_feed := 0;
CELL.F_out:= 0.15;	CELL.F_out:= 0.15;
CELL.F_in_glc := 0;	CELL.F_in_glc := 0;
END	END
CONTINUE FOR 0.1	CONTINUE FOR 0.1
RESET	RESET
CELL.F_in_feed := 0;	CELL.F_in_feed := 0;
CELL.F_out:= 0;	CELL.F_out:= 0;
CELL.F_in_glc := 0;	CELL.F_in_glc := 0;
END	END
CONTINUE FOR 23.15	CONTINUE FOR 23.90
RESET	
CELL.F_in_feed := 0.8;	
CELL.F_out:= 0.15;	
CELL.F_in_glc := 0.033;	
END	
CONTINUE FOR 0.1	
RESET	
CELL.F_in_feed := 0;	
CELL.F_out:= 0;	
CELL.F_in_glc := 0;	
END	
CONTINUE FOR 23.9	
RESET	
CELL.F_in_feed := 0;	
CELL.F_out:= 0.15;	
CELL.F_in_glc := 0;	
END	
CONTINUE FOR 0.1	
RESET	
CELL.F_in_feed := 0;	
CELL.F_out:= 0;	
CELL.F_in_glc := 0;	
END	
CONTINUE FOR 23.90	
RESET	
CELL.F_in_feed :=0.8;	
CELL.F_out:=0.15;	
CELL.F_in_glc := 0.043;	
END	
CONTINUE FOR 0.1	

RESET	
CELL.F_in_feed := 0;	
CELL.F_out:= 0;	
CELL.F_in_glc := 0;	
END	
CONTINUE FOR 23.90	
RESET	
CELL.F_in_feed := 0;	
CELL.F_out:= 0.15;	
CELL.F_in_glc := 0;	
END	
CONTINUE FOR 0.1	
RESET	
CELL.F_in_feed := 0;	
CELL.F_out:= 0;	
CELL.F_in_glc := 0;	
END	
CONTINUE FOR 23.90	
RESET	
CELL.F_in_feed := 0.8;	
CELL.F_out:= 0.15;	
CELL.F_in_glc := 0;	
END	
CONTINUE FOR 0.1	
RESET	
CELL.F_in_feed := 0;	
CELL.F_out:= 0;	
CELL.F_in_glc := 0;	
END	
CONTINUE FOR 23.9	
RESET	
CELL.F_in_feed := 0;	
CELL.F_out:= 0.15;	
CELL.F_in_glc := 0;	
END	
CONTINUE FOR 0.1	
RESET	
CELL.F_in_feed := 0;	
CELL.F_out:= 0;	
CELL.F_in_glc := 0;	
END	
CONTINUE FOR 23.9	
END	

Appendix Table 2. List of parameters used in cell dynamic models for both temperatures.

Parameter	Values		Units
	36.5 °C	32 °C (Day 6)	
Growth/death related			
μ_{max}	1.10E-01	7.49E-01	h^{-1}
$\mu_{d,max}$	9.70E-02	3.96E-02	h^{-1}
K_{glc}	1.82E+00	4.90E+01	mM
K_{lac}	3.87E+00	5.80E-03	mM
K_{arg}	3.80E-02	2.90E-01	mM
K_{asn}	1.07E-02	1.41E-01	mM
K_{asp}	1.00E-10	2.18E-01	mM
K_{glu}	1.55E-01	2.92E-01	mM
K_{lys}	1.00E-08	1.78E+00	mM
K_{pro}	4.09E-07	6.54E-01	mM
KI_{lac}	3.87E+00	3.79E+01	mM
KI_{amm}	2.75E+00	3.86E+00	mM
$K_{d,amm}$	8.04E+00	3.43E-04	mM
K_{lysis}	4.47E-01	2.14E-01	h^{-1}
Metabolism related			
$Y_{arg,glu}$	1.59E-02	1.10E-01	mmol $mmol^{-1}$
$Y_{asp,asn}$	9.50E-04	7.92E-01	mmol $mmol^{-1}$
$Y_{gln,glu}$	1.00E+00	1.00E+00	mmol $mmol^{-1}$
$Y_{glu,gln}$	1.00E-10	7.47E-01	mmol $mmol^{-1}$
$Y_{lac,glc}$	2.00E+00	5.32E-03	mmol $mmol^{-1}$
$Y_{lys,glu}$	1.19E-01	1.13E-01	mmol $mmol^{-1}$
$Y_{pro,glu}$	8.10E-01	7.95E-01	mmol $mmol^{-1}$
$Y_{mAb,\mu}$	4.40E-01	4.33E-01	mg h^{-1}
$Y_{x,amm}$	2.21E+10	1.00E+19	cell $mmol^{-1}$
$Y_{x,arg}$	2.64E+10	1.74E+13	cell $mmol^{-1}$
$Y_{x,asn}$	7.76E+10	4.84E+10	cell $mmol^{-1}$
$Y_{x,asp}$	3.59E+09	9.93E+14	cell $mmol^{-1}$
$Y_{x,gln}$	3.20E+12	4.01E+14	cell $mmol^{-1}$
$Y_{x,glu}$	6.10E+09	3.43E+09	cell $mmol^{-1}$
$Y_{x,lac}$	6.10E+13	4.57E+09	cell $mmol^{-1}$
$Y_{x,lys}$	1.75E+10	9.86E+14	cell $mmol^{-1}$
$Y_{x,pro}$	3.26E+11	6.40E+12	cell $mmol^{-1}$
$Y_{x,glc}$	9.00E+08	4.45E+10	cell $mmol^{-1}$
m_{glc}	1.48E-11	1.07E-11	mmol $cell^{-1}$ h^{-1}
p_{gln}	3.11E-12	4.87E-11	mmol $cell^{-1}$ h^{-1}
$K_{T,[asn\_ext]}$	4.37E-12	1.68E-11	h^{-1}
$K_{T,[lac\_ext]}$	5.83E-12	5.27E-13	h^{-1}
$Km_{amm,gln}$	0.00E+00	1.34E+00	mM
$Km_{lac,\mu}$	3.05E+00	1.72E-01	mM
mAb synthesis related			
K_A	1.38E-01	1.94E-03	molecule $cell^{-1}$ h^{-1}

K_{ER}	4.56E+02	9.03E+02	h^{-1}
K_G	2.00E+03	2.30E+04	h^{-1}
N_H	1.20E+02	1.20E+02	gene $cell^{-1}$
N_L	1.02E+02	1.02E+02	gene $cell^{-1}$
S_H	1.59E+01	1.11E+02	mRNAs $gene^{-1}$ h^{-1}
S_L	9.31E+01	1.58E+02	mRNAs $gene^{-1}$ h^{-1}
T_H	1.35E+00	2.17E+00	chain $mRNA^{-1}$ h^{-1}
T_L	3.84E-01	5.66E-01	chain $mRNA^{-1}$ h^{-1}
ε_1	1.00E+00	7.46E-01	n/a
K_h	9.77E-03	1.68E-03	h^{-1}
K_l	1.15E-03	1.13E-03	h^{-1}
mAb secretion related			
ε_2	1.11E+01	6.14E+00	n/a

Appendix Table 3. List of parameters used in NSD models for both temperatures.

Parameter	Values		Units
	36.5 °C	32 °C (Day 6)	
Nucleotide related			
$K_{T,glc}$	8.25E-01	8.25E-01	$mmol_{glc(int)}$ (dm^2_{cell} $mmol_{glc(ext)}$ $h)^{-1}$
$K_{T,gln}$	2.56E+00	2.56E+00	$mmol_{glc(int)}$ (dm^2_{cell} $mmol_{glc(ext)}$ $h)^{-1}$
$K_{glc,ATP}$	2.71E+00	3.02E-03	mM
$K_{gln,ATP}$	2.04E+01	8.34E+00	mM
$V_{max,\ ATP}$	1.37E+01	2.11E+00	mmol L_{cell}^{-1} h^{-1}
$V_{max,\ GTP}$	4.42E+01	2.68E+03	mmol L_{cell}^{-1} h^{-1}
$V_{max,\ UTP}$	3.49E+01	9.26E+02	mmol L_{cell}^{-1} h^{-1}
$V_{max,\ CTP}$	8.09E-03	7.61E+01	mmol L_{cell}^{-1} h^{-1}
$N_{ATP,\ GTP}$	2.00E+00	2.00E+00	mmol $mmol^{-1}$
$N_{ATP,\ UTP}$	4.00E+00	4.00E+00	mmol $mmol^{-1}$
$N_{ATP,CTP}$	1.00E+00	1.00E+00	mmol $mmol^{-1}$
$K_{CTP,ATP}$	1.00E-04	4.46E+02	mM
$K_{CTP,UTP}$	0.00E+00	2.83E+01	mM
$K_{GTP,ATP}$	1.00E-10	5.00E+03	mM
$K_{UTP,ATP}$	8.47E+01	1.45E+00	mM
$K_{CTP,Gln}$	1.00E-04	1.07E+04	mM
$K_{GTP,Glc}$	1.48E+01	8.85E+00	mM
$K_{GTP,Gln}$	1.36E+02	2.51E+00	mM
$K_{UTP,Glc}$	1.01E+00	1.45E+03	mM
$K_{UTP,Gln}$	1.36E+02	2.01E+02	mM
NSD related			
$K_{TP,UDPGlc}$	4.11E-03	0.00E+00	mM
$K_{TP,UDPGal}$	4.68E-02	3.47E-04	mM
$K_{TP,UDPGlcNAc}$	0.00E+00	9.76E+00	mM
$K_{TP,UDPGalNAc}$	1.26E-02	9.69E+00	mM
$K_{TP,GDPMan}$	1.00E-02	1.40E+00	mM
$K_{TP,GDPFuc}$	1.25E-01	7.42E-02	mM
$K_{TP,CMPNeu5Ac}$	1.90E+01	9.98E+01	mM
$V_{max,\ UDPGlc}$	5.00E-01	5.84E-01	mmol L_{cell}^{-1} h^{-1}
$V_{max,\ UDPGal}$	2.26E-03	0.00E+00	mmol L_{cell}^{-1} h^{-1}
$V_{max,\ UDPGlcNAc}$	2.17E+00	7.66E+00	mmol L_{cell}^{-1} h^{-1}
$V_{max,\ UDPGalNAc}$	6.23E-03	7.18E+01	mmol L_{cell}^{-1} h^{-1}
$V_{max,GDPMan}$	6.57E-01	2.18E-01	mmol L_{cell}^{-1} h^{-1}
$V_{max,GDPFuc}$	1.17E+01	5.28E+01	mmol L_{cell}^{-1} h^{-1}
$V_{max,CMPNeu5Ac}$	4.04E-02	5.37E+00	mmol L_{cell}^{-1} h^{-1}
K_{UDPGlc}	6.66E+02	1.05E+01	mM

K_{UDPGal}	4.73E-01	4.40E+02	mM
$K_{UDPGlcNAc}$	1.82E-01	4.53E-01	mM
$K_{UDPGalNAc}$	1.73E-02	4.57E+02	mM
K_{GDPMan}	1.71E+02	3.48E+01	mM
K_{GDPFuc}	8.80E+02	5.62E+03	mM
$K_{CMPNeu5Ac}$	1.50E+03	6.19E+03	mM
$N_{glyc,cell}$	1.72E-12	5.27E-12	mmol $cell^{-1}$
$N_{UDPGlc,glyc}$	5.04E-01	1.00E+00	mmol $mmol^{-1}$
$N_{UDPGal,glyc}$	1.07E+00	5.14E-01	mmol $mmol^{-1}$
$N_{UDPGlcNAc,glyc}$	5.47E-01	9.98E-01	mmol $mmol^{-1}$
$N_{UDPGalNAc,glyc}$	0.00E+00	0.00E+00	mmol $mmol^{-1}$
$N_{GDPMan,glyc}$	9.00E+00	9.00E+00	mmol $mmol^{-1}$
$N_{GDPFuc,glyc}$	3.97E-01	3.97E-01	mmol $mmol^{-1}$
$N_{CMPNeu5Ac,glyc}$	9.73E-02	9.73E-02	mmol $mmol^{-1}$
$N_{glyc,mAb}$	2.00E+00	2.00E+00	mol_{glyc} mol_{mAbFc}^{-1}
$N_{UDPGlc,mAb}$	3.00E+00	3.00E+00	$mmol_{NSD}$ $mmol_{mAb}^{-1}$
$N_{UDPGal,mAb}$	3.79E-01	1.91E-01	$mmol_{NSD}$ $mmol_{mAb}^{-1}$
$N_{UDPGlcNAc,mAb}$	3.88E+00	2.00E+00	$mmol_{NSD}$ $mmol_{mAb}^{-1}$
$N_{GDPMan,mAb}$	9.00E+00	9.00E+00	$mmol_{NSD}$ $mmol_{mAb}^{-1}$
$N_{GDPFuc,mAb}$	9.32E-01	9.25E-01	$mmol_{NSD}$ $mmol_{mAb}^{-1}$

Appendix III

Chapter 7 supplementary materials

Appendix Table 1. Feeding schedules used in gPROMS for all TGE conditions.

SCHEDULE (TGE 36.5°C)	SCHEDULE (TGE 32°C)						
From Day 0	From Day 2						
SEQUENCE	SEQUENCE						
RESET	RESET	RESET	RESET	RESET	RESET	RESET	RESET
Balance.F_in_feed := 0;	CELL.F_in_feed := 0;	Balance.F_in_feed := 0.8;	CELL.F_in_feed := 0;	Balance.F_in_feed := 0;	CELL.F_in_feed := 0;	Balance.F_in_feed := 0;	CELL.F_in_feed := 0.8;
Balance.F_out:= 0;	CELL.F_out := 0;	Balance.F_out:= 0.15;	CELL.F_out:= 0.15;	Balance.F_out:= 0;	CELL.F_out:= 0;	Balance.F_out:= 0.15;	CELL.F_out:= 0.15;
Balance.F_in_glc := 0;	CELL.F_in_glc := 0;	Balance.F_in_glc := 0;	CELL.F_in_glc := 0;	Balance.F_in_glc := 0;	CELL.F_in_glc := 0;	Balance.F_in_glc := 0;	CELL.F_in_glc := 0.065;
Balance.PEI_in := 0;	CELL.PEI_in := 0;	Balance.PEI_in := 0;	CELL.PEI_in := 0;	Balance.PEI_in := 0;	CELL.PEI_in := 0;	Balance.PEI_in := 0;	CELL.PEI_in := 0;
Balance.N_H := 0;	CELL.N_H := 111;	Balance.N_H := 28;	CELL.N_H := 26;	Balance.N_H := 8;	CELL.N_H := 7;	Balance.N_H := 2;	CELL.N_H := 3;
Balance.N_L := 0;	CELL.N_L := 128;	Balance.N_L := 86;	CELL.N_L := 83;	Balance.N_L := 47;	CELL.N_L := 42;	Balance.N_L := 21;	CELL.N_L := 31;
END	END	END	END	END	END	END	END
CONTINUE FOR 20.42	CONTINUE FOR 23.90	CONTINUE FOR 0.1	CONTINUE FOR 0.1	CONTINUE FOR 23.15	CONTINUE FOR 23.9	CONTINUE FOR 0.1	CONTINUE FOR 0.1
RESET	RESET	RESET	RESET	RESET	RESET	RESET	RESET
Balance.F_in_feed := 0;	CELL.F_in_feed := 0.8;	Balance.F_in_feed := 0;	CELL.F_in_feed := 0;	Balance.F_in_feed := 0.8;	CELL.F_in_feed := 0;	Balance.F_in_feed := 0;	CELL.F_in_feed := 0;
Balance.F_out:= 0.25;	CELL.F_out:= 0.15;	Balance.F_out:= 0;	CELL.F_out:= 0;	Balance.F_out:= 0.15;	CELL.F_out:= 0.15;	Balance.F_out:= 0;	CELL.F_out:= 0;
Balance.F_in_glc := 0;	CELL.F_in_glc := 0.0467;	Balance.F_in_glc := 0;	CELL.F_in_glc := 0;	Balance.F_in_glc := 0.05;	CELL.F_in_glc := 0;	Balance.F_in_glc := 0;	CELL.F_in_glc := 0;
Balance.PEI_in := 0.1295;	CELL.PEI_in := 0;	Balance.PEI_in := 0;	CELL.PEI_in := 0;	Balance.PEI_in := 0;	CELL.PEI_in := 0;	Balance.PEI_in := 0;	CELL.PEI_in := 0;
Balance.N_H := 0;	CELL.N_H := 111;	Balance.N_H := 19;	CELL.N_H := 33;	Balance.N_H := 8;	CELL.N_H := 7;	Balance.N_H := 4;	CELL.N_H := 2;
Balance.N_L := 0;	CELL.N_L := 128;	Balance.N_L := 71;	CELL.N_L := 76;	Balance.N_L := 47;	CELL.N_L := 42;	Balance.N_L := 31;	CELL.N_L := 28;
END	END	END	END	END	END	END	END
CONTINUE FOR 0.1	CONTINUE FOR 0.1	CONTINUE FOR 21.90	CONTINUE FOR 23.90	CONTINUE FOR 0.1	CONTINUE FOR 0.1	CONTINUE FOR 23.90	CONTINUE FOR 23.9
RESET	RESET	RESET	RESET	RESET	RESET	RESET	RESET
Balance.F_in_feed := 0;	CELL.F_in_feed := 0;	Balance.F_in_feed := 0;	CELL.F_in_feed := 0.8;	Balance.F_in_feed := 0;	CELL.F_in_feed := 0;	Balance.F_in_feed := 0.8;	CELL.F_in_feed := 0;
Balance.F_out := 0;	CELL.F_out:= 0;	Balance.F_out:= 0.15;	CELL.F_out:= 0.15;	Balance.F_out:= 0;	CELL.F_out:= 0;	Balance.F_out:= 0.15;	CELL.F_out:= 0.15;
Balance.F_in_glc := 0;	CELL.F_in_glc := 0;	Balance.F_in_glc := 0;	CELL.F_in_glc := 0;	Balance.F_in_glc:= 0;	CELL.F_in_glc := 0;	Balance.F_in_glc := 0.065;	CELL.F_in_glc := 0;
Balance.PEI_in := 0;	CELL.PEI_in := 0;	Balance.PEI_in := 0;	CELL.PEI_in := 0;	Balance.PEI_in := 0;	CELL.PEI_in := 0;	Balance.N_H := 4;	CELL.N_H := 2;
Balance.N_H := 97;	CELL.N_H := 58;	Balance.N_H := 19;	CELL.N_H := 33;	Balance.N_H := 5;	CELL.N_H := 5;	Balance.N_L := 31;	CELL.N_L := 28;
Balance.N_L := 148;	CELL.N_L := 114;	Balance.N_L := 71;	CELL.N_L := 76;	Balance.N_L := 38;	CELL.N_L := 33;	END	END
END	END	END	END	END	END		
CONTINUE FOR 23.90	CONTINUE FOR 26.15	CONTINUE FOR 0.1	CONTINUE FOR 0.1	CONTINUE FOR 23.9	CONTINUE FOR 23.90	CONTINUE FOR 0.1	CONTINUE FOR 0.1
RESET	RESET	RESET	RESET	RESET	RESET	RESET	RESET
Balance.F_in_feed := 0.8;	CELL.F_in_feed := 0;	Balance.F_in_feed := 0;	CELL.F_in_feed := 0;	Balance.F_in_feed := 0;	CELL.F_in_feed :=0.8;	Balance.F_in_feed := 0;	CELL.F_in_feed := 0;
Balance.F_out:= 1.0;	CELL.F_out:= 0.15;	Balance.F_out:= 0;	CELL.F_out:= 0;	Balance.F_out:= 0.15;	CELL.F_out:=0.15;	Balance.F_out:= 0;	CELL.F_out:= 0;
Balance.F_in_glc := 0.045;	CELL.F_in_glc := 0;	Balance.F_in_glc := 0;	CELL.F_in_glc := 0;	Balance.F_in_glc:= 0;	CELL.F_in_glc := 0.0;	Balance.F_in_glc := 0;	CELL.F_in_glc := 0;
Balance.PEI_in := 0;	CELL.PEI_in := 0;	Balance.PEI_in := 0;	CELL.PEI_in := 0;	Balance.PEI_in := 0;	CELL.PEI_in := 0;	Balance.PEI_in := 0;	CELL.PEI_in := 0;
Balance.N_H := 97;	CELL.N_H := 58;	Balance.N_H := 16;	CELL.N_H := 18;	Balance.N_H := 5;	CELL.N_H := 5;	Balance.N_H := 2;	CELL.N_H := 3;
Balance.N_L := 148;	CELL.N_L := 114;	Balance.N_L := 59;	CELL.N_L := 60;	Balance.N_L := 38;	CELL.N_L := 33;	Balance.N_L := 22;	CELL.N_L := 26;
END	END	END	END	END	END	END	END
CONTINUE FOR 0.1	CONTINUE FOR 0.1	CONTINUE FOR 23.90	CONTINUE FOR 23.9	CONTINUE FOR 0.1	CONTINUE FOR 0.1	CONTINUE FOR 23.9	CONTINUE FOR 23.9;
RESET	RESET	RESET	RESET	RESET	RESET	RESET	END
Balance.F_in_feed := 0;	CELL.F_in_feed := 0;	Balance.F_in_feed := 0.8;	CELL.F_in_feed := 0;	Balance.F_in_feed := 0;	CELL.F_in_feed := 0;	Balance.F_in_feed := 0;	
Balance.F_out:= 0;	CELL.F_out:= 0;	Balance.F_out:= 0.15;	CELL.F_out:= 0.15;	Balance.F_out:= 0;	CELL.F_out:= 0;	Balance.F_out:= 0.15;	
Balance.F_in_glc := 0;	CELL.F_in_glc := 0;	Balance.F_in_glc := 0.055;	CELL.F_in_glc := 0;	Balance.F_in_glc := 0;	CELL.F_in_glc := 0;	Balance.F_in_glc := 0;	
Balance.PEI_in := 0;	CELL.PEI_in := 0;	Balance.PEI_in := 0;	CELL.PEI_in := 0;	Balance.PEI_in := 0;	CELL.PEI_in := 0;	Balance.PEI_in := 0;	
Balance.N_H := 41;	CELL.N_H := 64;	Balance.N_H := 16;	CELL.N_H := 18;	Balance.N_H := 3;	CELL.N_H := 2;	Balance.N_H := 2;	
Balance.N_L := 97;	CELL.N_L := 116;	Balance.N_L := 59;	CELL.N_L := 60;	Balance.N_L := 26;	CELL.N_L := 23;	Balance.N_L := 22;	
END	END	END	END	END	END	END	
CONTINUE FOR 26.15	CONTINUE FOR 23.40	CONTINUE FOR 0.1	CONTINUE FOR 0.1	CONTINUE FOR 23.90	CONTINUE FOR 23.90	CONTINUE FOR 0.1	
RESET	RESET	RESET	RESET	RESET	RESET	RESET	
Balance.F_in_feed := 0;	CELL.F_in_feed := 0.8;	Balance.F_in_feed := 0;	CELL.F_in_feed := 0;	Balance.F_in_feed :=0.8;	CELL.F_in_feed := 0;	Balance.F_in_feed := 0;	
Balance.F_out:= 0.15;	CELL.F_out:= 0.15;	Balance.F_out:= 0;	CELL.F_out:= 0;	Balance.F_out:=0.15;	CELL.F_out:= 0.15;	Balance.F_out:= 0;	
Balance.F_in_glc := 0;	CELL.F_in_glc := 0.01;	Balance.F_in_glc := 0;	CELL.F_in_glc := 0;	Balance.F_in_glc := 0.0;	CELL.F_in_glc := 0;	Balance.F_in_glc := 0;	
Balance.PEI_in := 0;	CELL.PEI_in := 0;	Balance.PEI_in := 0;	CELL.PEI_in := 0;	Balance.PEI_in := 0;	CELL.PEI_in := 0;	Balance.PEI_in := 0;	
Balance.N_H := 41;	CELL.N_H := 64;	Balance.N_H := 9;	CELL.N_H := 9;	Balance.N_H := 3;	CELL.N_H := 2;	Balance.N_H := 2;	
Balance.N_L := 97;	CELL.N_L := 116;	Balance.N_L := 48;	CELL.N_L := 43;	Balance.N_L := 26;	CELL.N_L := 23;	Balance.N_L := 22;	
END	END	END	END	END	END	END	
CONTINUE FOR 0.1	CONTINUE FOR 0.1	CONTINUE FOR 23.9	CONTINUE FOR 23.15	CONTINUE FOR 0.1	CONTINUE FOR 0.1	CONTINUE FOR 23.9;	
						END	
RESET	RESET	RESET	RESET	RESET	RESET		
Balance.F_in_feed := 0;	CELL.F_in_feed := 0;	Balance.F_in_feed := 0;	CELL.F_in_feed := 0.8;	Balance.F_in_feed := 0;	CELL.F_in_feed := 0;		
Balance.F_out:= 0;	CELL.F_out:= 0;	Balance.F_out:= 0.15;	CELL.F_out:= 0.15;	Balance.F_out:= 0;	CELL.F_out:= 0;		
Balance.F_in_glc := 0;	CELL.F_in_glc := 0;	Balance.F_in_glc := 0.03;	CELL.F_in_glc := 0;	Balance.F_in_glc := 0;	CELL.F_in_glc := 0;		
Balance.PEI_in := 0;	CELL.PEI_in := 0;	Balance.PEI_in := 0;	CELL.PEI_in := 0;	Balance.PEI_in := 0;	CELL.PEI_in := 0;		
Balance.N_H := 28;	CELL.N_H := 26;	Balance.N_H := 9;	CELL.N_H := 9;	Balance.N_H := 2;	CELL.N_H := 3;		
Balance.N_L := 86;	CELL.N_L := 83;	Balance.N_L := 48;	CELL.N_L := 43;	Balance.N_L := 21;	CELL.N_L := 31;		
END	END	END	END	END	END		
CONTINUE FOR 23.40	CONTINUE FOR 21.9	CONTINUE FOR 0.1	CONTINUE FOR 0.1	CONTINUE FOR 23.90	CONTINUE FOR 23.90		

Appendix Table 2. List of parameters used in cell dynamics models for both temperatures in TGE.

Symbol	Values		Units
	TGE 36.5 °C	TGE 32 °C	
Growth/death related			
μ_{max}	1.12E+00	1.58E-01	h^{-1}
$\mu_{d,max}$	2.88E-02	2.66E-02	h^{-1}
K_{glc}	0.00E+00	1.49E-02	mM
K_{lac}	1.15E+01	2.15E+01	mM
K_{arg}	0.00E+00	3.66E-08	mM
K_{asn}	6.04E-01	9.51E-03	mM
K_{asp}	6.81E-05	4.62E-01	mM
K_{glu}	0.00E+00	5.69E-07	mM
K_{lys}	2.90E+00	5.75E-07	mM
K_{pro}	2.48E+00	1.22E-02	mM
KI_{lac}	4.47E+00	1.00E+03	mM
KI_{amm}	1.25E+02	7.20E-01	mM
$K_{d,amm}$	1.00E+00	5.67E+00	mM
K_{lysis}	1.39E-01	2.94E-01	h^{-1}
KI_{PEI}	8.74E+03	1.00E+04	mM
Metabolism related			
$Y_{arg,glu}$	2.41E-01	1.80E-02	mmol $mmol^{-1}$
$Y_{asp,asn}$	5.42E-02	1.00E-03	mmol $mmol^{-1}$
$Y_{gln,glu}$	4.85E-01	1.00E+00	mmol $mmol^{-1}$
$Y_{glu,gln}$	2.84E-03	1.00E+00	mmol $mmol^{-1}$
$Y_{lac,glc}$	2.00E+00	1.11E-15	mmol $mmol^{-1}$
$Y_{lys,glu}$	8.08E-01	2.90E-01	mmol $mmol^{-1}$
$Y_{pro,glu}$	1.00E+00	9.28E-01	mmol $mmol^{-1}$
$Y_{mAb,\mu}$	9.54E-01	1.00E+01	mg
$Y_{x,amm}$	4.79E+10	1.95E+09	cell $mmol^{-1}$
$Y_{x,arg}$	2.98E+10	2.76E+10	cell $mmol^{-1}$
$Y_{x,asn}$	9.40E+19	1.57E+10	cell $mmol^{-1}$
$Y_{x,asp}$	1.00E+07	2.01E+09	cell $mmol^{-1}$
$Y_{x,gln}$	8.91E+16	5.59E+10	cell $mmol^{-1}$
$Y_{x,glu}$	1.78E+10	4.10E+09	cell $mmol^{-1}$
$Y_{x,lac}$	1.45E+08	1.00E+14	cell $mmol^{-1}$
$Y_{x,lys}$	2.24E+10	9.50E+09	cell $mmol^{-1}$
$Y_{x,pro}$	2.54E+10	1.09E+10	cell $mmol^{-1}$
$Y_{x,glc}$	9.20E+08	6.54E+08	cell $mmol^{-1}$
m_{glc}	3.26E-11	9.66E-12	mmol $cell^{-1}$ h^{-1}
p_{gln}	1.91E-10	2.63E-12	mmol $cell^{-1}$ h^{-1}
$K_{T,[asn\_ext]}$	4.29E-12	5.07E-12	h^{-1}
$K_{T,[lac\_ext]}$	9.52E-13	7.63E-12	h^{-1}
$Km_{amm,gln}$	3.68E+02	1.85E-01	mM
$Km_{lac,\mu}$	3.95E+01	2.99E+02	mM

mAb synthesis related			
K_A	4.15E-02	1.87E-03	molecule cell^{-1} h^{-1}
K_{ER}	2.79E+03	3.00E+03	h^{-1}
K_G	1.35E-03	7.22E-03	h^{-1}
N_H	variable	variable	gene cell^{-1}
N_L	variable	variable	gene cell^{-1}
S_H	1.40E+01	7.52E+00	mRNAs gene^{-1} h^{-1}
S_L	2.33E+02	4.64E+01	mRNAs gene^{-1} h^{-1}
T_H	4.90E+00	4.71E+02	chain mRNA^{-1} h^{-1}
T_L	1.36E+00	4.70E+00	chain mRNA^{-1} h^{-1}
ε_1	1.00E+00	1.00E+00	n/a
K_h	0.00E+00	0.00E+00	h^{-1}
K_l	1.80E-01	1.00E-12	h^{-1}
mAb secretion related			
ε_2	6.50E+01	9.61E-01	n/a

Appendix Table 3. List of parameters used in NSD models for both temperatures in TGE.

Parameter	Values		Units
	TGE 36.5 °C	TGE 32 °C	
Nucleotide related			
$K_{T,glc}$	8.25E-01	8.25E-01	$mmol_{glc(int)}$ (dm^2_{cell} $mmol_{glc(ext)}$ $h)^{-1}$
$K_{T,gln}$	2.56E+00	2.56E+00	$mmol_{glc(int)}$ (dm^2_{cell} $mmol_{glc(ext)}$ $h)^{-1}$
$K_{glc,ATP}$	3.05E-13	6.13E+00	mM
$K_{gln,ATP}$	1.00E+00	6.57E+00	mM
$V_{max,\ ATP}$	5.46E+01	3.20E+00	mmol L_{cell}^{-1} h^{-1}
$V_{max,\ GTP}$	2.31E+02	2.85E+01	mmol L_{cell}^{-1} h^{-1}
$V_{max,\ UTP}$	4.74E+02	2.46E+00	mmol L_{cell}^{-1} h^{-1}
$V_{max,\ CTP}$	1.00E+02	1.87E-01	mmol L_{cell}^{-1} h^{-1}
$N_{ATP,\ GTP}$	2.00E+00	2.00E+00	mmol $mmol^{-1}$
$N_{ATP,\ UTP}$	4.00E+00	4.00E+00	mmol $mmol^{-1}$
$N_{ATP,CTP}$	1.00E+00	1.00E+00	mmol $mmol^{-1}$
$K_{CTP,ATP}$	1.20E+01	1.00E-06	mM
$K_{CTP,UTP}$	0.00E+00	0.00E+00	mM
$K_{GTP,ATP}$	5.36E+00	0.00E+00	mM
$K_{UTP,ATP}$	2.38E+01	9.76E+00	mM
$K_{CTP,Gln}$	3.20E+02	9.53E-01	mM
$K_{GTP,Glc}$	3.32E+04	2.55E+03	mM
$K_{GTP,Gln}$	6.95E+02	0.00E+00	mM
$K_{UTP,Glc}$	2.34E+00	0.00E+00	mM
$K_{UTP,Gln}$	2.33E+01	1.00E-02	mM
NSD related			
$K_{TP,UDPGlc}$	1.00E+00	4.89E-01	mM
$K_{TP,UDPGal}$	1.26E-02	0.00E+00	mM
$K_{TP,UDPGlcNAc}$	5.02E+00	6.14E+01	mM
$K_{TP,UDPGalNAc}$	1.26E-02	1.26E-02	mM
$K_{TP,GDPMan}$	1.00E-02	1.00E-02	mM
$K_{TP,GDPFuc}$	1.00E-05	1.00E-05	mM
$K_{TP,CMPNeu5Ac}$	8.01E-02	7.03E-01	mM
$V_{max,\ UDPGlc}$	4.86E+00	7.17E-04	mmol L_{cell}^{-1} h^{-1}
$V_{max,\ UDPGal}$	2.06E-03	5.76E-02	mmol L_{cell}^{-1} h^{-1}
$V_{max,\ UDPGlcNAc}$	1.00E+00	4.95E-01	mmol L_{cell}^{-1} h^{-1}
$V_{max,\ UDPGalNAc}$	3.35E-03	2.65E-03	mmol L_{cell}^{-1} h^{-1}
$V_{max,GDPMan}$	1.00E-10	2.45E+01	mmol L_{cell}^{-1} h^{-1}
$V_{max,GDPFuc}$	2.16E-01	5.82E+00	mmol L_{cell}^{-1} h^{-1}
$V_{max,CMPNeu5Ac}$	3.28E-07	3.28E-07	mmol L_{cell}^{-1} h^{-1}

K_{UDPGlc}	9.67E+02	0.00E+00	mM
K_{UDPGal}	5.00E-01	2.00E+02	mM
$K_{UDPGlcNAc}$	2.22E+01	0.00E+00	mM
$K_{UDPGalNAc}$	1.02E-02	9.91E-04	mM
K_{GDPMan}	0.00E+00	4.98E+01	mM
K_{GDPFuc}	4.50E+00	5.98E+01	mM
$K_{CMPNeu5Ac}$	1.50E+03	4.50E+00	mM
$N_{glyc,cell}$	1.41E-11	3.44E-10	$mmol\ cell^{-1}$
$N_{UDPGlc,glyc}$	1.99E+00	5.00E+00	$mmol\ mmol^{-1}$
$N_{UDPGal,glyc}$	1.88E+00	1.00E-01	$mmol\ mmol^{-1}$
$N_{UDPGlcNAc,glyc}$	7.93E+00	1.00E-10	$mmol\ mmol^{-1}$
$N_{UDPGalNAc,glyc}$	8.32E-01	8.32E-01	$mmol\ mmol^{-1}$
$N_{GDPMan,glyc}$	1.51E+00	1.51E+00	$mmol\ mmol^{-1}$
$N_{GDPFuc,glyc}$	6.68E-02	6.68E-02	$mmol\ mmol^{-1}$
$N_{CMPNeu5Ac,glyc}$	1.03E+00	1.03E+00	$mmol\ mmol^{-1}$
$N_{glyc,mAb}$	2.00E+00	2.00E+00	$mol_{glyc}\ mol_{mAbFc}^{-1}$
$N_{UDPGlc,mAb}$	3.00E+00	3.00E+00	$mmol_{NSD}\ mmol_{mAb}^{-1}$
$N_{UDPGal,mAb}$	2.15E-01	2.15E-01	$mmol_{NSD}\ mmol_{mAb}^{-1}$
$N_{UDPGlcNAc,mAb}$	4.01E+00	4.01E+00	$mmol_{NSD}\ mmol_{mAb}^{-1}$
$N_{GDPMan,mAb}$	9.00E+00	9.00E+00	$mmol_{NSD}\ mmol_{mAb}^{-1}$
$N_{GDPFuc,mAb}$	8.33E-01	8.33E-01	$mmol_{NSD}\ mmol_{mAb}^{-1}$

Appendix IV

Copy right licence

Page Number	Type of work: text, figure, map, etc.	Source work	Copyright holder & year	Satisfied terms and conditions of use or Creative Commons Attribution License	Permission to reproduce	Permission requested	permission refused	Orphan work
Page 16	Figure	Proc Natl Acad Sci U S A. 2011 Aug2;108(31):12669-74	© 2011 PNAS	✓				
Page 17	Figure	Curr Opin Immunol. 2008 Aug;20(4):471-8	© 2008 Elsevier		✓			
Page 33	Figure	Mol Biotechnol. 2008 May;39(1):69-77	© 2008 Springer		✓			
Page 42	Figure	Biotechnol Bioeng. 1997 Sep 20;55(6):890-908	© 1997 John Wiley & Sons, Inc		✓			
Page 43	Figure	Biotechnol Prog. 2010 Nov-Dec;26(6):1505-27	© 2010 American Institute of Chemical Engineers		✓			
Page 44	Figure	BIOTECHNOLOGY PROGRESS, Vol: 27, Pages: 1730-1743	© 2011 American Institute of Chemical Engineers		✓			
Page 56-72 (Chapter 4)	Whole paper	Biotechnol Bioeng. 2015 Jun;112(6):1165-76	© 2014 Wiley Periodicals, Inc.		✓			
Page 86	Figure	Int. J. Mol. Sci. 2014, 15(3), 4492-4522	© 2014 Special Issue Glycosylation and Glycoproteins	✓				
Page 166	Figure	International Journal of Genomics, vol. 2014, Article ID 970607, 15 pages, 2014.	© 2014 Ayla Valinezhad Orang et al.	✓				

Page 17

ELSEVIER LICENSE
TERMS AND CONDITIONS

Jan 21, 2016

This is a License Agreement between Si Nga Sou ("You") and Elsevier ("Elsevier") provided by Copyright Clearance Center ("CCC"). The license consists of your order details, the terms and conditions provided by Elsevier, and the payment terms and conditions.

All payments must be made in full to CCC. For payment instructions, please see information listed at the bottom of this form.

Supplier	Elsevier Limited The Boulevard,Langford Lane Kidlington,Oxford,OX5 1GB,UK
Registered Company Number	1982084
Customer name	Si Nga Sou
Customer address	Imperial College London London, SW7 2AZ
License number	3793730682853
License date	Jan 21, 2016
Licensed content publisher	Elsevier
Licensed content publication	Current Opinion in Immunology
Licensed content title	Terminal sugars of Fc glycans influence antibody effector functions of IgGs
Licensed content author	T Shantha Raju
Licensed content date	August 2008
Licensed content volume number	20
Licensed content issue number	4
Number of pages	8
Start Page	471
End Page	478
Type of Use	reuse in a thesis/dissertation
Portion	figures/tables/illustrations
Number of figures/tables/illustrations	1
Format	both print and electronic
Are you the author of this Elsevier article?	No
Will you be translating?	No
Original figure numbers	Figure 4
Title of your thesis/dissertation	Understanding the impact of bioprocess conditions on monoclonal antibody glycosylation in mammalian cell cultures through experimental and computational analyses
Expected completion date	Oct 2015

Page 33

SPRINGER LICENSE
TERMS AND CONDITIONS

Jan 21, 2016

This is a License Agreement between Si Nga Sou ("You") and Springer ("Springer") provided by Copyright Clearance Center ("CCC"). The license consists of your order details, the terms and conditions provided by Springer, and the payment terms and conditions.

All payments must be made in full to CCC. For payment instructions, please see information listed at the bottom of this form.

License Number	3793740272267
License date	Jan 21, 2016
Licensed content publisher	Springer
Licensed content publication	Molecular Biotechnology
Licensed content title	Metabolic Rates, Growth Phase, and mRNA Levels Influence Cell-Specific Antibody Production Levels from In Vitro-Cultured Mammalian Cells at Sub-Physiological Temperatures
Licensed content author	Rosalyn J. Marchant
Licensed content date	Jan 1, 2008
Volume number	39
Issue number	1
Type of Use	Thesis/Dissertation
Portion	Figures/tables/illustrations
Number of figures/tables/illustrations	1
Author of this Springer article	No
Order reference number	None
Original figure numbers	Figure 3
Title of your thesis / dissertation	Understanding the impact of bioprocess conditions on monoclonal antibody glycosylation in mammalian cell cultures through experimental and computational analyses
Expected completion date	Oct 2015
Estimated size(pages)	200
Total	0.00 GBP

Page 42

JOHN WILEY AND SONS LICENSE TERMS AND CONDITIONS

Jan 21, 2016

This Agreement between Si Nga Sou ("You") and John Wiley and Sons ("John Wiley and Sons") consists of your license details and the terms and conditions provided by John Wiley and Sons and Copyright Clearance Center.

License Number	3793770161334
License date	Jan 21, 2016
Licensed Content Publisher	John Wiley and Sons
Licensed Content Publication	Biotechnology & Bioengineering
Licensed Content Title	A mathematical model of N-linked glycoform biosynthesis
Licensed Content Author	Pablo Umaña,James E. Bailey
Licensed Content Date	Sep 20, 1997
Pages	19
Type of use	Dissertation/Thesis
Requestor type	University/Academic
Format	Print and electronic
Portion	Figure/table
Number of figures/tables	1
Original Wiley figure/table number(s)	Figure 2
Will you be translating?	No
Title of your thesis / dissertation	Understanding the impact of bioprocess conditions on monoclonal antibody glycosylation in mammalian cell cultures through experimental and computational analyses
Expected completion date	Oct 2015
Expected size (number of pages)	200
Requestor Location	Si Nga Sou Imperial College London C509 Roderic Hill building South Kensington Campus London, United Kingdom SW7 2AZ Attn: Si Nga Sou
Billing Type	Invoice
Billing Address	Si Nga Sou Imperial College London C509 Roderic Hill building South Kensington Campus London, United Kingdom SW7 2AZ Attn: Si Nga Sou
Total	0.00 GBP

Page 43

JOHN WILEY AND SONS LICENSE TERMS AND CONDITIONS

Jan 21, 2016

This Agreement between Si Nga Sou ("You") and John Wiley and Sons ("John Wiley and Sons") consists of your license details and the terms and conditions provided by John Wiley and Sons and Copyright Clearance Center.

License Number	3793770346847
License date	Jan 21, 2016
Licensed Content Publisher	John Wiley and Sons
Licensed Content Publication	Biotechnology Progress
Licensed Content Title	Towards the implementation of quality by design to the production of therapeutic monoclonal antibodies with desired glycosylation patterns
Licensed Content Author	Ioscani Jimenez del Val,Cleo Kontoravdi,Judit M. Nagy
Licensed Content Date	Jun 1, 2010
Pages	23
Type of use	Dissertation/Thesis
Requestor type	University/Academic
Format	Print and electronic
Portion	Figure/table
Number of figures/tables	1
Original Wiley figure/table number(s)	Figure 2
Will you be translating?	No
Title of your thesis / dissertation	Understanding the impact of bioprocess conditions on monoclonal antibody glycosylation in mammalian cell cultures through experimental and computational analyses
Expected completion date	Oct 2015
Expected size (number of pages)	200
Requestor Location	Si Nga Sou Imperial College London C509 Roderic Hill building South Kensington Campus London, United Kingdom SW7 2AZ Attn: Si Nga Sou
Billing Type	Invoice
Billing Address	Si Nga Sou Imperial College London C509 Roderic Hill building South Kensington Campus London, United Kingdom SW7 2AZ Attn: Si Nga Sou
Total	0.00 GBP

Page 44

JOHN WILEY AND SONS LICENSE TERMS AND CONDITIONS

Jan 21, 2016

This Agreement between Si Nga Sou ("You") and John Wiley and Sons ("John Wiley and Sons") consists of your license details and the terms and conditions provided by John Wiley and Sons and Copyright Clearance Center.

License Number	3793761466719
License date	Jan 21, 2016
Licensed Content Publisher	John Wiley and Sons
Licensed Content Publication	Biotechnology Progress
Licensed Content Title	A dynamic mathematical model for monoclonal antibody N-linked glycosylation and nucleotide sugar donor transport within a maturing Golgi apparatus
Licensed Content Author	Ioscani Jimenez del Val,Judit M. Nagy,Cleo Kontoravdi
Licensed Content Date	Sep 28, 2011
Pages	14
Type of use	Dissertation/Thesis
Requestor type	University/Academic
Format	Print and electronic
Portion	Figure/table
Number of figures/tables	1
Original Wiley figure/table number(s)	Figure 2
Will you be translating?	No
Title of your thesis / dissertation	Understanding the impact of bioprocess conditions on monoclonal antibody glycosylation in mammalian cell cultures through experimental and computational analyses
Expected completion date	Oct 2015
Expected size (number of pages)	200
Requestor Location	Si Nga Sou Imperial College London C509 Roderic Hill building South Kensington Campus London, United Kingdom SW7 2AZ Attn: Si Nga Sou
Billing Type	Invoice
Billing Address	Si Nga Sou Imperial College London C509 Roderic Hill building South Kensington Campus London, United Kingdom SW7 2AZ Attn: Si Nga Sou
Total	0.00 GBP

Chapter 4

JOHN WILEY AND SONS LICENSE TERMS AND CONDITIONS

Feb 04, 2015

This Agreement between Si Nga Sou ("You") and John Wiley and Sons ("John Wiley and Sons") consists of your license details and the terms and conditions provided by John Wiley and Sons and Copyright Clearance Center.

License Number	3561960411078
License date	Feb 04, 2015
Licensed Content Publisher	John Wiley and Sons
Licensed Content Publication	Biotechnology & Bioengineering
Licensed Content Title	How does mild hypothermia affect monoclonal antibody glycosylation?
Licensed Content Author	Si Nga Sou,Christopher Sellick,Ken Lee,Alison Mason,Sarantos Kyriakopoulos,Karen M. Polizzi,Cleo Kontoravdi
Licensed Content Date	Dec 29, 2014
Pages	1
Type of use	Dissertation/Thesis
Requestor type	Author of this Wiley article
Format	Print and electronic
Portion	Full article
Will you be translating?	No
Title of your thesis / dissertation	Understanding the impact of bioprocess conditions on monoclonal antibody glycosylation in mammalian cell cultures through experimental and computational analyses
Expected completion date	Oct 2015
Expected size (number of pages)	200
Requestor Location	Si Nga Sou Imperial College London C509 Roderic Hill building South Kensington Campus London, United Kingdom SW7 2AZ Attn: Si Nga Sou
Billing Type	Invoice
Billing Address	Si Nga Sou Imperial College London C509 Roderic Hill building South Kensington Campus London, United Kingdom SW7 2AZ Attn: Si Nga Sou
Total	0.00 GBP
Terms and Conditions	

TERMS AND CONDITIONS